Crowd dynamics : modeling pedestrian movement and associated generated forces

Bachar Kabalan

UNIVERSITÉ PARIS-EST

ECOLE DOCTORALE SCIENCES INGÉNIERIE ET ENVIRONNEMENT

THÈSE

présentée pour l'obtention du diplôme de

DOCTEUR DE

L'UNIVERSITÉ PARIS-EST

Spécialité : *Structures et Matériaux*

par

Bachar KABALAN

Sujet de la thése :

Dynamique des foules : modélisation du mouvement des piétons et forces associées engendrées

Soutenue le 12 Janvier 2016 devant le jury composé de :

Rapporteurs	Abdelilah HAKIM	Université Cadi Ayyad
	Jean-Mathieu MENCIK	Institut National des Sciences Appliquées Centre Val de Loire
Examinateurs	Patrice AKNIN	SNCF
	Gwendal CUMUNEL	École des Ponts ParisTech
	Stefano DAL PONT	Université Joseph Fourier
	Silvano ERLICHER	EGIS Industries
	Fabien LEURENT	Laboratoire Ville Mobilité Transport
Invité	Bruno SOULIER	ENS de Cachan
Directeur de Thèse	Pierre ARGOUL	École des Ponts ParisTech

To my mother Afaf, my father Ali,
To my country Lebanon

Acknowledgments

Accomplishing this dissertation would have been impossible if not for the incredible amount of help and support by many people in my life.

My adviser, Pierre Argoul, has been an amazing mentor. He has helped during and after my PhD. I learned a lot from him and appreciated all the advice he gave me on a personal and professional level. I very much enjoyed all the scientific discussions we had together not to mention the jokes and the laughs we shared.

I would also like to thank my supervisor, Gwendal Cumunel, for all the help that he gave me in order to finish my work rapidly and efficiently. I am grateful for his patience in helping me find the errors in my work and correcting them.

I would also like to extend my appreciation to the president of my thesis committee Professor Fabien Leurent and the reviewers who accepted to evaluate my thesis Professor Abdelilah Hakim and Jean-Mathieu Mencik.

I would like to show my gratitude to all my colleagues especially those with whom I have shared the office and who became dear friends. My deepest appreciation to all the friends I made in France during the past three years. I would particularly like to thank two of my closest friends Hassan Shukor and Mohammad Rammal for being there for me whenever I needed.

My deepest heartfelt appreciation goes to my family. Amal, Mahmoud and Leila all lived abroad and where examples for me on how to deal with the hardships of being away from home. To my parents Afaf and Ali to whom I owe everything I am grateful for. They have been the major motive for me to pursue this path and finish it successfully. It would take me several lifetimes to thank them for what they have done for me and my siblings.

Knowledge is better than wealth. Knowledge guards you while you have to guard wealth. Wealth decreases by spending while knowledge increases by spending, and the results of wealth die as wealth decay. With knowledge a man acquires obedience during his lifetime and a good name after his death. Knowledge is a ruler while wealth is ruled upon.

Ali ibn Abi Taleb

The noblest pleasure is the joy of understanding.

Leonardo Da Vinci

Résumé

Que ce soit dans une rue commerçante, un supermarché ou un aéroport, les phénomènes de foule sont incontournables et nous affectent au quotidien. Elles constituent un système complexe dont la dynamique collective, résultant des interactions individuelles, est difficile à appréhender et a toujours intrigué les scientifiques de différents domaines. Grâce au progrès technologique, il est aujourd'hui possible de modéliser les mouvements de foule et de les reproduire en simulation. Les simulations de mouvement de foule permettent aux chercheurs de plusieurs disciplines, comme les sciences sociales ou la biomécanique, de mieux étudier et comprendre les mouvements des piétons et leurs interactions. Quant aux sciences de la sécurité et du transport, ils y voient des applications concrètes comme le développement de modèles de foule capables de simuler l'évacuation d'un lieu public de moyenne ou de forte affluence, afin que les futures constructions ou aménagements publics puissent offrir une qualité de sécurité et de service optimale pour les usagers.

Dans le cadre de cette thèse, nous avons travaillé sur le perfectionnement du modèle discret proposé et développé par l'équipe dynamique du laboratoire Navier. Dans ce modèle, les actions et les décisions de chaque piéton sont traitées individuellement. Trois aspects du modèle ont été traités dans cette thèse.

Le premier concerne la navigation des piétons vers leurs destinations. Dans notre modèle, un piéton est représenté par une particule ayant une direction et une allure souhaitées. Cette direction est obtenue par la résolution d'une équation eikonale. La solution de cette équation permet d'obtenir un champ de vitesses qui attribue à chaque piéton, en fonction de sa position, une direction vers sa destination. La résolution de l'équation une fois ou à une période quelconque donne la stratégie du chemin le plus court ou le plus rapide respectivement. Les effets des deux stratégies sur la dynamique collective de la foule sont comparées.

Le deuxième consiste à gérer le comportement des piétons. Après avoir choisi son chemin, un piéton doit interagir avec l'environnement (obstacles, topologie, ...) et les autres piétons. Nous avons réussi à intégrer trois types de comportement dans notre modèle: (i) la poussée en utilisant une approche originale, basée sur la théorie des collisions des corps rigides dans un cadre thermodynamique rigoureux, (ii) le passage agressif (forcer son chemin) modélisé par une force sociale répulsive et (iii) l'évitement "normal" en adoptant une approche cognitive basée sur deux heuristiques. Les performances des trois méthodes ont été comparées pour plusieurs critères.

Le dernier aspect concerne la validation et la vérification du modèle. Nous avons réalisé une étude de sensibilité et validé le modèle qualitativement et quantitativement. À l'aide d'un plan d'expérience numérique nous avons réussi à identifier les paramètres d'entrée ayant les effets principaux sur les résultats du modèle. De plus, nous avons trouvé les différentes interactions entre ces paramètres. En ce qui concerne la validation qualitative, nous avons réussi à reproduire plusieurs phénomènes d'auto-organisation. Enfin, nous avons testé la capacité de notre modèle à reproduire des résultats expérimentaux issus de la littérature. Nous avons choisi le cas du goulot d'étranglement. Les résultats du modèle et ceux de l'expérience ont été comparés.

Ce modèle de foule a également été appliqué à l'acheminement des piétons dans la gare de Noisy-Champs. L'objectif de cette application est d'estimer le temps de stationnement des trains dans la gare.

Mots clés: Mouvement de foule, stratégie de déplacement, navigation, interactions piéton-piéton, validation et vérification, phénomènes d'auto-organisation.

Abstract

Crowds are present almost everywhere and affect several aspects of our lives. They are considered to be on of the most complex systems whose dynamics, resulting from individual interactions and giving rise to fascinating phenomena, is very difficult to understand and have always intrigued experts from various domains. The technological advancement, especially in computer performance, has allowed to model and simulate pedestrian movement. Research from different disciplines, such as social sciences and bio-mechanics, who are interested in studying crowd movement and pedestrian interactions were able to better examine and understand the dynamics of the crowd. Professionals from architects and transport planners to fire engineers and security advisors are also interested in crowd models that would help them to optimize the design and operation of a facility.

In this thesis, we have worked on the imporvement of a discrete crowd model developed by the researchers from the dynamics group in Navier laboratory. In this model, the actions and decisions taken by each individual are treated. In its previous version, the model was used to simulate urgent evacuations. Three main aspects of the model were addressed in this thesis.

The first one concerns pedestrian navigation towards a final destination. In our model, a pedestrian is represented by a disk having a willingness to head to a certain destination with a desired direction and a desired speed. A desired direction is attributed to each pedestrian, depending on his position from the exit, from a floor field that is obtained by solving the eikonal equation. Solving this equation a single time at the beginning of the simulation or several times at during the simulation allows us to obtain the shortest path or the fastest path strategy respectively. The influence of the two strategies on the collective dynamics of the crowds is compared.

The second one consists of managing pedestrian-pedestrian interactions. After having chosen his/her direction according to one of the available strategies, a pedestrian is bound to interact with other pedestrians present on the chosen path. We have integrated three pedestrian behaviors in our model: (i) pushing by using an original approach based on the theory of rigid body collisions in a rigorous thermodynamics context, (ii) forcing one's way by introducing a social repulsive force and (iii) "normal" avoidance by using a cognitive approach based on two heuristics. The three methods are compared for different criteria.

The last aspect is the validation and verification of the model. We have performed a sensibility study and validated the model qualitatively and quantitatively. Using a numerical experimental plan, we identified the input parameters that are the most statistically significant and estimated the effects of their interactions. Concerning qualitative validation, we showed that our model is able to reproduce several self-organization phenomena such as lane formation. Finally, our model was validated quantitatively for the case of a bottleneck. The experimental results are very close to the ones obtained from simulations.

The model was also applied to pedestrian movement in the Noisy-Champs train station. The objective of the study was to estimate the train dwell time. The simulation results were similar to the observations.

Keywords : Crowd movement, displacement strategies, navigation, pedestrian-pedestrian interactions, validation and verification, self-organization phenomena.

Contents

List of Figures

List of Tables

Notations

Table 1: Table of notations. Scalars are in normal font and vectors are in bold.

$q_i^x(t)$	abscissa of the position of a pedestrian
$q_i^y(t)$	ordinate of the position of a pedestrian
$\dot{\theta}_i(t)$	rotational velocity of a pedestrian
r_i	radius of a pedestrian
m_i	mass of a pedestrian
$u_{d,i}$	desired speed of a pedestrian
u^*	optimal speed according to a particular strategy
l_i^a	restoring torque
k_i	torsional stiffness
c_i	rotational damping
$h(\alpha)$	the distance before the first collision in the direction α
d_{max}	the range of the pedestrians' vision field
$\alpha_{i,0}$	the direction of the destination point
$\theta_i(t)$	orientation of a pedestrian about the $\mathbf{e}_z$-axis
τ_i	relaxation time
λ	reflects the anisotropic nature of the force
I_i	moment of inertia
A	maximum value of the magnitude of the social repulsion force
B	fall-off length of the social repulsion force
G	center of the disk representing a pedestrian
M	inertial matrix
N	number of pedestrians in a certain environment
N_c	number of contacts or collisions
$N_{subgroup}$	number of pedestrians who belong to a group
K_n	dissipation coefficient for the normal component of the dissipative percussion
K_{tg}	dissipation coefficient for the tangential component of the dissipative percussion
K_v	coefficient of viscous dissipation
T	velocity field
D	dynamic velocity field
S	static velocity field
V	wavefront velocity
J	flow for a given facility
J_s	specific flow for a given facility
Φ	pseudo-potential of dissipation
$\mathbf{u}_i(t)$	velocity vector of a pedestrian
$\mathbf{f}^a$	acceleration force
$\mathbf{f}^{soc}$	social repulsion force
$\mathbf{f}^{phys}$	physical contact force
$\mathbf{e}_{d,i}$	unit vector of the desired direction of a pedestrian

$\mathbf{u}_{d,i}$	desired velocity vector of a pedestrian
$\mathbf{f}^{ext}$	exterior force vector
$\mathbf{f}^{int}$	interior force vector
$\mathbf{p}^{int}$	interior percussions
$\mathbf{p}^{ext}$	exterior percussions
$\mathbf{e}_{ij}^{n}$	a unit vector pointing from pedestrian i to j
$\mathbf{q}_{[t,T)}$	trajectory of a pedestrian between instants t and T
$\mathbf{u}_{[t,T)}$	control path or the velocity on a certain trajectory between instants t and T
$\mathbf{u}^{*}$	optimal velocity according to a particular strategy
$\mathbf{e}^{*}$	optimal direction according to a particular strategy

Chapter 1

Introduction

Contents

1.1 Crowd Management-History

The history of crowd management is not very recent. In ancient Rome, the architects and builders of the Flavian Amphitheater, or Colosseum designed and built the biggest arena in the world at that time, capable of holding between 50,000 - 80,000 people not to mention the wild animals such as elephants and tall giraffes. They came up with an ingenious system of entrances, corridors, and staircases that allowed the crowds to enter, be seated and exit the Colosseum quickly, easily and efficiently. To solve the problem of crowd control, 80 separate entrance arches were made (see Fig. 1.1)so that the Colosseum could be cleared in less than 10 minutes [1]. These entrances lead to a corridor that spans uninterruptedly around the building leading to staircases and passages to the seats. However, the crowd management methods that were used gave very little importance for the well-being of the audience. Nowadays, crowd management has become a scientific study where crowd dynamics, crowd psychology, and staff training all contribute in ensuring the safety of crowds.

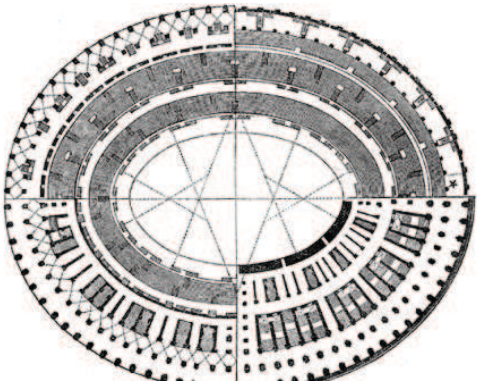

Figure 1.1: The architectural plan of the Flavian amphitheather or the colosseum [2].

In the scope of this work, we are interested in studying crowd dynamics. Crowd dynamics is about studying the formation and displacement of crowds for densities above one person per square meter. Since at high densities individual safety becomes at risk, understanding the dynamics of crowds, how pedestrians understand and interpret information, and how their behavior is affected by management systems is crucial and form the basis of the science of crowd dynamics [3]. A more commonly used term than the science of crowd dynamics is the "Crowd Science" which includes the science of crowd dynamics, psychology and behavior. The broad definition of this domain is Crowd Modeling, Monitoring and Management. Three topics aimed at developing crowd management plans with safer and more robust standards.

The objective of crowd modeling is to model how pedestrians behave and crowds form and move. Its use has become crucial since it is thought that the major contributing factor in crowd related disasters is the lack of understanding of crowd dynamics and crowd psychology [3]. For this reason, pedestrians have been the subject of several empirical studies since 4 decades now [4–6]. The obtained direct observations, photographs, and time-lapse films were used as the main evaluation methods. The main objective of these studies was to develop a level-of-service concept [7], design elements of pedestrian facilities [8–10], or planning guidelines [11]. With more complex architecture, large facilities and events, these studies have become insufficient to evaluate the evacuation of challenging situations. As a result, a number of simulation models were developed such as the queuing models [12], transition matrix models [13], stochastic models [14], and models for the route choice behavior of pedestrians [15].

However, these models failed to take into account the self-organization phenomena occurring in pedestrians crowds. The first model that was able to reproduce spatio-temporal patterns of motion was proposed by Henderson [16, 17] who used principles from the fluid-dynamic theory. While this approach could be partially confirmed, it is does not take into consideration certain particular interactions (i.e. avoidance and deceleration maneuvers) that does not obey momentum and energy conservation. The attention was then shifted to modeling individual pedestrian motion. Agent-based modeling is now the main focus of pedestrian research. The most well-known types of agent-based models are the force-based

models [18–21], cellular automata [22–25], and artificial intelligence-based models [26, 27].

1.2 What is a crowd?

The definitions of a crowd are still controversial. The term is sometimes used without a concrete definition. One of the definitions of a crowd is that it is a group of interacting individuals forming a social system. Crowds are not to be considered as homogeneous entities since they are made up of several individuals with different motives. According to empirical data gathered by scientists, crowds are more of a process (see Fig. 1.2)- they have a beginning, middle and end [28]. The cognitive and social processes involved in crowd movement allows us to describe it on different levels [29]:

- Physical/physiological
- Psychological
- social

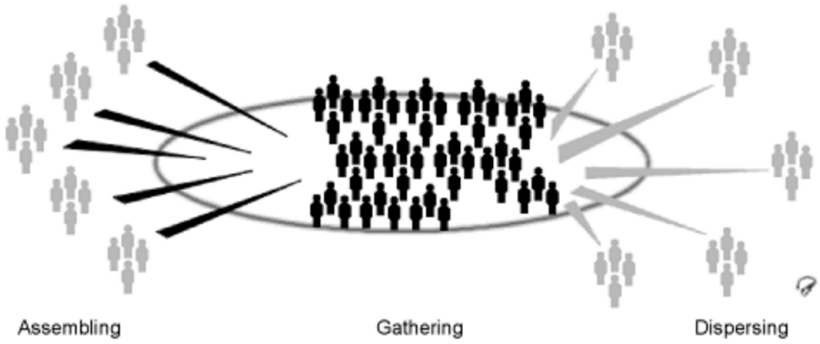

Figure 1.2: Crowd is a process of assembling, gathering and dispersing [30].

Pedestrian behavior is related to the psychological and social level. This behavior is not the same in groups as in crowds making it important to distinguish between the two. A group is formed by two or more individuals. A large group is called a mass. Only when this group occupy a single location and share a common focus, does it form a crowd (see Fig. 1.3).

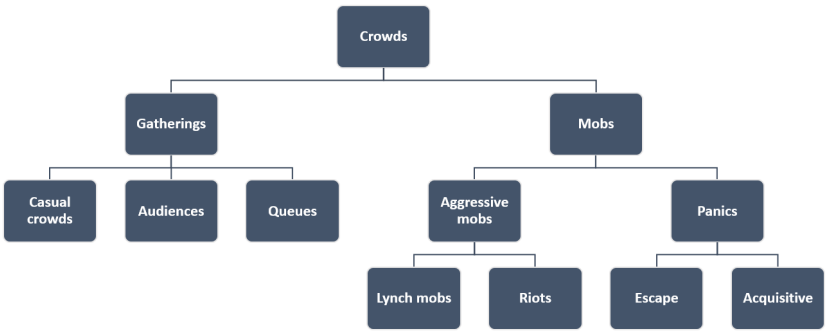

Figure 1.3: Classification of crowds [31]. Crowds are large groups that occupy a single location and share a common focus.

1.3 Why simulate crowd motion and evacuation processes?

Over the last decade, the field of pedestrian movement has received growing interest. This has been due to several reasons.

- Growing mobility: walking is inevitable. It is necessary for every other form of traveling (e.g., walking to the bus, car, train platform, airport terminal,...). In addition, it is probably one of the most time-intensive form of mobility [29]. Simulation can help increase the level of comfort for pedestrians and decrease the waiting times by assessing the design of facilities.
- Large facilities: more and more large facilities (e.g., shopping centers, theme parks, stadiums, ...) are being built destined to accommodate large crowds. This can result in densely packed crowds that create high pressure that poses a threat to people's health. Therefore, detailed planning of the walkways and crowd management are crucial to ensure a safe and comfortable environment for large crowds.
- Large events: large events such as rallies, marches, parades, or rock concerts usually attract a huge number of people. To manage crowds safely, a deep knowledge of the laws of crowd motion is necessary. Scientific research helps acquire the knowledge needed to channel flows, increase capacity by decreasing orientation problems or holding back people (creating waiting areas) to avoid peak flows in critical areas.
- Emergency evacuations: by using simulations, buildings or passenger vessels' (e.g., ships, airplanes) layouts can be improved and optimized so that they can be evacuated in a short time even under stress conditions.
- Safety requirements: new passenger vessels are being designed to carry more and more people. This is being accompanied with additional and more strict safety requirements.
- Collective motion: to increase our knowledge on crowd motion, it is important to understand the principles and mechanisms behind collective motion and self-organization phenomena such as shock waves, oscillation at bottlenecks, lane formation, etc.
- Crowd related disasters: the use of crowd modeling has become crucial since it is thought that the major contributing factor in crowd related disasters is the lack of understanding of crowd dynamics and crowd psychology [32]. Table 1.1 shows that the numerical analysis of flow rates, fill times and capacity are potentially the primary elements where improvements to crowd safety would have most impact [32]. While writing this dissertation, one of deadliest disasters in years to hit the Muslim Hajj in Saudi Arabia [33] happened where at least 717 people died and hundreds of others hurt in a stampede of pilgrims outside Mecca.

For all of the above reasons, it is necessary to study the laws of crowd motion and what influences it especially in urgent evacuations. Computer simulations seem to be the best tool to investigate crowd movement and assess evacuation processes. The potential areas of application are numerous: buildings, urban systems like pedestrian crossings, buses, trains, aircrafts, ships, shopping malls, theme parks, railway and subway stations airports, etc.

The outline of this thesis is divided into 8 chapters. In the second chapter, an extended abstract of all the thesis is done in french. The accomplished work and the obtained results in this PhD thesis are briefly presented. In the third chapter, an overview of crowd modeling is given. The two main approaches to modeling pedestrian movement are explained followed by a survey on the three main types of models that exist in literature. Our discrete model is then introduced and positioned with respect to other works. The new modifications that have been done to the model are demonstrated.

The fourth chapter is dedicated to pedestrian navigation and route choice. The first part of the chapter assesses the different types of classification of pedestrian navigation levels and the existing route choice models. In the second part, the different displacement strategies that have been developed in our model are demonstrated. Their influences on the overall crowd dynamics are compared.

In the fifth chapter, pedestrian-pedestrian interactions are addressed. The effect and the importance of pedestrian interactions at the microscopic level on the overall crowd dynamics on the macroscopic level

Table 1.1: Incidents related to crowd events [32].

Year	Casualties	Cause	Place
1989	96 dead, 400 injured (too many people)	**Design (throughput)**	Hillsborough, UK
1990	1426 pilgrims crushed (too many people)	**Design (throughput)**	Mina Valley, Saudi Arabia
1994	266 pilgrims crushed, 98 injured (too many people)	**Design (throughput)**	Jamarat, Saudi Arabia
1996	83 crushed, 180 injured (too many people)	Information (Forged Tickets)	Guatemala City
1997	22 pilgrims crushed, 43 injured (too many people)	**Design (throughput)**	Jamarat, Saudi Arabia
1998	118 pilgrims crushed, 434 injured (too many people)	**Design (throughput)**	Jamarat, Saudi Arabia
1999	51 killed, 150 injured in stampede (reaction)	Information (Weather)	Kerala, India
1999	53 killed, 190 injured in stampede (reaction)	Information (Weather)	Minsk, Belarus
2001	35 pilgrims crushed, 179 injured (too many people)	**Design (throughput)**	Jamarat, Saudi Arabia
2001	4 dead, including 3 children (reaction)	Information (Handouts - crazing)	Aracaju, Brazil
2002	10 trampled, Mall crowd craze (reaction)	Information (Handouts - crazing)	Yakohama, Hapan
2004	249 pilgrims crushed, 252 injured (too many people)	**Design (throughput)**	Jamarat, Saudi Arabia
2004	37 dead , 15 injured in crowd crush (too many people)	**Design (throughput)**	Beijing, China
2006	363 dead, 389 injured in crowd crush (reaction)	**Design (throughput)**	Jamarat, Saudi Arabia
2006	74 dead, 300 injured in crowd crush (reaction)	**Design (throughput)**	Manila, Philippines
2006	51 dead, 238 injured in crowd crush (reaction)	Information (political rally)	Yemen, Middle East
2008	146 dead, 50 injured in stampede (narrow road)	**Design (throughput)**	Himachal Pradesh, India
2008	23 dead, dozens injured in Ramadan (reaction)	Information (handouts)	Pasuran, Java
2008	1 dead, 4 injured - store sales (reaction)	Information (Black Friday sales)	Wal-Mart, New York, USA
2009	22 dead, 132 injured - football (reaction)	**Design (throughput)**	Abidjan, Ivory Coast
2009	60 injured, 4 hospitalized (JLS) (reaction)	**Design (capacity)**	Birmingham (JLS), UK
2010	26 dead, 55 injured (too many people)	**Design (Throughput)**	Timbuktu, Mali, West Africa
2010	63 dead, 44 injured (too many people - narrow road)	**Design (throughput)**	Kunda, North India
2010	10 police officers injured (reaction) (too many people)	**Design (capacity+crazing)**	
2010	60 injured (reaction)	Information (screamer)	Amesterdam, The Netherlands
2010	14 injured (too many people at entry gates)	Information (forged tickets)	Johannesburg, South Africa
2010	Over 100 injured (reaction)	**Design (choice of barriers)**	EDC - Los Angeles, USA
2010	21 dead, 511 injured (too many peopl)	**Design (throughput)**	Duisburg, Germany
2010	10 dead, dozens injured (reaction)	Information (over reaction)	Bihar, India
2010	7 dead, 70 injured (reaction)	Information (rain stopped)	Nairobi, Kenya
2010	347 dead, 395 injured (too many people)	**Design (capacity)**	Phnom Penh, Cambodia
2011	102 dead, 44 injured (too many people)	**Design (capacity)**	Kerala, India
2011	11 dead, 29 injured (reaction)	Information (shots fired)	Port Harcourt, Nigeria
2011	36 dead, 70 injured (too many people)	**Design (capacity)**	Bamako, Mali
2011	7 dead, 30 injured (too many people)	**Design (capacity)**	Brazzaville, Congo
2011	2 dead, 13 injured (too many people)	Information (poor ticket allocation)	Jakarta, Indonesia
2012	1 dead, 13 injured (too many people)	**Design (throughput)**	Johannesburg, South Africa
2012	74 dead, over 1000 injured (too many people + rioting)	**Design (throughput) + riot**	Port Said, Egypt
2012	3 dead, dozens injured (too many people)	**Design (throughput)**	Cairo (copic), Egypt
2013	62 dead, dozens injured (too many people)	**Design (capacity + crazing)**	Abidjan, Ivory Coast

is first explained through the concept of self-organization phenomena. The types of pedestrian behaviors and interactions that were integrated into our model are shown. The methods that we used to model these behaviors are then compared using several criteria.

The sixth chapter concerns the validation and verification (V&V) of pedestrian models. First, a bibliographical study on the different V&V methods available in literature is carried out. Then, an experimental design is used in order to identify the input parameters of our model that significantly influence the flow values for the case of a bottleneck. Finally, for the same previous case, the capacity of our model to reproduce experimental results is examined.

The seventh chapter is dedicated to a study on modeling pedestrian flows in the Noisy-Champs train station in île-de-France. In the first place, the methods that were used to obtain the geometrical, train, and pedestrian data is shown. These data were then used to create a simulation scenario and to model pedestrian movement in the aforementioned train station. The obtained results are then compared to observations.

In the last chapter, the hybrid version of the Van der Pol self-sustained oscillator that is developed to model the lateral walking force of a pedestrian on a rigid floor is further validated by processing the experimental data of 31 pedestrians walking on a treadmill. In addition, the obtained results of the male and female participants are compared to identify the differences.

Bibliography

[1] K. Fernando, "Roman colosseum-A grand monument to raw pleasure?," *Ceylontoday*, 2014.

[2] "Tickets to the Colosseum." http://www.tribunesandtriumphs.org/colosseum/tickets-to-the-colosseum.htm.

[3] G. K. Still, *Crowd dynamics*. PhD thesis, University of Warwick, 2000.

[4] B. D. Hankin and R. A. Wright, "Passenger flow in subways," *OR*, vol. 9, pp. 81–88, June 1958.

[5] S. Older, "Movement of pedestrians on footways in shopping streets," *Traffic Engineering and Control*, vol. 10, pp. 160–163, 1968.

[6] U. Weidmann, "Transporttechnik der fußgänger," report Schriftenreihe Ivt- Berichte 90, ETH Zürich, 1993.

[7] J. J. Fruin, "Designing for pedestrians: a level of service concept," in *Highway research record*, 1971.

[8] J. Pauls, "The movement of people in buildings and design solutions for means of egress," *Fire Technology*, vol. 20, pp. 27–47, Feb. 1984.

[9] D. Helbing, *Verkehrsdynamik*. Berlin, Heidelberg: Springer Berlin Heidelberg, 1997.

[10] D. Helbing, L. Buzna, A. Johansson, and T. Werner, "Self-organized pedestrian crowd dynamics: experiments, simulations, and design solutions," *Transportation Science*, vol. 39, pp. 1–24, Feb. 2005.

[11] *Highway capacity manual*. Washington, D.C.: Transportation Research Board, lslf sub ed., Dec. 1994.

[12] S. J. Y. Jr and J. M. Smith, "Modeling circulation systems in buildings using state dependent queueing models," *Queueing Systems*, vol. 4, pp. 319–338, Dec. 1989.

[13] D. Garbrecht, "Describing pedestrian and car trips by transition matrices," *Traffic Quarterly*, vol. 27, no. 1, 1973.

[14] N. Ashford, M. O'LEARY, and P. D. McGinity, "Stochastic modelling of passenger and baggage flows through an airport terminal," *Traffic Engineering & Control*, vol. 17, no. 5, 1976.

[15] A. Borgers and H. J. P. Timmermans, "City centre entry points, store location patterns and pedestrian route choice behaviour: A microlevel simulation model," *Socio-Economic Planning Sciences*, vol. 20, no. 1, pp. 25–31, 1986.

[16] L. Henderson, "The statistics of crowd fluids," vol. Nature,229, pp. 381–383, 1971.

[17] L. F. Henderson, "On the fluid mechanics of human crowd motion," *Transportation Research*, vol. 8, pp. 509–515, Dec. 1974.

[18] M. Chraibi, A. Seyfried, and A. Schadschneider, "Generalized centrifugal-force model for pedestrian dynamics," *Physical Review E*, vol. 82, no. 4, p. 046111, 2010.

[19] D. Helbing and P. Molnàr, "Social force model for pedestrian dynamics," *Physical Review E*, vol. 51, pp. 4282–4286, May 1995.

[20] R. Löhner, "On the modeling of pedestrian motion," *Applied Mathematical Modelling*, vol. 34, pp. 366–382, Feb. 2010.

[21] W. J. Yu, R. Chen, L. Y. Dong, and S. Q. Dai, "Centrifugal force model for pedestrian dynamics," *Physical Review E*, vol. 72, p. 026112, Aug. 2005.

[22] A. Kirchner and A. Schadschneider, "Simulation of evacuation processes using a bionics-inspired cellular automaton model for pedestrian dynamics," *Physica A: Statistical Mechanics and its Applications*, vol. 312, pp. 260–276, Sept. 2002.

[23] M. Fukui and Y. Ishibashi, "Jamming transition in cellular automaton models for pedestrians on passageway," *Journal of the Physical Society of Japan*, vol. 68, no. 11, pp. 3738–3739, 1999.

[24] V. Blue and J. Adler, "Emergent fundamental pedestrian flows from cellular automata microsimulation," *Transportation Research Record: Journal of the Transportation Research Board*, vol. 1644, pp. 29–36, Jan. 1998.

[25] C. Burstedde, K. Klauck, A. Schadschneider, and J. Zittartz, "Simulation of pedestrian dynamics using a two-dimensional cellular automaton," *Physica A: Statistical Mechanics and its Applications*, vol. 295, no. 3, pp. 507–525, 2001.

[26] S. Gopal and T. R. Smith, "Human way-finding in an urban environment: a performance analysis of a computational process model," *Environment and Planning A*, vol. 22, no. 2, pp. 169 – 191, 1990.

[27] C. W. Reynolds, "Evolution of corridor following behavior in a noisy world," *From animals to animats*, vol. 3, pp. 402–410, 1994.

[28] J. M. Kenny, C. McPhail, P. Waddington, S. Heal, S. Ijames, D. N. Farrer, J. Taylor, and D. Odenthal, "Crowd behavior, crowd control, and the use of non-lethal weapons," tech. rep., DTIC Document, 2001.

[29] H. L. Klüepfel, *A cellular automaton model for crowd movement and egress simulation*. PhD thesis, Universität Duisburg-Essen, Fakultät für Physik, 2003.

[30] A. Hunsicker, *Behind the Shield: Anti-Riot Operations Guide*. Universal-Publishers, 2011.

[31] D. Forsyth, *Group Dynamics 3rd*. Wadsworth, Belmont, CA, 1998.

[32] "PhD - Crowd cynamics | Prof. Dr. G. Keith Still," 1990.

[33] A. A. O. i. Hofuf, S. Arabia, S. D. i. Amman, and Jordan, "More Than 700 People Killed in Mecca Stampede," *Wall Street Journal*, Sept. 2015.

Chapter 2

Resumé étendu

Contents

2.1 Introduction

Ces dernières années, des mouvements de panique ont provoqué de nombreux morts, écrasés dans des bousculades, lors d'évènements de masse toujours plus fréquents et importants. Deux exemples marquants de l'année 2010 sont le mouvement de panique en marge de la Love Parade de Duisbourg (Allemagne), ayant coûté la vie à 20 personnes et fait environ 340 blessés, et celui sur un pont de Phnom Penh (Cambodge) ayant fait au moins 375 morts et 755 blessés, le dernier jour de la fête de l'eau. Ces drames ont des causes variées, mais tous font naître chez les piétons un sentiment d'insécurité qui les amène à vouloir évacuer très rapidement les lieux. Pour atténuer l'ampleur de telles catastrophes, des études du comportement des piétons en situation d'évacuation et des théories capables de prédire la dynamique des foules sont réalisées. La modélisation du mouvement de la foule, pour simuler des situations d'évacuation, devient un outil intéressant pour améliorer la qualité de service des bâtiments et lieux publics, et reste encore un sujet ouvert.

L'objectif de cette thèse est d'améliorer un modele de piétons développé au laboratoire Navier depuis 2008. Nous présentons les travaux réalisés sur les stratégies de déplacement, les interactions piéton-piéton et la validation et la vérification du modèle. Dans ce chapitre, nous présentons un résumé étendu de la thèse en français. Le reste du manuscrit est rédigé en anglais.

2.2 Etude bibliographique

Dans cette section, nous présentons une étude bibliographique concernant la modélisation des mouvements de foule. Ainsi, les différents modèles de mouvement de foule existants sont présentés ci-après.

2.2.1 Etat de l'art des modèles de mouvement de foule

Par définition, une foule est une multitude de personnes regroupées en un même lieu. Face à la complexité du comportement de l'homme, de nombreux modèles de simulation ont été proposés ces dernières années, afin de reproduire un comportement ou une situation précise. Les premières études menées pour décrire le comportement des piétons durant la marche étaient des observations afin de recueillir des informations qualitatives (i.e. la détermination des préférences des piétons) et quantitatives (i.e. la vitesse de marche des piétons) sur la foule. Ces observations ont permis de lister certaines caractéristiques dans le comportement des piétons et de visualiser des phénomènes d'auto-organisation de la foule. Elles ont inspiré par la suite les chercheurs qui ont proposé des modèles de foule afin de les simuler efficacement. Les premiers modèles caractérisant le comportement des piétons ont été des modèles statistiques [1, 2]. Ils ont permis de définir les valeurs de densités et de débits observables, et ainsi de trouver les vitesses moyennes de déplacement des piétons. Les premiers modèles informatiques simulant les mouvements de foule sont les modèles de simulation macroscopique [1–4]. Les comportements simulés restent simples car les piétons sont représentés dans leur ensemble. Pour prendre en compte des comportements de piétons plus complexes, les modèles de mouvement de foule microscopiques ont été développés [5–8]. Chaque piéton a son propre comportement, prend ses propres décisions et réagit individuellement aux modifications de son environnement.

Les modèles de mouvement de foule ont été développés afin de reproduire dans l'idéal tous les comportements des piétons ainsi que les phénomènes de foule observés. Évidemment, la complexité des comportements et phénomènes observés font que chaque modèle cible une ou des applications spécifiques.

Parmi les modèles qui se focalisent sur le déplacement à court terme du piéton et de ses interactions avec les individus qu'il croise sur son chemin, les différentes approches existantes peuvent être classées selon différents critères. Tout d'abord, il est possible de distinguer les modèles de type microscopique et ceux de type macroscopique. Dans les premiers, le mouvement de chaque individu est représenté dans le temps et l'espace. Chaque individu a son propre comportement, ses propres décisions et interagit avec les autres. Au contraire, les modèles macroscopiques sont complémentaires des modèles microscopiques et consistent à formaliser la dynamique globale du système sans se référer directement aux comportements des individus. Cette approche suppose que les piétons sont soumis à des lois d'écoulement.

Un second élément de classification concerne la représentation continue ou discrète de l'environnement dans lequel évolue les piétons. Les variables décrivant l'état de la simulation, notamment le temps,

l'espace ou les états internes des piétons (vitesse de déplacement par exemple), peuvent être représentées de manière discrète ou continue. Dans la représentation continue, la localisation d'un individu est décrite par des coordonnées réelles et le piéton peut se trouver à n'importe quelle position de l'environnement. Dans le cas d'un modèle discret, il existe un nombre fini de positions que peuvent occuper les piétons car l'environnement est divisé en un certain nombre de cellules.

Enfin, il est possible de différencier les modèles déterministes et les modèles stochastiques. Dans le premier cas, la dynamique du déplacement des piétons est déterministe et le résultat des actions de cheminement des piétons est entièrement déterminé par l'état courant du système. Dans le deuxième cas, le comportement des piétons est soumis à des lois stochastiques, une même action pouvant entraîner des résultats différents pour des situations de départ identiques.

Dans les sections suivantes, sans chercher à être exhaustif, nous détaillons quelques modèles de déplacement: les modèles macroscopiques basés sur des analogies avec la dynamique des fluides ; les automates cellulaires qui sont les premiers représentants des modèles discrets ; et enfin les modèles basés sur une combinaison de forces autour de la description détaillée du modèle des forces sociales.

2.2.2 Modèles de dynamique des fluides ou des gaz

Pour illustrer les modèles de dynamique des fluides ou des gaz [3, 4, 9–11], on peut prendre l'exemple du modèle de foule de Bodgi [4] dans lequel les piétons sont représentés dans leur ensemble par un fluide compressible. Cette approche est utilisée pour la modélisation du traffic routier. On s'intéresse au comportement de la foule en un point donné et les variables utilisées sont des variables locales qui dépendent du temps t et de l'espace x (par exemple $x \in [0; L]$ si l'on considère la position longitudinale des piétons sur une passerelle de longueur L). Ainsi le comportement de la foule est assimilé à celui d'un liquide compressible gouverné par l'équation de conservation de la masse, où η représente la densité locale des piétons et v leur vitesse locale :

$$\frac{\partial \eta}{\partial t} + \frac{\partial}{\partial x}(\eta, v) = 0 \tag{2.1}$$

Ayant deux variables, une deuxième équation sera nécessaire pour compléter le système. Elle est généralement connue sous le nom d'équation de fermeture et met en relation les variables η et v. D'autres modèles fondés sur la dynamique des fluides ou des gaz sont présentés dans [12].

2.2.3 Modèles d'automates cellulaires

Les modèles d'automates cellulaires sont des modèles où la zone de déplacement 2D des piétons est discrétisée [8, 13–15]. Une grille uniforme de cellules comporte des cellules inaccessibles pour représenter les obstacles, des cellules occupées par les piétons et des cellules vides (Fig. 2.1). A chaque pas de temps, les piétons se déplacent de cellule en cellule voisine selon certaines règles. Il y a deux façons de déplacer les piétons à chaque pas de temps. Soit les piétons se déplacent chacun à leur tour (individu par individu) de manière aléatoire. La gestion du contact se fait alors de manière intrinsèque, le piéton ne peut pas se déplacer dans une cellule occupée. Soit la mise à jour de la position des piétons est simultanée et le hasard est utilisé si deux piétons veulent se déplacer dans la même cellule. Le principal avantage de ce type de modèles est la réalisation de simulations dans des espaces vastes avec beaucoup de piétons car les temps de calcul des simulations sont intéressants. L'inconvénient majeur est le manque de réalisme car le mouvement des piétons est restreint par la grille et les contacts ne sont pas gérés directement.

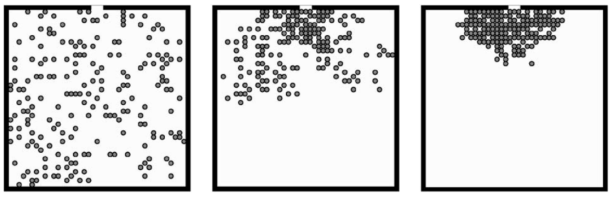

Figure 2.1: Exemple d'une simulation d'évacuation de salle réalisée avec un modèle d'automate cellulaire [13].

2.2.4 Modèles de forces sociales

Le modèle de forces sociales [6, 16–19], développé principalement par Helbing, est un modèle qui permet de gérer le mouvement de chaque piéton, représenté par un disque, par l'utilisation de trois forces: une force d'accélération, une force de répulsion et une force d'attraction (facultative) (Fig. 2.2). La force motrice d'accélération permet au piéton de se déplacer vers sa destination souhaitée. Elle est dirigée à chaque instant vers cette destination.

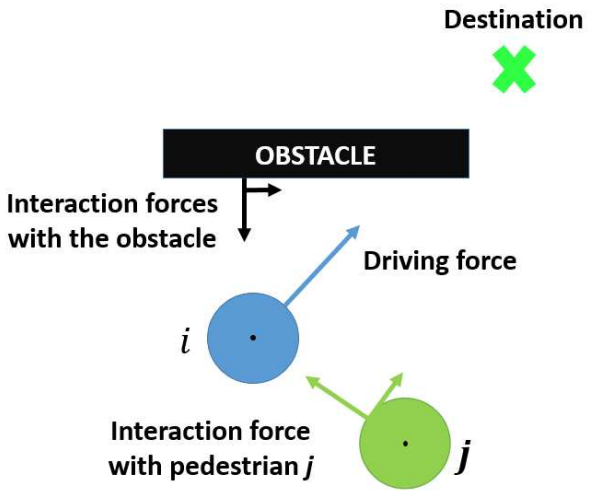

Figure 2.2: Les forces agissant sur le piéton i.

La force de répulsion est inspirée d'une approche utilisée pour les milieux granulaires [20]. Chaque piéton possède sa propre masse et a une certaine direction et allure qu'il adapte en fonction de l'environnement qui l'entoure (piétons et obstacles). Il peut se déplacer continûment dans un environnement 2D car il n'y a pas de discrétisation spatiale de l'environnement. Ce modèle est principalement utilisé pour simuler des situations d'évacuation. Le principal avantage de ce modèle est sa faible complexité. Son inconvénient majeur est qu'il n'est pas adapté pour les foules trop denses car les piétons oscillent sur place de part l'utilisation de la force de répulsion à distance [21].

Après un aperçu général et succinct de l'état de l'art des modèles de mouvement de foule, nous présentons dans la section suivante notre modèle 2D discret.

2.3 Modèle discret

Un modèle de foule discret est developpé depuis 2008 au sein de l'Equipe Dynamique des Structures et Identification du Laboratoire Navier dans lequel les actions et les décisions de chaque piéton sont traitées individuellement. Afin de gérer les contacts piéton-piéton et piéton-obstacle, nous avons adopté une approche originale fondée sur la théorie des collisions des corps rigides proposée par Frémond [105, 106], dans un cadre thermodynamique rigoureux, et inspirée des travaux de Moreau [126]. Ensuite, une "volonté" a été ajoutée pour chaque piéton afin d'adapter le modèle aux mouvements de piétons [22–25]. Dans cette section, nous présentons brièvement le modèle discret et les travaux qui ont été effectués durant cette thèse sur la rotation des piétons.

Nous considérons un système constitué de N particules se déplaçant dans le plan. Chaque particule est représentée par un disque dont le centre est G_i. Les vecteurs et les matrices sont en gras. Pour une particule i, nous notons:

- m_i: la masse

- I_i: le moment d'inertie autour de l'axe vertical
- r_i: le rayon
- $\mathbf{q}_i(t) = (q_i^x(t), q_i^y(t), \theta_i(t)) \in \mathbb{R}^3$: la position de G_i
- $\mathbf{v}_i(t) = (\mathbf{u}_i(t), \dot{\theta}_i(t)) = (u_i^x(t), u_i^y(t), \dot{\theta}_i(t))$: la vitesse de G_i.

où $\theta_i(t) \in [-\pi, \pi]$ est la rotation de la particule i autour de l'axe $\mathbf{e}_z$ et $\dot{\theta}_i(t) = d\theta_i/dt$ sa vitesse angulaire. La description du comportement d'un ensemble de corps discrets est fondée sur la considération que le système global est déformable même si les particules sont rigides. Considérons ainsi l'ensemble des N particules comme un système déformable composé de solides rigides. La vitesse de déformation locale (vitesse relative) entre les $i^{ème}$et $j^{ème}$ particules en contact au point C est définie par:

$$\mathbf{\Delta}_{ij}(\mathbf{v}) = \mathbf{u}_i + \dot{\theta}_i \mathbf{e}_z \times \mathbf{G}_i\mathbf{C} - (\mathbf{u}_j + \dot{\theta}_j \mathbf{e}_z \times \mathbf{G}_j\mathbf{C}) \tag{2.2}$$

où ${}^t\mathbf{v} = ({}^t\mathbf{v}_i, {}^t\mathbf{v}_j)$ est le vecteur vitesse de toutes les particules qui évoluent dans le système. Une autre expression de la vitesse de déformation permet de modéliser un cas particulier des groupes: les piétons qui se tiennent par la main. La méthode proposée utilise la notion de vitesse de déformation à distance pour décrire la cohésion d'un groupe au lieu d'utiliser des forces [26, 27]. Inspirée par des travaux de Caselli and Frémond [28], la notion d'interaction à distance entre des particules rigides a été introduite dans notre modèle afin de modéliser la dynamique d'un sous-groupe par une déformation continue du système composé des particules liées entre elles (les membres du sous-groupe). Cette vitesse de déformation à distance est une quantité scalaire definie par la derivée, par rapport au temps, de la distance au carré entre les épaules de deux piétons, i.e. les points C_i et C_j pour les piétons i et j (Fig. 2.3). Pour deux piétons, la vitesse de déformation à distance est définie par:

$$\Delta^*_{ij}(\mathbf{v}) = 2\Big(\mathbf{u}_i + \dot{\theta}_i \mathbf{e}_z \times \mathbf{G}_i\mathbf{C}_i - \big(\mathbf{u}_j + \dot{\theta}_j \mathbf{e}_z \times \mathbf{G}_j\mathbf{C}_j\big)\Big) \cdot \mathbf{C}_j\mathbf{C}_i \tag{2.3}$$

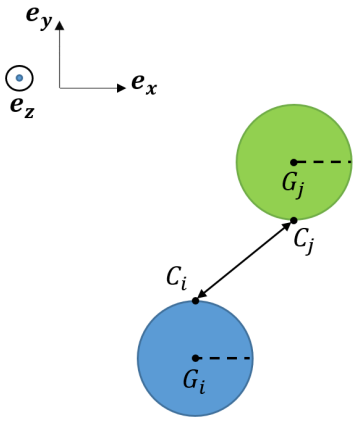

Figure 2.3: Deux piétons en groupe àl'aide d'un lien existant entre eux.

La description de l'évolution du système multi-particules doit être réalisée aussi bien pendant l'évolution régulière que pendant l'évolution non-régulière des particules, à savoir à l'instant d'une collision. La discontinuité de la vitesse des particules à l'instant de la collision ne permet pas de résoudre l'équation régulière du mouvement car la vitesse n'est pas différentiable. Le système 2.2 est alors réécrit dans le cadre de cette approche :

$$\begin{cases} \mathbf{M}\,\dot{\mathbf{v}} = -\mathbf{f}^{int} + \mathbf{f}^{ext} & \text{presque partout} \quad (2.4) \\ \mathbf{M}\,(\mathbf{v}^+ - \mathbf{v}^-) = -\mathbf{p}^{int} + \mathbf{p}^{ext} & \text{partout} \quad (2.5) \end{cases}$$

où $\mathbf{M}$ est la matrice d'inertie des particules de dimension $3N \times 3N$ (Eq. (2.6)); $\mathbf{f}^{ext}$ (resp. $\mathbf{f}^{int}$) est le vecteur des forces extérieures (resp. forces intérieures) appliquées au système de dimension $3N$ et $\mathbf{v}^+$ et $\mathbf{v}^-$ sont les vitesses des particules après et avant contact respectivement.

$$\mathbf{M} = \begin{pmatrix} \ddots & 0 & \dots & \dots & 0 \\ 0 & m_i & \ddots & & \vdots \\ \vdots & \ddots & m_i & \ddots & \vdots \\ \vdots & & \ddots & I_i & 0 \\ 0 & \dots & & 0 & \ddots \end{pmatrix} \tag{2.6}$$

Une solution à ce système (Eqs. (2.4) et (2.5)) existe [29–31]. La première équation du système (Eq. (2.4)), qui décrit l'évolution régulière du système multi-particules, est appliquée presque partout, excepté à l'instant de la collision où elle est remplacée par la seconde. Quand un contact est détecté, les vitesses des particules en collision sont discontinues et nous introduisons alors dans la seconde équation du système (Eq. (2.5)) des percussions intérieures, $\mathbf{p}^{int}$, et des percussions extérieures, $\mathbf{p}^{ext}$, au système. Les deux premières composantes de ces percussions ont la dimension d'une quantité de mouvement ($kg.m.s^{-1}$) et la dernière celle d'un moment angulaire ($kg.m^2.s^{-1}$). Les percussions intérieures, $\mathbf{p}^{int}$, sont des inconnues du problème. Frémond a montré dans [28, 31, 32] que ces percussions intérieures sont définies en dualité avec la vitesse de déformation à l'instant du choc, $\mathcal{D}(\frac{\mathbf{v}^+ + \mathbf{v}^-}{2})$ (où $\mathcal{D}(\mathbf{v}) = (\mathbf{\Delta}(\mathbf{v}), \mathbf{\Delta}^*(\mathbf{v}))$), au sens du travail des efforts intérieurs. Il utilise la notion de pseudo-potentiel de dissipation $\Phi = \Phi(\mathcal{D})$, qui est une fonction positive, convexe et nulle à l'origine [33], pour définir les percussions intérieures:

$$\mathbf{p}^{int} \in \partial\Phi\left(\mathcal{D}\left(\frac{\mathbf{v}^+ + \mathbf{v}^-}{2}\right)\right) \tag{2.7}$$

où l'opérateur ∂ est le sous différentiel qui généralise la dérivée pour les fonctions convexes [31]. La fonction convexe Φ est définie par la somme de deux pseudo-potentiels [33]:

$$\Phi = \Phi^d + \Phi^r \tag{2.8}$$

où Φ^d est le pseudo-potentiel de dissipation qui permet de définir les percussions intérieures dissipatives et Φ^r celui qui permet de définir les percussions intérieures réactives.

Dans l'Eq. (2.5), pour déterminer $\mathbf{v}^+$, il faut résoudre le problème de minimisation sous contraintes suivant:

$$\mathbf{X} = \arg\min_{\mathbf{Y}\in\mathbb{R}^{3N_c}} \left[{}^t\mathbf{Y}\,\mathbf{M}\,\mathbf{Y} + \Phi\big(\mathcal{D}(\mathbf{Y})\big) - {}^t\left(2\mathbf{v}^- + \mathbf{M}^{-1}\mathbf{p}^{ext}\right)\mathbf{M}\,\mathbf{Y}\right] \tag{2.9}$$

où $\mathbf{Y} = \frac{\mathbf{v}^+ + \mathbf{v}^-}{2}$ et N_c le nombre de piétons en contact. La solution est donnée par $\mathbf{X} = \frac{\mathbf{v}^+ + \mathbf{v}^-}{2}$ [31]. Une démonstration de l'existence et de l'unicité des vitesses après la collision simultanée de plusieurs solides rigides, ainsi que de la dissipativité de la collision, est faite dans [30–32].

2.3.1 Loi de comportement

Pour contrôler le comportement après contact de particules en collisions, une loi de comportement doit être établie pour définir le pseudo-potentiel de dissipation [29, 31]. Ce pseudo-potentiel, Φ^d, permet de choisir le type de collision: parfaitement inélastique, inélastique ou élastique. Pendant la collision, les percussions intérieures ont des composantes normale et tangentielle. Il existe plusieurs choix pour Φ^d qui permettent d'obtenir une large variété de comportements après contact [29, 31]. Pour le cas des piétons, nous avons choisi la même loi de comportement pour exprimer les deux composantes. Ainsi, pour déterminer la percussion intérieure normale, nous avons choisi un pseudo-potentiel quadratique qui permet de retrouver les résultats classiques du coefficient de restitution de Newton [29]:

$$\begin{aligned} \Phi^d\big(\mathcal{D}(\mathbf{v})\big) = \ & \tfrac{1}{2} \sum_{1\le i\le j\le N} \left[K_n \Big({}^t\mathbf{\Delta}_{ij}(\mathbf{v}) \cdot \mathbf{e}_{ij}^n \Big)^2 + K_{tg} \Big({}^t\mathbf{\Delta}_{ij}(\mathbf{v}) \cdot \mathbf{e}_{ij}^{tg} \Big)^2 \right] \\ + & \sum_{1\le i\le j\le N_{subgroup}} \frac{1}{2} K_v \Big(\Delta_{ij}^*(\mathbf{v}) \Big)^2 \end{aligned} \tag{2.10}$$

où $\mathbf{e}_{ij}^{tg} = \mathbf{e}_z \times \mathbf{e}_{ij}^{n}$ et $N_{subgroup}$ est le nombre de membres des groupes. La composante normale de la percussion du coefficient de dissipation de la percussion, K_n (kg), reflète la nature inélastique des collisions entre les particules. Une valeur infinie de K_n donne une collision parfaitement élastique. La composante tangentielle, K_{tg} (kg), peut être associée aux effets de type visqueux. K_v ($kg.m^{-2}$) est le coefficient de dissipation visqueuse. Il contrôle la rigidité du lien entre les membres de groupe.

2.3.2 Volonté de déplacement d'un piéton

Dans notre modèle, un piéton est représenté par une particule ayant une direction et une allure souhaitées. Une vitesse souhaitée, actualisée à chaque instant, donne une volonté au piéton et une force permet d'introduire cette vitesse souhaitée dans le modèle de mouvement de particules [22–24].

L'idée est d'introduire, dans le modèle de mouvement de particule, une force $\mathbf{f}_i^a$ qui permet de donner une vitesse souhaitée aux piétons à chaque instant. Il s'agit de la force d'accélération intérieure introduite par Helbing [19]. Cette force ajoutée est une des composantes de la force intérieure $\mathbf{f}_i^{int}$ présente dans l'Eq. (2.5). Nous avons choisi d'utiliser cette force car elle décrit un comportement réaliste en utilisant peu de paramètres. $\mathbf{f}_i^a$ est la force motrice des piétons nécessaire pour donner la trajectoire et l'allure désirées de chaque piéton. Elle a pour expression:

$$\mathbf{f}_i^a = m_i \frac{\mathbf{u}_i - \parallel \mathbf{u}_{d,i} \parallel \mathbf{e}_{d,i}}{\tau_i} \tag{2.11}$$

où $\mathbf{u}_i$ (en $m.s^{-1}$) est la vitesse réelle du piéton i, $\mathbf{e}_{d,i}$ la direction désirée, $\mathbf{u}_{d,i}$ la vitesse désirée et τ_i (s) un temps de relaxation permettant au piéton i de retrouver la vitesse désirée après un contact ou un changement soudain de direction pendant son mouvement.
Plus la valeur de τ_i est petite, plus le piéton est "agressif" et retrouve rapidement sa vitesse souhaitée, lorsqu'elle est différente de sa vitesse réelle. Helbing a choisi $\tau_i = 0.5\,s$. Un exemple est illustré sur la Fig. 2.4. Les trajectoires de deux piétons identiques i et j se déplaçant dans des directions opposées, après une collision et en fonction de différentes valeurs de τ, sont représentées.

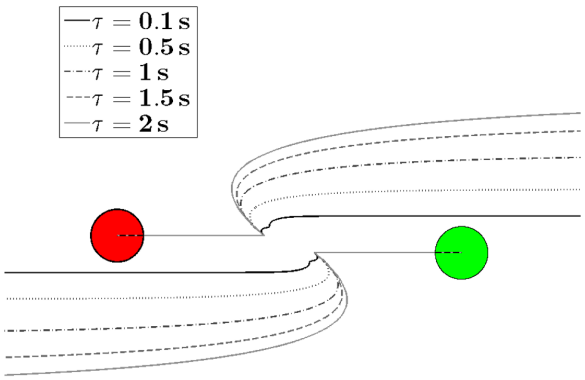

Figure 2.4: Trajectoires de deux piétons identiques i et j se déplaçant dans des directions opposées, pour des valeurs différentes de τ. Après la collision, pour chaque piéton, la force d'accélération intérieure permet de modifier progressivement la vitesse réelle après le choc pour retrouver la vitesse souhaitée. La rapidité du changement de vitesse dépend des valeurs de τ_i et τ_j. Dans cet exemple, $\tau_i = \tau_j = \tau$.

Nous nous intéressons à la rotation des piétons car elle est essentielle pour modéliser les piétons qui se tiennent à la main. La rotation d'un piéton est modélisée par un pendule de torsion. Un couple de rappel l_i^a $(kg.m^2.s^{-2})$ permet au piéton de retrouver sa direction souhaitée après une perturbation (choc, changement de direction, etc.). Ce couple est representé par la troisième composante de $\mathbf{f}_i^{int}$ et a pour expression:

$$l_i^a = k_i\big(\theta_i - \theta_{d,i}\big) + c_i\dot{\theta}_i = -I_i\ddot{\theta}_i \tag{2.12}$$

où $\theta_{d,i}$ est l'angle entre $\mathbf{e}_x = [1;0]$ et $\mathbf{e}_{d,i}$ représentant la direction souhaitée, I_i ($kg.m^2$) le moment d'inertie, k_i ($kg.m^2.s^{-2}.rd^{-1}$) la constante de rigidité, c_i ($kg.m^2.s^{-1}.rd^{-1}$) l'amortissement et $\omega_i = \sqrt{\frac{k_i}{I_i}}$ ($rd.s^{-1}$) est la pulsation propre.
Pour $\zeta_i = \frac{c_i}{2\sqrt{I_i\, k_i}} \geq 1$, un piéton i retrouve la direction souhaitée sans oscillations. Il la retrouve le plus rapidement pour $\zeta_i = 1$. Si l'amortissement est faible ($\zeta_i < 1$), un piéton retrouve la direction souhaitée après plusieurs oscillations. Dans la Fig. 2.5, un choc entre deux piétons a lieu à $t = 0.1\,s$ et le pas de temps est $\Delta t = 0.01\,s$. La ligne continue tracée dans chaque particule représente la direction souhaitée et celle en pointillé la direction actuelle. Nous avons choisi $\zeta_i = 1$ afin de retrouver le plus rapidement possible la rotation souhaitée.

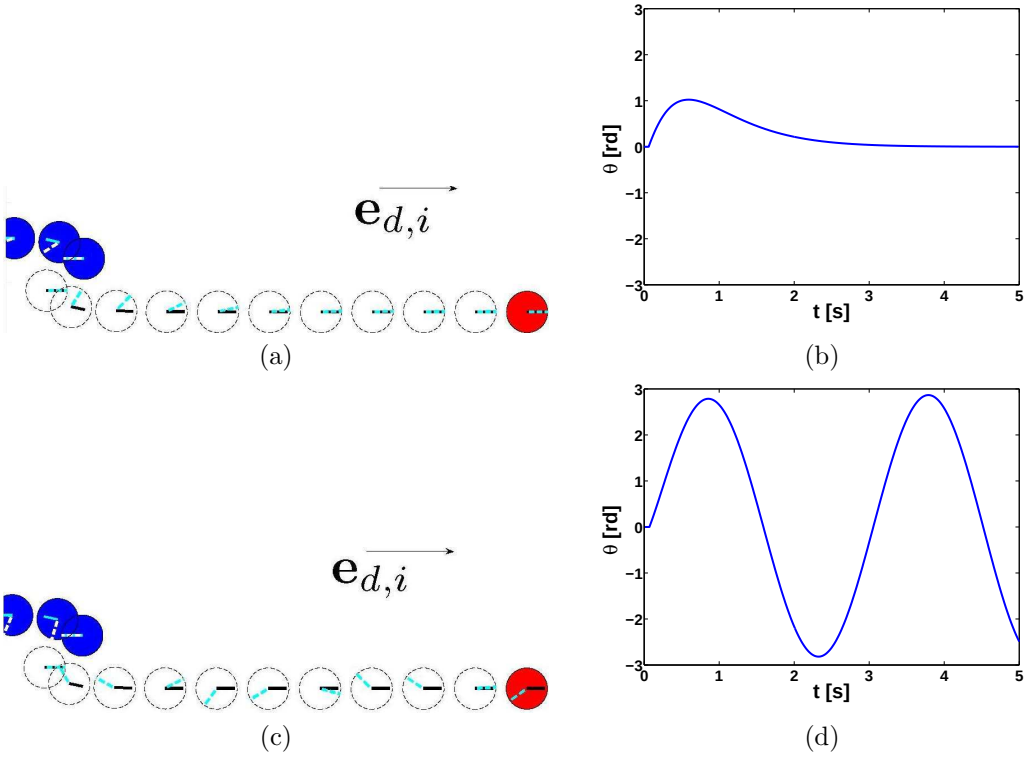

Figure 2.5: Interaction piéton-piéton sans force répulsive: les représentations à gauche montrent le mouvement d'un piéton après une collision pour (haut) $\zeta_i = 1$ et (bas) $\zeta_i = 0$, où $\theta_{d,i} = 0$. A droite, la rotation du piéton est tracée en fonction du temps.

Un autre aspect important de la rotation d'un piéton est sa valeur maximale. Après une perturbation, il peut arriver que le piéton tourne plus que π. La valeur maximale de rotation doit donc être limitée. En resolvant l'Eq. (2.12), l'expression de la rotation en fonction du temps est obtenue:

$$\theta_i(t) = \dot{\theta}_0(K_{tg}, K_n) t e^{-\omega_i t} + \theta_{d,i} \tag{2.13}$$

où $\dot{\theta}_0(K_{tg}, K_n)$ est calculé par le modèle après un choc (Eq. (2.9)) et $k_i = I_i \cdot \omega_i^2$ est choisie par l'utilisateur (par soucis de simplicité $k_i = k$). La Fig. 2.6 montre que la valeur de $\dot{\theta}_0$, calculée après un choc, varie en fonction de K_{tg} et est indépendante de K_n, pour $K_n \geq 2 \cdot 10^3\, kg$. L'Eq. (2.13) donne l'expression de θ_{max}:

$$\theta_{max} = \frac{\dot{\theta}_0(K_{tg})}{\omega_i \cdot e} + \theta_{d,i} \tag{2.14}$$

où e désigne l'exponentielle. En faisant varier k ($kg.m^2.s^{-2}.rd^{-1}$) dans l'intervalle [0.5,18.5], et $\dot{\theta}_0$ ($rad.s^{-1}$) dans l'intervalle [0,5] (chaque valeur de $\dot{\theta}_0$ correspond à une valeur de K_{tg}), l'Eq. (2.14) donne la surface illustrée sur la Fig. 2.7. Alors, pour limiter la rotation maximale d'un piéton, il suffit

de choisir de la Fig. 2.7 un point $(\dot{\theta_0}, k)$ au-dessous de l'isoligne qui représente la valeur désirée de la rotation maximale.

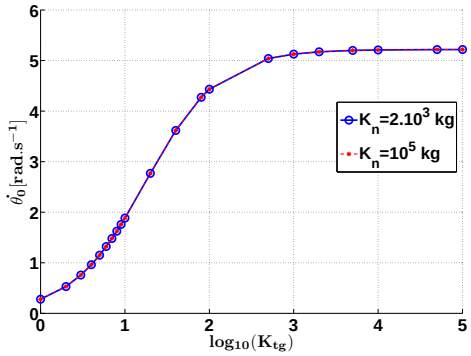

Figure 2.6: Variation de $\dot{\theta}_0$ en fonction de $\log_{10}(K_{tg})$

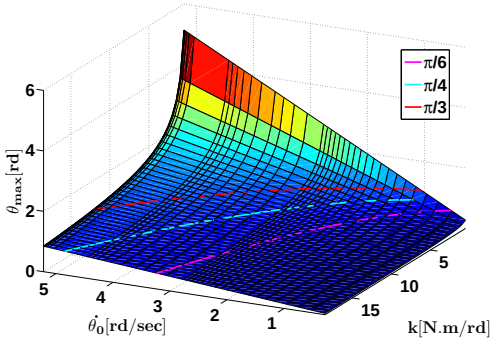

Figure 2.7: Variation de θ_{max} en fonction de $\dot{\theta}_0$ et k

Comme nous l'avons déja mentionné, dans notre modèle, un piéton est représenté par une particule ayant une direction et une allure souhaitées. Dans la section suivante, nous présentons les stratégies de déplacement utilisées pour trouver la direction souhaitée d'un piéton.

2.4 Stratégies de déplacement

Comme nous l'avons précisé dans la section précédente, pour gérer le mouvement des piétons dans une foule, il est nécessaire de contrôler le déplacement d'un piéton seul dans un espace prédéfini. Pour cela, on définit le champ de "vitesses souhaitées" qu'utiliserait un piéton pour trouver la direction vers la sortie d'un espace connu. Dans cette section, nous allons décrire les deux stratégies de déplacement que nous avons introduites dans le modèle: la stratégie du chemin (i) le plus court et (ii) le plus rapide. Dans les deux cas, le champ de vitesses souhaitées est obtenu par la résolution d'une équation eikonale [34].

2.4.1 Méthode d'obtention du champ de vitesses souhaitées

Deux étapes sont nécessaires pour générer le champ de vitesses souhaitées: réaliser une cartographie de l'espace étudié puis créer les vecteurs définissant le champ de vitesses.

Cartographie

Pour définir le champ de vitesses souhaitées, il faut tout d'abord réaliser une "cartographie" de l'espace étudié, c'est-à-dire connaître le temps nécessaire en tout point de l'espace pour rejoindre une sortie choisie. Pour cela, on considère une onde dont l'origine est la sortie $\partial\Upsilon$ et qui se propage dans l'espace étudié Υ

où les obstacles sont représentés par Γ. La fonction scalaire $T(\mathbf{x}, t)$ définit le temps d'arrivée de l'onde en chaque point de l'espace. Cette fonction peut être obtenue en résolvant l'équation eikonale [35]:

$$|| \nabla T(\mathbf{x}, t) || = \frac{1}{V(\mathbf{x}, t)} \quad \text{for } \mathbf{x} \in \Upsilon \tag{2.15}$$

$$T(\mathbf{x}, t) = 0 \quad \text{for } \mathbf{x} \in \partial\Upsilon \tag{2.16}$$

où $V(\mathbf{x}, t)$ est la vitesse de l'onde.
Dans les zones non accessibles aux piétons (obstacles, murs,...), $V(\mathbf{x}, t)$ est choisie nulle. Il existe plusieurs méthodes pour construire la solution d'une équation eikonale comme les méthodes Fast Marching [34] et Fast Iterative [36]. Nous avons retenu la première.

Champs de vitesses souhaitées

Une fois la cartographie de l'espace étudié réalisée, la fonction $T(\mathbf{x}, t)$ est utilisée pour trouver les vecteurs composant le champ de vitesses souhaitées. Pour chaque point de l'espace $\mathbf{x}$ un vecteur "direction" unitaire $\mathbf{e}^*(\mathbf{x})$ est attribué. Ensuite, les piétons auront leurs vitesses instantanées suivant la direction définie au niveau des points qu'ils occupent. Le vecteur unitaire a pour expression:

$$\mathbf{e}^*(\mathbf{x}, t) = -\frac{\nabla T(\mathbf{x}, t)}{|| \nabla T(\mathbf{x}, t) ||} \tag{2.17}$$

Par conséquent, si un piéton désire suivre le chemin le plus court, alors $\mathbf{e}_{d,i}(t) = \mathbf{e}^*(\mathbf{q}_i(t))$ et la vitesse souhaitée est donnée par $\mathbf{u}_{d,i} = u_{d,i} \cdot \mathbf{e}_{d,i}$ où $u_{d,i}$ représente l'amplitude de la vitesse. Cette dernière est choisie aléatoirement par le bias d'une distribution normale de moyenne 1.34 $m.s^{-1}$ et d'écart type 0.26 $m.s^{-1}$ [37].

Dans la suite, nous montrons comment les stratégies du chemin le plus court et du chemin le plus rapide peuvent être obtenues à partir de la solution de l'équation eikonale.

2.4.2 Champ statique de vitesses

Comme l'indique son nom, le champ de vitesses statique, $S(\mathbf{x})$, est calculé une seule fois au début de la simulation. Par conséquent, la présence d'autres piétons et l'évolution du trafic ne sont pas prises en compte. De plus, la vitesse de l'onde est constante par rapport au temps $V(\mathbf{x}, t) = V(\mathbf{x}) = cst$. Pour $V(\mathbf{x}) = 1$, le temps d'arrivée de l'onde à un endroit donné coïncide avec la distance parcourue. Le résultat obtenu représente donc les distances géodésiques par rapport à la sortie de l'espace étudié (Fig. 2.8(a) et Fig. 2.9(a)). Pour que les piétons évitent les obstacles, nous choisissons une vitesse de l'onde tel que $0 < V(\mathbf{x}) < 1$ à une certaine distance des obstacles (Fig. 2.8(b) et Fig. 2.9(b)).

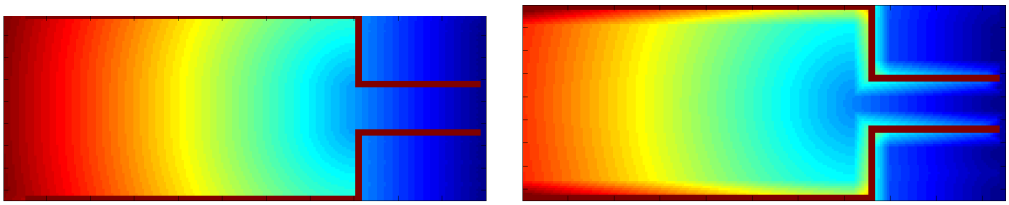

(a) (b)

Figure 2.8: $S(\mathbf{x})$ obtenu pour (a) $V(\mathbf{x}) = 1$ partout et (b) $V(\mathbf{x}) = 1/50$ près des murs.

2.4.3 Champ dynamique de vitesses

Afin de prendre en compte l'évolution du trafic, le champ de vitesses doit être calculé au cours du temps. Ce champ dynamique permet aux piétons d'éviter les endroits congestionnés. Pour cela, un critère de congestion et ainsi que l'évolution de $V(\mathbf{x}, t)$ doivent être choisis.

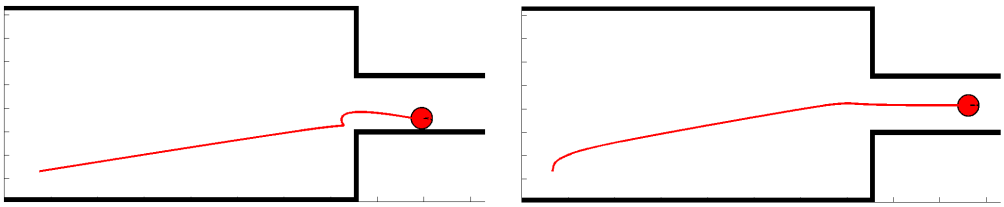

(a) (b)

Figure 2.9: Trajectoire d'un piéton pour (a) $V(\mathbf{x}) = 1$ partout et (b) $V(\mathbf{x}) = 1/50$ près des murs.

Le critère de congestion que nous proposons est l'espace personnel d'un piéton, construit à l'aide d'un diagramme de Voronoï. Cette approche originale a été utilisée pour mesurer la densité des piétons dans une section [38] mais jamais comme un critère de congestion pour calculer le champ dynamique de vitesses. Un diagramme de Voronoï est un découpage du plan (pavage) à partir d'un ensemble discret de points appelés "germes". Autour de chaque germe, une cellule de Voronoï, A_i^c, est construite. Cette cellule contient l'ensemble des points de l'espace qui sont les plus proches du germe de la cellule que de tous les autres germes. On peut considérer qu'un germe a une zone d'influence représenté par sa cellule de Voronoï. Dans notre cas, les germes sont les centres des disques représentant les piétons et les zones d'influence, ou cellules, représentent les espaces personnels de ces derniers. Une congestion est détectée lorsque cet espace personnel, z_b, devient plus petit qu'un seuil choisi (Fig. 2.10).

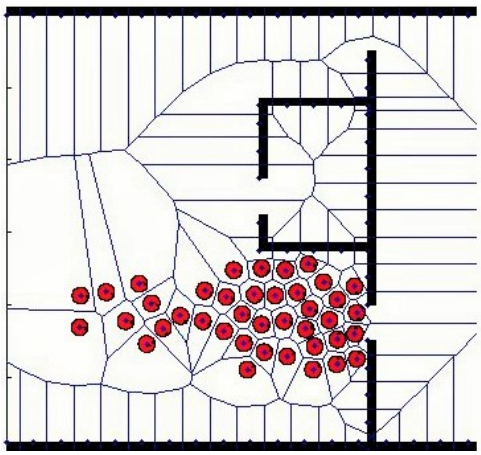

Figure 2.10: Discretisation de l'environnement à l'aide d'un diagramme de Voronoï.

Concernant l'évolution de $V(\mathbf{x}, t)$, nous nous sommes inspirés du mécanisme utilisé par les fourmis pour signaler une source de nourriture. Lorsqu'une fourmi trouve de la nourriture, elle dépose une phéromone qui va attirer les autres fourmis (Fig. 2.11). Une fois que la source de nourriture est épuisée, les fourmis arrêtent de déposer la phéromone. Avec le temps, cet agent chimique s'évapore et les fourmis n'empruntent plus ce chemin. Le mécanisme inverse est appliqué dans notre modèle. Lorsque l'espace personnel d'un piéton devient plus petit qu'un seuil choisi, la valeur de $V(\mathbf{x}, t)$ est diminuée dans la cellule de Voronoï correspondante (Eq. 2.18). Elle est augmentée à nouveau lorsque la congestion disparaît (Eq. 2.19).

$$V(\mathbf{x}, t_{i+1}) = V(\mathbf{x}, t_i) - i_V \quad \text{si } A_i^c \leq z_b \quad (2.18)$$

$$V(\mathbf{x}, t_{i+1}) = min\big(V(\mathbf{x}, t_0), V(\mathbf{x}, t_i) + j_V\big) \quad \text{si } A_i^c > z_b \quad (2.19)$$

où i_v et j_v sont un décrément et un incrément, respectivement.
L'influence des champs de vitesses statique et dynamique sur l'évolution du système est illustré dans la Fig. 2.12.

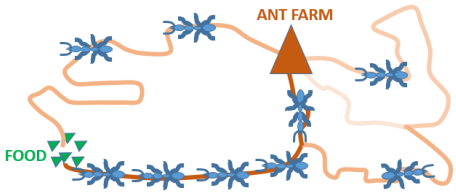

Figure 2.11: Dépôt de phéromones attirant de plus en plus de fourmis vers la source de nourriture.

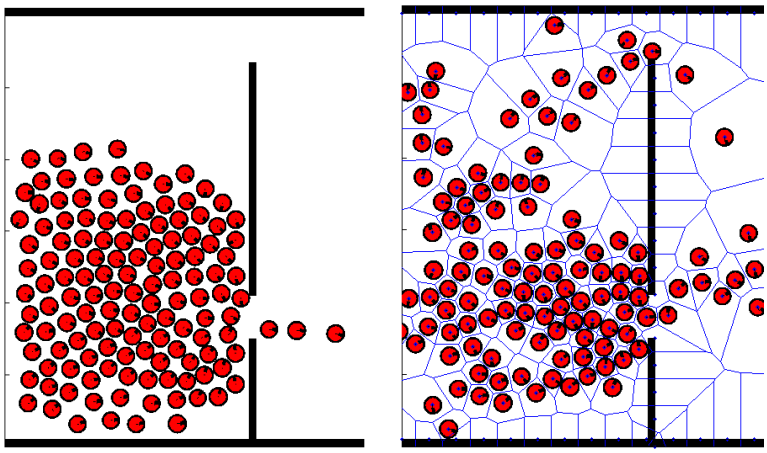

(a) (b)

Figure 2.12: Evolution de la simulation en utilisant un champ de vitesses (a) statique (chemin plus court) et (b) dynamique (chemin plus rapide).

Après avoir choisi son chemin par une des deux stratégies de déplacement, un piéton devra interagir avec les autres individus qu'il va croiser. Dans la section suivante, les différents types de comportements que nous avons modélisés sont présentés.

2.5 Interactions piéton-piéton

Dans cette section, nous traitons l'évitement entre les piétons. Nous détaillons une approche fondée sur des forces répulsives et une approche cognitive.

2.5.1 Force de répulsion sociale

Un des modèles très répandu dans la littérature est le modèle des forces sociales, introduit par Dirk Helbing en 1995 [6]. Le modèle des forces sociales repose sur certains concepts issus de la physique newtonienne. Les piétons interagissent à l'aide d'une combinaison de forces, à la manière des forces électromagnétiques qui agissent sur les particules d'un gaz. Le piéton est "repoussé" par les autres piétons sous l'effet d'une force d'interaction, $\mathbf{f}_i^{soc}$, qui est le coeur de ce modèle et qui définit de quelle manière un piéton se comporte lorsqu'il fait face à un autre individu. Les différentes spécifications du modèle des forces sociales se distinguent les unes des autres par la forme de cette fonction. Nous utilisons la fonction d'interaction définie dans [19] par:

$$\mathbf{f}_i^{soc} = \sum_{j \neq i} \mathbf{f}_{ij}^{soc} = \sum_{j \neq i} A e^{\frac{(R_{ij} - d_{ij})}{B}} \left[\lambda + (1 - \lambda) \frac{1 + \cos\phi_{ij}}{2} \right] \mathbf{e}_{ji} \tag{2.20}$$

où $R_{ij} = r_i + r_j$ est la somme des rayons des piétons i et j, d_{ij} est la distance entre leurs centres, A

et B sont deux paramètres du modèle qui caractérisent l'amplitude et la portée de l'interaction répulsive respectivement, λ $(0 < \lambda < 1)$ permet de considérer le caractère anisotropique des interactions des piétons, $\mathbf{e}_{ji}$ est le vecteur unitaire dirigé du centre du piéton j vers le centre du piétons i et ϕ_{ij} est l'angle entre la direction souhaitée $\mathbf{e}_{d,i}$ et $\mathbf{e}_{ji}$. Un exemple de deux piétons qui s'évitent grâce à la force répulsive est illustré sur la Fig. 2.13.

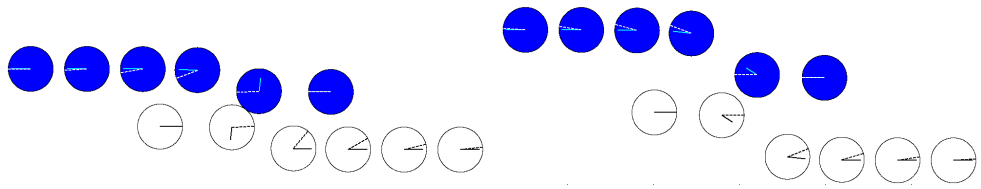

(a) (b)

Figure 2.13: Interaction piéton-piéton (a) sans et (b) avec force répuslive (pour $A = 2000\,N$ et $B = 0.08\,m$)

2.5.2 Approche cognitive

Une nouvelle approche de modélisation fondée sur des heuristiques comportementales, s'appuyant sur le champ visuel des piétons, a été proposée dans [39]. Soit l'intervalle $[-\phi, \phi]$ le champ de vision du piéton. Pour toutes les directions $\alpha \in [-\phi, \phi]$, celui-ci va évaluer la distance avant la première collision $h(\alpha)$. Par défaut, en l'absence de collision, le modèle fixe la valeur de $h(\alpha)$ à la distance maximale du champ de vision d_{max}. La fonction $h(\alpha)$ permet d'évaluer la distance totale parcourue pour atteindre la destination finale, situé dans la direction α_0:

$$d^2(\alpha) = d_{max}^2 + h(\alpha)^2 - 2d_{max}h(\alpha)\cos(\alpha_0 - \alpha) \tag{2.21}$$

Le piéton choisit alors sa direction de déplacement optimale α_{opt} en minimisant cette distance. Quant à sa vitesse de déplacement, elle est définie par:

$$v_{adap,i} = min(||\mathbf{u}_i||, \frac{d_{obs}}{\tau_i}) \tag{2.22}$$

où $\mathbf{u}_i$ est la vitesse du piéton i et d_{obs} est la distance le séparant du premier obstacle suivant sa direction actuelle.

Après avoir effectué une recherche bibliographique, nous avons pu constater que peu d'informations étaient fournies pour expliquer l'allure de la fonction $h(\alpha)$, qui évalue la distance avant la première collision dans la direction α.

2.5.3 Expression de $h(\alpha)$

Nous avons dévéloppé deux méthodes afin de calculer $h(\alpha)$. Dans la première méthode, nous approchons la courbe de $h(\alpha)$ (Fig 2.14 (b)) par une fonction polynomiale. Dans la deuxième méthode, nous la calculons numériquement. L'application choisie pour tester ces méthodes est le cas de deux piétons face à face se croisant (Fig. 2.15).

Méthode 1: approximation de la courbe

Nous commençons par la définition des notations qui seront utilisées dans la suite :

- α_j : l'angle auquel se trouve le piéton j dans le champ de vision du piéton i
- $h_j = h(\alpha = \alpha_j)$ la distance avant collision avec le piéton j $(\alpha = \alpha_j)$

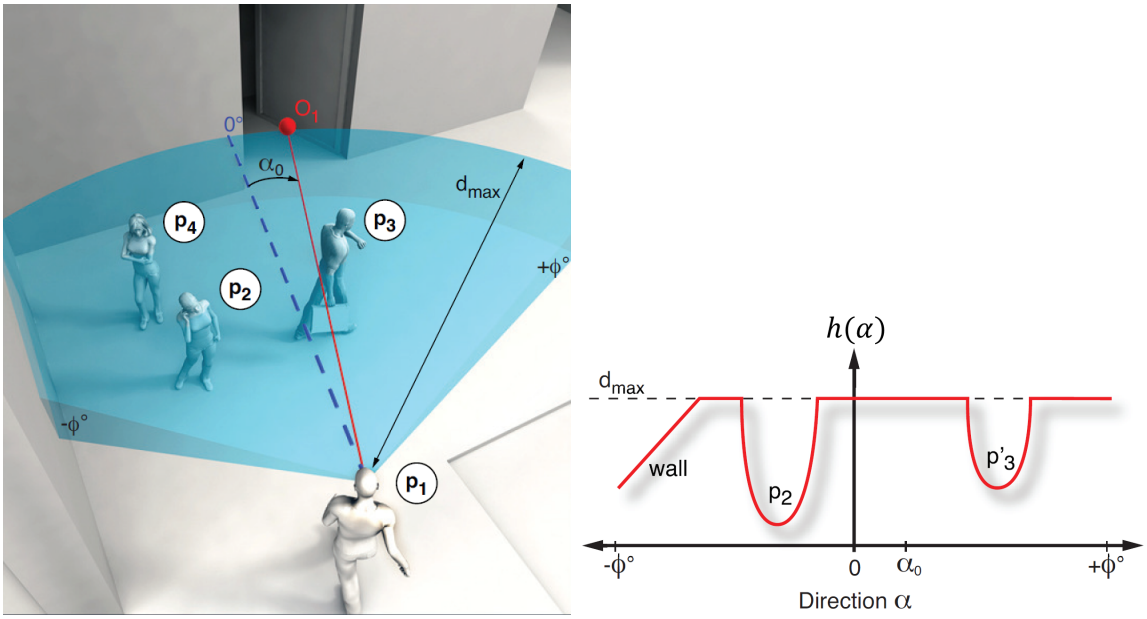

(a) (b)

Figure 2.14: (a) Illustration d'un piéton p_1 ayant 3 piétons dans son champ de vision et essayant de rejoindre la porte marquée par le point rouge. (b) Représentation graphique de la fonction $h(\alpha)$ [39].

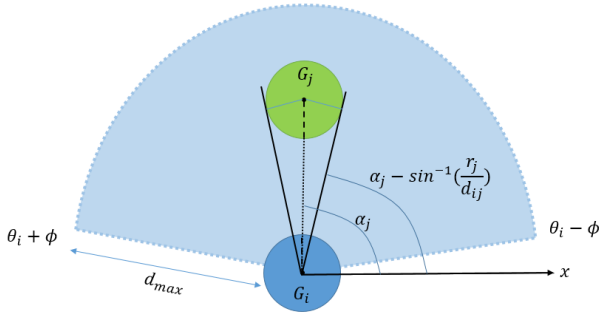

Figure 2.15: Deux piétons i et j face à face se croisant.

Dans cette approche, la fonction $\alpha \to h(\alpha)$ est approchée par une parabole centrée sur h_j. Après avoir trouvé h_j, la fonction $\alpha \to H_j(\alpha)$ est définie par:

$$H_j(\alpha) = a_{ij}(\alpha - \alpha_j)^2 + h_j \tag{2.23}$$

$$\text{où } a_{ij} = \frac{d_{max} - h_j}{arcsin^2\left(\frac{r_j}{d_{ij}}\right)}$$

Dans le champ de vision du piéton i, le centre du piéton j se trouve à α_j. Du fait de ses dimensions (disque de rayon r_j), il occupe l'intervalle angulaire $[\alpha_j - arcsin(r_i/d_{ij}), \alpha_j + arcsin(r_i/d_{ij})]$ du champ de vision du piéton i. Alors, la fonction $\alpha \to h(\alpha)$ est définie par:

$$h(\alpha) = \begin{cases} d_{max} & \text{si } \alpha \in \left[\theta_i - \phi, \alpha_j - arcsin(\frac{r_i}{d_{ij}})\right[\cup \left]\alpha_j + arcsin(\frac{r_i}{d_{ij}}), \theta_i + \phi\right] \\ H_j(\alpha) & \text{si } \alpha \in \left[\alpha_j - arcsin(\frac{r_i}{d_{ij}}), \alpha_j + arcsin(\frac{r_i}{d_{ij}})\right] \end{cases} \tag{2.24}$$

L'allure de la fonction $h(\alpha)$ obtenue est illustrée sur la Fig. 2.16.

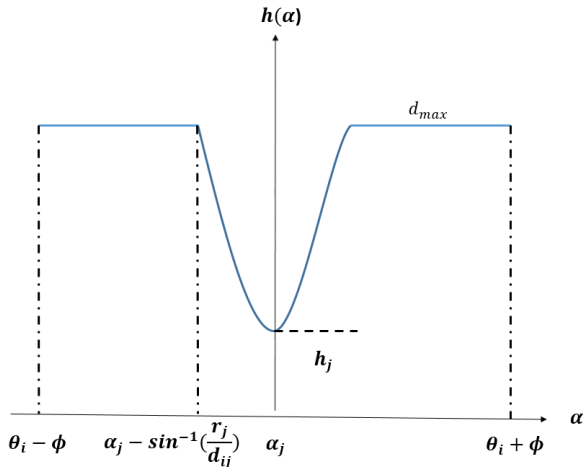

Figure 2.16: Fonction $h(\alpha)$ définie par une parabole centrée au point (α_j, h_j).

Méthode 2: résolution numérique

Dans cette méthode, nous discrétisons le champ de vision de piéton i en N_α directions possibles (Fig. 2.17). Ensuite, nous évaluons pour chaque direction possible d'angle α par rapport au piéton i, la valeur de la fonction $h(\alpha)$. Tout d'abord, nous redéfinissons quelques notations utilisées dans la suite:

- $\boldsymbol{\alpha} = {}^t(\alpha_1, ..., \alpha_{N_\alpha})$ est désormais un vecteur, de dimension $N_\alpha \times 1$, qui contient toutes les directions possibles (dans le champ de vision) pour la vitesse $\mathbf{u}_i$ du piéton i
- $\mathbf{h}(\boldsymbol{\alpha}) = {}^t(h(\alpha_1), ..., h(\alpha_{N_\alpha}))$ est le vecteur, de dimension $N_\alpha \times 1$, des distances avant collision pour le piéton i et pour toutes les directions possibles α_n, $n \in [1, \cdots, N_\alpha]$
- $\Delta t(\alpha_n^i)$ est le temps jusqu'à la collision dans la direction α_n, pour le piéton i

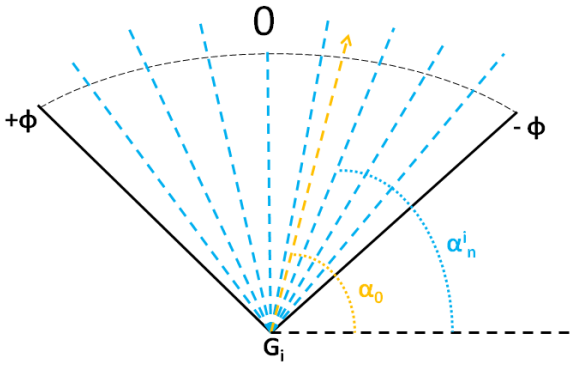

Figure 2.17: Champs de vision discrétisé du piéton i.

Le temps avant collision $\Delta t(\alpha_n)$ est calculé pour chaque α_n de $\boldsymbol{\alpha}$ ($n \in [1, ..., N_\alpha]$) . Ensuite, ce temps est multiplié par la vitesse du piéton afin d'obtenir le vecteur des distances avant collision :

$$\forall n \in [1, ..., N_\alpha],\ h(\alpha_n) = ||\mathbf{u}_i(\alpha_n)|| * \Delta t(\alpha_n)$$

Pour le cas de deux piétons face à face se croisant (Fig. 2.15), la Fig. 2.18 représente le vecteur $\mathbf{h}(\boldsymbol{\alpha^i})$ en fonction de $\boldsymbol{\alpha^i}$ et $\alpha \to h(\alpha)$, où α est un scalaire $\in [-\phi, +\phi]$. Dans cet exemple, les coordonnées des centres des piétons i et j sont respectivement $(1, 0.2)$ et $(1, 3.5)$ exprimées en mètre:

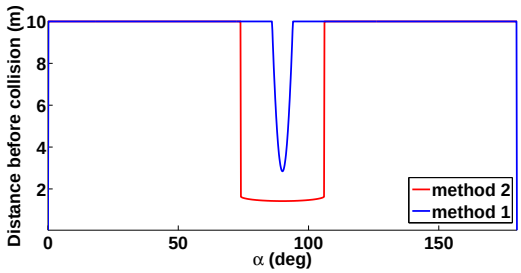

Figure 2.18: Distance avant collision - deux piétons face à face se croisant. La méthode 1 (en bleu) et la méthode 2 (en rouge).

2.5.4 Simulations numériques

Dans ce paragraphe, nous simulons le croisement de deux groupes de piétons suivant les quatre versions du modèle suivantes (Fig. 2.19):

- Modèle de collision sans évitement
- Modèle de collision avec force répulsive
- Modèle de collision avec approche coginitive: méthode 1
- Modèle de collision avec approche coginitive: méthode 2

Pour le groupe qui avance de bas en haut, nous avons fixé une destination finale au point de coordonnées $(9, 9.5)$ (Fig. 2.19). Pour l'autre groupe, les membres ont une direction souhaitée de -45 degrés par rapport à l'horizontale. Pour comparer les différentes versions du modèle, nous évaluons les trois critères suivants:

- le nombre de collisions,
- le temps de calcul,
- la capacité des piétons à marcher à leurs vitesses souhaitées.

Nombre des collisions

Nous avons calculé le nombre de collisions qui ont eu lieu pendant les simulations pour chacun des quatre cas. Les résultats sont illustrés sur la Fig. 2.20. En utilisant une force répulsive, il n'y a eu aucune collision. Comme attendu, notre modèle de collision est à l'opposé avec le maximum nombre de collisions. Concernant les deux méthodes avec approche cognitive, la deuxième génère moins de collisions.

Temps de calcul

L'évolution du temps de calcul en fonction du nombre de piétons est un critère très important lorsque l'on vise à simuler les mouvements de milliers de personnes. La Fig. 2.21 montre que notre modèle de collision est le plus rapide et que les versions avec l'approche cognitive sont les plus lentes. En revanche, ces méthodes apportent un niveau "d'intelligence" plus élevé.

Maintient de la vitesse souhaitée

Dans les simulations, nous avons donné la même valeur de vitesse souhaitée à tous les piétons. Ensuite, nous avons vérifié leur capacité à marcher à leurs vitesses souhaitées pour chacune des versions du modèle. Sur la Fig. 2.22, les moyennes des amplitudes des vitesses des piétons au cours des simulations pour les 4 versions du modèle sont tracées. Nous remarquons que la méthode 2 de l'approche cognitive est la plus

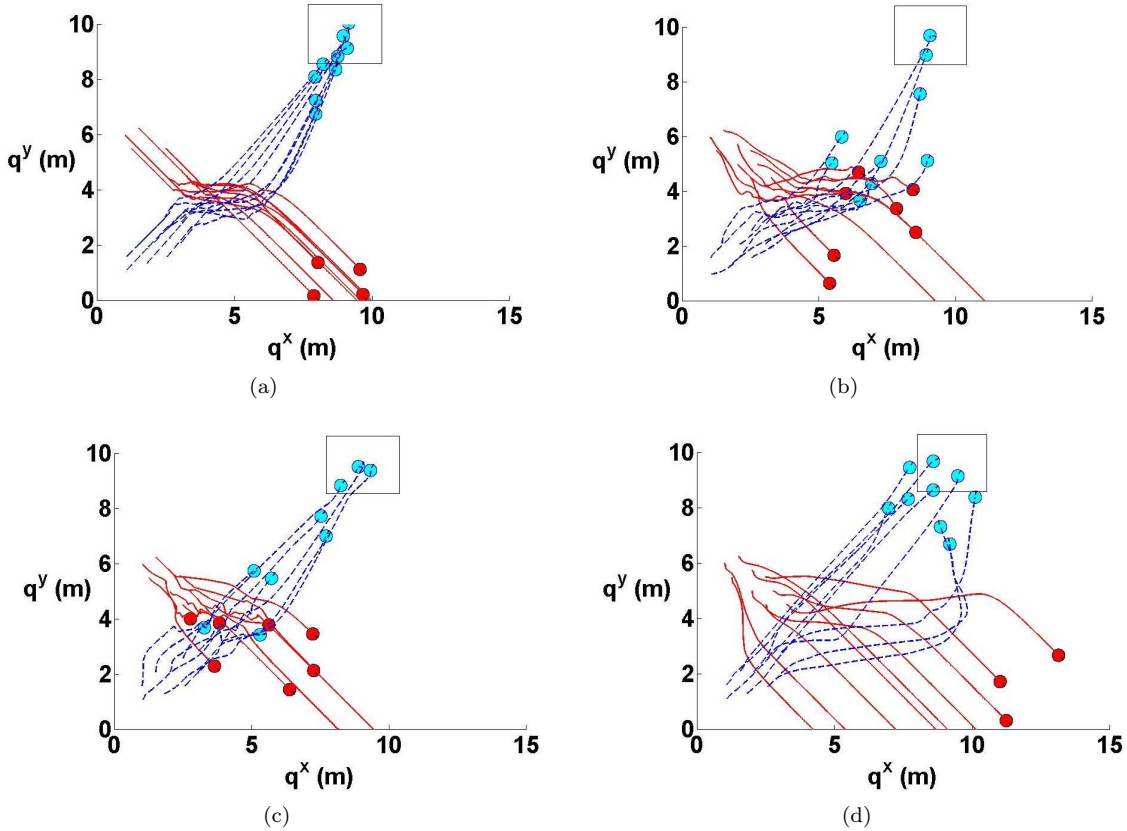

Figure 2.19: Croisement de deux groupes de piétons: (a) sans évitement, (b) évitement avec force répulsive et évitement avec approche cognitive avec (c) la méthode 1 et (d) la méthode 2.

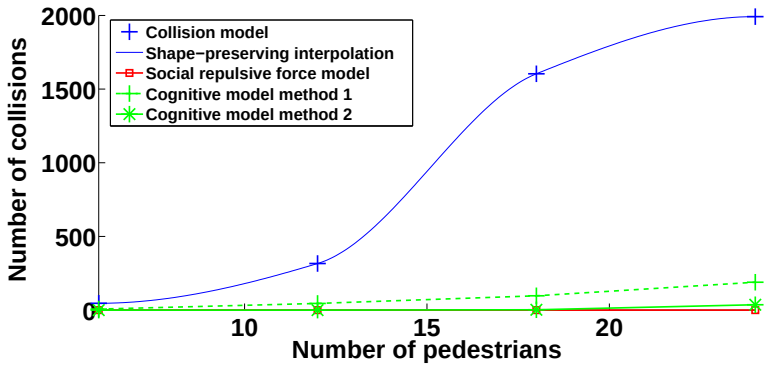

Figure 2.20: Croisement de deux groupes de piétons: nombre de collisions pour les différentes versions du modèle et pour differents nombres de piétons.

performante par rapport à la capacité des piétons à éviter les collisions tout en marchant à leurs vitesses souhaitées.

Dans cette section, nous avons présenté les trois types d'interaction piéton-piéton du notre modèle. Nous avons montré que la performance de chacune des 4 versions du modèle varie selon le critère choisi. Dans la section suivante, nous présentons les travaux qui ont été faits sur la validation de notre modèle.

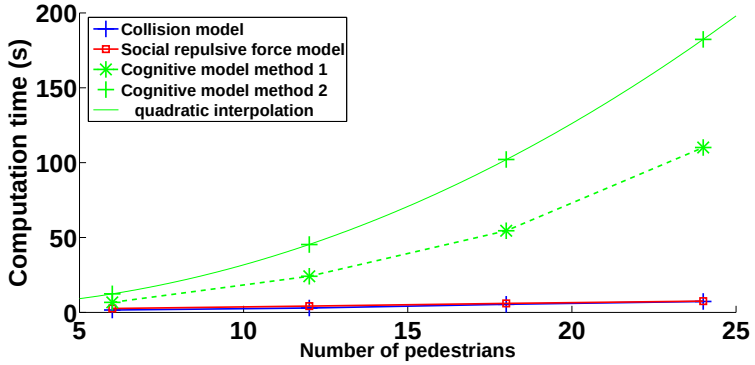

Figure 2.21: Croisement de deux groupes de piétons: temps de calcul pour les différentes versions du modèle et pour différents nombres de piétons (temps de simulation = 9 s).

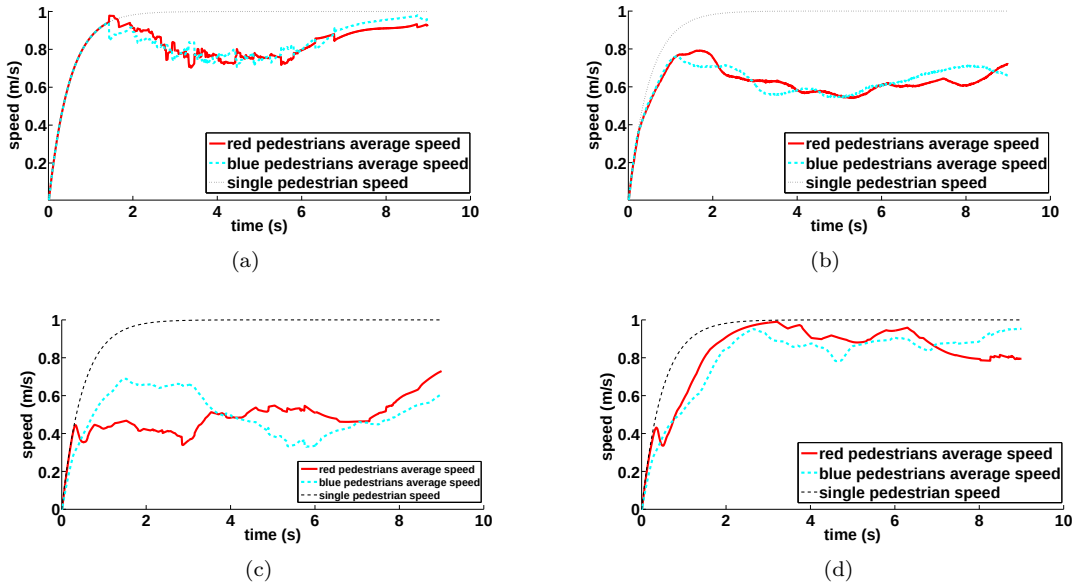

Figure 2.22: La vitesse souhaitée moyenne pour 18 piétons pour les différentes versions du modèle.

2.6 Validation et verification du modèle

Dans cette section, nous abordons la problématique de la vérification et de la validation de notre modèle de piétons. Dans un premier temps, nous présentons une phase de validation quantitative de notre modèle. Dans l'étape suivante, à l'aide d'un plan d'expérience numérique, nous identifions les facteurs significativement influents (au sens statistique) parmi l'ensemble des paramètres du modèle pris en compte pour l'étude .

2.6.1 Validation quantitative: cas du goulot d'étranglement

Dans cette section, nous examinons la capacité de notre modèle à reproduire des résultats expérimentaux. Plusieurs études ont été réalisées sur les goulots d'étranglement [40–42]. Nous avons choisi de reproduire l'expérience présentée dans [41]. L'environnement de l'expérience est illustré sur la Fig. 2.23(a).

Dans [41], différentes largeurs de goulot ($b \in [0.8\,m, 1.2\,m]$ avec un incrément de $0.1m$) et plusieurs nombres de piétons ($N = 20, 40$ et 60) ont été testés. Le flux de piétons et les effets du positionnement,

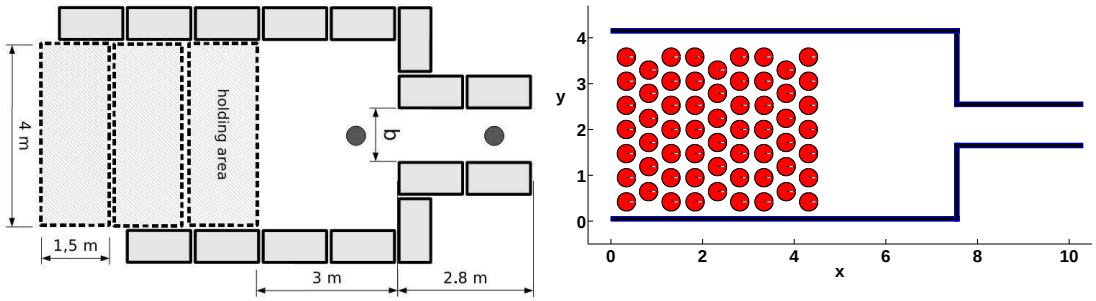

(a) (b)

Figure 2.23: Environnement de l'expérience (a) réelle et (b) modélisé pour les simulations numériques.

en files ou en quinconce, ont été étudiés. Les auteurs ont utilisé la notion de "specific flow" qui a pour expression:

$$J_s = \frac{J}{b} = \frac{N_b}{\Delta t \cdot b} \tag{2.25}$$

où J est le flux défini par le rapport entre le nombre de piétons, qui sont passés à une position précise, et l'intervalle de temps Δt, mesuré à partir de la sortie du premier piéton.

Table 2.1: Valeurs de $J_{s,exp}$ $(personnes.m^{-1}.s^{-1})$ mesurées [41].

$b(m)$	$N_b = 20$	$N_b = 40$	$N_b = 60$
0.8	**1.86**	**1.77**	**1.61**
0.9	**2.06**	**1.91**	**1.86**
1.0	**2.19**	**2.08**	**1.9**
1.1	**1.78**	**1.93**	**1.93**
1.2	**2.31**	**1.81**	**1.97**

Calibration des paramètres de la force répulsive

Dans cette première étude, nous voulons trouver les valeurs des deux de paramètres de la force répulsive $A(kg.m.s^{-2})$ et $B(m)$ nous permettant de retrouver les résultats expérimentaux issus de [41]. Pour cela, nous avons choisi 20 valeurs de A et de B répartiées uniformément sur les intervalles $[10; 1000]$ et $[0.01; 0.2]$ respectivement. Tous les essais réalisés dans [41] ont été simulés (400 simulations pour chaque essai). Les valeurs des autres paramètres du modèle sont répertoirées dans le tableau 2.2. les seuls paramètres qui varient d'une simulation à l'autre sont A, B, N_b et b.

Nous avons calculé l'erreur entre les valeurs expérimentales et simulées en utilisant l'expression suivante:

$$\varepsilon_T(A,B) = \frac{1}{n_g\, n_b} \sum_{j=1}^{n_g} \sum_{i}^{n_b} \left(\frac{J_s(A,B,b_i,N_b^j)}{J_{s,exp}(b_i,N_b^j)} - 1 \right)^2 \tag{2.26}$$

où n_b est le nombre de largeurs du goulot (tableau 2.1), n_g est le nombre de groupes de piétons, $J_{s,exp}$ est la valeur expérimentale de J_s (tableau 2.1) et J_s est la valeur obtenue par notre modèle.

Les valeurs optimisées $\tilde{A}$ and $\tilde{B}$ sont obtenues en minimisant ε_T:

$$(\tilde{A}, \tilde{B}) = \arg\min \varepsilon_T(A,B) \tag{2.27}$$

Table 2.2: Valeurs des paramètres fixés dans les simulations numériques.

Paramètre	Symbole	Valeur	Unité
Vitesse	$\parallel \mathbf{u}_{d,i} \parallel$	$\mathcal{N}$ (1.34,0.26)	m.s^{-1}
Rayon	r_i	0.23	m
Masse	m_i	83	kg
Agressivité	τ_i	0.5	s
Coefficient de dissipation (collision)	K_n	10^5	kg
Coefficient de friction (collision)	K_{tg}	0	kg
Pas de temps	h	10^{-2}	s

En traçant ε_T en fonction de A et B, nous obtenons la surface illustrée sur la Fig. 2.24. Parmi plusieurs fonctions, la fonction exponentielle était la meilleure représentation des minima locaux indiqués par des cercles rouges sur Fig. 2.24. Nous avons ensuite choisi 3 points de coordonnées (B, A) sur la courbe ajustée avec une valeur de B proche de celle choisie dans [19]. Les résultats simulés pour ces 3 points sont conformes avec ceux obtenus expérimentalement (Fig. 2.25).

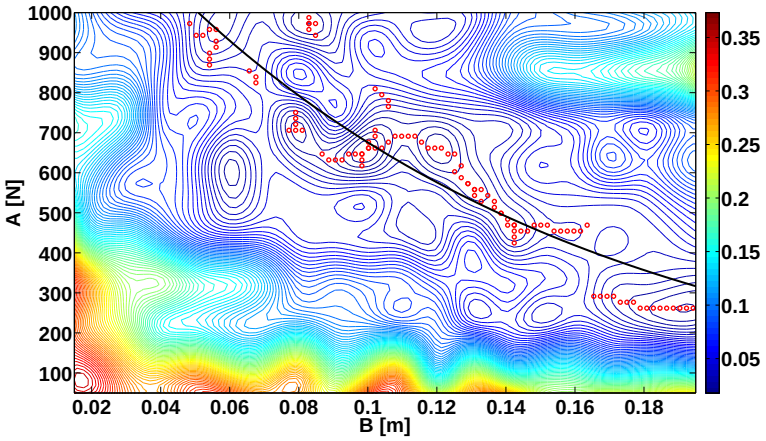

Figure 2.24: Surface représentant ε_T en fonction de A et B. La fonction exponentielle, représentée par la courbe noire, a pour equation $A = 1501 * e^{-7.98B}$

Bien que nous avons obtenu des informations et des résultats très importants de cette étude, ils ne sont pas suffisants pour le nombre des simulations que nous avons dû faire. Pour cela, nous utilisons les plans d'expériences numériques.

2.6.2 Plans d'expériences numériques

Les plans d'expériences permettent de planifier, d'organiser les expériences scientifiques et industrielles et de retirer l'information correspondant à l'objectif que l'on s'est préalablement fixé. En général, la méthodologie du plan d'expériences a deux objectifs principaux [43]: (i) repérer les facteurs (paramètres d'entrées d'un modele) significativement influents (au sens statistique) parmi l'ensemble de ceux qui ont été pris en compte dans l'étude et (ii) construire des modèles de régression ou d'analyse de la variance de bonne qualité dans un but de compréhension et/ou de prédiction et/ou de recherche d'optimum. Dans la suite, nous illustrons les travaux qui ont été réalisés sur notre modèle de foule afin d'atteindre ces deux objectifs.

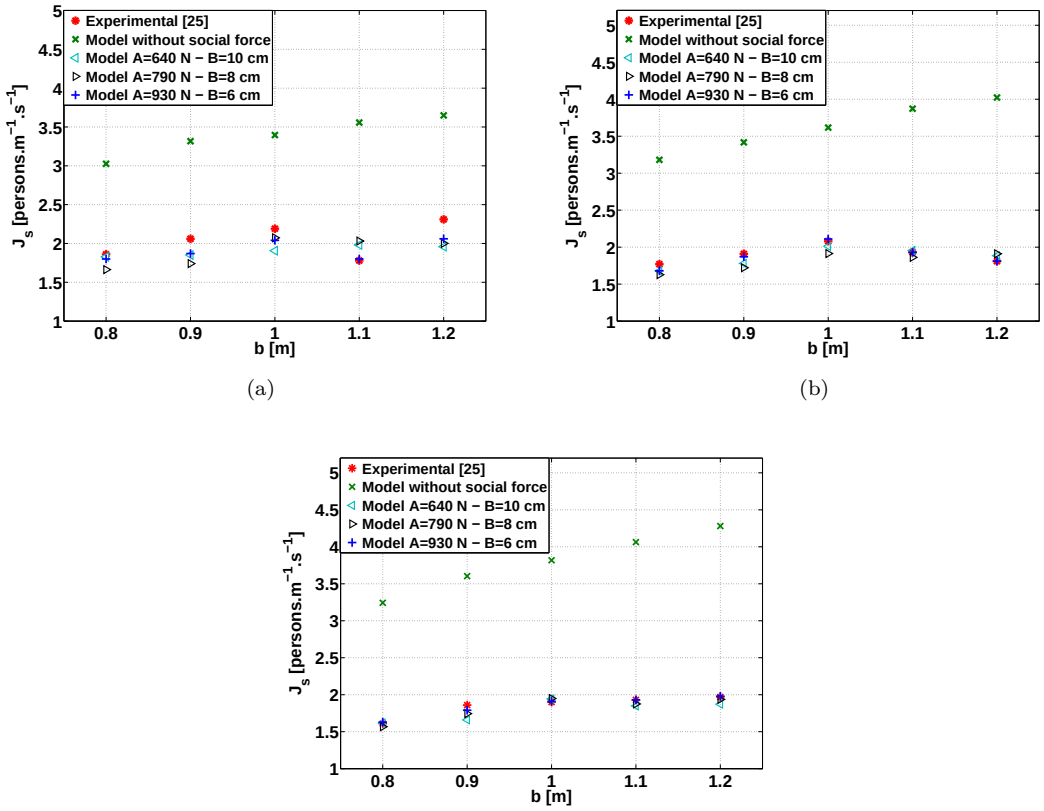

Figure 2.25: Valeurs du flux spécifique données par notre modèle avec force répulsive et celles obtenues expérimentalement [41] pour N= (a) 20, (b) 40, et (c) 60

L'expérience

Pour effectuer un plan d'expérience, nous avons choisi de simuler les mouvements des piétons au travers d'un goulot d'entranglement (Fig. 2.23) car plusieurs études ont été menées sur ce cas particulier. La réponse à mesurer est le flux de piétons $J = \frac{\Delta N}{\Delta t}$. Dans notre modèle, les paramètres d'entrées n'ont pas de valeurs spécifiques. Pour cela, nous avons attribué à chaque paramètre un intervalle défini par une valeur maximale et une valeur minimale. Les facteurs que nous avons retenus pour cette étude et leurs intervalles sont listés dans le tableau 2.3.

Le plan d'experience

Comme le montre le tableau 2.3, chacun des facteurs possède deux niveaux, une valeur minimale et une maximale. Nous avons choisi un plan factoriel complet 2^{k_f} où k_f est le nombre de facteurs pris en compte pour l'étude ($k_f = 13$ pour notre étude). Un plan complet nous permet d'obtenir les effets principaux de tous les facteurs et leurs interactions jusqu'à l'ordre 13 en faisant $2^{13}(= 8192)$ expériences ou simulations. Le plan d'expérience que nous avons construit est illustré dans le tableau 2.4. Les signes $+$ et $-$ représentent respectivement les valeurs minimale et maximale des facteurs.

2.6.3 Estimation des effets principaux et leurs interactions

Nous avons utilisé l'algorithme de Yates afin d'estimer les effets des facteurs et leurs interactions. L'algorithme opère de la manière suivante [44]:

Table 2.3: Les facteurs choisis et leurs intervalles de variation.

Facteur	**Symbole**	**Intervalle**
Evitement obstacle: vitesse de l'onde	$V_b(\mathbf{x})$	[0.1,0.3]
Evitement obstacle: distance	D_{shy}	[0.1,0.35]
Viscosité de la collision (kg)	K_{tg}	$[0, 1e^4]$
Elasticité de la collision (kg)	K_n	$[500, 1e^5]$
Force sociale-anistotropie	λ	[0,1]
Force sociale-zone répulsive	z_{rep}	[0.8,5]
Force sociale-portée	B	[0,0.25]
Force sociale-amplitude	A	[0,800]
Rayon des piétons	R	[0.18,0.24]
Nombre des piétons	N	[20,40]
Agressivité	τ	[0.4,1]
Vitesse souhaitée	v_0	[0.5,2.2]
Pas de temps	h	[0.001,0.01]

Table 2.4: Plan factoriel 2^{13}*complet*.

	Facteurs												
Numéro de l'essai	$V_b(\mathbf{x})$	D_{shy}	K_{tg}	K_n	λ	z_{rep}	B	A	R	N	τ	v_0	h
1	-	-	-	-	-	-	-	-	-	-	-	-	-
2	+	-	-	-	-	-	-	-	-	-	-	-	-
3	-	+	-	-	-	-	-	-	-	-	-	-	-
4	+	+	-	-	-	-	-	-	-	-	-	-	-
5	-	-	+	-	-	-	-	-	-	-	-	-	-
6	+	-	+	-	-	-	-	-	-	-	-	-	-
							⋮						
							⋮						
8192	+	+	+	+	+	+	+	+	+	+	+	+	+

1. Créer une table de $k + 2$ colonnes et placer le plan d'experience (tableau 2.4) dans la première colonne.
2. Mettre les réponses (les valeurs de flux) dans la deuxième colonne.
3. Mettre la somme des éléments $2 * i - 1$ et $2 * i$ de la deuxième colonne dans la première moitié de la troisième colonne et leurs différences dans la deuxième moitié.
4. Répéter la même procédure pour les colonnes $4, 5, \ldots, k+2$. Par exemple, pour construire la colonne 6, la colonne 5 est utilisée.
5. Tous les facteurs qui ont un signe + (plan d'expérience) dans une ligne donnée, se trouvent en variables de la fonction g dans la colonne $k + 2$. Par exemple, pour la ligne 2, seul le facteur $V_b(\mathbf{x})$ a un signe + dans le plan d'expérience. La ligne 2 de la colonne $k + 2$ est alors représentée par $g(V_b(\mathbf{x}))$. La moyenne globale est obtenue en divisant $g(T)$ (la première ligne de la colonne $k + 2$) par $N = 2^k$ ($k = 13$ ici). Les estimations des effets et leurs interactions sont obtenues en divisant $g(\ldots)$ par $N/2$. Les estimations, $E(\ldots)$, se trouvent dans la dernière colonne.

Les résultats obtenus par notre étude sont illustrés dans le tableau 2.5.

2.6.4 Analyse de variance: quels sont les effets principaux?

Maintenant que nous avons calculé tous les effets, nous cherchons ceux qui sont significativement influents (au sens statistique). D'abord, nous calculons pour chaque effet l'intervalle suivant:

Table 2.5: Analyse de Yates en utilisant les données du tableau 2.4.

$V_b(\mathbf{x})$ D_{shy} $\cdots$h	2 (Réponses)	3	4	$\cdots$	15			Estimations des effets		
- - - $\cdots$ −	2.4655	4.9310	9.8619		**1.5788e^4**	=	$g(T)$	Moyenne	=	1.9272
+ - - $\cdots$ −	2.4655	4.9310	5.4636		7.566	=	$g(V_b(\mathbf{x}))$	$E(V_b(\mathbf{x}))$	=	0.0018
- + - $\cdots$ −	2.4655	2.7318	9.0567		10.8394	=	$g(D_{shy})$	$E(D_{shy})$	=	0.0026
+ + - $\cdots$ −	2.4655	2.7318	8.7169	$\cdots$	-2.3343	=	$g(V_b(\mathbf{x}),\, D_{shy})$	$E(V_b(\mathbf{x})\, D_{shy})$	=	$-5.7e^{-4}$
- - + $\cdots$ −	1.3659	4.5284	9.8619		$-7.9e^3$	=	$g(K_{tg})$	$E(K_{tg})$	=	-1.9276
+ - + $\cdots$ −	1.3659	4.5284	5.4636		14.7048	=	$g(V_b(\mathbf{x}),\, K_{tg})$	$E(V_b(\mathbf{x})\, K_{tg})$	=	0.0036
			$\vdots$							
+ + + $\cdots$ +	0.6135	0.0106	0.0106		-73.9056	=	$g(V_b(\mathbf{x})\cdots, h)$	$E(V_b(\mathbf{x})\cdots h)$	=	-0.018
Totale	**1.5788e^4**									
Somme des carrées	5.8508e^4				4.7929$e^8/2^{13}$	=	5.8508e^4			

$$\text{Effet} \pm t_{\nu,\alpha/2} * (SE(\text{effet})) \tag{2.28}$$

où $t_{\nu,\alpha/2}$ est la distribution t de student, ν est le nombre de degrès de liberté, $100(1-\alpha)\%$ est l'intervalle de confiance et SE(effet) est l'erreur standard.

SE est défini par:

$$SE(\text{effet}) = SE(\bar{y}_+ - \bar{y}_-) = 2s/\sqrt{N} \tag{2.29}$$

où s^2 est une estimation de la variance des erreurs σ^2. Pour un plan d'expérience avec répétition, une estimation de σ^2 peut être obtenue en regroupant les estimations de variances calculées pour chaque ensemble de réplicats. Dans notre étude, nous n'avons pas fait de répétitions. Dans ce cas, il faut une autre procédure pour trouver une estimation de σ^2. Nous utilisons l'analyse de variance pour un plan factorial complet 2^k.

Il est possible de mesurer la variabilité des observations en calculant $\sum (y_i - \bar{y})^2 = \sum y_i^2 - (\sum y_i)^2/N$, pour $i = 1, 2, \ldots, N$ où y_i sont les réponses et $\bar{y}$ leur moyenne globale [44]. Dans ce cas, une estimation de σ^2 est donnée par $s^2 = \sum (y_i - \bar{y})^2/(N-1)$. Par contre, les influences des facteurs choisis pour l'étude contribuent aussi à la variance des observations. Afin de trouver la contribution de chaque facteur, nous calculons la somme des carrés donnée par $SSq = N * (\text{effet})^2/4$ avec un seul degré de liberté (tableau 2.6).

Table 2.6: Analyse de variance pour le plan factoriel 2^{13}.

Source of Variation			SSq	DF
Totale	=	$\sum (y_i - \bar{y})^2$	2.8082e^4	8192
$V_b(\mathbf{x})$ effet	=	$2^{13}(0.0018)^2/4$	0.007	1
D_{shy} effet	=	$2^{13}(0.0026)^2/4$	0.0143	1
$V_b(\mathbf{x})\, D_{shy}$ effet	=	$2^{13}(-5.7e^4)^2/4$	6.65e^{-4}	1
K_{tg} effet	=	$2^{13}(-1.9276)^2/4$	7.6093e^3	1
$V_b(\mathbf{x})\, K_{tg}$ effet	=	$2^{13}(0.0036)^2/4$	0.0264	1
		$\vdots$		
$V_b(\mathbf{x}) \cdots h$ effet	=	$2^{13}(-0.018)^2/4$	0.6668	1
Somme des carrés des résidus			0	0

Après avoir attribué une variance à chaque effet, la variance qui reste est représentée par la somme des carrés des résidus. Dans le tableau 2.6, la somme des carrés des résidus est égale à 0 car toutes les sources de variance (8192 effets) ont été considérés.

Pour estimer σ^2 pour ce plan d'expérience sans répétition, il est nécessaire de considérer que certains effets sont des manifestations de bruits et n'ont aucune véritable influence [44]. Nous avons décidé de négliger les interactions de l'ordre 7 et plus. En sommant leurs SSq et leurs degrés de liberté nous obtenons une estimation de la variance $s^2 = 602.81/4096 = 0.1472$ avec $\nu = 4096$ degrés de liberté. L'estimation de l'écart type est $s = 0.3837$. L'erreur standard est alors $SE(\text{effet}) = 2s/\sqrt{N} = 0.0085$ et l'intervalle de confiance à $100(1-\alpha)\%$ est:

$$\pm\, t_{\nu,\alpha/2} * SE(effect) = \pm t_{4096,0.025} * 0.0085 = \pm 0.0167 \tag{2.30}$$

Les effets restants (4096) ont un intervalle de confiance à 95% donné par Effet $\pm$ 0.0167. Si, pour un effet donné, son intervalle contient 0, il est considéré comme non influent. Nous avons ainsi trouvé 461 effets significativement influents dont 10 effets principaux, 41 interactions d'ordre 2, 74 d'ordre 3, 112 d'ordre 4, 121 d'ordre 5 et 103 d'ordre 6. Un diagramme de Pareto (Fig. 2.26) montre les effets significativement influents dans l'ordre décroissant. Pour des raisons de clarté, seuls 30 effets parmi les 461 sont illustrés. Les effets principaux et les interactions d'ordre deux sont présentés sur les Fig. 2.27 et 2.28. Dans la Fig. 2.27, plus la ligne est inclinée plus l'effet du facteur est influent. Dans la Fig. 2.28, si la ligne continue et celle pointée sont parallèles alors il n'y a aucune interaction entre les deux facteurs.

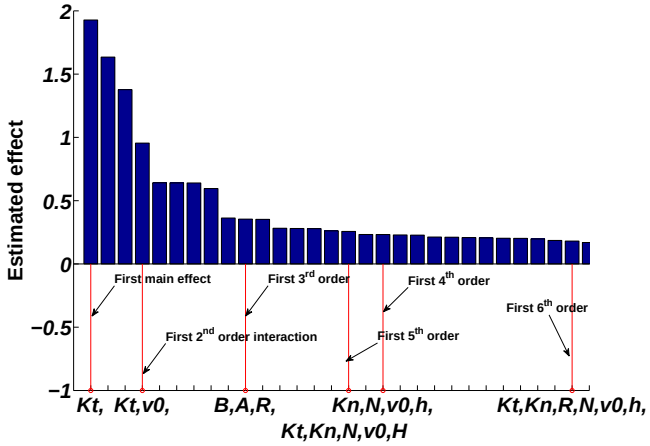

Figure 2.26: Effets significativement influents dans l'ordre décroissant en prenant en compte les interactions jusqu'à l'ordre 6.

2.6.5 Modèles de regression

Après avoir identifié les p effets significativement influents, nous construisons les modèles de regression qui predisent la réponse du modèle de foule. Ces modèles ont pour expression:

$$\hat{\mathbf{y}}_i = \mathbf{E}\beta \tag{2.31}$$

où $\beta = [\beta_0, \beta_1, \cdots, \beta_{p-1}]^T$ est un vecteur qui regroupe les coefficients du modèle et $\mathbf{E}$ est appelée matrice des effets et peut s'écrire de façon formelle par:

$$\mathbf{E} = \begin{pmatrix} 1 & e_{11} & e_{12} & \dots & e_{1p-1} \\ 1 & e_{21} & e_{22} & \dots & e_{2p-1} \\ \vdots & \vdots & \vdots & \ddots & \vdots \\ 1 & e_{N1} & e_{N2} & \dots & e_{Np-1} \end{pmatrix} \tag{2.32}$$

où e_{ij} représente l'état d'un facteur. Nous construisons 12 modèles en augmentant à chaque fois l'ordre des interactions prises en compte afin d'examiner la précision de chaque modèle de regression. Par exemple, pour le modèle d'ordre 1, aucune interaction n'est prise en compte. Pour le modèle 2 les interactions juqu'à l'ordre 2 sont prises en compte et ainsi de suite. Ensuite, nous effectuons une analyse de variance (ANOVA) pour chaque modèle afin d'estimer le niveau de variablité. Pour cela, nous calculons la somme des carrés, SS, associée aux sources indiquées dans la première colonne du tableau 6.9 où $SST = SSM + SSE$. Le coefficient de détermination R^2, compris entre 0 et 1, représente la part de variance de y expliqué par le modèle. Sa définition est donnée par le rapport entre la variance de $\hat{y}_i$ et celle de y_i

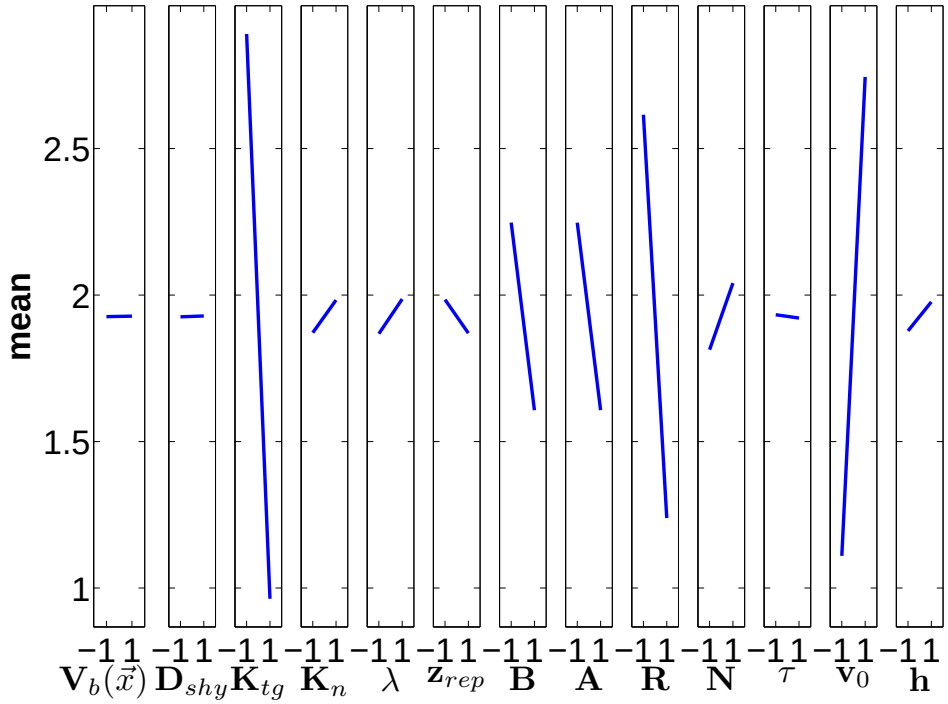

Figure 2.27: Effets principaux du plan d'expérience 2^{13}.

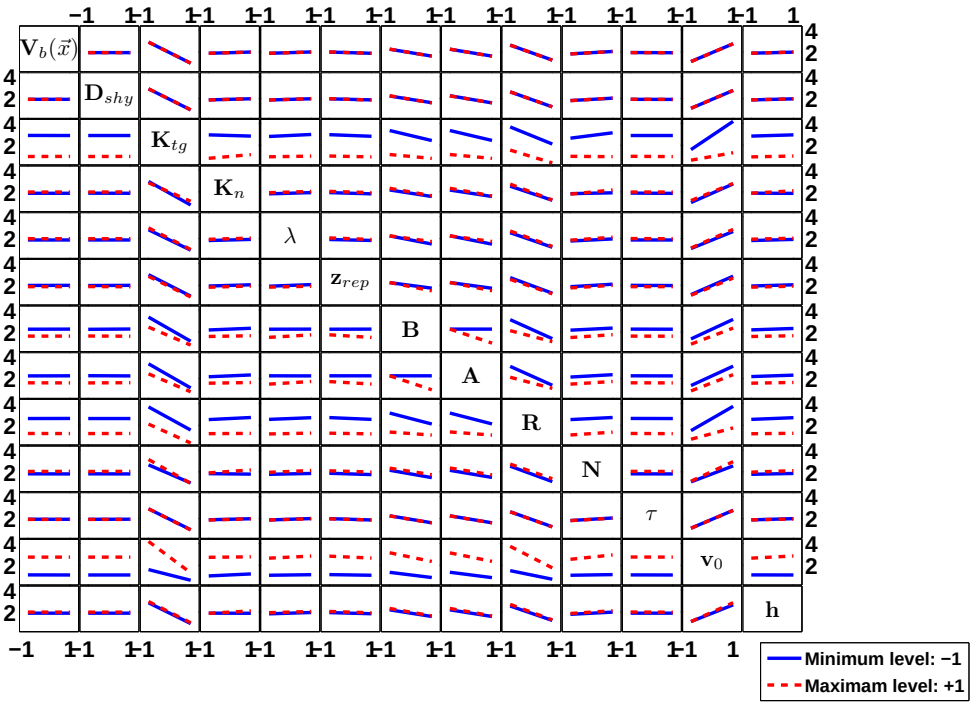

Figure 2.28: Interactions d'ordre 2 des facteurs du plan d'expérience 2^{13}.

Table 2.7: Tableau de l'analyse de variance (ANOVA).

Source	SS	ddl
Régression	$SSM = \sum_{i=1}^{N} (\hat{y}_i - \bar{y})^2$	p-1
Résidus	$SSE = \sum_{i=1}^{N} (y_i - \hat{y}_i)^2$	N-p
Total	$SST = \sum_{i=1}^{N} (y_i - \bar{y})^2$	N-1

$$R^2 = \frac{SS_r}{SS_t} \tag{2.33}$$

Si R^2 est nul, le modèle n'explique rien et un R^2 égal à 0,9 signifie que 90% des variations sont expliquées par le modèle. La Fig. 6.19 montre la valeur de R^2 obtenue pour chacun des 12 modèles construits.

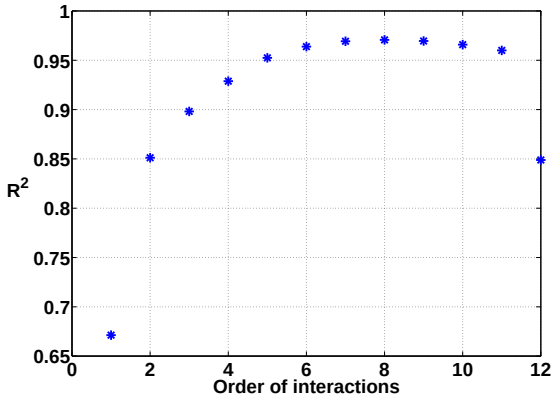

Figure 2.29: Valeur de R^2 pour chacun des 12 modèles construits.

Parmi ces modèles, nous avons ainsi trouvé que celui qui contient les interactions jusqu'à l'ordre 8 (avec 664 coefficients correspondant aux effets significativement influents) donne la plus grande valeur de $R^2 = 97\%$. En revanche, le modèle construit avec les effets jusqu'à l'ordre 3 (104 coefficients) donne $R^2 = 90\%$. Le choix du modèle de régression est donc un compromis entre sa complexité et la précision requise.

La prochaine étape sera de valider le modèle de régression choisi par rapport au modèle numérique (notre modèle de piéton) pour des valeurs intermédiaires des facteurs (entre les valeurs maximum et minimum utilisées pour cette étude). Ensuite, le modèle de régression doit être validé par rapport aux résultats empiriques. Finalement, on pourra l'utiliser pour calculer les valeurs de flux au travers d'un goulot d'étranglement sans faire des simulations.

Après avoir présenté les travaux qui on été faits sur les stratégies de déplacement, les interactions piéton-piéton, nous présentons dans la section suivante une application de notre modèle sur le cheminement des piétons en gare.

2.7 Cheminement des piétons en gare

En collaboration avec le Laboratoire Ville Mobilité Transport (LVMT), nous avons utilisé notre modèle de foule pour simuler le cheminement des piétons à la gare de Noisy-Champs. L'objectif de cette étude est d'estimer le temps de stationnement des trains dans cette gare.

2.7.1 Géométrie de la gare de Noisy-Champs

La gare de Noisy-champs a deux entrées/sorties et le quai s'étend sur 300 m (Fig. 2.30). Pour la modéliser, nous avons divisé la gare en trois zones principales en considérant les trois étapes suivantes: Entrer-sortir, accéder au quai, embarquer-débarquer. Ces trois zones sont illustrées dans les Figures 2.31 et 2.32. La zone 1 est divisée en trois sous-zones car il existe trois entrées-sorties dans la gare.

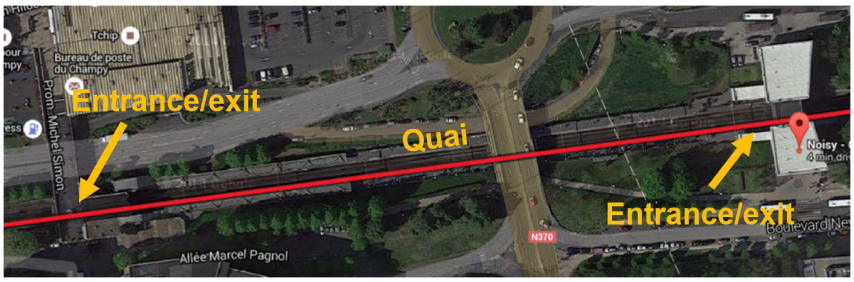

Figure 2.30: Vue aérienne de la gare de Noisy-Champs.

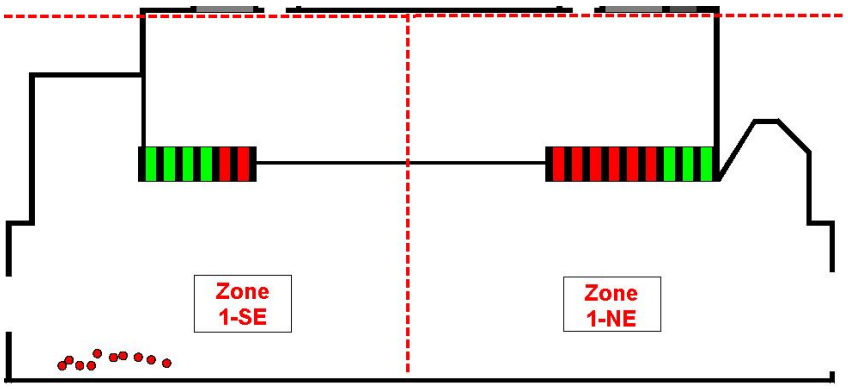

(a)

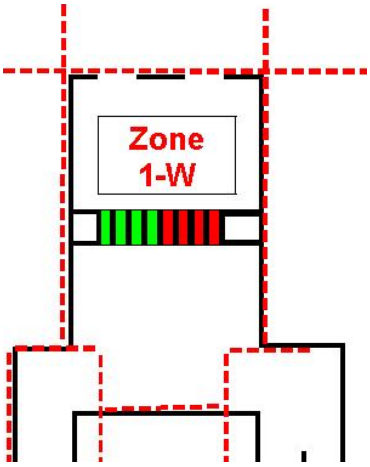

(b)

Figure 2.31: Entrées-sorties de la gare de Noisy-champs coté (a) est et (b) ouest.

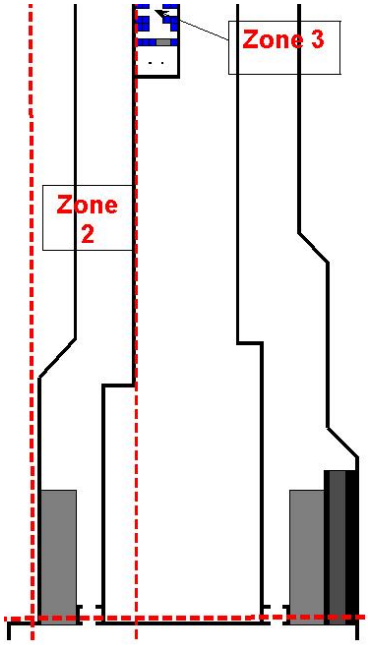

Figure 2.32: Quai de la gare de Noisy-Champs (direction Paris).

2.7.2 Trafic des trains

Nous nous intéressons à l'intervalle de temps entre deux trains consécutifs aux heures de pointe. Cet intervalle de temps est appelé headway et a pour expression:

$$H = \frac{60}{f} \tag{2.34}$$

où H est le headway en minute et f la fréquence réelle (observée) des trains par heure.

En théorie, 12 trains par heure sont censés passer par la gare de Noisy-Champs pendant les heures de pointe. En réalité, il n'y a en moyenne que 10 trains par heure ce qui donne un headway H de $6\,min$. Par conséquent, nous avons construit le scénario de simulation, illustré dans la Fig. 2.33, à partir de cette valeur de Headway. Le train arrive dans la gare à la $4^{ième}$ minute et les portes s'ouvrent 30 secondes après. Pour ces simulations, le temps d'embarquement sera considéré comme atteint lorsqu'il n'y a aucun piéton à moins de 3 mètres des extrémités du train. Il reste maintenant à intégrer les données du trafic des voyageurs afin de réaliser les simulations numériques.

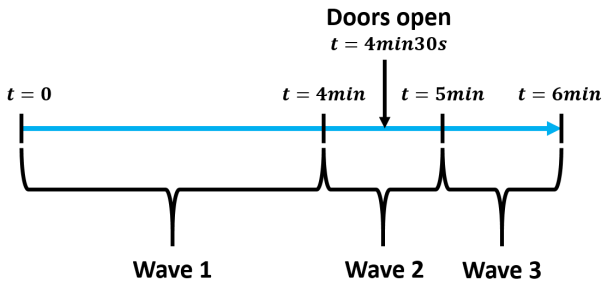

Figure 2.33: Scenario de la simulation numérique.

2.7.3 Trafic des voyageurs

Afin d'estimer le temps de stationnement des trains à quai, il est important de recueillir les données des flux de passagers et leurs caractéristiques. Dans la suite, nous présentons comment les flux des passagers et leurs répartitions spatiale et temporelle ont été obtenues.

Flux des voyageurs

Le modèle CapTA, développé au sein du laboratoire LVMT, affecte les trafics des voyageurs aux itinéraires sur un réseau de transport collectif soumis aux contraintes de capacité suivantes : à l'intérieur du véhicule, dans les mouvements de montée-descente, ainsi que dans loccupation de la voie [45]. A l'aide de ce modèle, nous avons pu obtenir le flux des usagers de la ligne A (direction est- ouest). Nous avons listé, dans le Tableau 2.8, le flux des passagers qui montent - à partir des stations entre Marne-la-Vallée et Noisiel et descendent à Noisy Champs. Dans le tableau 2.9, le flux des passagers qui montent à Noisy-Champs et descendent dans chaque station de la ligne A en aval, est indiqué.

Table 2.8: Flux des voyageurs descendant à Noisy-Champs

Station	**Train freq.**	**Flux** (par heure)	**Flux** (par train)
Marne-la-Vallée	7	115	16
Val d'Europe	7	49	7
Bussy-Saint-Georges	7	99	14
Torcy	14	161	12
Lognes	10	84	8
Noisiel	10	15	2
Totale		**522**	**59**

Table 2.9: Flux des voyageurs montant à Noisy-Champs.

Station	**Train freq.**	**Flux** (par heure)	**Flux** (par train)
Noisy-le-Grand	14	134	9
Bry-sur-Marne	5	0	0
Neuilly plaisance	9	34	4
Val de Fontenay	14	176	13
Vincennes	14	70	5
Nation	14	811	58
Gare de Lyon	14	446	32
Chatelet	14	629	45
Auber	14	699	50
Charles de Gaulle-Etoile	14	620	44
La Défense	14	438	31
Nanterre Pr.	7	19	3
Sartrouville	6	8	1
Achères Ville	4	15	1
Conflans- fin d'Oise	4	2	1
Neuville Univ.	4	2	1
Cergy Pref.	4	23	5
Cergy St. Chris.	4	5	1
Cergy le Haut	4	1	0
Total		**4117**	**304**

Répartition spatiale des voyageurs sur le quai

Afin de déterminer la répartition des passagers sur le quai, nous avons choisi de diviser le train en trois zones (A,B,C), comme illustré sur la Fig. 2.34. Ensuite, nous avons observé sur le terrain pour chaque station en amont (et en aval) de Noisy-Champs, le pourcentage des passagers qui montent (et descendent) dans chacune des 3 zones. En nous basant sur les tableaux 2.8 et 2.9 et à partir des coefficients de répartition notés durant les observations, nous avons pu déterminer le flux des piétons dans les différentes zones de la plateforme de Noisy-Champs (Fig. 2.34).

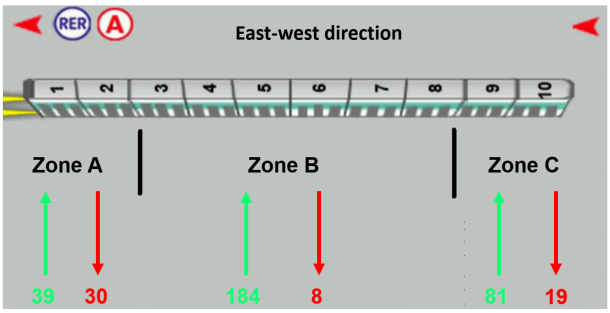

Figure 2.34: La répartition spatiale des voyageurs sur le quai.

Pendant les observations que nous avons faites dans la gare, nous avons pu déterminer trois profils de passagers. Pour chaque profil, nous avons mesuré la durée pendant laquelle les usagers arrivent à la gare et leur vitesse:

- **Profil 1**:
  - durée: 4 min
  - nombre de passagers: 202
  - vitesse moyenne: $1.15\,m/s$ pour ceux arrivant de coté est et $0.95\,m/s$ pour ceux arrivant de côté ouest
- **Profil 2**:
  - durée: 1 min
  - nombre de passagers: 51
  - vitesse moyenne: $1.91\,m/s$ pour ceux arrivant de coté est et $1.5\,m/s$ pour ceux arrivant de côté ouest
- **Profil 3**:
  - durée: 1 min
  - nombre de passagers: 52
  - vitesse moyenne: $3.28\,m/s$ pour ceux arrivant de coté est et $2\,m/s$ pour ceux arrivant de côté ouest

Nous avons fait plusieurs simulations (voir un extraits dans les Fig. 2.35 et 2.36) pour le scenario illustré dans la Fig. 2.33.

2.7.4 Résultats

Comme nous l'avons déja mentionné, l'objectif principal de cette étude est d'estimer l'influence du comportement des passagers à l'interface quai-train à la gare de Noisy-champs et de le comparer avec des observations réelles. Nous avons réalisé 10 simulations numériques. En moyenne, les résultats des simulations sont conformes avec les observations comme l'illustre le tableau 2.10.

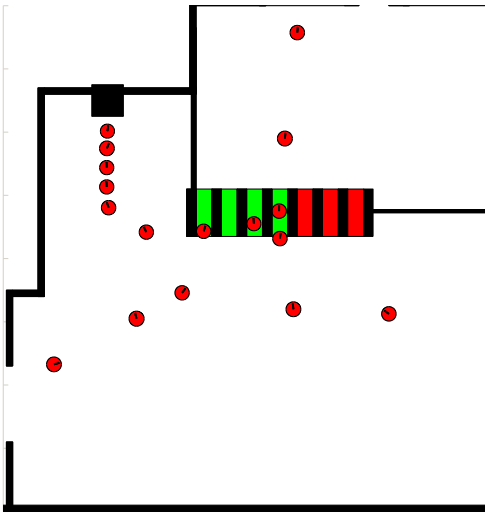

Figure 2.35: Passagers entrant dans la gare, achetant leurs billets et passant par les portiques pour accéder au quai.

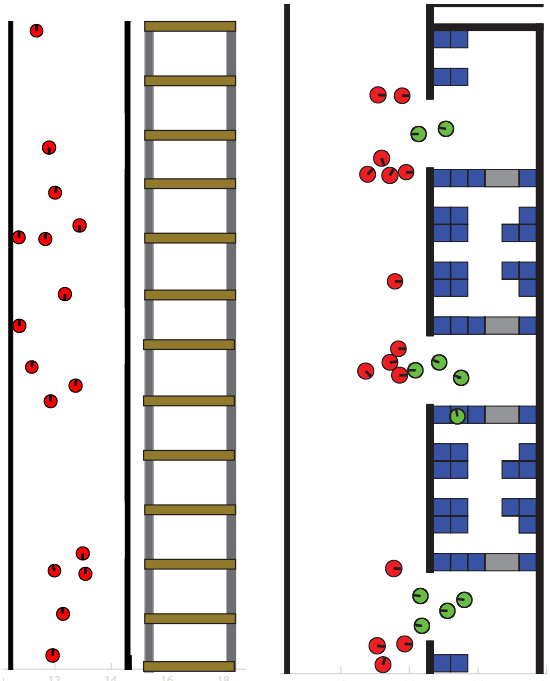

(a) (b)

Figure 2.36: Passagers (a) attendant le train sur le quai et (b) embarquant/débarquant.

De plus, notre modèle est capable de fournir d'autres résultats intéressants. Dans la Fig. 2.37, les nombres de passagers montés et descendus, avec le temps d'échange correspondant, ont été determinés pour chaque porte du train. Il serait intéressant de les comparer avec des observations réelles pour comprendre comment les temps d'échange varient et pour quelles raisons. Nous pouvons aussi étudier la demande sur des zones particulières dans les gares. Par exemple, la Fig. 2.38 montre la demande sur les portiques du côté sud de la zone 1 de la gare. Ce résultat permettra d'estimer si la capacité des portiques est atteinte ou pas.

L'étude que nous avons faite sur le cheminement des piétons à la gare de Noisy-Champs a donné

Table 2.10: Temps de stationnement des trains à quai à la gare de Noisy-Champs.

	Observations			Simulation
Passagers montés	257	242	240	238
Passagers descendus	57	28	64	59
Total	314	270	304	297
Temps de stationnement	27	35	38	32

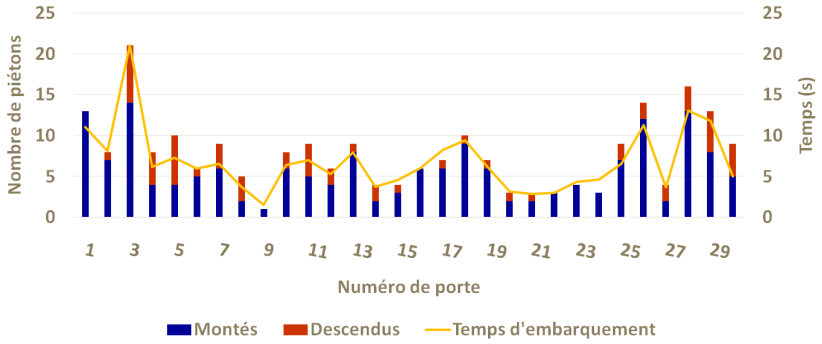

Figure 2.37: Nombre de passagers montés et descendus, avec le temps d'échange correspondant, pour chaque porte du train.

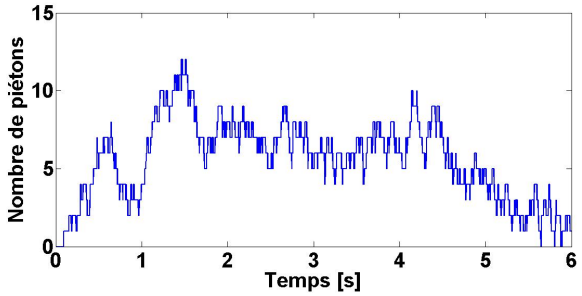

Figure 2.38: Demande au niveau des portiques du coté sud de la zone 1 de la gare.

des résultats prometteurs. Nous souhaitons continuer l'étude en pernant en compte des nouveaux caractérisiques des piétons comme leur âge, physique, agressivité, etc. Nous pouvons aussi élargir l'environnement de simulation afin de prendre en compte l'arrivée des bus à la gare et étudier l'efficacité de l'intermodalité à la gare.

Cette section termine la partie sur la modélisation du mouvement des piétons. Dans la section suivante, nous étudions la modélisation de la force latérale engendrée par un piéton par un oscillateur auto-entretenu.

2.8 Modélisation de la force latérale engendrée par un piéton par un oscillateur auto-entretenu

Le corps humain est un système mécanique très complexe, composé de plusieurs parties en interaction réciproque. Il peut être modélisé suivant le degré de raffinement souhaité et les objectifs à atteindre. Dans le but d'étudier l'interaction foule-structure sur les passerelles piétonnes, on s'intéresse à la modélisation de la force latérale engendrée par un piéton. Un modèle hybride de l'oscillateur auto-entretenu de Van der Pol a été développé dans [46] afin de modéliser cette force. Tout d'abord, en utilisant la transformée de Fourier, la quasi-périodicité de la force latérale est montrée, ce qui a permis d'écrire cette dernière

sous la forme d'une série de Fourier composée des harmoniques impairs. Ensuite, les auteurs se sont inspirés des allures des diagrammes obtenus en traçant la force latérale en fonction du déplacement et de la vitesse, afin de proposer un oscillateur de Van de Pol Modifié (VdPM). Puis, les paramètres du modèle VdPM ont été identifiés par la méthode des moindres carrés. Enfin, la pertinence du modèle VdPM a été confirmée par la correspondance satisfaisante entre celui-ci et l'approximation périodique de la mesure de la force latérale, pour différents piétons et des vitesses de marche différentes.

Dans [46], l'étude précédente a été faite pour 12 sujets et 4 vitesses de marche comprises entre $3.75\,km/h$ et $6\,km/h$. Nous répétons la procédure pour 31 sujets, dont 20 masculins et 11 féminins, et 4 vitesses de marche (entre $1.87\,km/h$ et $3.35\,km/h$), différentes de celles utilisées dans [46] . En outre, cette mixité des participants (masculins/féminins) nous permettra d'identifier les différences éventuelles dans la façon de marcher entre les deux genres. Ces 31 individus ont participé à une expérience concernant l'étude des forces dues à la marche d'un piéton sur un plancher rigide (i.e. non susceptible de vibrer sous l'action de la marche) réalisée par l'Université de Sheffield.

En effet, des mesures de forces, engendrées par la marche de piétons sur un plancher rigide, ont été réalisées par l'Université de Sheffield. Ces données ont été analysées afin de déterminer certaines caractéristiques de la marche des piétons et de modéliser la force qu'ils engendrent. Dans ce qui suit, nous décrivons dans un premier temps l'expérience réalisée par l'Université de Sheffield, puis nous présentons le traitement des données, et enfin les résultats de l'analyse effectuée.

2.8.1 Description de l'expérience

Les mesures ont été réalisées sur un tapis roulant équipé de sorte à mesurer les composantes verticale, latérale ($F_y(t)$) et longitudinale de la force qui lui est appliquée (Fig. 8.1). Plusieurs personnes de caractéristiques différentes ont participé à l'expérience. Des séquences de marche de durées différentes à vitesse de marche constante ont été enregistrées pour différentes vitesses de marche (entre 1,87 km/h et 9 km/h). Il faut savoir que 4.5 km/h est une vitesse proche de la vitesse moyenne de marche libre ($v_M = 5,4km/h$) à laquelle la majorité des personnes marche confortablement et naturellement [37]. A chaque fois, les différentes composantes de la force engendrée par le piéton ont été enregistrées avec une fréquence d'acquisition de 200Hz. Les caractéristiques des sujets masculins et féminins sont répertoriées dans les tableaux 8.1 et 8.2 respectivement. Afin d'éviter la confusion, nous faisons référence aux participants masculins et féminins en ajoutant un "msc" et un "fmn" respectivement (exemple : $1-msc$ et $1-fmn$).

Table 2.11: Masse et taille des 20 participants masculins.

Participant	**1**	**2**	**3**	**4**	**5**	**6**	**7**	**8**	**9**	**10**
Masse (kg)	67.5	81.6	81.2	86.6	89.9	86.3	79.6	63.3	89.8	81.7
Taille (cm)	180	175	180	173	174	188	173	188	180	175
Participant	**11**	**12**	**13**	**14**	**15**	**16**	**17**	**18**	**19**	**20**
Masse (kg)	77.1	94.8	80.3	69.2	95.9	68.1	75.4	82.7	73.2	79.8
Taille (cm)	173	173	173	176	183	175	167	178	175	181

Table 2.12: Masse et taille des 11 participantes féminines.

Participant	**1**	**2**	**3**	**4**	**5**	**6**	**7**	**8**	**9**	**10**	**11**
Masse (kg)	55.8	59.6	57.3	50.7	61.9	49.7	49.1	54.5	69.9	55.9	71.6
Taille (cm)	160	160	170	160	171	163	158	166	165	165	160

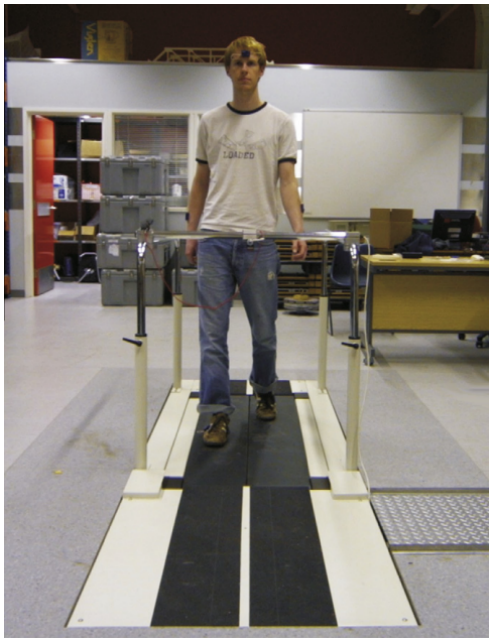

Figure 2.39: Installation expérimentale [47].

2.8.2 Analyse de Fourier de la force latérale

Les signaux expérimentaux ont été analysés en utilisant la transformée de Fourier rapide (FFT) afin d'examiner leur périodicité. Le signal enregistré de la force latérale, $F_y(t)$ et son approximation par serie de Fourier $F_y^{(5)}(t)$ (composée des harmoniques impaires jusqu'à l'ordre 9) pour les piétons 1-msc et 1-fmn sont tracés dans les Fig. 2.40 et 2.41. A part les signaux reconstruits pour (1-msc,$v_x = 2.88\,km/h$) et (1-fmn,$v_x = 2.38\,km/h$), la concordance entre les signaux enregistrés et ceux reconstruits est satisfaisante.

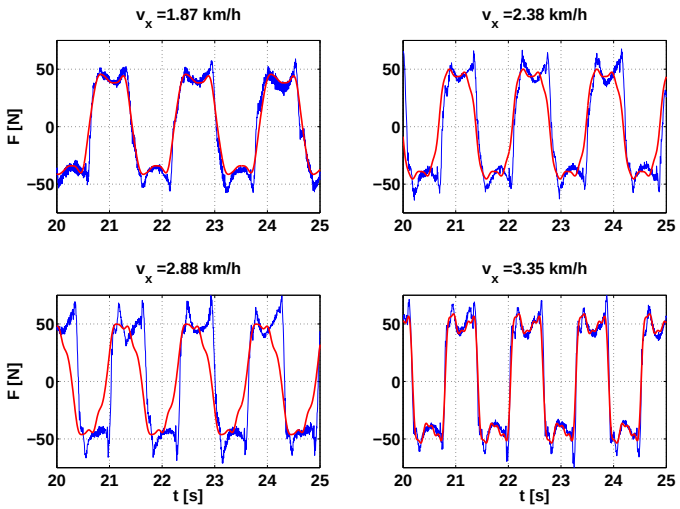

Figure 2.40: Piéton 1-msc : évolution temporelle de la force latérale pour quatre vitesses de marche différentes. Mesure vs. Série de Fourier (ligne en gras)

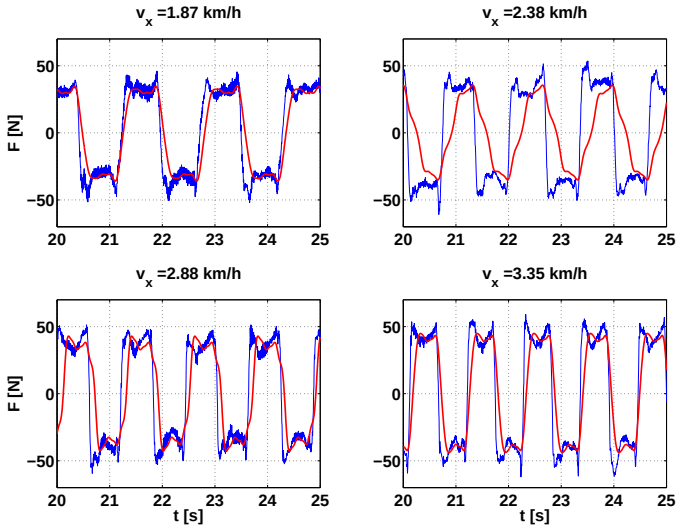

Figure 2.41: Piéton 1-fmn : évolution temporelle de la force latérale pour quatre vitesses de marche différentes. Mesure vs. Série de Fourier (ligne en gras)

2.8.3 Modélisation de la force latérale par un oscillateur auto-entretenu

Dans ce paragraphe, nous testons la validité de la modélisation de la force latérale d'un piéton par un oscillateur hybride Van der Pol/Rayleigh (VdPM) [46]. Dans [46], deux aspects de la force latérale ont poussé les auteurs à se questionner sur la validité d'utiliser un oscillateur auto-entretenu pour la modéliser. Le premier aspect est d'avoir traité la force latérale, $F_y(t)$, le déplacement, $u_y(t)$ et la vitesse, $\dot{v}_{y(t)}$ comme des signaux du temps périodiques. Le deuxième aspect est que les piétons auto-entretiennent leur mouvement pendant la marche. Ainsi, les auteurs ont cherché un oscillateur satisfaisant les critères suivants:

- une équation du mouvement donnée par l'Eq. (2.35) et une force de rappel donnée par l'Eq. (2.36) où $h(u_y(t), \dot{u}_y(t))$ est sous forme polynômiale.

$$m\ddot{u}_y(t) + F_y(u_y(t), \dot{u}_y(t)) = 0 \tag{2.35}$$

$$F_y(u_y(t), \dot{u}_y(t)) = 2\mu m\omega_0 \dot{u}_y(-1 + h(u_y(t), \dot{u}_y(t))) + m\omega_0^2 u_y \tag{2.36}$$

- un cycle limite stable
- un cycle limite de même taille et forme des diagrammes dans le plan de phase similaire à celles obtenues par l'analyse expérimentale des mesures de la force latérale. De plus, tout au long du cycle limite, la valeur force engendrée par l'oscillateur, F_y, doit être proche des valeurs expérimentales.

Après avoir examiné les tracés de la phase et de la force pour les oscillateurs Van der Pol, Rayleigh ainsi que pour les mesures expérimentales, un oscillateur hybride Van der Pol/Rayleigh avec un terme additionnel $F_\gamma = m2\gamma u_y \dot{u}_y^2$ a été proposé. Ce terme est responsable de l'effet adoucissant observé dans l'allure de la force expérimentale pour les grandes valeurs du déplacement (Fig. 2.42 et 2.43) . La force de rappel de cet oscillateur hybride est donnée par :

$$F_y(u_y, \dot{u}_y, \mu, \omega_0, \beta, \gamma, \delta) = 2\mu\omega_0 m\dot{u}_y(-1 + \beta u_y^2 + \frac{\gamma}{\omega_0} u_y \dot{u}_y + \frac{\delta}{\omega_0^2}\dot{u}_y^2) + m{\omega_0}^2 u_y \tag{2.37}$$

où $\beta \geq 0$, $\delta \geq 0$ avec $\beta + \delta \neq 0$, γ est un réel, $\omega_0 > 0$ et $\mu > 0$. En remplaçant l'Eq. (2.37) dans l'Eq. (2.35), on obtient :

$$\ddot{u}_y(t) - 2\mu\omega_0 m\dot{u}_y(1 - \beta u_y^2 - \frac{\gamma}{\omega_0}u_y\dot{u}_y - \frac{\delta}{\omega_0^2}\dot{u}_y^2) + m{\omega_0}^2 u_y = 0 \tag{2.38}$$

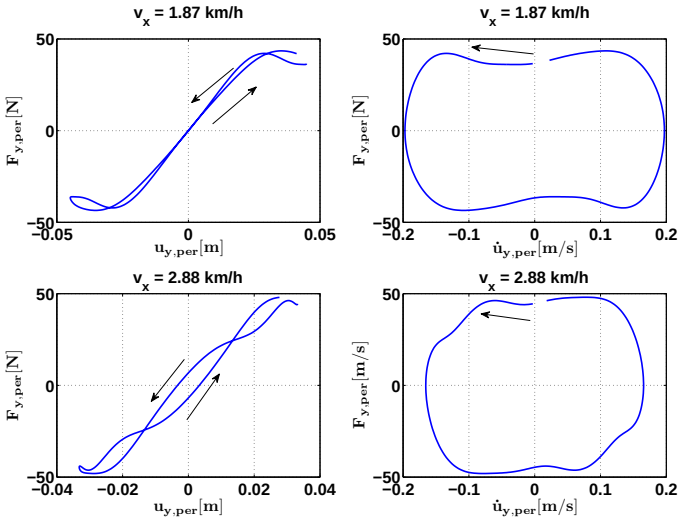

Figure 2.42: Série de Fourier de la force, de la vitesse et du déplacement du piéton 1-msc pour quatre vitesses de marche différentes pour un cycle : $F_y(t) - u_y(t)$ (gauche) et $F_y(t) - \dot{u}_y(t)$ (droite)

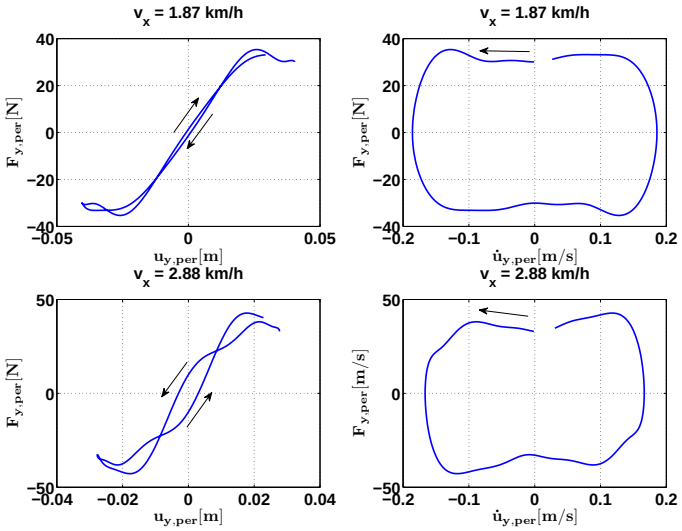

Figure 2.43: Série de Fourier de la force, de la vitesse et du déplacement du piéton 1-fmn pour quatre vitesses de marche différentes pour un cycle : $F_y(t) - u_y(t)$ (gauche) et $F_y(t) - u_y(t)$ (droite)

Afin de calculer les paramètres du modèle VdPM, une méthode basée sur une procédure d'identification des moindres carrés est utilisée [46]. Pour cela, l'Eq. (2.37) est réécrite sous la forme suivante:

$$F = F(u_y, \dot{u}_y, b) = b_1 u_y + b_2\dot{u}_y + b_3{u_y}^2\dot{u}_y + b_4 u_y\dot{u}_y^2 + b_5\dot{u}_y^3 \;\text{ avec }\; b = [b_1, b_2, b_3, b_4, b_5]^T \tag{2.39}$$

Les composantes du vecteur b correspondent alors aux paramètres du modèle VdPM:

$$b = [m{\omega_0}^2,\ -2\mu m\omega_0,\ 2\mu m\omega_0\beta,\ 2\mu m\gamma,\ \frac{2\mu m}{\omega_0}\delta]^T \tag{2.40}$$

Les paramètres optimaux, b^*, sont donc obtenus en minimisant l'erreur entre la nouvelle expression de F et sa série de Fourier obtenue précédemment:

$$b^* = min[\frac{1}{2}\sum_{i=1}^{N_{id}}((F_{y,per}^{(i)} - F(u_{y,per}^{(i)}, \dot{u}_{y,per}^{(i)}, b)))^2] \tag{2.41}$$

où $F_{y,per}^{(i)}$ est calculée par série de Fourier, $\dot{u}_{y,per}^{(i)}$ et $u_{y,per}^{(i)}$ ont été obtenus par intégrations successives de $\ddot{u}_{y,per}^{(i)} = F_{y,per}^{(i)}/m_i$ et N_{id} est le nombre de points utilisé pour la procédure d'identification correspondant à une période.

Les contraintes d'optimisation sont données par:

$$b_1 \geq 0, b_2 \leq 0, b_3 \geq 0 \text{ et } b_5 \geq 0 \tag{2.42}$$

Les Eqs. (2.41) et (2.42) définissent un problème d'optimisation linéaire avec contraintes. Plusieurs fonctions existent dans Matlab pour résoudre ce type de problème. Nous avons choisi d'utiliser la fonction *fmincon*. Une fois b^* calculé, nous pouvons recalculer les paramètres sachant que :
$\omega_0 = \sqrt{\frac{{b_1}^*}{m}}$, $\mu = -\frac{{b_2}^*}{2{b_1}^*}\sqrt{\frac{{b_1}^*}{m}}$, $\beta = -\frac{{b_3}^*}{{b_2}^*}$, $\gamma = -\frac{{b_4}^*}{{b_2}^*}\sqrt{\frac{{b_1}^*}{m}}$, $\delta = -\frac{1}{m}\frac{{b_1}^*}{{b_2}^*}{b_5}^*$, $R = \frac{1}{n}\int\frac{F_{y,per}}{F_y}dt$.

Les paramètres des piétons 1-msc et 1-fmn ont été calculés par la méthode décrite ci-dessus (voir tableaux 2.13 et 2.14). Enfin, en utilisant les paramètres identifiés, la resolution de l'Eq. (2.38) à l'aide d'un solveur ODE de Matlab donne la réponse de l'oscillateur VdPM. Les Fig. 2.44-2.46 illustrent la comparaison entre le modéle VdPM et l'approximation périodique de la mesure pour les piétons 1-msc et 1-fmn et pour deux vitesses de marche. Les paramètres pour tous les piétons ont également été identifiés et sont illustrés sur les Fig. 2.50 et 2.51.

Table 2.13: Paramètres du modèle VdPM du piéton 1-msc.

	1.87 km/h	**2.38 km/h**	**2.88 km/h**	**3.35 km/h**
$\omega_0(rad/s)$	3.468	4.092	4.531	4.223
μ	0.844	0.024	0.044	0.026
$\beta(m^{-2})$	592.3	2601.7	3396.6	3105.4
$\gamma(m^{-2})$	248.6	11037.6	3632.6	26708.5
$\delta(m^{-2})$	308.5	0	0	0
R	0.99	0.99	0.99	0.99

Table 2.14: Paramètres du modèle VdPM du piéton 1-fmn.

	1.87 km/h	**2.38 km/h**	**2.88 km/h**	**3.35 km/h**
$\omega_0(rad/s)$	3.612	4.696	4.663	5.212
μ	0.692	0.001	0.049	0.418
$\beta(m^{-2})$	697.5	160.9	4511.2	1882.0
$\gamma(m^{-2})$	403.8	38325.2	12103.7	1634.8
$\delta(m^{-2})$	387.5	1758.7	0	975.5
R	0.99	0.99	0.99	0.99

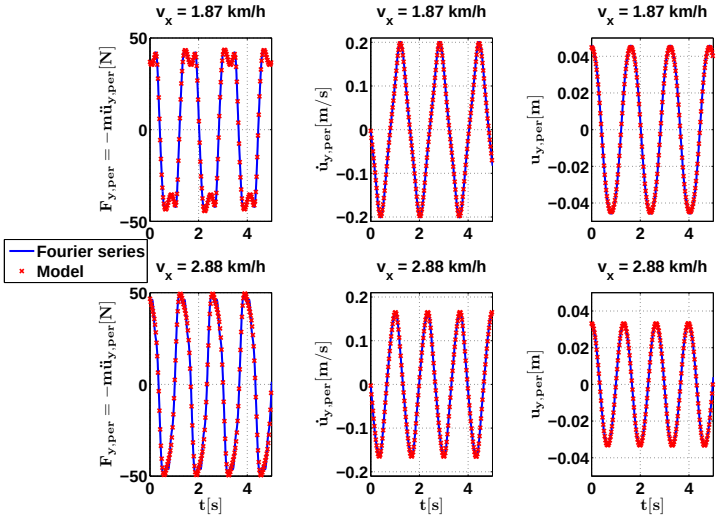

Figure 2.44: Oscillations latérales du piéton 1-msc. Modèle VdPM (croix) vs. série de Fourier (ligne continue): La force latérale (gauche), la vitesse latérale (centre) et le déplacement latéral (droite)

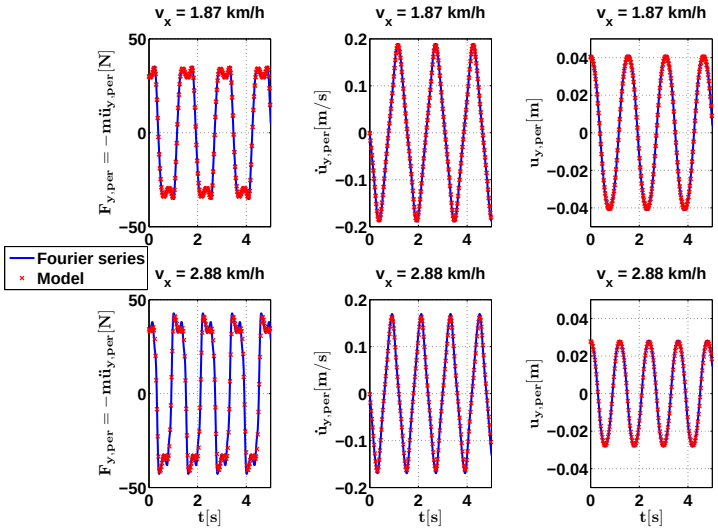

Figure 2.45: Oscillations latérales du piéton 1-fmn. Le Modèle VdPM (croix) vs. série de Fourier (ligne continue): La force latérale (gauche), la vitesse latérale (centre) et le déplacement latéral (droite)

2.8.4 Conclusion

Le but de cette section est de valider la représentation du comportement dynamique d'un piéton par un oscillateur auto-entretenu [46]. Il s'agit d'une version modifiée de l'oscillateur de Van der Pol qui nécessite que la force latérale engendrée par un piéton soit périodique.

Nous avons réalisé l'étude décrite dans cette section pour 20 sujets masculins et 11 féminins afin de déterminer s'il existe des différences entre les deux genres. En premier lieu, nous avons trouvé que les femmes possèdent une fréquence de marche plus élevée que les hommes. Les amplitudes des harmoniques diminuent plus rapidement chez les hommes que chez les femmes. Ensuite, en moyenne, la différence de phase entre la première et le troisième harmonique était supérieure à π chez les femmes et inférieure à π chez les hommes. En dernier lieu, les cycles limites tendent à converger pour les femmes lorsque la vitesse de marche augmente, ce qui n'est pas le cas chez les hommes (pour les quatre vitesses de marche étudiées).

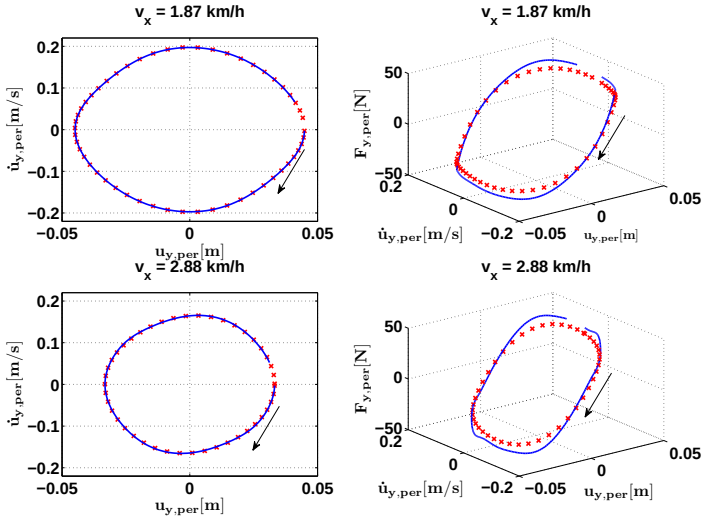

Figure 2.46: Oscillation latérale du piéton 1-msc. Modèle VdPM (croix) vs. Série de Fourier (ligne continue): Cycle limite dans le plan de phase (gauche); Diagramme paramétrique 3D avec déplacement, vitesse et force latérale (droite)

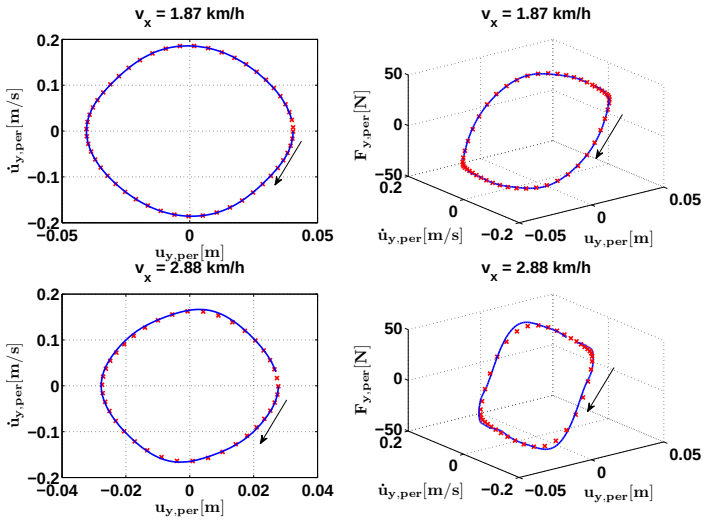

Figure 2.47: Oscillation latérale du piéton 1-fmn. Le Modèle VdPM (croix) vs. Série de Fourier (ligne continue): Cycle limite dans le plan de phase (gauche); Diagramme paramétrique 3D avec déplacement, vitesse et force latérale (droite)

Pour conclure, il est difficile de prononcer sur l'origine de la différence trouvée entre les hommes et les femmes. La faible diversité des participantes féminines, trop peu nombreuses, peut être à l'origine de cette différence. Une étude avec des sujets ayant des caractéristiques plus diverses serait nécessaire.

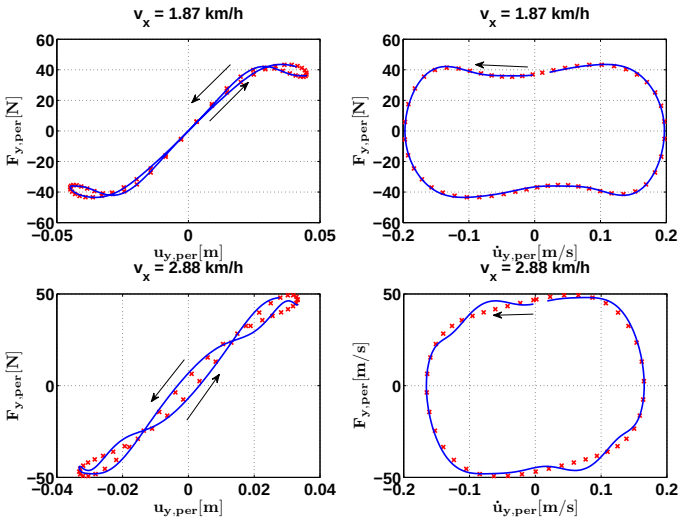

Figure 2.48: Oscillation latérale du piéton 1-msc. Modèle VdPM (croix) vs. Série de Fourier (ligne continue): la série de Fourier de la force, de la vitesse et du déplacement du piéton 1-msc pour quatre vitesses de marche différentes pour un cycle $F_y(t) - u_y(t)$ (gauche) et $F_y(t) - \dot{u}_y(t)$ (droite)

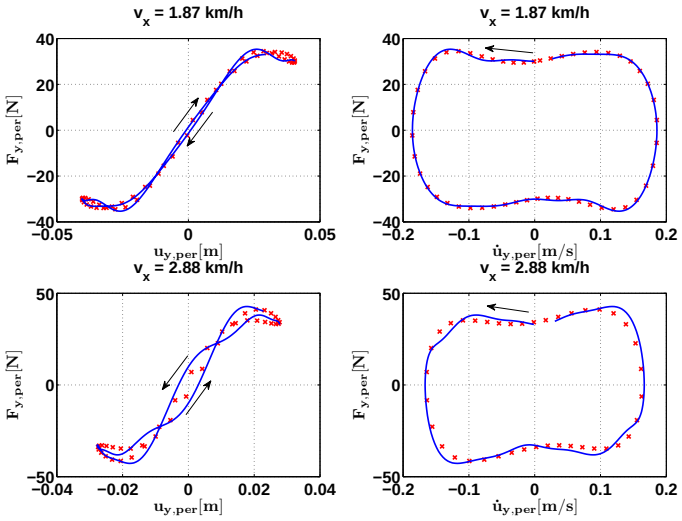

Figure 2.49: Oscillation latérale du piéton 1-fmn. Modèle VdPM (croix) vs. Série de Fourier (ligne continue): la série de Fourier de la force, de la vitesse et du déplacement du piéton 1-fmn pour quatre vitesses de marche différentes pour un cycle $F_y(t) - u_y(t)$ (gauche) et $F_y(t) - \dot{u}_y(t)$ (droite)

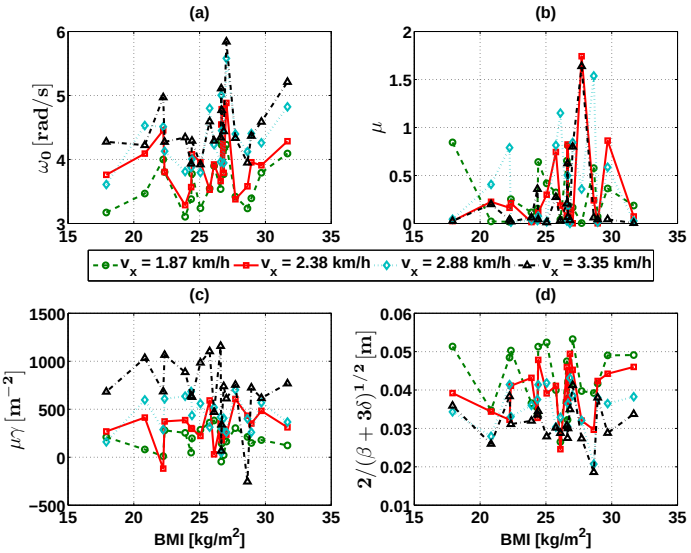

Figure 2.50: Paramètres du modèle VdPM pour les piétons masculins

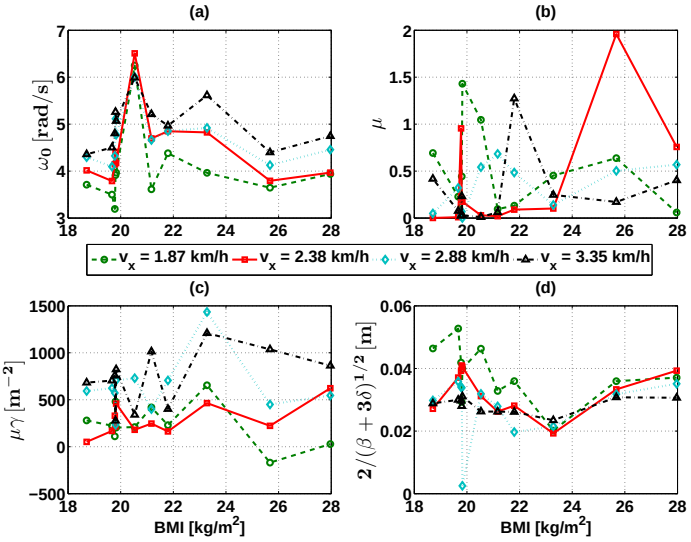

Figure 2.51: Paramètres du modèle VdPM pour les piétons féminins

Bibliography

[1] J. J. Fruin, "Designing for pedestrians: a level-of-service concept," in *Highway Research Record-50th Annual Meeting of the Highway Research Board*, pp. 1–15, 1971.

[2] J. Milazzo, N. Rouphail, J. Hummer, and D. Allen, "Effect of pedestrians on capacity of signalized intersections," *Transportation Research Record: Journal of the Transportation Research Board*, no. 1646, pp. 37–46, 1998.

[3] R. L. Hughes, "A continuum theory for the flow of pedestrians," *Transportation Research Part B: Methodological*, vol. 36, no. 6, pp. 507–535, 2002.

[4] J. Bodgi, *Synchronisation piétons-structure: Applications aux vibrations des passerelles souples*. PhD thesis, Ecole Nationale des Ponts et Chaussees, 2008.

[5] C. W. Reynolds, "Flocks, herds and schools: A distributed behavioral model," *ACM SIGGRAPH Computer Graphics*, vol. 21, no. 4, pp. 25–34, 1987.

[6] D. Helbing and P. Molnàr, "Social force model for pedestrian dynamics," *Physical Review E*, vol. 51, no. 5, pp. 4282–4286, 1995.

[7] J. Venel and B. Maury, *Modélisation mathématique des mouvements de foule*. PhD thesis, Laboratoire de Mathématiques, Université Paris XI, Orsay, France, 2008.

[8] V. Blue and J. Adler, "Cellular automata microsimulation of bidirectional pedestrian flows," *Transportation Research Record: Journal of the Transportation Research Board*, no. 1678, pp. 135–141, 1999.

[9] N. Bellomo, M. Delitala, and V. Coscia, "On the mathematical theory of vehicular traffic flow I: Fluid dynamic and kinetic modelling," *Mathematical Models and Methods in Applied Sciences*, vol. 12, no. 12, pp. 1801–1843, 2002.

[10] B. Piccoli and A. Tosin, "Pedestrian flows in bounded domains with obstacles," *Continuum Mechanics and Thermodynamics*, vol. 21, no. 2, pp. 85–107, 2009.

[11] B. Piccoli and A. Tosin, "Time-evolving measures and macroscopic modeling of pedestrian flow," *Archive for Rational Mechanics and Analysis*, vol. 199, no. 3, pp. 707–738, 2011.

[12] S. Paris, *Caractérisation des niveaux de services et modélisation des circulations de personnes dans les lieux d'échanges*. PhD thesis, Université de Rennes 1, 2007.

[13] W. Song, Y. Yu, B. Wang, and W. Fan, "Evacuation behaviors at exit in CA model with force essentials: A comparison with social force model," *Physica A*, vol. 371, no. 2, pp. 658–666, 2006.

[14] K. Yamamoto, S. Kokubo, and K. Nishinari, "Simulation for pedestrian dynamics by real-coded cellular automata (RCA)," *Physica A: Statistical Mechanics and its Applications*, vol. 379, no. 2, pp. 654–660, 2007.

[15] H. Yue, H. Hao, X. Chen, and C. Shao, "Simulation of pedestrian flow on square lattice based on cellular automata model," *Physica A: Statistical Mechanics and its Applications*, vol. 384, no. 2, pp. 567–588, 2007.

[16] D. Helbing, I. J. Farkas, P. Molnar, and T. Vicsek, "Simulation of pedestrian crowds in normal and evacuation situations," *Pedestrian and evacuation dynamics*, vol. 21, pp. 21–58, 2002.

[17] D. Helbing, "Traffic and related self-driven many-particle systems," *Reviews of modern physics*, vol. 73, no. 4, p. 1067, 2001.

[18] D. R. Parisi, M. Gilman, and H. Moldovan, "A modification of the Social Force Model can reproduce experimental data of pedestrian flows in normal conditions," *Physica A: Statistical Mechanics and its Applications*, vol. 388, no. 17.

[19] D. Helbing, I. Farkas, and T. Vicsek, "Simulating dynamical features of escape panic," *Nature*, vol. 407, pp. 487–490, 2000.

[20] P. Cundall, "A computer model for simulating progressive, large-scale movements in blocky rock systems," in *Proceedings of the international symposium on rock fracture*, vol. 1, (Nancy, France), pp. 129–136, International Society for Rock Mechanics (ISRM), 1971.

[21] N. Pelechano, J. M. Allbeck, and N. I. Badler, "Controlling individual agents in high-density crowd simulation," in *Proceedings of the 2007 ACM SIGGRAPH/Eurographics symposium on Computer animation*, pp. 99–108, Eurographics Association, 2007.

[22] P. Pécol, S. D. Pont, S. Erlicher, and P. Argoul, "Modelling crowd-structure interaction," in *XVIIth Symposium Vibrations, Chocs et Bruit, Ecole Centrale de Lyon*, (Ecully, France), 2010.

[23] P. Pécol, S. Dal Pont, S. Erlicher, and P. Argoul, "Smooth/non-smooth contact modeling of human crowds movement: numerical aspects and application to emergency evacuations," *Annals of Solid and Structural Mechanics*, vol. 2, no. 2-4, pp. 69–85, 2011.

[24] P. Pécol, P. Argoul, S. D. Pont, and S. Erlicher, "The non-smooth view for contact dynamics by Michel Frémond extended to the modeling of crowd movements," *Discrete and Continuous Dynamical Systems - Series S*, vol. 6, no. 2, pp. 547–565, 2012.

[25] P. Pécol, P. Argoul, S. Dal Pont, and S. Erlicher, "A new crowd movement modeling for pedestrians who hold hands," *Vibrations, Shocks and Noise*, 2012.

[26] M. Moussaïd, N. Perozo, S. Garnier, D. Helbing, and G. Theraulaz, "The walking behaviour of pedestrian social groups and its impact on crowd dynamics," *PLoS ONE*, vol. 5, no. 4, p. e10047, 2010.

[27] H. Singh, R. Arter, L. Dodd, P. Langston, E. Lester, and J. Drury, "Modelling subgroup behaviour in crowd dynamics DEM simulation," *Applied Mathematical Modelling*, vol. 33, no. 12, pp. 4408–4423, 2009.

[28] F. Caselli and M. Frémond, "Collision of three balls on a plane," *Computational Mechanics*, vol. 43, no. 6, pp. 743–754, 2008.

[29] C. Cholet, "Collisions d'un point et d'un plan," *Comptes Rendus de l'Académie des Sciences - Series I - Mathematics*, vol. 328, no. 5, pp. 455–458, 1999.

[30] S. Dal Pont and E. Dimnet, "Theoretical approach to and numerical simulation of instantaneous collisions in granular media using the A-CD2 method," *Communications in Applied Mathematics and Computational Science*, vol. 3, no. 1, pp. 1–24, 2008.

[31] M. Frémond, *Collisions*. Roma, Italie: Università di Roma Tor Vergata, dipartimento di ingegneria civile, 2007.

[32] M. Frémond, "Rigid bodies collisions," *Physics Letters A*, vol. 204, no. 1, pp. 33–41, 1995.

[33] J. J. Moreau, "Sur les lois de frottement, de plasticité et de viscosité," *Comptes Rendus de l'Académie des Sciences Paris 271 - Series A*, pp. 608–611, 1970.

[34] R. Kimmel and J. Sethian, "Fast marching methods for computing distance maps and shortest paths," Tech. Rep. 669, University of California, Berkley, 1996.

[35] H. Bruns, "Das eikonal," *Abhandlungen der Mathematisch-Physischen Classe der Königlich Sächsischen Gesellschaft der Wissenschaften*, 1895.

[36] W.-K. Jeong and R. Whitaker, "A fast eikonal equation solver for parallel systems," in *SIAM conference on Computational Science and Engineering*, 2007.

[37] L. Henderson, "The Statistics of Crowd Fluids," vol. Nature, 229, pp. 381–383, 1971.

[38] B. Steffen and A. Seyfried, "Methods for measuring pedestrian density, flow, speed and direction with minimal scatter," *Physica A: Statistical mechanics and its applications*, vol. 389, no. 9, pp. 1902–1910, 2010.

[39] M. Moussaïd, D. Helbing, and G. Theraulaz, "How simple rules determine pedestrian behavior and crowd disasters," *Proceedings of the National Academy of Sciences*, vol. 108, no. 17, pp. 6884–6888, 2011.

[40] T. Kretz, A. Grünebohm, and M. Schreckenberg, "Experimental study of pedestrian flow through a bottleneck," *Journal of Statistical Mechanics: Theory and Experiment*, vol. 2006, no. 10, p. P10014, 2006.

[41] A. Seyfried, O. Passon, B. Steffen, M. Boltes, T. Rupprecht, and W. Klingsch, "New insights into pedestrian flow through bottlenecks," *Transportation Science*, vol. 43, no. 3, pp. 395–406, 2009.

[42] W. Song, W. Lv, and Z. Fang, "Experiment and modeling of microscopic movement characteristic of pedestrians," *Procedia Engineering*, vol. 62, pp. 56–70, Jan. 2013.

[43] D. Duhamel, *Faire une mesure en mécanique.* Presses des Ponts, 2014.

[44] J. Juran and A. Joseph, *Juran's Quality Handbook: The Complete Guide to Performance Excellence, Sixth Edition.* McGraw Hill, 1999.

[45] E. Chandakas, F. Leurent, and A. Poulhès, "Les contraintes de capacité dans les trafics de voyageurs et de véhicules en transport collectif: un modèle de simulation et son application au Grand Paris," pp. 1–10, Congrès ATEC ITS France 2014 : Les Rencontres de la Mobilité Intelligente, 2014.

[46] S. Erlicher, A. Trovato, and P. Argoul, "Modeling the lateral pedestrian force on a rigid floor by a self-sustained oscillator," *Mechanical Systems and Signal Processing*, vol. 24, no. 5, pp. 1579–1604, 2010.

[47] V. Racic and J. Brownjohn, "Mathematical modelling of random narrow band lateral excitation of footbridges due to pedestrians walking," *Computers & Structures*, vol. 90-91, pp. 116–130, Jan. 2012.

Chapter 3

Modeling pedestrian and crowd dynamics

Contents

3.1 Introduction

Modeling helps to better understand complex systems and gain an insight into how they function. When building a model, it is necessary to define the different rules governing individual behavior and interactions with its surrounding. Then, the numerical simulations, obtained by implementing the model, allow to evaluate the dynamics of the system in a collective context. Using modeling as a tool to study complex systems offers several interests and advantages. First of all, it allows to examine the emergence of collective phenomena and find if they are caused or related to a particular individual behavior. Secondly, modeling allows to reproduce certain scenarios that are difficult or impossible to reproduce experimentally (situations that put pedestrians at risk). In these cases, the obtained results might not be validated experimentally but they still offer an important insight into the system's properties in those conditions. Lastly, crowd models can be used to examine the quality of the flow of pedestrian traffic (ingress-circulation-egress) through a certain structure (building, stadium, airport..) and how it is affected by architectural design. In the first section of this chapter, we discuss the two main approaches for modeling crowds and the three main families of pedestrian models. In the second section, we introduce the model that has been developed in Navier laboratory since 2008.

3.2 Two approaches for modeling crowd dynamics

When modeling a real world system that has not been described before, two possible approaches exist. In the first approach, one uses the principle of analogy and searches if there is a familiar system that has been successfully modeled, showing qualitatively comparable trends to those observed in the new one. The familiar system's model setup can then be used as a starting point to mathematize the new system. In the second approach, the new system is considered novel and necessitates to be mathematized starting from very basic principles.

3.2.1 Modeling by analogy

Human crowds is one of the new complex systems that mathematics started to deal with in relatively recent times. At first, the main modeling approach was the one by analogy with particle systems of gas dynamics. This choice was justified by the similarity of the observed qualitative flow patterns of the two systems. Some authors even borrowed terminology proper to fluid dynamics. Expressions such as *laminar* and *turbulent* flow were used to describe different regimes of crowd movement. Following this reasoning, a macroscopic representation of crowds was adopted. In macroscopic models, one is interested in quantities like the flow, density and speed that represent pedestrian movement. In this approach, the crowd is modeled as a continuous fluid made up of "unintelligent" particles. Therefore, different individual behavior becomes insignificant with respect to the overall dynamics of the crowd. Macroscopic analysis may be suited for very large systems and dense crowds where collective motion is dominant. The advantage of macroscopic models is that they can usually be treated analytically.

3.2.2 The crowd: a social complex system

Social systems are the most complex systems we know [1]. They are even more complex than physical or biological systems. Indeed, social systems possess a number of properties, which distinguish them from most physical ones. A full list of these properties can be found in [1]. In the following we list some of them:

- Social systems have a much larger number of variables and parameters than most of the physical ones.
- Most of these variables and parameters are unknown and hard to measure.
- When they exist, the laws of social behavior are masked by the considerable statistical variation of measurements.
- Technical, financial, and ethical issues often limit empirical studies.

- Subdividing the system into simple, non-interacting subsystems to be studied separately is difficult or even impossible.
- The observer participates in the system and modifies social reality.
- The non-linear and/or network dependance between several variables usually leads to complex dynamics and structures, and sometimes paradoxical effects.
- Interaction effects are very strong especially emergent phenomena
- Analysis and modeling are rendered difficult by factors such as a large degree of randomness and heterogeneity, memory, anticipation, decision-making, communication, consciousness, and the relevance of intentions and individual interpretations.
- Information has a greater impact on the behavior of social systems than physical aspects or biological heritage.
- The interactions between the elements of a social system may change over time unlike the case for the fundamental laws and forces of physics.

For such reasons, social systems are the most complex systems we know. They are certainly more complex than physical systems. That is why, more recently, the modeling approach that considers the crowd as a social complex system rather than a physical one has begun to impose itself. Unlike the case of fluid particles, in this approach it is not possible to predict the behavior of several pedestrians from the detailed knowledge of the behavior of one. In fact, individuals continuously modify their movement due to interactions with their surrounding. This leads to emergence of collective motion that is not part of the simple behavioral rules followed by each pedestrian. This is made possible since pedestrians are able to actively influence the laws of physics through personal decisions whose impact is not necessarily similar to that of external force fields. Considering crowds as complex systems necessitates a microscopic representation of crowds. Microscopic models represent each pedestrian of a crowd as an individual agent occupying a certain space at a certain time. The movement of each walker is then described using state variables, mainly position and velocity. In this approach, each individual navigates towards his/her destination while interacting with its surrounding (other pedestrians, obstacles,...). A more realistic representation of pedestrian movement doesn't come without cost. The microscopic models can rarely be manipulated analytically and require computation effort and cost.

After choosing how to represent the crowd, the next step concerns the representation of space. If a macroscopic representation of the crowds is adopted, then a continuous representation of the environment is necessary. For microscopic approaches, a continuous or a discrete representation of space is possible. In the the continuous approach, pedestrians move freely in available space with almost no constraint on their desired direction. For example, force based models use a continuous representation of the environment. In the second approach, the space is divided into a finite number of cells similar to a cellular automaton [2–4] or described by a graph where each node represents a possible position like in the Lattice-gas models [5].

3.3 Classes of crowd models

In order to illustrate the different modeling approaches, we have chosen to present three classes of pedestrian models that are the mostly used and frequently cited in literature. These are the fluid dynamics models, cellular automata models, and force-based models.

3.3.1 Fluid dynamics models

One of the first attempts to model crowd movement was done by Henderson [6, 7]. Inspired by some obvious similarities between crowd and fluid dynamics, Henderson developed a macroscopic model. He noticed that the pedestrian velocity distribution in different environmental conditions can be described using certain equations from fluid mechanics [6]. This model performs best for relatively high densities.

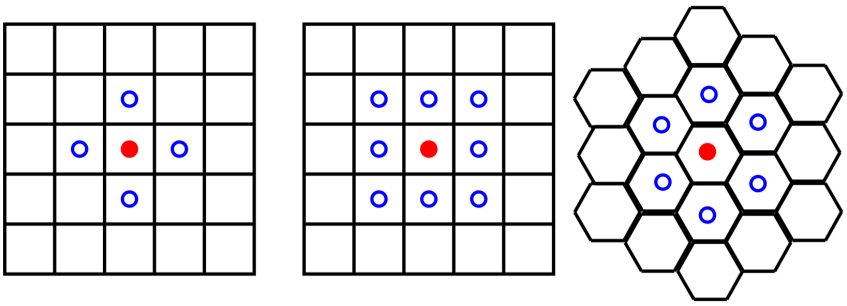

Figure 3.1: Von-Neumann neighborhood (left), Moore neighborhood (middle), and Hexagonal neighborhood (right) [17].

However, several studies have shown that certain corrections are needed to be taken into consideration so that the laws of crowd dynamics include the fact that people do not follow the laws of physics. They have different desired directions, have no conservation of momentum and can stop and start at will [8, 9]. In addition, crowd models based on the analogies with fluid mechanics aren't capable of reproducing certain collective phenomena like lane formation or bottleneck oscillations. Despite its shortcomings, this modeling approach is used frequently in evacuation simulations to estimate the pedestrian flow intensity as a function of the density of individuals and the topology of the environment.

3.3.2 Cellular automata models

Cellular automata are microscopic models where agents move in an environment discretized into a regular lattice made up of cells. A natural discretization can be derived from the fact that maximal densities of about $6\,persons/m^2$ can be observed in dense crowds (except in very extreme situations)[10]. According to this density, a pedestrian occupies an area of $40 \times 40\,cm^2$ [11] which can be used as the size of the cells making up the lattice. Fig 3.1 illustrates the three most commonly used space discretization in cellular automata. Time is also discretized where pedestrians can change position at each time step. Their movement is governed by a set of deterministic or stochastic behavioral rules. Accoriding to these rules, three main families of cellular automata can be identified. The first and the most simple one is the deterministic model of Fukui-Ishibashi [12, 13]. In this approach, bidirectional flow is simulated using the following rules: (i) a pedestrian moves in its desire direction if the cell in front of him is empty, (ii) waits if it is occupied by another pedestrian moving in the same direction or (iii) moves to the right or to the left (chosen randomly) if it is occupied by a pedestrian moving in the opposite direction. Several additions were later introduced [14–16].

The second family of cellular automata is frequently used in literature and is based on the floor field concept developed by Andrea Schadschneir and his team (Fig. 3.2) [3, 4]. In this approach, each cell is given an attractiveness parameter. For evacuation simulations, the cells that are closer to the exit have a greater attractiveness value. Then, similar to the pheromone deposit by ants, the more a cell is traversed by pedestrians the higher its attractiveness value. This high value is later dissipated if the cell is no more traversed. Using this mechanism is justified by the hypothesis that pedestrians have the tendency to follow their neighbors especially in panic situations.

The third family proposes a model that lies between cellular automata and continuous models [18, 19]. Each pedestrian interacts with its surroundings using a half circle of radius equal to 1.5 times its actual velocity placed in front of it. This zone is then discretized with each cell having a probability to be chosen (see Fig. 3.3). A cell occupied by another individual will have a zero probability to be chosen.

The advantage of cellular automata models is that they are simple and can be used for large scale simulations. In addition, they perform better than continuous models in numerical simulation speed.

3.3.3 Force-based models

Force-based models are one of the most important tools used to simulate crowd movement. Amongst them, the Social Force Model developed by Helbing [20] is probably the most known especially for being

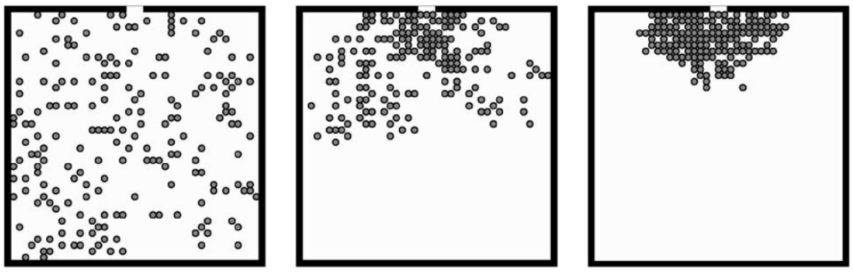

Figure 3.2: Three snapshots of an evacuation simulation made using the model developed by Andrea Schadschneider and his team [10].

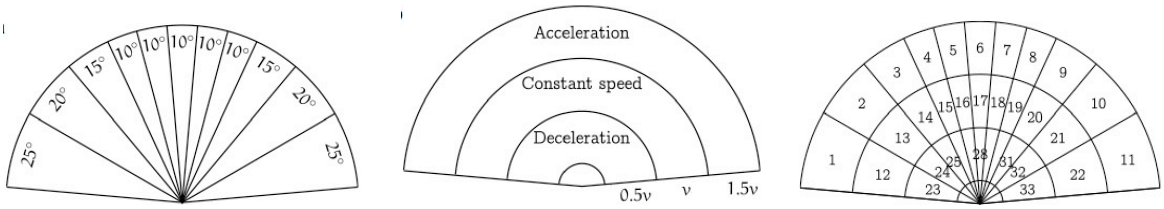

(a) (b) (c)

Figure 3.3: Illustration of how the cellular automata model proposed in [19] functions. An interaction zone in the shape of a half circle is defined in front of each pedestrian such that: (a) it is first discretized angularly, (b) then radially, (c) and finally into 33 parts where each part has a probability to be chosen by the pedestrian.

the first to use concept of self-organization to explain lane formation and oscillations at bottlenecks. It is based on the works of Lewin [21] who proposed that behavioral changes are guided by so-called social fields or social forces. Helbing translated this idea into mathematical equations and introduced the social force model [22]. This model was then applied to opinion formation [23], pedestrian motion [22], and vehicular traffic [24]. Despite its simplicity, the social force model was the first to reproduce self-organized pedestrian movement. The social force model is based on continuous space and time:

$$\frac{d\mathbf{q}_i(t)}{dt} = \mathbf{u}_i(t) \tag{3.1}$$

where $\mathbf{q}_i(t)$ denotes the position and $\mathbf{u}_i(t)$ the velocity of pedestrian i who is represented by a disk of radius r_i. In this microscopic continuous model, three hypothesis based on Newtonian physics define pedestrian behavior:

- Whether searching to reach a destination or just walking around, each pedestrian has a desired direction.
- Each pedestrian tries to walk at its desired speed.
- Individuals try to maintain a certain distance from others that they don't know.

These three hypothesis imply that the basic equation for a pedestrian of mass m_i is then of the general form:

$$m_i \frac{d\mathbf{u}_i(t)}{dt} = \mathbf{f}_i^a + \mathbf{f}_i^{soc} + \mathbf{f}_i^{phys} + \boldsymbol{\xi} \tag{3.2}$$

where $\boldsymbol{\xi}$ is a vector of random fluctuation. Pedestrian i, wishing to move in a direction $\mathbf{e}_{d,i}$ at a desired speed $u_{d,i}$, is attracted toward its destination by a force $\mathbf{f}_i^a$ that adapts the current velocity of the pedestrian, $\mathbf{u}_i$, to its desired velocity. This force is given by :

Table 3.1: Typical parameter values for the social-force model [10].

Parameter	Value
$\mathbf{u}_i$	$0.6 - 1.5\, m/s$
r_i	$[0.25m, 0.35m]$
A_i	$2 \cdot 10^3\, N$
B_i	$0.08\, m$
τ_i	$0.5\, s$
κ'	$1.1 - 1.2 \cdot 10^5\, kg/s^2$
κ''	$2.4 \cdot 10^5\, kg/m/s$

$$\mathbf{f}_i^a = m_i \frac{\mathbf{u}_i - u_{d,i}\mathbf{e}_{d,i}}{\tau_i} \tag{3.3}$$

where τ_i is the relaxation time. As a pedestrian moves in its desired direction, he/she tries to keep a distance from obstacles on his/her way (other pedestrians and obstacles) which gives rise to a repulsive force between them. It is difficult to determine this social force empirically. In [25], it has been defined using an exponential form:

$$\mathbf{f}_i^{soc} = \sum_{j \neq i} \mathbf{f}_{ij}^{soc} = \sum_{j \neq i} A_i e^{\left((R_{ij} - d_{ij})/B_i\right)} \left(\lambda_i + (1 - \lambda_i)\frac{1 + \cos\phi_{ij}}{2}\right) \mathbf{e}_{ji}^n \tag{3.4}$$

where $R_{ij} = r_i + r_j$ is the sum of the radii of pedestrians i and j, d_{ij} is the distance between their centers, A_i and B_i are constant parameters of the model representing the magnitude of the maximum sociopsychological force and its fall-off length respectively, λ_i reflects the anisotropic nature of the force and grows with the strength of interactions from behind ($0 < \lambda_i < 1$), $\mathbf{e}_{ji}^n$ is the vector pointing from pedestrian j to i, and ϕ_{ij} is the angle between the desired direction $\mathbf{e}_{d,i}$ and the vector $\mathbf{e}_{ji}^n$. The social force does not satisfy Newton's third law (action=reaction) because of its anisotropic nature (e.g., if $\lambda_i \neq \lambda_j$). This means that for two pedestrians i and j, $\mathbf{f}_j^{soc} \neq -\mathbf{f}_i^{soc}$.

When two pedestrians are in contact, a physical force $\mathbf{f}_i^{phys}$ is introduced to prevent interpenetration. This force has a pushing and a friction component. The pushing component is a "body force" counteracting body compression (preventing overlapping) and the friction component is a "sliding friction force" impeding relative tangential motion such that:

$$\begin{aligned} \mathbf{f}_i^{phys} &= \mathbf{f}_i^{push} + \mathbf{f}_i^{fric} \\ &= \sum_{j \neq i} \kappa' g(r_i + r_j - \parallel \mathbf{q}_i - \mathbf{q}_j \parallel)\mathbf{e}_{ji}^n + \sum_{j \neq i} \kappa" g(r_i + r_j - \parallel \mathbf{q}_i - \mathbf{q}_j \parallel)\Delta u_{ij}^{tg}\mathbf{e}_{ji}^{tg} \end{aligned} \tag{3.5}$$

where κ' and κ" are constants and the function $g(s)$ is 0 if the pedestrians are not in contact, otherwise equal to the argument s. The tangential velocity difference between pedestrians i and j is given by $\Delta u_{ij}^{tg} = -(\mathbf{u}_j - \mathbf{u}_i) \cdot \mathbf{e}_{ij}^{tg}$. Unlike the social force, the physical force obeys the Newton's third law. With the aforementioned value of κ' (Table 3.1), the human body acts like a very stiff string that resists penetration. At the same time, this value of κ' results in a very high contact force capable of crushing an individual [26]. In this approach, only perfectly elastic pedestrian-pedestrian collisions can be obtained. The typical parameter values for the social force model are shown in Table 3.1. However, in other publications and for other situations, different parameters sets have been used. The model has also been calibrated several times using empirical data [27–31].

Several versions of the repulsive force were developed in the aim of reproducing more realistic avoidance behavior (Fig. 3.4). The most successful were the approaches that incorporate the relative velocity $\mid \mathbf{v}_j - \mathbf{v}_i \mid$ of pedestrian j with respect to pedestrian i [32–34]. Other types of interaction forces (attraction, imitation, or friction) can be added to the social force model making it possible to simulate several phenomena like situations of panic [25] and trail formation [35]. However, while successful in reproducing pedestrian behavior or collective phenomena in some situations, these approaches fail to do so for others.

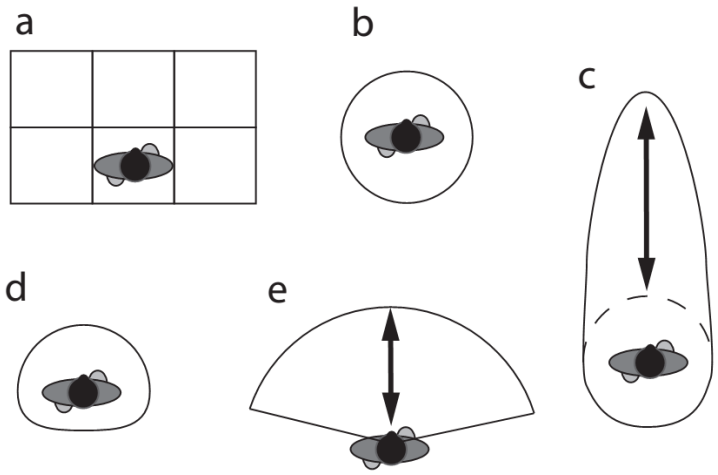

Figure 3.4: Different forms of the interaction zones suggested by different models: (a) for cellular automata [16], (b) circular, (c) elliptical or (d) anisotropic form for the social force model [29] and (e) the dynamic form that changes in length (hence the black arrow) proposed by [19].

The social forces concept still suffers from major disadvantages such as pedestrian oscillations at high densities and backward movement.

3.4 Commercial models

The increase in computer processing power and the advances in programming skills have lead to the development of several transportation and urban planning computer models from a macroscopic to a microscopic scale. Concerning pedestrian models, they have been modeled to simulate pedestrian behavior in various contexts. The aim of this thesis is not to present a full discussion on the pedestrian simulation techniques available on the market. However, we do provide some references to some of the existing simulation tools, referring the interested reader to the reported references:

- PedSim [36] is a software tool for microscopic pedestrian and crowd simulation. It implements the social force model described in [37].
- Nomad[38] is a microscopic model developed at the Transport & Planning department of the Delft University of Technology. It uses the minimal effort principle and is based on microscopic characteristics of pedestrians, such as walking speed, pedestrian size, etc..
- Exodus [39] is developed by the Fire Safety Engineering Group at the University of Greenwich to be used to perform evacuation simulation and pedestrian dynamics/circulation analysis for the safety industry.
- Legion is a simulator that uses a multi-agent pedestrian model where each pedestrian is modeled as a two-dimensional “entity” with a circular body, which moves in 2D continuous space where it moves towards its current target by selecting a step which seeks to minimize a perceived objective cost function [40].
- PTV Viswalk is an add-on module to PTV Vissim which is a simulation program developed by the PTV Group. It is based on the Viswalk is based on the social force model by developed by Helbing et Molnàr [37].
- Pathfinder [41] is an agent-based egress simulator that uses steering behaviors (first presented in [42]) to model pedestrian motion.

The previous section was dedicated to offer the reader a general background overview of crowd modeling. Two main approaches that were used to model the complex system that is the crowd were addressed. This lead us to the three big families of crowd models that currently exist in literature. In the following section, the model that has been developed in Navier laboratory since 2008 is detailed.

3.5 The 2D crowd movement model

In Navier laboratory, crowds were first studied to inspect how do they interact with vibrating structures mainly footbridges. In her PhD thesis (2005-2008) [43], Joanna Bodgi developed a continuous crowd model to study pedestrian-structure interaction. The crowd was considered as a fluid and applied a spatially distributed force to the footbridge inducing it to resonate for certain conditions. The researchers at Navier were then interested in finding out if more precise results would be obtained by using a discrete model where each pedestrian applies a single force to the footbridge. During the thesis of Philippe Pécol (2008-2011) [44], crowd-structure interaction was addressed in addition to a new research field which is the urgent evacuation of crowds. The developed 2D discrete model successfully modeled urgent evacuation of buildings [45–48]. The research team then started investigating modeling pedestrian flows in public spaces (train stations, airports,...) for normal situations. In this section, the 2D model that has been developed at Navier laboratory is explained along with the modifications and the additions that were done in this PhD thesis.

3.5.1 A non-smooth microscopic model based on Frémond's approach for collision modeling

In the following, scalars are written in normal font. Vectors and matrices are written in bold font and are represented by lower case and upper case respectively unless precised. Let us consider a system of N circular particles moving in a horizontal plane each defined by:

- a mass m_i
- a moment of inertia I_i about its vertical axis
- a radius r_i
- a center of gravity G_i, whose position with respect to a reference system with axes $x-y$ and origin O, is described by the vector ${}^t\mathbf{q}_i(t) = (q_i^x(t), q_i^y(t), \theta_i(t)) \in \mathbb{R}^3$
- a velocity denoted by ${}^t\mathbf{v}_i(t) = (\mathbf{u}_i(t), \dot{\theta}_i(t)) = (u_i^x(t), u_i^y(t), \dot{\theta}_i(t))$

where $\theta_i(t) \in [-\pi, \pi]$ represents the walking direction of the particles about the $\mathbf{e}_z$-axis ($\theta_i(t) = 0$ when the particle's walking direction is parallel to the x-axis in the positive direction and $\theta_i(t) > 0$ when the particle turns counterclockwise) and $\dot{\theta}_i(t) = d\theta_i/dt$ their rotational velocity. Contacts between particles are assumed to be punctual. For the sake of notation simplicity, we shall omit the time dependence in the following, unless this leads to ambiguities.

The description of the behavior of this collection of discrete bodies is based on the consideration that the global system they constitute is deformable even if each particle is rigid. Making use of the principle of virtual work, the equations describing the regular (smooth) as well as the discontinuous (non-smooth collisions) evolutions of the movement of the system can be obtained. The deformation velocity involving the i^{th} and j^{th} particles at the contact point C is given by:

$$\mathbf{\Delta}_{ij}(\mathbf{v}) = \mathbf{u}_i + \dot{\theta}_i \mathbf{e}_z \times \mathbf{G}_i\mathbf{C} - (\mathbf{u}_j + \dot{\theta}_j \mathbf{e}_z \times \mathbf{G}_j\mathbf{C}) \tag{3.6}$$

where ${}^t\mathbf{v} = ({}^t\mathbf{v}_i, {}^t\mathbf{v}_j)$ collects the velocities of all the particles evolving in the studied system and $\times$ the cross product.

A different form of the deformation velocity allows to represent a particular case of subgroup: pedestrians holding hands. While existing methods depict the cohesion of a subgroup with forces [49, 50], the proposed method to describe this particular type of subgroups uses an at-a-distance deformation velocity.

Inspired by the works of Caselli and Frémond [51], an at-a-distance interaction between rigid particles is introduced to model the effects of the subgroup as a continuous deformation of the system constituted by all the linked pedestrians. The at-a-distance deformation velocity is a scalar quantity defined by the derivative with respect to time of the squared distance between linked shoulders, i.e. for pedestrians i and j points C_i and C_j are considered and illustrated in Fig. 3.5.

For a group of two individuals, the at-a-distance deformation velocity is expressed as:

$$\Delta^*_{ij}(\mathbf{v}) = 2\Big(\mathbf{u}_i + \dot{\theta}_i \mathbf{e}_z \times \mathbf{G}_i\mathbf{C}_i - \big(\mathbf{u}_j + \dot{\theta}_j \mathbf{e}_z \times \mathbf{G}_j\mathbf{C}_j\big)\Big) \cdot \mathbf{C}_j\mathbf{C}_i \tag{3.7}$$

The dynamics equations for the set of all particles can be written as follows:

$$\begin{cases} \mathbf{M}\,\dot{\mathbf{v}} = -\mathbf{f}^{int} + \mathbf{f}^{ext} & \text{almost everywhere} \quad (3.8) \\ \mathbf{M}\,(\mathbf{v}^+ - \mathbf{v}^-) = -\mathbf{p}^{int} + \mathbf{p}^{ext} & \text{everywhere} \quad (3.9) \end{cases}$$

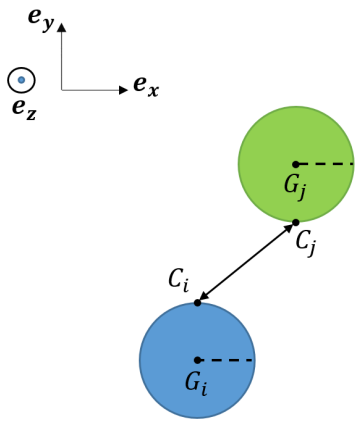

Figure 3.5: Two holding hands pedestrians - Example of linked shoulders

where $\mathbf{M}$ is the $3N \times 3N$ inertial matrix of the set of particles (Eq. (3.10)); $\mathbf{f}^{ext}$ (resp. $\mathbf{f}^{int}$) is the external force vector (resp. internal force vector) of dimension $3N$ applied to the deformable system of all the particles. For instance, the social repulsion force introduced by Helbing [25] would be considered as an external force, while the force driving an individual to a certain destination would be introduced as an interior one.

$$\mathbf{M} = \begin{pmatrix} \ddots & 0 & \dots & \dots & 0 \\ 0 & m_i & \ddots & & \vdots \\ \vdots & \ddots & m_i & \ddots & \vdots \\ \vdots & & \ddots & I_i & 0 \\ 0 & \dots & & 0 & \ddots \end{pmatrix} \tag{3.10}$$

The existence of a solution of the system given by Eqs. (3.8) and (3.9) is proven in [52–54]. Eq. (3.8) describes the smooth evolution of the multi-particles system whereas Eq. (3.9) describes its non-smooth evolution during a collision, where $\mathbf{v}^+$ and $\mathbf{v}^-$ are the particle's velocities before and after a collision. Hence, Eq. (3.8) applies almost everywhere, except at the instant of collision, where it is replaced by Eq. (3.9).

When a contact is detected, the velocities of colliding particles become discontinuous. Therefore, Eq. (3.9), where the interior and exterior percussions ($\mathbf{p}^{int}$ and $\mathbf{p}^{ext}$ respectively) are introduced, is used to calculate the velocity after the shock. By definition, percussions have the dimension of a linear momentum: a force multiplied by time ($kg.m.s^{-1}$). The $\mathbf{p}^{int}$ percussions are unknown; they take into

account the dissipative interactions between the colliding particles (dissipative percussions $\mathbf{p}^d$) and the reaction forces that permit the avoidance of overlapping among particles (reactive percussions $\mathbf{p}^{reac}$), and hence $\mathbf{p}^{int} = \mathbf{p}^d + \mathbf{p}^{reac}$. Frémond [51, 54, 55] defined the deformation velocity $\mathcal{D}(\frac{\mathbf{v}^+ + \mathbf{v}^-}{2})$ in duality with $\mathbf{p}^{int}$ according to the work of internal forces, where $\mathcal{D}(\mathbf{v}) = (\mathbf{\Delta}(\mathbf{v}), \mathbf{\Delta}^*(\mathbf{v}))$, $\mathbf{\Delta}(\mathbf{v})$ represents the vector containing all the velocities of deformation of all the particles in contact, and $\mathbf{\Delta}^*(\mathbf{v})$ represents the vector containing all the at-a-distance deformation velocities of the particles belonging to groups. He then introduced a pseudopotential of dissipation $\Phi = \Phi(\mathcal{D})$, where , that allows us to express $\mathbf{p}^{int}$ as:

$$\mathbf{p}^{int} \in \partial\Phi\left(\mathcal{D}(\frac{\mathbf{v}^+ + \mathbf{v}^-}{2})\right) \tag{3.11}$$

where the operator ∂ is the sub-differential that generalizes the derivative for convex functions [54].

The convex function Φ is defined as the sum of two pseudopotentials [56]:

$$\Phi = \Phi^d + \Phi^r\,, \tag{3.12}$$

where Φ^d and Φ^r characterize respectively the dissipative and reactive interior percussions.

The introduced system (Eqs.(3.9-3.12)) leads to a constrained minimization problem:

$$\mathbf{X} = \arg\min_{\mathbf{Y}\in\mathbb{R}^{3N_c}} \left[{}^t\mathbf{Y}\,\mathbf{M}\,\mathbf{Y} + \Phi\big(\mathcal{D}(\mathbf{Y})\big) - {}^t\left(2\mathbf{v}^- + \mathbf{M}^{-1}\mathbf{p}^{ext}\right)\mathbf{M}\,\mathbf{Y}\right] \tag{3.13}$$

with $\mathbf{Y} = \frac{\mathbf{v}^+ + \mathbf{v}^-}{2}$ and N_c the number of pedestrians in contact. $\mathbf{X}$ and $\mathbf{Y}$ are vectors. The solution is given by $\mathbf{X} = \frac{\mathbf{v}^+ + \mathbf{v}^-}{2}$ [54]. Proof of the existence and uniqueness of the velocity $\mathbf{v}^+$ after the simultaneous collisions of several rigid solids, as well as the dissipative nature of the collisions, is presented in [53–55].

3.5.2 Choice of the pseudopotentials

The reactive percussion $\mathbf{p}^{reac}$ ensures the non-interpenetration between particles. It is equal to 0 if contact is not maintained after collision (i.e., $\Delta_{ij}(\mathbf{v}^+)\cdot\mathbf{e}_{ij}^n < 0$) and positive if contact is maintained after collision (i.e., $\Delta_{ij}(\mathbf{v}^+)\cdot\mathbf{e}_{ij}^n = 0$) where $\mathbf{e}_{ij}^n$ is the unit vector pointing from G_i to G_j. These conditions allow us to define $\mathbf{p}^{reac}$ using the indicator function $\Phi^r = I_{\mathbb{R}^-}(\Delta_{ij}(\mathbf{v}^+)\cdot\mathbf{e}_{ij}^n)$ such that $\mathbf{p}^{reac} \in \partial\Phi^r$ [51]. Since Ω is convex and contains the origin, I_Ω can be considered as a pseudopotential of dissipation.

A large variety of behaviors after impact can be obtained by giving Φ^d different forms [52, 54]. A quadratic pseudopotential gives the same classical results obtained by using the coefficient of restitution. In the following, a quadratic pseudopotential Φ^d is chosen :

$$\begin{aligned}\Phi^d\big(\mathcal{D}(\mathbf{v})\big) = \;& \tfrac{1}{2}\sum_{1\le i\le j\le N}\left[K_n\Big({}^t\mathbf{\Delta}_{ij}(\mathbf{v})\cdot\mathbf{e}_{ij}^n\Big)^2 + K_{tg}\Big({}^t\mathbf{\Delta}_{ij}(\mathbf{v})\cdot\mathbf{e}_{ij}^{tg}\Big)^2\right] \\ & + \sum_{1\le i\le j\le N_{subgroup}} \frac{1}{2}K_v\Big(\Delta_{ij}^*(\mathbf{v})\Big)^2\end{aligned} \tag{3.14}$$

where $\mathbf{e}_{ij}^{tg} = \mathbf{e}_z \times \mathbf{e}_{ij}^n$ and $N_{subgroup}$ is the number of pedestrians that belong to groups. The dissipation coefficient K_n (in kg) for the normal component of the dissipative percussion characterizes the inelastic nature of the collisions between particles; an infinite value of K_n implies a perfectly elastic collision. K_{tg} (in kg) is the dissipation coefficient for the tangential component of the percussion while K_v (in $kg.m^{-2}$) is the coefficient of viscous dissipation. The higher its value is, the more rigid the link between the particles forming a group is. In other words, for a high value of K_v, a free grain colliding with a group of particles won't be able to break their bond.

3.5.3 Adaptation to crowd movement

In our 2D model a pedestrian is represented by a circular particle having a "willingness", i.e. a desire to move in a particular direction with a specific speed at each time [25, 45–47]. In addition, the particle's desired direction can be considered [48].

The first step of the approach is to give a desired trajectory to each particle. Several definitions of the desired trajectory of a pedestrian are possible: (i) the most comfortable trajectory, where the individual exerts the least effort, e.g. by avoiding stairs or making the fewest changes in direction, etc.; (ii) the shortest path; or (iii) the fastest one [57]. It is possible to combine two strategies in the same simulation or to change the preferred strategy for any reason during the simulation. In the current model, pedestrians use the shortest path to get to the exit. To do so, we consider a wavefront that starts at the exit $\partial\Upsilon$ of a 2D environment Υ where the areas occupied by obstacles are represented by Γ. As the wavefront propagates in Υ, its arrival times can be found for each node of the discretized space. These arrival times form a scalar function $T(x, y)$ whose values can be obtained by solving the eikonal equation [58] given by :

$$|| \boldsymbol{\nabla} T(x,y) || = \frac{1}{V(x,y)} \quad \text{for } (x,y) \in \Upsilon \tag{3.15}$$

$$T(x,y) = 0 \quad \text{for } (x,y) \in \partial\Upsilon \tag{3.16}$$

where $V(x, y)$ is the velocity of the wavefront. By setting $V(x, y) = 0$ in Γ, the wavefront cannot penetrate this area. In this way, zones that cannot be used by pedestrians can be defined (obstacles, walls,...). By setting $V(x, y) = 1\, m/s$ in $\Upsilon\backslash\Gamma$, the arrival times $T(x, y)$ coincide with the Euclidean distances to the exit. In this way, the shortest path from one point to another can be calculated. By setting $0 < V(x, y) < 1$ in $\Upsilon\backslash\Gamma$, areas that are not frequently used by pedestrians can be defined (areas near to obstacles and walls, wet floor, streets...). Several numerical methods exist to solve the eikonal equation, for example the Fast Marching Method [59] and the Fast Iterative Method [60]. In our model we set $V(x, y) = 1$ in $\Upsilon\backslash\Gamma$ and $V(x, y) = 0$ in Γ. Then by using the Fast Marching Algorithm to solve the eikonal equation, a geodesic map is obtained that can be used to find the direction of the shortest path towards the exit defined by:

$$\mathbf{e}^* = -\frac{\boldsymbol{\nabla} T(x,y)}{|| \boldsymbol{\nabla} T(x,y) ||} \tag{3.17}$$

If pedestrian i wishes to move on the shortest path towards the exit then $\mathbf{e}^* = \mathbf{e}_{d,i}$ his/her desired velocity is defined by $\mathbf{u}_{d,i} = u_{d,i} \cdot \mathbf{e}_{d,i}$ where $u_{d,i}$ represents the amplitude of the desired velocity at which the i-th pedestrian wants to move. For normal conditions, this speed is chosen to be following a normal distribution with an average of 1.34 $m.s^{-1}$ and a standard deviation of 0.26 $m.s^{-1}$ [6].

The second step is to introduce the desired velocity into the original discrete model to simulate crowd movement. Let $\mathbf{f}^{int} = \mathbf{h}^a$, where $\mathbf{h}^a$ gives the desired direction, the amplitude of the velocity and the walking direction of each pedestrian. Each vector $\mathbf{h}_i^a$ associated with pedestrian i represents a component of the vector ${}^t\mathbf{h}^a = ({}^t\mathbf{h}_1^a, {}^t\mathbf{h}_2^a, ..., {}^t\mathbf{h}_N^a)$ of dimension $3N$. It can be expressed as ${}^t\mathbf{h}_i^a = ({}^t\mathbf{f}_i^a, l_i^a)$, where $\mathbf{f}_i^a$ (in $kg.m.s^{-2}$) is the so-called acceleration force [25] giving the desired direction and amplitude of the velocity of the i-th pedestrian. $\mathbf{f}_i^a$ is defined in [25, 45–47] by:

$$\mathbf{f}_i^a = m_i \frac{\mathbf{u}_i - || \mathbf{u}_{d,i} || \mathbf{e}_{d,i}}{\tau_i} \tag{3.18}$$

where $\mathbf{u}_i$ (in $m.s^{-1}$) is the actual velocity and τ_i (in s) is the relaxation time, which specifies how long the pedestrian will take to recover his desired velocity after a contact or after a sudden change in path. For example, Helbing [25] chose $\tau_i = 0.5\, s$ in his numerical simulations. When the value of τ_i is less than or equal to $0.5\, s$, the pedestrians walk "aggressively" and several contacts may occur successively. Its influence has been studied in [47].

As for l_i^a (in $kg.m^2.s^{-2}$), it represents the restoring torque in order to return the pedestrian to his desired direction after a perturbation. It is modeled as the combination of a linear rotational spring and of a linear rotational damper [48], and is defined for the i-th pedestrian by:

$$l_i^a = k_i(\theta_i - \theta_{d,i}) + c_i\dot{\theta}_i = -I_i\ddot{\theta}_i \tag{3.19}$$

where $\theta_{d,i}$ is the angle between $\mathbf{e}_{d,i}$ and the reference direction $\mathbf{e}_x = [1; 0]$, I_i (in $kg.m^2$) is the moment of inertia, k_i (in $kg.m^2.s^{-2}.rd^{-1}$) is the torsional stiffness, c_i (in $kg.m^2.s^{-1}.rd^{-1}$) is the rotational

damping, and $\omega_i = \sqrt{\frac{k_i}{I_i}}$ (in $rd.s^{-1}$) is the undamped resonant frequency for pedestrian i. After a perturbation, a pedestrian returns the fastest without oscillations to its desired direction when its rotation is critically damped ($\zeta_i = \frac{c_i}{2\sqrt{I_i\, k_i}} = 1$). For $\zeta_i > 1$, the individual returns more slowly to its desired position. For $\zeta_i < 1$, it oscillates before returning to its desired direction. In Fig. 3.6, the collision occurs at $t = 0.1\,s$ and the time step is $\Delta t = 0.01\,s$. The solid line plotted inside the particle represents the pedestrian's desired direction while the dotted line represents his current walking direction. We have chosen $\zeta_i = 1$. The choice of k_i will be discussed later. As we have mentioned earlier, adding rotation to the pedestrians' movement is essential to model subgroup behavior.

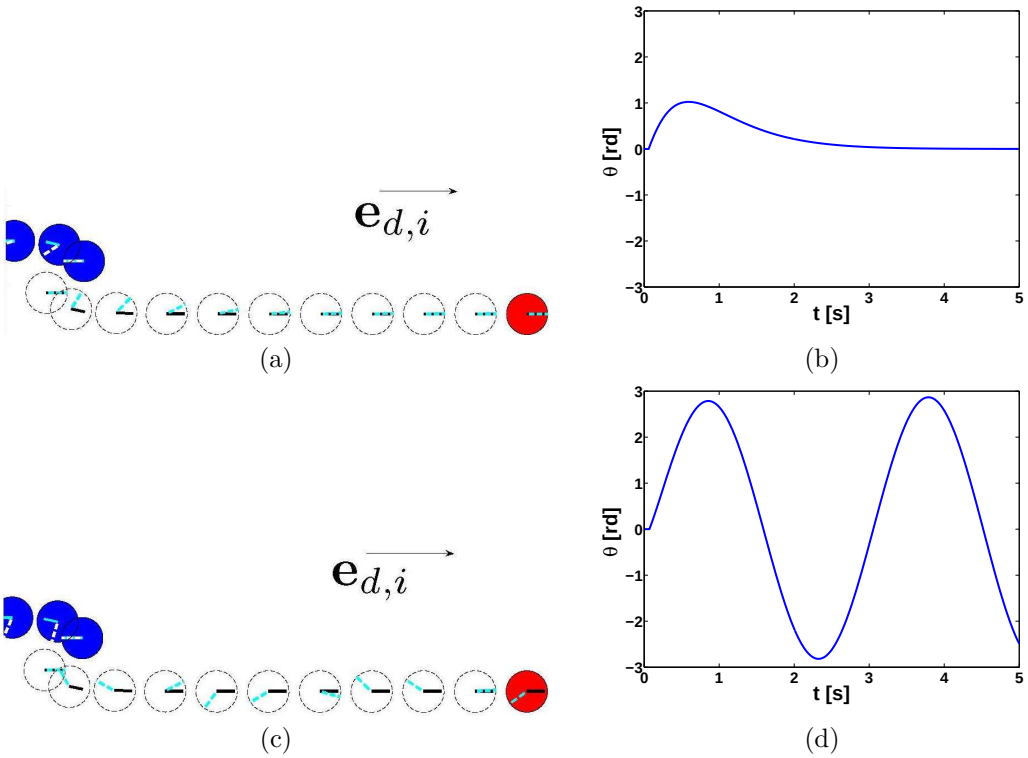

Figure 3.6: Pedestrian-pedestrian interaction without repulsive forces: the left column shows the pedestrian's movement after "collision" for $\zeta_i = 1$ (top) and $\zeta_i = 0$ (bottom), where $\theta_{d,i} = 0$. The right column is a plot of the pedestrian's rotation as a function of time

3.5.4 Calibrating the parameters that govern a collision

Velocity after collision

In the proposed model, the main parameter controlling the velocity after a collision between two individuals is K_n (in kg). Let us consider a head on collision of two points of masses m_1 and m_2 respectively, illustrated in Fig. 3.7, where $K_{tg} = K_v = 0$ and rotation is not considered. The after collision velocities $\mathbf{u}_1^+$ and $\mathbf{u}_2^+$ of the masses m_1 and m_2 respectively, can be found analytically by solving the following system (derived from Eqs. (3.9) and (3.11)):

$$\begin{cases} m_1(\mathbf{u}_1^+ - \mathbf{u}_1^-) = -\mathbf{p}^{int} = -\frac{K_n}{2}(\mathbf{u}_1^+ - \mathbf{u}_2^+ + \mathbf{u}_1^- - \mathbf{u}_2^-) - \mathbf{p}^{reac} \\ m_2(\mathbf{u}_2^+ - \mathbf{u}_2^-) = \mathbf{p}^{int} \\ \mathbf{p}^{reac} \in \partial I_{\mathbb{R}^-}\left(\mathbf{u}_1^+ - \mathbf{u}_2^+\right) \end{cases}$$

The solution of this system can be found [54]:

- If $K_n \leq \frac{m_1 m_2}{m_1+m_2}$ then

$$\mathbf{u}_1^+ = \mathbf{u}_2^+ = \frac{m_1\mathbf{u}_1^- + m_2\mathbf{u}_2^-}{m_1+m_2} \tag{3.20}$$

- If $K_n \geq \frac{m_1 m_2}{m_1+m_2}$ then

$$\mathbf{u}_1^+ = \frac{(m_1m_2 + K_nm_1 - K_nm_2)\mathbf{u}_1^- + 2K_nm_2\mathbf{u}_2^-}{m_1m_2 + K_nm_1 + K_nm_2}$$
$$\mathbf{u}_2^+ = \frac{(m_1m_2 + K_nm_2 - K_nm_1)\mathbf{u}_2^- + 2K_nm_1\mathbf{u}_1^-}{m_1m_2 + K_nm_1 + K_nm_2}$$

It can be noticed in Eq. (3.20) that when $K_n \leq \frac{m_1 m_2}{m_1+m_2}$, the after collision velocities are not dependent on K_n and when $K_n > \frac{m_1 m_2}{m_1+m_2}$, the particles move in opposite directions after colliding. Finally when K_n tends towards infinity, the after collision velocities become:

$$\begin{aligned} \mathbf{u}_1^+ &= \frac{(m_1-m_2)\mathbf{u}_1^- + 2m_2\mathbf{u}_2^-}{m_1+m_2} \\ \mathbf{u}_2^+ &= \frac{(m_2-m_1)\mathbf{u}_2^- + 2m_1\mathbf{u}_1^-}{m_1+m_2} \end{aligned} \tag{3.21}$$

and in the case of $m_1 = m_2$, Eq. (3.21) can be simplified:

$$\begin{aligned} \mathbf{u}_1^+ &= \mathbf{u}_2^- \\ \mathbf{u}_2^+ &= \mathbf{u}_1^- \end{aligned} \tag{3.22}$$

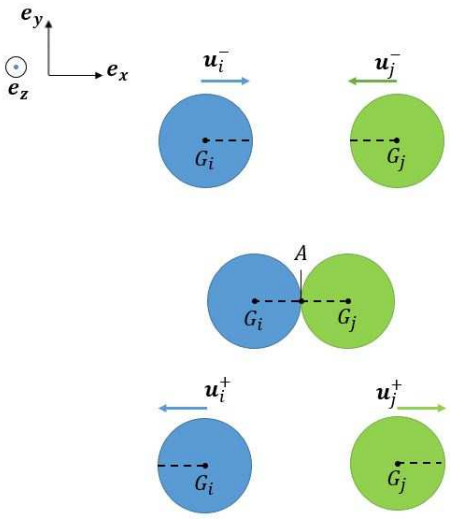

Figure 3.7: Two colliding pedestrians. The dotted line represents each pedestrian's current walking direction

A comparison between analytical and numerical solutions: The collision illustrated in Fig. 3.7 has been studied for two cases. In the first case, $m_1 = m_2 = 62\,kg$ and $|\,\mathbf{u}_1^-\,| = |\,\mathbf{u}_2^-\,| = 1\,m/s$ while in the second one $m_1 = 62\,kg$, $m_2 = 20\,kg$, $|\,\mathbf{u}_1^-\,| = 2\,m/s$ and $|\,\mathbf{u}_2^-\,| = 0.5\,m/s$. The plot of u_i^+ as a function of $\log_{10}(K_n)$ illustrated in Fig. 3.8, shows the validity of the used scheme and the influence of the normal coefficient of dissipation on the after collision velocities. It can be observed that for $K_n > 10^4\,kg$ the collisions become perfectly elastic. The nature of the pedestrian-pedestrian collision controls the choice of K_n. In [45–48], the author chose $K_n = 10^5\,kg$ which results in perfectly elastic collisions when social forces are not considered. The simulations done using this value for K_n gave satisfying results for the case of emergency evacuation.

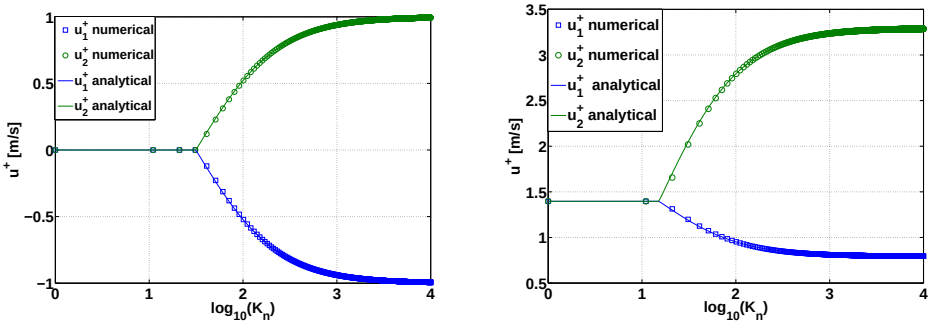

Figure 3.8: Velocity after head on collision of two particles for (a) $m_1 = m_2 = 62\,kg$ and $\mid \mathbf{u}_1^- \mid = \mid \mathbf{u}_2^- \mid = 1\,m/s$ and (b) $m_1 = 62\,kg$, $m_2 = 20\,kg$, $\mid \mathbf{u}_1^- \mid = 2\,m/s$ and $\mid \mathbf{u}_2^- \mid = 0.5\,m/s$

Pedestrian's rotation

In the available crowd models, pedestrians' rotation is seldom treated. Since it must be introduced in our model if we want to model subgroup behavior, we will study its effect on evacuation. By solving Eq. (3.19), we obtain the rotation time-evolution of an individual about himself:

$$\theta_i(t) = \dot{\theta}_0(K_{tg}, K_n) t e^{-\omega_i t} + \theta_{d,i} \tag{3.23}$$

where $\dot{\theta}_0(K_{tg}, K_n)$ is calculated by the model (by solving Eq. (3.13)) after a shock takes place and $k_i = I_i \cdot \omega_i^2$, the torsional stiffness (Eq. (3.19)), is introduced by the user ($k_i = k$ for the sake of simplicity). Fig. 3.9 shows that the value of $\dot{\theta}_0$, calculated after a shock, varies with K_{tg} and is independent of K_n for values greater than $2 \cdot 10^3\,kg$. From Eq. (3.23), we can easily obtain the expression of θ_{max}:

$$\theta_{max} = \frac{\dot{\theta_0}(K_{tg})}{\omega_i \cdot e} + \theta_{d,i} \tag{3.24}$$

By varying k (in $kg.m^2.s^{-2}.rd^{-1}$) between [0.5,18.5], and for each value of $\dot{\theta}_0$ obtained from Fig. 3.9 (each value of $\dot{\theta}_0$ corresponds to a value of K_{tg}), Eq. (3.24) gives the surface illustrated in Fig. 3.10. Now the user can specify the desired value of θ_{max} by choosing from Fig. 3.10 a point $(\dot{\theta_0}, k)$ which corresponds to a couple (K_{tg}, k). The couple must be on or below the isoline representing the chosen value of the maximal rotation.

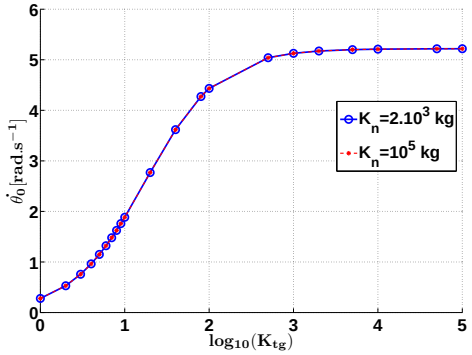

Figure 3.9: Variation of $\dot{\theta}_0$ as a function of $\log_{10}(K_{tg})$

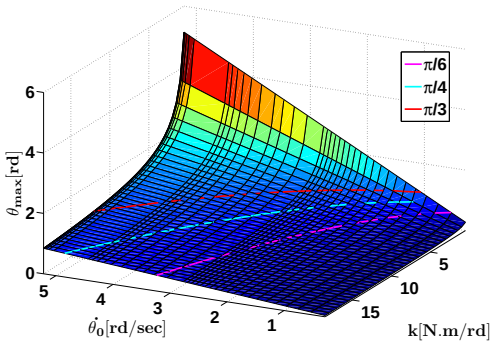

Figure 3.10: Variation of θ_{max} as a function of $\dot{\theta_0}$ and k

3.6 Conclusion

This chapter was dedicated to crowd models. After a bibliographical study on pedestrian modeling, the most basic version of the 2D discrete model that has been been developed in Navier laboratory was demonstrated. First, the original approach based on the theory of rigid bodies' collisions proposed by Frémond was shown. Then several modifications and additions to the model concerning pedestrian rotation were illustrated. The relationship between the collision parameters and the rotation of a pedestrian was identified. It has also been shown that the maximal rotation of an individual can be limited by properly choosing the values of the torsional stiffness and the dissipation coefficient for the tangential component of the percussion. In the next chapter, we address one of the most important aspects of crowd models which is route choice or displacement strategies.

Bibliography

[1] D. Helbing, ed., *Social self-organization.* Understanding complex systems, Springer Berlin Heidelberg, 2012.

[2] V. Blue and J. Adler, "Emergent fundamental pedestrian flows from cellular automata microsimulation," *Transportation Research Record: Journal of the Transportation Research Board*, vol. 1644.

[3] C. Burstedde, K. Klauck, A. Schadschneider, and J. Zittartz, "Simulation of pedestrian dynamics using a two-dimensional cellular automaton," *Physica A: Statistical Mechanics and its Applications*, vol. 295, no. 3, pp. 507–525, 2001.

[4] A. Kirchner and A. Schadschneider, "Simulation of evacuation processes using a bionics-inspired cellular automaton model for pedestrian dynamics," *Physica A: Statistical Mechanics and its Applications*, vol. 312, no. 1â2, pp. 260–276, 2002.

[5] D. H. Rothman and S. Zaleski, "Lattice-gas models of phase separation: interfaces, phase transitions, and multiphase flow," *Reviews of Modern Physics*, vol. 66, no. 4, pp. 1417–1479, 1994.

[6] L. Henderson, "The Statistics of Crowd Fluids," vol. Nature,229, pp. 381–383, 1971.

[7] L. F. Henderson, "On the fluid mechanics of human crowd motion," *Transportation Research*, vol. 8, no. 6.

[8] D. Helbing, "A Fluid dynamic model for the movement of pedestrians," *Complex Systems*, vol. 6, no. 391-415, 1992. arXiv: cond-mat/9805213.

[9] G. K. Still, *Crowd dynamics.* PhD thesis, University of Warwick, 2000.

[10] A. Schadschneider, D. Chowdhury, and K. Nishinari, "Chapter Eleven - Pedestrian dynamics," in *Stochastic transport in complex systems* (A. Schadschneider, D. Chowdhury, and K. Nishinari, eds.), pp. 407–460, Amsterdam: Elsevier, 2011.

[11] U. Weidmann, "Transporttechnik der FuÃgÃ¤nger," report Schriftenreihe Ivt- Berichte 90, ETH ZÃ¼rich, 1993.

[12] M. Fukui and Y. Ishibashi, "Jamming transition in cellular automaton models for pedestrians on passageway," *Journal of the Physical Society of Japan*, vol. 68, no. 11, pp. 3738–3739, 1999.

[13] M. Fukui and Y. Ishibashi, "Self-organized phase transitions in cellular automaton models for pedestrians," *Journal of the Physical Society of Japan*, vol. 68, no. 8.

[14] S. Maniccam, "Effects of back step and update rule on congestion of mobile objects," *Physica A Statistical Mechanics and its Applications*, vol. 346.

[15] R. Nagai and T. Nagatani, "Jamming transition in counter flow of slender particles on square lattice," *Physica A: Statistical Mechanics and its Applications*, vol. 366.

[16] V. J. Blue and J. L. Adler, "Cellular automata microsimulation for modeling bi-directional pedestrian walkways," *Transportation Research Part B: Methodological*, vol. 35, no. 3, pp. 293–312, 2001.

[17] M. Chraibi, *Validated force-based modeling of pedestrian dynamics*. PhD thesis, Forschungszentrum J'ulich GmbH.

[18] G. Antonini, M. Bierlaire, and M. Weber, "Discrete choice models of pedestrian walking behavior," *Transportation Research Part B: Methodological*, vol. 40, no. 8, pp. 667–687, 2006.

[19] T. Robin, G. Antonini, M. Bierlaire, and J. Cruz, "Specification, estimation and validation of a pedestrian walking behavior model," tech. rep., Ecole Polytechnique Fédérale de Lausanne, Switzerland, 2007.

[20] D. Helbing, *Quantitative Sociodynamics*. Dordrecht: Springer Netherlands, 1995.

[21] K. Lewin, *Field theory in social science: selected theoretical papers*. Harper, 1951.

[22] D. Helbing, "A mathematical model for the behavior of pedestrians," *Behavioral Science*, vol. 36, no. 4, pp. 298–310, 1991.

[23] D. Helbing, "A mathematical model for the behavior of individuals in a social field," *The Journal of Mathematical Sociology*, vol. 19, no. 3.

[24] B. Tilch and D. Helbing, "Evaluation of single vehicle data in dependence of the vehicle-type, lane, and site," in *Traffic and Granular Flow 99*, pp. 333–338, Springer, 2000.

[25] D. Helbing, I. Farkas, and T. Vicsek, "Simulating dynamical features of escape panic," *Nature*, vol. 407, pp. 487–490, 2000.

[26] T. I. Lakoba, D. J. Kaup, and N. M. Finkelstein, "Modifications of the Helbing-Molnàr-Farkas-Vicsek Social Force Model for Pedestrian Evolution," *SIMULATION*, vol. 81, no. 5.

[27] S. P. Hoogendoorn and W. Daamen, "A novel calibration approach of microscopic pedestrian models," in *Pedestrian behavior: models, data collection and applications* (H. J. P. Timmermans, ed.), pp. 195–214, Emerald Group Publishing, 2009.

[28] S. P. Hoogendoorn and W. Daamen, "Microscopic Calibration and Validation of Pedestrian Models: Cross-Comparison of Models Using Experimental Data," in *Traffic and Granular Flow'05* (A. Schadschneider, T. Pöschel, R. Kühne, M. Schreckenberg, and D. E. Wolf, eds.), pp. 329–340, Springer Berlin Heidelberg, 2007.

[29] A. Johansson, D. Helbing, and P. K. Shukla, "Specification of the social force pedestrian model by evolutionary adjustment to video tracking data," *Advances in complex systems*, vol. 10, no. supp02, pp. 271–288, 2007.

[30] T. Kretz, S. Hengst, and P. Vortisch, "Pedestrian flow at bottlenecks: validation and calibration of VISSIM's social force model of pedestrian traffic and its empirical foundations," *International symposium on transport simulation, 8th, 2008, Surfers Paradise, Queensland, Australia*.

[31] D. R. Parisi, M. Gilman, and H. Moldovan, "A modification of the Social Force Model can reproduce experimental data of pedestrian flows in normal conditions," *Physica A: Statistical Mechanics and its Applications*, vol. 388, no. 17, pp. 3600–3608, 2009.

[32] S. P. Hoogendoorn, "Walker behaviour modelling by differential games," in *Interface and transport dynamics* (H. Emmerich, B. Nestler, and M. Schreckenberg, eds.), no. 32 in Lecture Notes in Computational Science and Engineering, pp. 275–294, Springer Berlin Heidelberg, 2003.

[33] W. J. Yu, R. Chen, L. Y. Dong, and S. Q. Dai, "Centrifugal force model for pedestrian dynamics," *Physical Review E*, vol. 72, no. 2.

[34] A. Johansson, *Data-driven modeling of pedestrian crowds*. PhD thesis, TU Dresden, 2008.

[35] D. Helbing, *Verkehrsdynamik*. Springer Berlin Heidelberg, 1997.

[36] "Pedsim." http://pedsim.silmaril.org/.

[37] D. Helbing and P. Molnàr, "Social force model for pedestrian dynamics," *Physical Review E*, vol. 51, no. 5.

[38] M. Campanella, S. Hoogendoorn, and W. Daamen, "The Nomad Model: Theory, Developments and Applications," *Transportation Research Procedia*, vol. 2, pp. 462–467, 2014.

[39] "Exodus Introduction." http://fseg.gre.ac.uk/exodus/.

[40] J. L. Berrou, J. Beecham, P. Quaglia, M. A. Kagarlis, and A. Gerodimos, "Calibration and validation of the Legion simulation model using empirical data," *Pedestrian and evacuation dynamics*, pp. 167–181, 2005.

[41] Thunderhead, "Pathfinder: technical reference." http://www.thunderheadeng.com/downloads/pathfinder/tech_ref.pdf, 2015.

[42] C. W. Reynolds, "Steering behaviors for autonomous characters," in *Game developers conference*, vol. 1999, pp. 763–782, 1999.

[43] J. Bodgi, *Synchronisation pietons-structure: Applications aux vibrations des passerelles souples*. PhD thesis, Ecole Nationale des Ponts et Chaussees, 2008.

[44] P. Pécol, *Modélisation 2D discrète du mouvement des piétons: application à l'évacuation des structures du génie civil et à l'interaction foule-passerelle*. PhD thesis, Université Paris-Est, 2011.

[45] P. Pécol, S. D. Pont, S. Erlicher, and P. Argoul, "Modelling crowd-structure interaction,"

[46] P. Pécol, S. Dal Pont, S. Erlicher, and P. Argoul, "Smooth/non-smooth contact modeling of human crowds movement: numerical aspects and application to emergency evacuations," *Annals of Solid and Structural Mechanics*, vol. 2, no. 2-4, pp. 69–85, 2011.

[47] P. Pécol, P. Argoul, S. D. Pont, and S. Erlicher, "The non-smooth view for contact dynamics by Michel Frémond extended to the modeling of crowd movements," *Discrete and Continuous Dynamical Systems - Series S*, vol. 6, no. 2.

[48] P. Pécol, P. Argoul, S. Dal Pont, and S. Erlicher, "A new crowd movement modeling for pedestrians who hold hands," *Vibrations, Shocks and Noise*, 2012.

[49] M. Moussaïid, N. Perozo, S. Garnier, D. Helbing, and G. Theraulaz, "The Walking Behaviour of Pedestrian Social Groups and Its Impact on Crowd Dynamics," *PLoS ONE*, vol. 5, no. 4.

[50] H. Singh, R. Arter, L. Dodd, P. Langston, E. Lester, and J. Drury, "Modelling subgroup behaviour in crowd dynamics DEM simulation," *Applied Mathematical Modelling*, vol. 33, no. 12.

[51] F. Caselli and M. Frémond, "Collision of three balls on a plane," *Computational Mechanics*, vol. 43, no. 6, pp. 743–754, 2008.

[52] C. Cholet, "Collisions d'un point et d'un plan," *Comptes Rendus de l'Académie des Sciences - Series I - Mathematics*, vol. 328, no. 5.

[53] S. Dal Pont and E. Dimnet, "Theoretical approach to and numerical simulation of instantaneous collisions in granular media using the A-CD2 method," *Communications in Applied Mathematics and Computational Science*, vol. 3, no. 1, pp. 1–24, 2008.

[54] M. Frémond, *Collisions*. Roma, Italie: Università di Roma Tor Vergata, dipartimento di ingegneria civile, 2007.

[55] M. Frémond, "Rigid bodies collisions," *Physics Letters A*, vol. 204, no. 1.

[56] J. J. Moreau, "Sur les lois de frottement, de plasticité et de viscosité„" *Comptes Rendus de l'Académie des Sciences Paris 271 - Series A*, pp. 608–611, 1970.

[57] S. P. Hoogendoorn, P. H. L. Bovy, and W. Daamen, "Microscopic pedestrian wayfinding and dynamics modelling," in *Pedestrian and evacuation dynamics* (M. Schreckenberg and S. Sharma, eds.), pp. 123–154, Berlin: Springer-Verlag, 2002.

[58] H. Bruns, "Das eikonal," *Abhandlungen der Mathematisch-Physischen Classe der Königlich Sächsischen Gesellschaft der Wissenschaften.*, 1895.

[59] R. Kimmel and J. Sethian, "Fast Marching Methods for Computing Distance Maps and Shortest Paths," Tech. Rep. Technical Report 669, University of California, Berkley, 1996.

[60] W. K. Jeong and R. Whitaker, "A fast eikonal equation solver for parallel systems," in *SIAM conference on Computational Science and Engineering*, 2007.

Chapter 4

Pedestrian route choice

Contents

4.1 State-of-the-art in pedestrian route choice

An emerging field in complexity science is the study of pedestrian dynamics. This domain has several real life applications such as evaluating the effects of a proposed policy on the pedestrian facilities before its implementation, optimizing alighting and boarding times of passengers in train and metro stations, or the optimization of egress strategies. Therefore, the realism of pedestrian models are crucial to ensure their utility and reliability. This is done differently depending on the adopted approach to describe the crowd. Since in our model each individual's behavior is resolved explicitly, this work will be restricted to agent-based models. We refer the reader interested in macroscopic models to [1–5].

In microscopic models, each pedestrian is represented by a particle having the will or desire to move in a certain direction at a certain speed. In most pedestrian models, the speed of pedestrians in normal situations is chosen from a normal distribution of mean $1.34\,m.s^{-1}$ and standard deviation $0.26\,m.s^{-1}$ [6]. Concerning a pedestrian's desire direction or its route choice, it is one of the most important difficulties faced by microscopic models. In real life, a pedestrian chooses the path that leads it through a complex topology to a desired final destination out of an infinite set of alternatives. Moreover, a pedestrian interacts with several factors and events (shortcuts, traffic conditions, other pedestrians, obstacles, changes in the environment,...) that forces it to deviate from its original path. Modeling this behavior is a very complex task. Therefore, it is important to simplify the problem by dividing the pedestrian route choice behavior into several categories or levels. This allows us to identify the different behavior types and tackle each one at a time. This chapter is defined into 5 sections. After the introduction, some essential terms with respect to pedestrian route choice are defined in section 2. In section 3, we go over two approaches concerning the classification or the categorization of pedestrian route choice levels. In section 4, a literature review on route choice modeling is done. The conclusions reached at the end of this chapter are found in section 5.

4.1.1 Pedestrian route choice: a glossary of key terminology

In the field of pedestrian and evacuation dynamics (PED), identical terms are often used with different significations. In this section, some essential terms related to route choice are defined in order to clarify how they will be employed in this work.

According to [7], a *route* is a chain of consecutive nodes joined by links, connecting the origin, the intermediate destinations, and the final destination. This definition can be applied to discrete networks that are made up of links and nodes. However, pedestrians usually move freely in their environment choosing a route from an infinite set of alternatives without being restricted to certain lanes or nodes. In this case, a route is the trajectory of a pedestrian that started at an origin and ended at a destination.

A *trajectory* is the graphical representation of the motion of an object, in our case an individual. A pedestrian's trajectory is usually obtained by saving its coordinates at each time step and finally connecting all the points (see Fig.4.1).

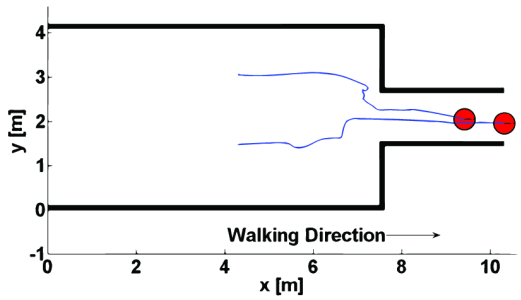

Figure 4.1: Pedestrian trajectories for a bottleneck

In [8], *navigation* is defined as "coordinated and goal-directed movement of one's self (one's body) through the environment" and *wayfinding* as the "goal-directed and planned movement of one's body around an environment in an efficient way".

A *route choice situation* [9] is when a pedestrian has to choose between several available routes to get to its destination. There are three types of choice processes [7]: (i) simultaneous choice (choice of the entire route), (ii) sequential choice (choice of sub-routes at intermediate destinations), and (iii) hierarchical choice which is similar to sequential choice but with a dependency on previous decisions. Different from these three types of choice processes is the adaptive route choice [7] where individuals make decisions based on prevailing conditions such as traffic.

A *route selection strategy* is the decision style that a pedestrian uses to choose a route. Among numerous decision variables, a route selection strategy might depend on travel distance or travel time between origin and destination, level of comfort or service, proximity to obstacles, attractiveness, etc. In literature, the focus seems to be both on the travel time and travel distance.

The *shortest distance* doesn't always refer to the shortest euclidean distance. The distance to target is usually measured using different metrics including the real Euclidean metric. Using spatially varying metrics leads to avoidance or attraction of certain areas (streets, construction sites, stairs vs. escalators...).

A *shy away distance* is the minimum distance that pedestrians keep with different elements of the surrounding environment (walls, obstacles, other pedestrians...). This distance depends on the elements' characteristics and the available space for pedestrians [9].

4.1.2 Classification of pedestrian route choice levels

Given the complexity of the pedestrian route choice problem, it was necessary to divide it into sub problems. This has been done by creating different levels of route choice, identifying pedestrian behaviors in each one and finally modeling them. In the following, two approaches for dividing route choice behavior are presented.

Strategical, tactical, and operational behaviors

Crowd models are ideally developed to reproduce all pedestrian behavior and the observed phenomena. The complexity of this task lead each model to target few aspects of human behavior related to public spaces. According to [10, 11], pedestrian behavior can be classified into three levels: (i) the strategical, (ii) the tactical, and (iii) the operational level.

The strategical level In most models, a pedestrian's behavior is influenced strictly by its surroundings or its local environment. In reality, people decide on which activities they want to perform and in what order even before entering a certain facility. Therefore they compute a preliminary path that will allow them to accomplish their objectives. For example, before arriving to a train station, a passenger might have already decided to first buy the ticket, then buy a newspaper and finally head to the platform. If the passenger is familiar with the environment, he/she would have already planned its route. If not, it can consult the train station's plan. In [10], it is considered that this process takes place at a strategic level. *The tactical level* At the strategical level, a preliminary path is planned that passes by the chosen the intermediary and final destinations. In the tactical level, at each decision point (intermediate destination) everything that was chosen at the strategical level is reexamined according to local conditions and circumstances such as weather, topology, traffic, etc. At this level, pedestrians might cancel certain activities and change their route. A traveler who risks missing his/her train would cancel all activities and head directly to the platform. To model this behavior, an algorithm should be capable of organizing the activities to be done (obligatory or optional) , localizing the areas where they can be accomplished (familiar with the environment or not), and computing the corresponding route.

The operational level At the operational level, pedestrians interact with their surroundings. Once on the path chosen at the upper levels, an individual interacts with other pedestrians and obstacles that it crosses on its way. Therefore the pedestrian is forced to deviate from its original route. This can be observed by comparing an individual's trajectory with its planned path. At this level, a pedestrian decides to walk, wait, or accomplish a task.

Long, medium, and short distance navigation

Another approach for classifying pedestrian route choice behavior depends on navigation as a function of distance. Navigation concerns basically all moving agents, biological or artificial, autonomous or remote-controlled. According to [12] three spatial scales exist for pedestrian navigation: (1)long range, (2) medium range, and (3) short range.

Long range navigation (10 $\sim$ 200 m) [12] considers strategic aspects, e.g. using the floor plan in a commercial center to get to a certain store. It is usually modeled by inserting a set of intermediate destinations that lead to the final target [13].

Medium range navigation (5 $\sim$ 50m) Whether a pedestrian possesses a definitive final target or not (tourists,shoppers...), it is bound to move from one intermediate destination to the next one by simply using visibility. Individuals navigate at this medium scale along the paths that corresponds to their motives (fastest, shortest, most enjoyable... path). This navigation skill can be modeled using floor field methods e.g.[14–16].

Short range navigation (1 $\sim$ 10 m) Once on the chosen path, an individual is bound to interact with other pedestrians and obstacles who happen to be in its way. This short range interaction is usually modeled by introducing pedestrian-pedestrian and pedestrian-obstacle repulsion forces.

4.1.3 Literature review on route choice models

This section focuses on modeling route choice at the tactical level or medium distance navigation. Very few studies exist on the strategical level of route choice or long distance navigation and thus will not be included in this study. Since the operational level or small distance navigation concerns pedestrian interactions, it will be left to chapter 5 dedicated to this end. In the rest of this chapter, we use the terms of the approach that classifies pedestrian route choices according to distance (Long, medium, and short range navigation) rather than the one based on pedestrian behavior (strategical, tactical and operational).

Normative pedestrian behavior theory and modeling

For an effective planning and design of infrastructure (e.g. airports, public transport stations, shopping malls, stadiums,...) and time tables provided by transit systems, it is crucial to better understand pedestrian behavior. Infrastructure designers and public transport planners tend to use modeling tools, such as pedestrian models, in order to optimize their design. In 2001, the normative pedestrian theory was introduced in [10] to provide such a tool and to address two main issues that were lacking in existing models at that time. A set of behavior rules were introduced in order to be able to simulate complex scenarios where the pedestrians' microscopic behavior is paramount. In addition, a generic theory of pedestrian flow, relating all relevant behavioral levels (see section 4.1.2), was developed. In this approach, all actions of a pedestrian, be it performing an activity or walking along a certain route, will provide *utility* (or equivalently, induce cost). The main behavioral assumption is that pedestrians are utility maximizers. They predict and optimize the expected utility while taking account the uncertainty caused by the expected traffic conditions. Hereafter, we demonstrate how the principal of utility maximization is used to model pedestrian route choice (medium distance navigation). For the other two levels of pedestrian behavior, namely activity scheduling/area choice and walking behavior, the reader is referred to [10].

In this section, we examine route choice modeling at the medium distance level using the normative theory [10]. The infrastructure is described by an area $\Upsilon \subset \mathbb{R}^2$ in which the pedestrians move except for the areas occupied by fixed obstacles Γ. Any position in Υ is denoted $\mathbf{x}$. Let us consider that a pedestrian wants to perform a single activity a such as buying a journal. The activity areas, denoted by A_j^{act}, are all the possible areas where a can be accomplished such that $A_j^{act} \subset \Upsilon$. An individual chooses an activity area depending on the walking cost to reach it and the utility (or gain) of performing the activity in it. This means that the path and the activity area are found simultaneously. Assuming that an individual arrives at A_j^{act} at time T, we denote by $\mathbf{x}_{[t,T)}$ a path that allows it to move from its current destination $\mathbf{x}(t)$ to $\mathbf{x}(T)$. The total generalized cost associated to $\mathbf{x}_{[t,T)}$ is given by:

$$C(t, \mathbf{x}, \mathbf{u}_{[t,T)}) = \int_t^T L[s, \mathbf{x}(s), \mathbf{u}^{adm}(s)]ds + \phi[T, \mathbf{x}(T)] \tag{4.1}$$

where L and ϕ represent the running cost and the terminal cost respectively and $\mathbf{u}_{[t,T)}$ the control path such that $\mathbf{u}_{[t,T)} = \{\mathbf{u}^{adm} \in \mathcal{V}(t,\mathbf{x}) \mid t \leq s < T\}$ and $\mathcal{V}(t,\mathbf{x})$ is the set of admissible velocities. $\phi[T,\mathbf{x}]$ is a gain if the pedestrians arrives at A_j^{act} on time $(t = T)$ and a cost if not. The running cost of a path is the cost incurred due to walking on it. It is the sum of the contributions of each attribute of a certain route such as the travel time, discomfort due to proximity to obstacles and walls, expected number of pedestrian interactions, etc. The running cost is defined as:

$$L(t,\mathbf{x},\mathbf{u}^{adm}) = \sum_k c_k L_k(t,\mathbf{x},\mathbf{u}^{adm}) \tag{4.2}$$

where L_k is the cost contribution of attribute k and c_k the latter's relative weight. More attributes and their costs' expressions can be found in [17]. It is assumed that the optimal route and the optimal activity area are obtained by choosing a velocity $\mathbf{u}^*_{[t,T)}$ that minimizes C:

$$\mathbf{u}^*_{[t,T)} = \arg\min\{C(t,\mathbf{x} \mid \mathbf{u}_{[t,T)})\} \tag{4.3}$$

Now to solve the path and activity area choice problem, the value function is defined as the following:

$$W(t,\mathbf{x}) = C(t,\mathbf{x};\mathbf{u}^*_{[t,T)}) \tag{4.4}$$

The value function describes the minimal expected cost of walking from $\mathbf{x}(t)$ to A_j^{act}. It can be found by solving the *Hamilton-Jacobi-Bellman*(HJB) equation [18]:

$$-\frac{\partial W}{\partial t} + H(t,\mathbf{x},\boldsymbol{\nabla} W) = 0 \tag{4.5}$$

with boundary conditions

$$W(T,\mathbf{x}) = \phi(T,\mathbf{x}) \tag{4.6}$$

In Eq.4.5, H denotes the *Hamilton function* defined as:

$$H(t,\mathbf{x},\boldsymbol{\nabla} W) \quad = \quad \min_{\mathbf{u}^{adm}\in\mathcal{V}(t,\mathbf{x})} [L + \boldsymbol{\nabla} W \cdot \mathbf{u}^{adm}] \tag{4.7}$$

Once the HJB equation is solved and $W(t,\mathbf{x})$ obtained, the latter can be plotted as isoline curves (see Fig.4.2). Finally, using $W(t,\mathbf{x})$ the optimal velocity $\mathbf{u}^* = u^*\mathbf{e}^*$ can be calculated at any position $\mathbf{x}$ and time t:

$$\mathbf{e}^*(t,\mathbf{x}) = -\frac{\boldsymbol{\nabla} W(t,\mathbf{x})}{||\boldsymbol{\nabla} W(t,\mathbf{x})||} \tag{4.8}$$

$$u^*(t,\mathbf{x}) = \max\{c_u^{-1}||\nabla_{\mathbf{x}} W(t,\mathbf{x})||, u_{max}(\mathbf{x})\} \tag{4.9}$$

where c_u is the relative weight of walking at a high speed. Eq.4.8 shows that the optimal direction is oriented towards the steepest descent of the total minimal cost $W(t,\mathbf{x})$. As a result, the optimal velocity depends on the rate of decrease $||(t,\mathbf{x})||$ of $W(t,\mathbf{x})$ in the direction of $\mathbf{e}^*(t,\mathbf{x})$.

Floor field methods

As we have mentioned earlier, floor field methods can be used to model medium scale navigation. The first step of the floor field method is to create a virtual grid structurally identical to the environmental one. Then, starting at the destination of the considered environment (Hall, building, airplane...), a wavefront is set to propagate at a normal speed towards the domain of interest. Consequently, an arrival time of this wavefront can be assigned to each point of the virtual grid. A floor field, which is a scalar function that increases with increasing distance from the destination, is then obtained. The perception of obstacles and pedestrians present in the environment depends on the choice of the wavefront velocity and leads to static or dynamic floor fields.

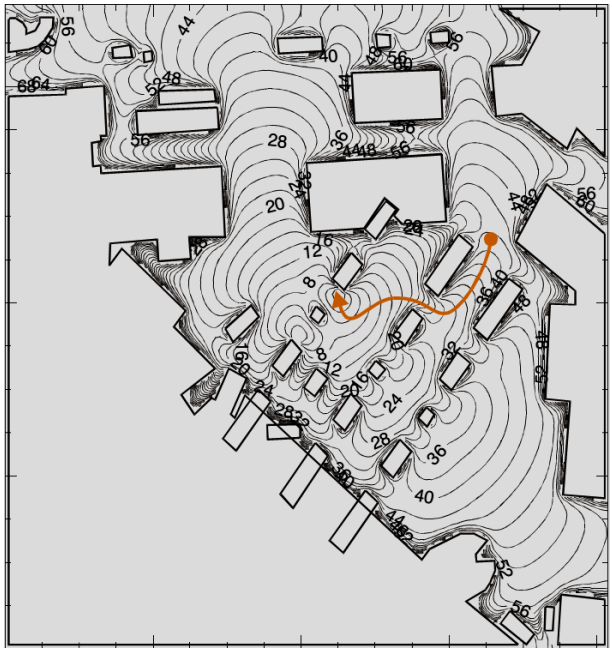

Figure 4.2: Value function $W(t, \mathbf{x})$ for pedestrians performing an activity located at the head of the arrow [19]. The optimal paths are perpendicular to the iso-value function curves.

Static floor fields

A static floor field $S(\mathbf{x})$ is calculated only once at the beginning of a simulation. It is constructed by an estimation of arrival times using the Eikonal equation:

$$\begin{aligned} V(\mathbf{x}) \mid\mid \boldsymbol{\nabla} S(\mathbf{x}) \mid\mid &= 1 \qquad in\ \Upsilon, \\ S(\mathbf{x}) &= 0 \qquad on\ \partial\Upsilon \end{aligned} \tag{4.10}$$

where $S(\mathbf{x})$ is the floor field obtained by calculating the arrival times of a wavefront starting at the destination $\partial\Upsilon$ and propagating at a normal velocity $V(\mathbf{x})$ in the domain Υ. Inside the obstacles, $V(\mathbf{x})$ is set to 0 since they cannot be penetrated by the wavefront. However, outside the obstacles and in the domain of interest, the choice of $V(\mathbf{x})$ leads to different results. If $V(\mathbf{x})$ is chosen to be equal to one, the arrival times $S(\mathbf{x})$ coincide with exact Euclidean distances to the destination. In other words, from every point of the virtual grid, the length of the shortest path towards the target is obtained. By varying the values of $V(\mathbf{x})$ ($V(\mathbf{x}) \neq 1$ and $V(\mathbf{x}) > 1$) from one region to the other, the wavefront speed varies and results in different weightings of distance. Consider for example the case of a wet floor. Setting a value of $V(\mathbf{x}) < 1$ leads to slower propagation of the wavefront in the precised region. Virtually, the path that passes through the wet floor will appear longer than the one that goes around it. Since pedestrians move along geodesics, they will avoid the wet area.

The floor field $S(\mathbf{x})$ is obtained by solving Eq. 4.10. This can be done using several methods such as the Fast Marching Method (FMM) [20, 21], the Fast Iterative Method (FIM)[22], or the Fast Sweeping Method (FSM) [23]. Finally, for a certain environment, $S(\mathbf{x})$ (Fig.4.3) can be used to find the direction from any point $\mathbf{x}$ towards the exit (see Fig.4.4):

$$\mathbf{e}^*(\mathbf{x}) = -\frac{\boldsymbol{\nabla} S(\mathbf{x})}{||\boldsymbol{\nabla} S(\mathbf{x})||} \tag{4.11}$$

Since static floor fields are calculated at the beginning of simulations, the presence of pedestrians is not taken into consideration. Agents will only perceive fixed obstacles (walls, columns, furniture,

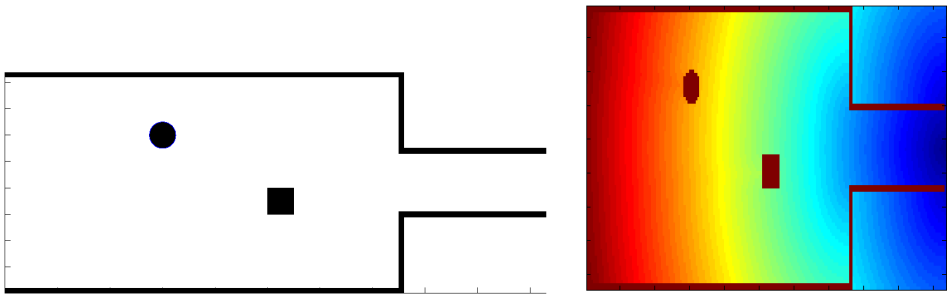

(a) (b)

Figure 4.3: An illustration of (a) an environment with walls and two obstacles and (b) the corresponding static field $S(\mathbf{x})$.

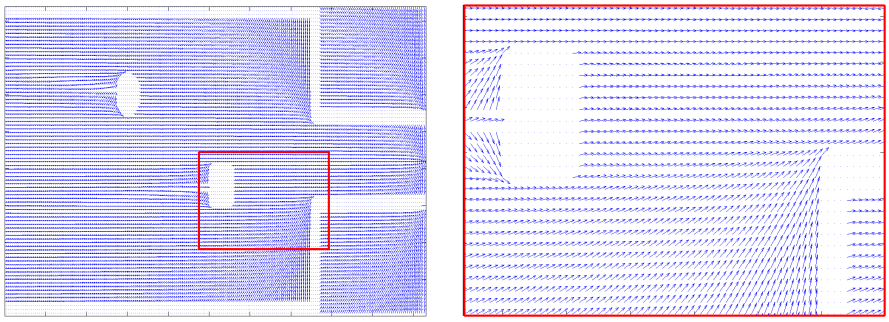

(a) (b)

Figure 4.4: The direction from any point $\mathbf{x}$ towards the exit of the environment shown in Fig. 4.3(a)

...). Pedestrian-pedestrian interactions will only take place at a short range if a social repulsive force is introduced. For this reason, pedestrians go through congestions instead of avoiding them (see Fig.4.5(a) and 4.6(a)). To eliminate unrealistic congestions, the dynamic floor field can be used.

Dynamic floor fields

To choose their path, individuals consider all the pedestrians and the congestions that are visible to them. To model this medium navigation behavior, dynamic floor fields can be used. They are calculated at every time step in order to take into consideration the traffic evolution. The dynamic floor field $D(\mathbf{x}, t)$ is constructed by solving the following Eikonal equation:

$$V(\mathbf{x}, t) \mid\mid \boldsymbol{\nabla} D(\mathbf{x}, t) \mid\mid = 1 \qquad in\ \Upsilon, \tag{4.12}$$

$$D(\mathbf{x}, t) = 0 \qquad on\ \partial\Upsilon \tag{4.13}$$

Here, the expression of $V(\mathbf{x}, t)$ depends on space and time. In this way, $D(\mathbf{x}, t)$ will represent expected travel times giving the fastest path displacement strategy. Using this strategy, the agents will avoid congested shortest paths for the longer fastest ones. Several expressions of $V(\mathbf{x}, t)$ exist. In [24], the expression of $V(\mathbf{x}, t)$ is chosen in a way so as to capture the effect of the current velocity of the agent that occupies a certain point of the virtual grid compared to the average velocity of the agents present in the domain of interest. $V(\mathbf{x}, t)$ is defined by :

$$\frac{1}{V(\mathbf{x}, t)} = 1 + max\Big(0, g_D(1 + h_D \frac{\mathbf{u}(\mathbf{x}, t) \cdot \boldsymbol{\nabla} S(\mathbf{x})}{u_0 \mid\mid \boldsymbol{\nabla} S(\mathbf{x}) \mid\mid})\Big) \tag{4.14}$$

where $\mathbf{u}(\mathbf{x},t)$ is the current velocity of the agent occupying the cell, u_0 the average desired speed of all the agents and g_D and h_D are free parameters of the method. The method's general impact strength is given by g_D, i.e. if $g_D = 0$, a static floor field is obtained since $V(\mathbf{x},t) = V(\mathbf{x}) = 1$. The effect of the agent's displacement direction is given by h. Let us consider two agents where i is walking in front of j and both have the same direction. If $||\ \mathbf{u}_i\ ||> u_0$, then Eq. 4.14 gives $V(\mathbf{x},t) = 1$ and both individuals continue walking normally. However, if $||\ \mathbf{u}_i\ ||< u_0$, then Eq. 4.14 gives $V(\mathbf{x},t) < 1$ and agent j will overtake agent i (see Fig.4.5).

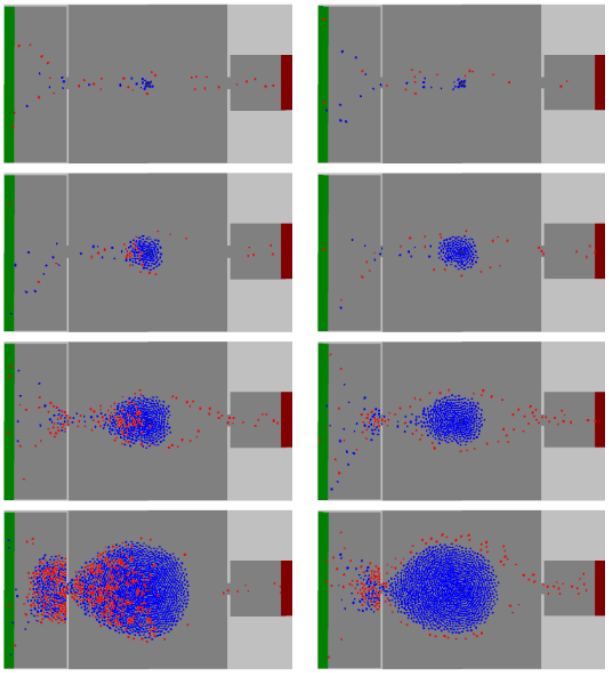

Figure 4.5: The red agents move from the green to the red zone while the blue agents head to the middle of the large room. The figure shows the different behavior when using a (left) static potential and (right) a dynamic one [24].

Another approach was introduced by [12] where the estimated travel speed $V(\mathbf{x},t)$ depends on the local pedestrian density. The expression of $V(\mathbf{x},t)$ is given by :

$$\frac{1}{V(\mathbf{x},t)} = \big(1 + w_D\rho(\mathbf{x},t)\big) \tag{4.15}$$

where w_D is a constant and $\rho(\mathbf{x},t)$ is the local pedestrian density (ped/m^2). Hartmann applied this approach for a cellular automaton model where $\rho(\mathbf{x},t)$ is considered to be piecewise constant on the cells such that

$$\rho(\mathbf{x},t) = \begin{cases} 0 & \text{if } \mathbf{q}_i(t) \neq \mathbf{x} \\ 5.4 & \text{if } \mathbf{q}_i(t) = \mathbf{x} \end{cases} \tag{4.16}$$

where $\mathbf{q}_i(t)$ is the position of a pedestrian i in 2D. Following this approach, regions with high pedestrian density are avoided by the incoming agents (see Fig. 4.6). The value of $\rho(\mathbf{x},t) = 5.4\,ped/m^2$ that is given to occupied cells comes from the choice of the size of the cells in the cellular automate model used in [12]. Each cell accommodates an average European male having a size of $0.185\,m^2$ [6] giving a density in each cell equal to $\rho = 1/0.185 = 5.4\,ped/m^2$.

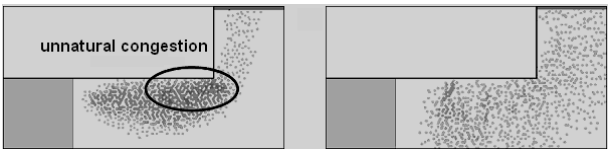

Figure 4.6: By considering densities (dynamic floor field-right), unnatural congestions (static floor field-left) can be avoided [12].

Multi-scale models

In crowd modeling, one uses macroscopic models to study large-scale behavior and navigation. It is then necessary to use microscopic models to be able to examine local phenomena that sometimes emerge as a result of large scale navigation. Both tasks can be accomplished using multi-scale models that combine both levels of modeling. The challenge in this case is to be able to keep the advantages or the realistic qualitative properties of each layer and overcome their drawbacks (difficulty to estimate travel times (macro) and extensive computation times (micro)). In what follows, a brief overview of existing multi-scale models shows us if and how information is exchanged between the microscopic and macroscopic levels.

In general, multi-scale models are made up of two layers: (i) a small-scale layer modeling a pedestrian's navigation towards a particular destination and (ii) a large-scale layer modeling long distance navigation by choosing the next intermediate destination.

On the small-scale layer, forces similar to those of Newtonian particle mechanics steer pedestrians towards their desired destination. To do so, continuous force-based models ([25–29]) usually use an attractive force while cellular automata models [16, 30–32] use a potential-based approach. The potentials are often referred to as floor fields or navigation fields. As was explained in 4.1.3, in potential-based approaches, pedestrians move in the direction of decreasing potential value.

On the large-scale layer, most multi-scale models use graph-based approaches to model the pedestrians' navigation strategy [33, 34]. In these approaches, for a given geometry, the possible routes are identified and used to construct the navigation graph. This graph is made up of vertices that represent crossings or landmarks and that will be used to orient pedestrians from their origin to their final destination (for example see Fig. 4.7). At each vertex or intermediate destination, a pedestrian must choose which path to take. This decision depends on each pedestrian's route selection strategy (e.g. shortest path, fastest path, avoiding congestions, following friends, following signage, ...).

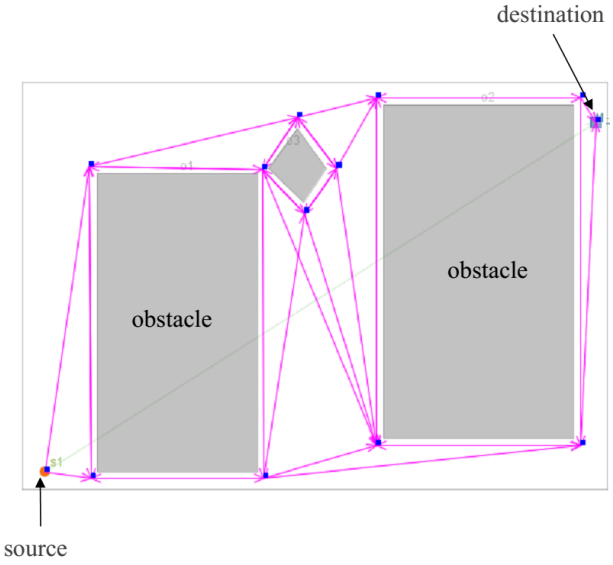

Figure 4.7: An example of a navigation graph [35].

By combining the small and large scale layers, the multi-scale model is obtained (see Fig. 4.8). The pedestrians' paths or routes (a series of intermediate destinations connecting the origin to the final destination) are calculated using the navigation graph and a chosen navigation strategy. The navigation field is then used to orient the pedestrians between each two intermediate destinations. Although multi-scale models are successful in improving the realism of simulations, there are still other troublesome aspects that need to be addressed on both levels.

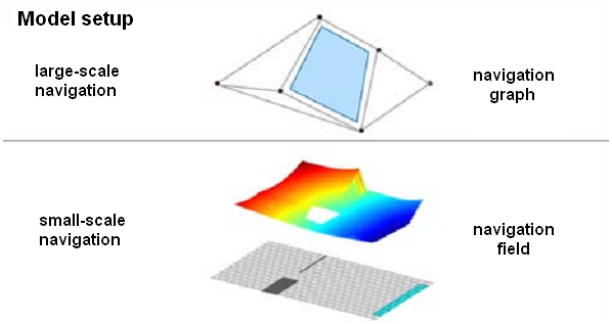

Figure 4.8: An illustration of the multi-scale model setup [36].

For small-scale navigation, static fields, calculated once in the initialization phase of the simulation, are widely used [14, 16, 31, 37, 38]. Static fields lead to unrealistic pedestrian behavior where individuals always take the shortest path even if it is highly congested. To resolve this issue, the dynamic field was introduced [38, 39]. Though successful, this approach needs a continuous update (i.e. computationally expensive) and allows pedestrians to avoid congestion even when it is still not 'visible' (Fig. 4.9).

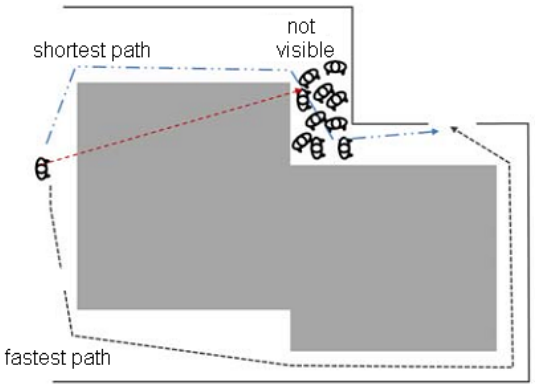

Figure 4.9: Using the dynamic floor field, the pedestrian to the left avoids the congestion even without having a 'visual' evidence that it exists [36].

Concerning large-scale navigation, each segment of a possible route is attributed a weight which is often a heuristic estimate of travel time. These estimates depend on the number of pedestrians using the corresponding route. However, using a local property, i.e. densities or congestions, to determine the weight of a possible route is problematic. A pedestrian would choose a longer route in order to unnecessarily avoid a congestion that will have already disappeared by the time he/she reaches it (see Fig. 4.10). Therefore, a better estimation of travel times is needed.

In [36], a hybrid multi-scale model was introduced that addressed several of the above mentioned problems. In this approach the information exchange between the two navigation levels is emphasized. First, we start at the large-scale layer where the navigation graph identifies visible and invisible areas for each pedestrian. Second, at the small-scale layer, the vertices are used to calculate the dynamic navigation fields. The navigation fields and mean travel times are to be used to estimate the weight of each segment (part of the whole route) in the visible and invisible areas respectively. Then, these weights go back to the navigation graphs to recalculate the possible routes to destination and assign one

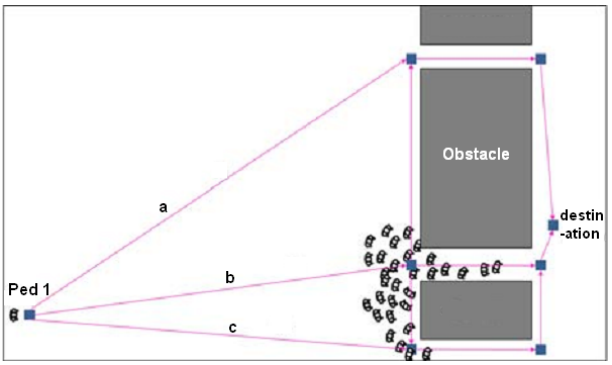

Figure 4.10: Ped 1 takes route a even though the congestion on routes b and c aren't important [36].

for each pedestrian. Finally, using the navigation fields, each individual's position is updated and the loop repeats itself. In conclusion, over intelligent behavior is dismissed (visible and non-visible areas), traveling time estimations are improved, and a more realistic pedestrian behavior is obtained (dynamic navigation fields). In addition, using the vertices to calculate the navigation fields makes it possible to construct the latter in a directed manner. Rather than calculating it for the whole environment, the navigation fields are computed for a minimal area (only where there are pedestrians). Directed floor fields will be discussed later in this chapter.

Event driven way finding

Using a graph-based structure (see Fig. 4.7), an event driven way finding was introduced in [40]. In this approach, pedestrians take decisions based on previously made observations of their surroundings and their knowledge of the environment. The latter reflects the long distance aspect of this method. Pedestrians who are familiar with the environment choose a global version of the shortest/quickest path i.e. their route is already planned from their starting point to the final destination. On the other hand, unfamiliar individuals can only use the local version of the shortest/quickest path. They plan their routes towards one visible intermediate destination at a time. Now the question is how do pedestrians switch between shortest or quickest path based on the made observations. According to [40], after starting with the shortest path (local or global) the procedure of finding the next suitable destination goes as follows:

- Pedestrian i reaches a decision area where it has to choose its next intermediate destination. A pedestrian is in a decisions area whenever it enters a new room or a corridor. These are connected via nodes (see Fig. 4.11) that can be chosen by agents as intermediate destinations. Another scenario is when pedestrian i is stuck in congestion i.e. $|| \mathbf{u}_i ||< u_{min}$ where $u_{min} = 0.2\, m.s^{-1}$ [40]. After a user-defined period t_{min} (patience time) has passed, the agent tries to find an intermediate destination different than the one it had previously chosen. For example, in Fig. 4.11(a), pedestrian 1 enters a new decision area while pedestrians 2, 3, and 4 have passed more than t_{min} in a jam and want to search for other possible destinations.

- Pedestrian i picks a visible reference pedestrian j from the jamming queue $Q(n_k)$ of each visible node n_k such that $P_{Ref}(i, n_k) = j$. For example in Fig. 4.11(a), agent 1 selects individuals 5, 6, and 8 as references for the exits n_2, n_3, and n_4 while agent 2 on exit n_2 cannot choose any reference due to restricted visibility. Now that the reference pedestrians are known, they are observed for t_{obs} seconds ($1\,s \leq t_{obs} \leq 3\,s$) [40]. At the end of the observation time, an expected travel time $t(\mathbf{q}_i, \mathbf{q}_{n_k})$ is associated to each node visible to pedestrian i using the following equation:

$$t(\mathbf{q}_i, \mathbf{q}_{n_k}) = \begin{cases} \frac{\|\mathbf{q}_i - \mathbf{q}_j\|}{\|\mathbf{u}_i\|} + \frac{\|\mathbf{q}_j - \mathbf{q}_{n_k}\|}{\|\mathbf{u}_{j,obs}\|} & \text{if } P_{ref}(i, n_k) \neq 0 \\ \frac{\|\mathbf{q}_i - \mathbf{q}_{n_k}\|}{\|\mathbf{u}_i\|} & \text{if } P_{ref}(i, n_k) = 0 \end{cases}$$

where $\mathbf{u}_{j,obs}$ is the average velocity of $P_{ref}(i, n_k)$ over the observation period t_{obs}:

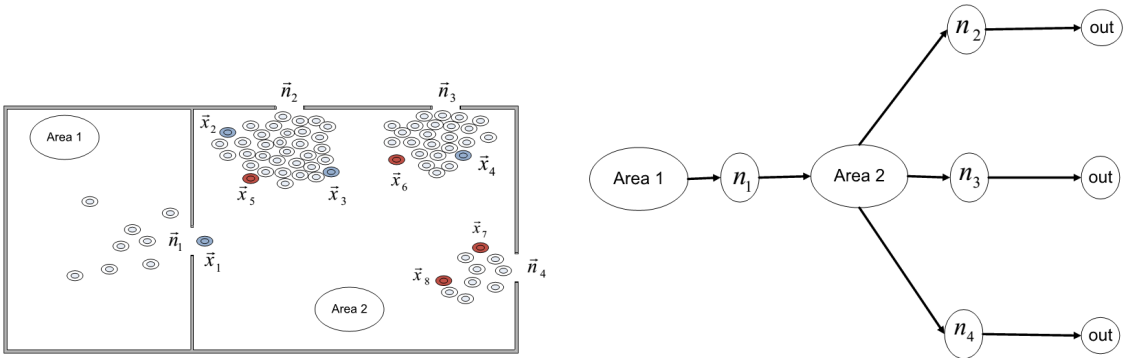

(a) (b)

Figure 4.11: An example of (a) an environment and the corresponding (b) network mapping [40].

$$\| \mathbf{u}_{j,obs} \| = \frac{1}{t_{obs}} \int_{t}^{t+t_{obs}} \| \mathbf{u}_j \| (t) dt \tag{4.17}$$

- The estimated time $t(\mathbf{q}_i, \mathbf{q}_{n_k})$ is then converted to a gain:

$$G(\mathbf{q}_i, \mathbf{q}_{n_k}) = G_{i,k} = \frac{1}{t(\mathbf{q}_i, \mathbf{q}_{n_k})} \tag{4.18}$$

- For each alternative destination the cost benefit analysis (C^{ba}) [40] is calculated:

$$C^{ba}_{i,k} = \frac{G_c - G_{i,k}}{G_c + G_{i,k}} \tag{4.19}$$

  where G_c represents pedestrian i's current destination.

Finally, agent i chooses alternative n_k only if $C^{ba}_{i,k}$ is greater than a threshold of 0.2 for individuals familiar with the environment and 0.15 for the unfamiliar ones [40]. No information was provided by the author on how these values were obtained. The evacuation of 1000 pedestrians, with an initial configuration shown in Fig. 4.12, using different strategies (shortest and quickest paths) for familiar (global path) and unfamiliar pedestrians (local path) is illustrated in Fig. 4.13.

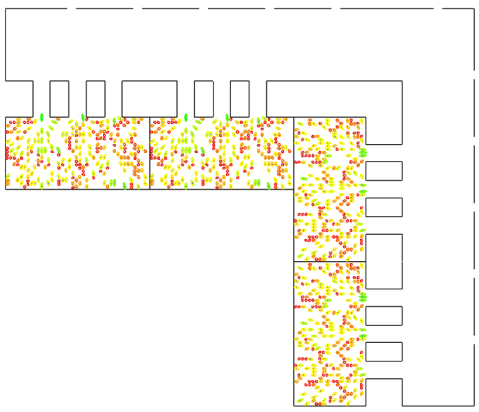

Figure 4.12: 1000 pedestrians distributed in four blocks [40].

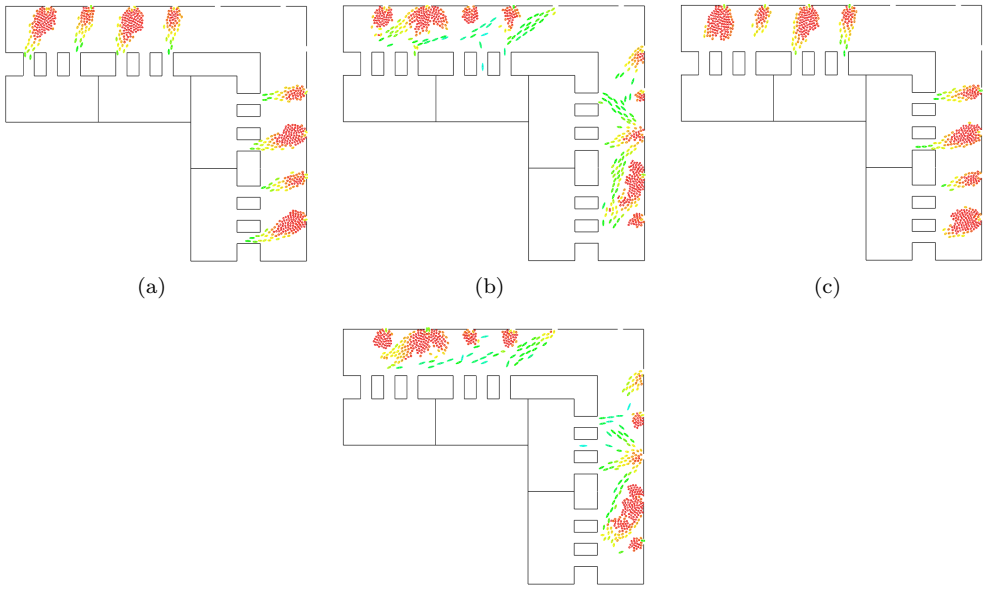

Figure 4.13: Simulation of an evacuation of 1000 pedestrians using (a) the local shortest path, (b) the local shortest with quickest path, (c) the global shortest path, and (d) the global shortest with quickest path [40].

In this section, we have done a bibliographical study on pedestrian route choice. First, we have defined several key terminology to clarify how they are employed and in which context. We then described two approaches that are used to divide the decision making process into three levels : (i) the strategic, tactical, and operational level on one hand and (ii) the long, medium, and short distance navigation on the other. Following this categorization, a brief literature review was done on approaches used to model pedestrian route behavior at the tactical level (medium distance navigation).

In the next section, the work that has been done on pedestrian route choice in our model is demonstrated.

4.2 Pedestrian route choice in the 2D discrete model

In the previous section, a bibliographical study was done on certain aspects of pedestrian route choice that are relevant to our interest. The aim of this section, is to precise what have we retained from this study and to present the work that has been done on our model concerning pedestrian route choice.

To begin with, we have decided to adopt the approach that classifies pedestrian route choices according to distance (Long, medium, and short range navigation) rather than the one based on pedestrian behavior (strategical, tactical and operational). We have found the former to be more easily conveyed leaving no room for confusion. At this stage, we are only interested in medium and short range navigation. Therefore, in the rest of this chapter, we illustrate the chosen methods that where used to model each level of navigation.

4.2.1 Medium distance navigation

As have been previously mentioned, medium scale ($5 \sim 50$m) navigation is moving from one intermediate destination to the next one. At this level, pedestrians can use several strategies, for example, fastest, shortest, most enjoyable... path (see Fig. 4.14). In the scope of this work, we are interested in modeling the shortest and fastest path strategies using the static and the dynamic floor fields respectively.

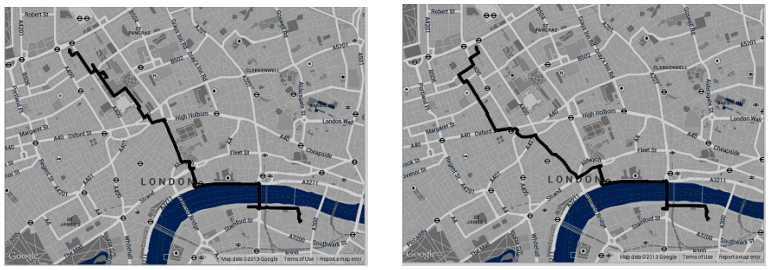

(a) (b)

Figure 4.14: Maps showing the (a)shortest and (b) the "happiest" paths between Euston Square and Tate Modern in London [41].

The floor fields method has already been introduced in section 4.1.3. To help the reader it is recalled here. A floor field $T(\mathbf{x}, t)$ is constructed by an estimation of arrival times using the Eikonal equation:

$$\begin{aligned} V(\mathbf{x}, t) \mid\mid \boldsymbol{\nabla} T(\mathbf{x}, t) \mid\mid &= 1 \qquad in\ \Upsilon, \\ T(\mathbf{x}, t) &= 0 \qquad on\ \partial\Upsilon \end{aligned}$$

where $T(\mathbf{x}, t)$ is the floor field obtained by calculating the arrival times of a wavefront starting at the destination $\partial\Upsilon$ and propagating at a normal velocity $V(\mathbf{x}, t)$ in the domain Υ. Inside the obstacles, $V(\mathbf{x}, t)$ is set to 0 since they cannot be penetrated by the wavefront. However, outside the obstacles and in the domain of interest, the choice of $V(\mathbf{x}, t)$ leads static or dynamic floor fields.

4.2.2 The static floor field

The static floor field has been already used in our model only for $V(\mathbf{x}, t) = V(\mathbf{x}) = 1$ [42] and the shortest path strategy was successfully modeled. In this section, we shed the light on certain aspects and parameters of floor fields that influence pedestrian trajectories. Later in this section, the static floor field will be denoted as $S(\mathbf{x})$ and the dynamic floor field as $D(\mathbf{x}, t)$.

The influence of floor field parameters on pedestrian trajectories

Using a static floor field with $V(\mathbf{x}) = 1$ everywhere except inside static obstacles allows to model the shortest path strategy. A unit vector in the shortest direction is assigned to the center of the agent not taking its dimensions into consideration (an agent is represented by a disk of radius r_i). As a result, when $V(\mathbf{x}) = 1$ everywhere in the environment (Fig. 4.15(a)) and the shortest path is very close to an obstacle (wall, column,...), the agent collides with the latter as illustrated in Fig. 4.16(a). However, it is possible to model repulsive and attractive areas using floor fields. By assigning a value of $0 < V(\mathbf{x}) < 1$ to the nodes that are found at a shy away distance D_{shy} from the obstacles (see Fig. 4.15(b)) the agents avoid the walls (Fig. 4.16(b)). If we want the agents to be attracted to a certain area, it is enough to set $V(\mathbf{x}) > 1$ in this area. The chosen value of $V(\mathbf{x})$ controls the intensity of the repulsion or attraction in the considered area and D_{shy} its dimensions. Two questions are raised: (1) What is the influence of D_{shy} and $V(\mathbf{x})$ on pedestrians trajectories and (2) how should their values be chosen?

To answer the first question, we consider the scenario illustrated in Fig. 4.17. In this scenario, a pedestrian starts at the left of the environment and wants to reach the destination to the right of it with two obstacles found in his/her way. To study the influence D_{shy} and $V(\mathbf{x})$ on the shape of the trajectory taken by the pedestrian, 400 simulations were done for 20 values of each of D_{shy} and $1/V(\mathbf{x})$ uniformly distributed in the intervals $[0, 100]\,cm$ and $[1.01, 100]\,s/m$ respectively. For each couple $(D_{shy}, 1/V(\mathbf{x}))$, the deviation of the corresponding trajectory y^{traj} from the line joining the pedestrian's initial and final position $\hat{y}$ (shown as dotted line in Fig. 4.17) was defined as the following:

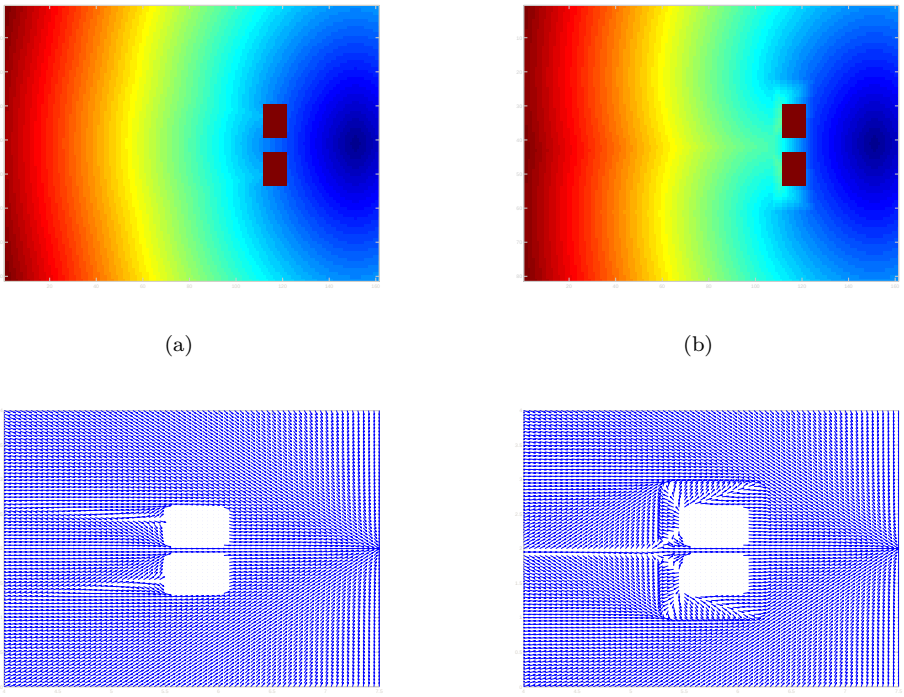

(a) (b)

(c) (d)

Figure 4.15: $S(\mathbf{x})$ obtained for (a) $1/V(\mathbf{x}) = 1\,s/m$ everywhere and $D_{shy} = 0\,cm$ and (b) $1/V(\mathbf{x}) = 50\,s/m$ near walls for $D_{shy} = 35\,cm$ and the corresponding directing unit vectors towards toward the shortest path for (c) $1/V(\mathbf{x}) = 1\,s/m$ everywhere and $D_{shy} = 0\,cm$ and (d) $1/V(\mathbf{x}) = 50\,s/m$ near walls for $D_{shy} = 35\,cm$.

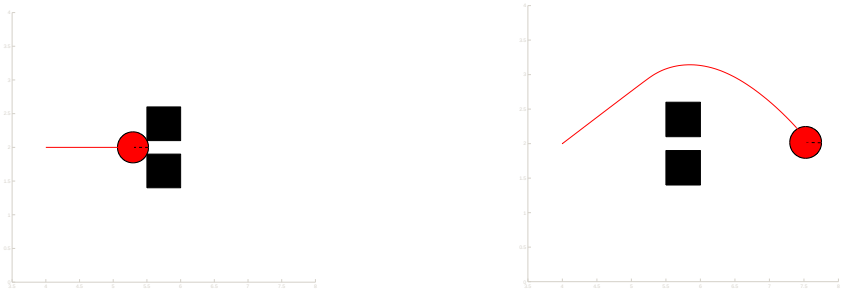

(a) (b)

Figure 4.16: The trajectory of an agent for (a) $1/V(\mathbf{x}) = 1\,s/m$ everywhere and $D_{shy} = 0\,cm$ and (b) $1/V(\mathbf{x}) = 50\,s/m$ near walls for $D_{shy} = 35\,cm$.

$$\epsilon = \frac{1}{N}\sum_{i=1}^{N}(1 - \frac{y_i^{traj}}{\hat{y}_i})^2 \tag{4.20}$$

where N depends on the sample rate used to trace the pedestrian's trajectory. The aim is not to precise an error criterion or find the optimal value of D_{shy} and $V(\mathbf{x})$ but to find out their influence on the

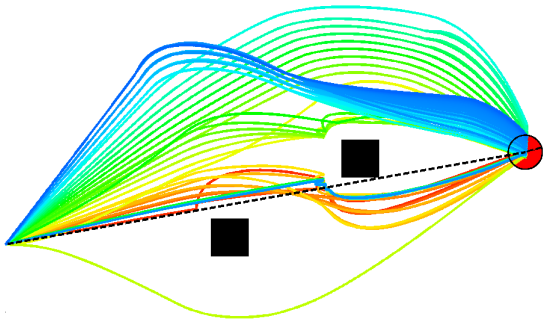

Figure 4.17: The effect of D_{shy} on pedestrians' trajectories. The dotted line joins the initial and final position of the pedestrian and the solid lines are his/her trajectories for different values of D_{shy}.

pedestrian's trajectory. By plotting ϵ as a function of D_{shy} and $V(\mathbf{x})$, it can be noticed from Fig. 4.18 that the pedestrian's trajectory is influenced by D_{shy} for $D_{shy} > 0.4\,m$ and by $V(\mathbf{x})$ for $1/V(\mathbf{x}) < 6\,s/m$.

Now that the influence of the shy away distance and the wavefront velocity is established, we try to answer the second question that was raised concerning the values of D_{shy} and $V(\mathbf{x})$ to be chosen. This is very important since very different trajectories can be obtained for different values of these two parameters (see Fig. 4.17). Ideally, an experiment can be done where pedestrians trajectories are tracked. Then we can search for the values of D_{shy} and $V(\mathbf{x})$ that reproduce the experimentally obtained trajectories. Unfortunately this data does not exist. In literature, we can only find values of the shy away distances with obstacles and other elements of the surrounding environment (see Table 4.1) without any data on pedestrian trajectories. For this reason, the choice of the values of these parameters has to be made by the modeler and depends on his/her experience. Visual inspection of the obtained trajectories is sometimes the only criterion.

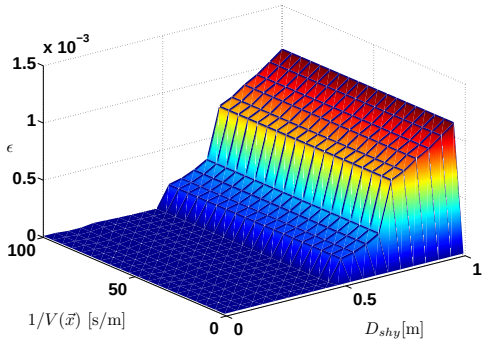

Figure 4.18: The value of ϵ as a function of D_{shy} and $1/V(\mathbf{x})$.

So far the microscopic effect of D_{shy} on pedestrian trajectories have been illustrated. However, the shy away distance also has a macroscopic effect. In the case of a bottleneck, when pedestrians keep a shy away distance from obstacles, a self-organization phenomenon appears called the funnel effect. This phenomenon can be modeled by using a static floor field that takes into consideration a distance D_{shy} with the walls (Fig. 4.19).

Choosing the exit area

In every simulation, an exit area must be defined as the final destination of the pedestrians. It also serves as a sink that removes individuals from the environment once they have reached the final destination. In floor fields, an exit area is defined by assigning a value of $V(\mathbf{x}) = 0$ to all the corresponding nodes. For example, if the exit area is $1\,m$ long and $1\,m$ wide, then all the nodes falling in this area are assigned a

Element	Distance(m)	Source
Concrete Walls	0.30-0.45	[11]
	0.45	[43]
	0.15	[44]
	0.40	[6]
	0.25	[45]
Metal walls	0.20	[6]
Obstacles	0.40	[45]
	0.10	[6]
Opposite flows	0.60	[43]
Pedestrians	0.27	[46]
Platform edges	0.80	[45]

Table 4.1: Shy away distance of pedestrians

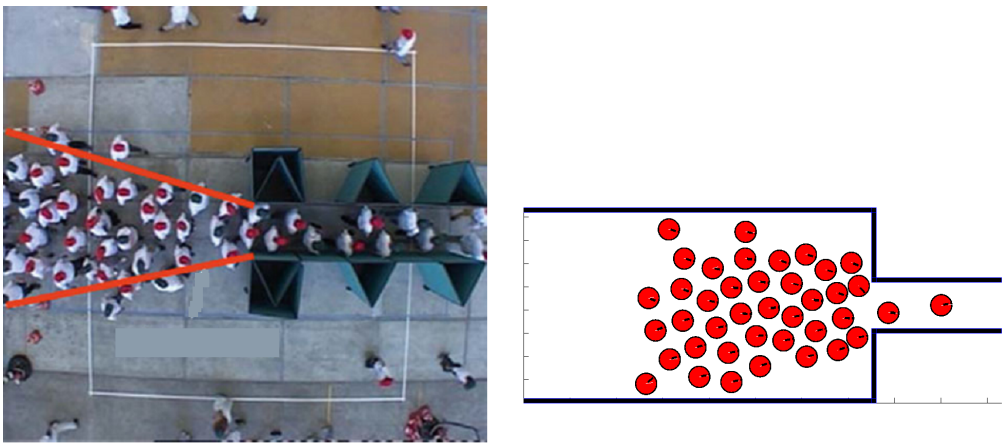

(a) (b)

Figure 4.19: The funnel shape upstream a bottleneck obtained (a) in an experiment [47] and (b) by our model.

value of $V(\mathbf{x}) = 0$. It has been found that the shape of the exit area can have an influence on pedestrian trajectories.

While studying the evacuation of pedestrians through a bottleneck, it has been noticed that pedestrians, in our model, had a 'preference' to one side of the latter (Fig. 4.20(b)). At first, it was thought that this result was related to the initial configuration as the pedestrians' initial positions were slightly offset to the right (Fig. 4.20(a)). Since correcting the offset had no effect, we then investigated the choice of the exit area.

A pedestrian's trajectory was studied for two types of exits as illustrated in Fig. 4.21: (i) exit area 1 is the one used in Fig. 4.20(a) which means that all the nodes falling in the blue rectangle are given a value of $V(\mathbf{x}) = 0$ and (ii) exit area 2 which is a single node at the midpoint of the bottleneck. The dotted line in Fig. 4.21 represents the trajectory of a pedestrian obtained for exit area 1 and the solid line represents the trajectory obtained for exit area 2. The deviation between the two trajectories starts at the entrance of the bottleneck. The reason behind this results is related to the algorithm used to calculate the floor field. Even though all the nodes inside the exit area 1 are considered to be exit points, the algorithm treats them one after the other. This leads to a global minimum represented only by the first treated node of the list containing all the exit nodes instead of global minima represented by all the exit nodes.

We now repeat the exact same experiment that was illustrated in Fig. 4.20(a) this time by choosing exit area 2 (Fig4.22(a)). The distribution of the pedestrians inside the bottleneck is similar to a bimodal

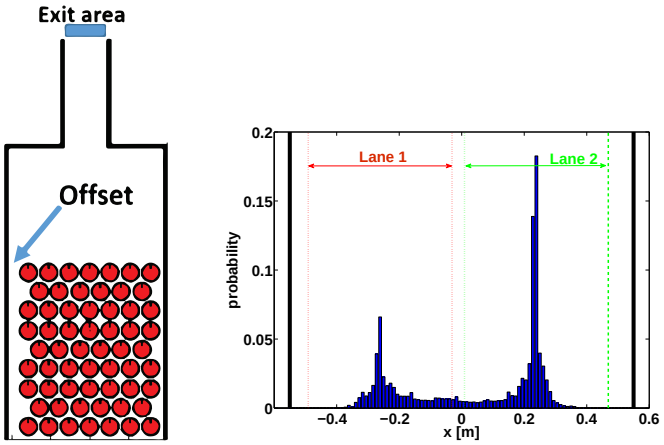

(a) (b)

Figure 4.20: Bottleneck evacuation: (a) the initial pedestrian positions and (b) the probability of finding a pedestrian at position x. The black solid lines in (b) are the boundaries of the bottleneck and the the dotted lines represent the two main lanes that formed inside it. The width of each lane is taken equal to the diameter of the disk representing each pedestrian ($diam_i = diam = 0.46\,m$).

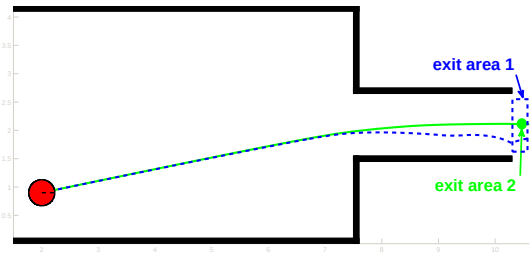

Figure 4.21: The influence of the chosen size of the exit area on pedestrian trajectories: (a) the dotted line is the trajectory of the agent for exit area 1 and (b) is the one for exit area 2.

distribution indicating the formation of two primary lanes (Fig. 4.22(b)). This result conforms with empirical data [48–50].

Important Remark: In the next paragraph, modeling medium distance navigation ($5\sim 50\,m$) using dynamic floor fields is illustrated. The reader will notice that to address some of the problematic aspects of applying dynamic floor fields in continuous models, certain cases of short range navigation ($1\sim 10\,m$) are used. This is done since the same problems occur for both levels of navigation but the short range one allows us to obtai more clear figures and illustrations. In our model, dynamic floor fields are not used to model short range navigation (even though they can be used) because of the computation cost. They are used to model medium distance navigation by taking the evolution of traffic into consideration.

4.2.3 The dynamic floor field

In literature floor field methods have been only applied for cellular automata models where the environment is discretized into cells. Take for example the cellular automaton shown in Fig. 4.23. Each

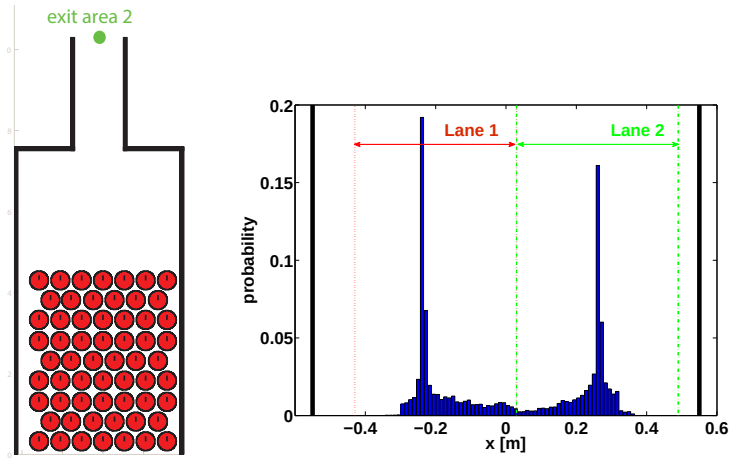

(a) (b)

Figure 4.22: Bottleneck evacuation for exit area 2: (a) the initial pedestrian positions and (b) the probability of finding a pedestrian at position x. The black solid lines in (b) are the boundaries of the bottleneck and the dotted lines represent the two main lanes that formed inside it. The width of each lane is taken equal to the diameter of the disk representing each pedestrian ($diam_i = diam = 0.46\,m$).

pedestrian occupies a single cell and can only move to unoccupied ones. For each occupied cell the value of $V(\mathbf{x}, t)$ is assigned to be lower than 1. The dynamic floor field is then calculated and the direction towards the fastest path is obtained for each cell.

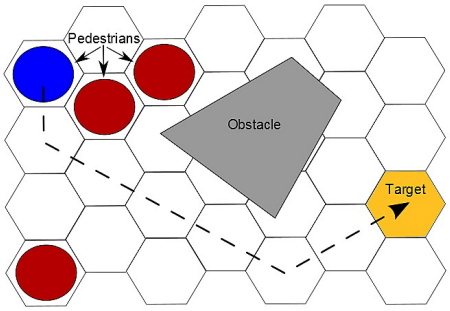

Figure 4.23: A Cellular automaton [51].

We now try to apply the same approach to continuous models. In these models, the desired direction is given by the node occupied by the center of the disk representing a pedestrian (represented by the red node in Fig. 4.24). Two other types of nodes exist. The ones that are found under the area of the disk, represented by blue nodes in Fig. 4.24, and the ones that are found outside of this area represented by the green nodes.

Now to decrease the value of $V(\mathbf{x}, t)$ for the areas occupied by pedestrians we have two options: (i) consider only the red node occupied by the center of the disk or (ii) the red and blue nodes which are found inside the disk. Two cases are considered: (i) a mobile pedestrian walking behind an immobile one and tries to overtake the latter and (ii) a mobile pedestrian walking behind a group of immobile pedestrians.

Case of overtaking an immobile pedestrian

Let us consider the case of a mobile pedestrian walking behind an immobile pedestrian. The former is expected to overtake the latter by taking the quickest path. We examine the first option which is

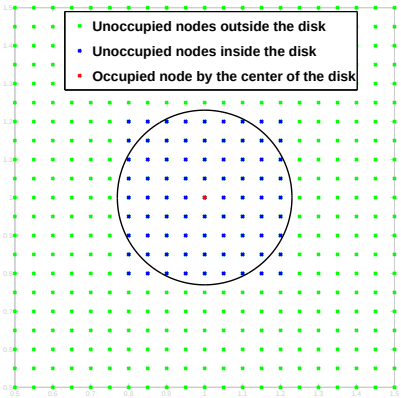

Figure 4.24: The nodes occupied by a disk of radius $0.23\,m$ representing a pedestrian.

decreasing the value of $V(\mathbf{x},t)$ for the red node. After this modification, we calculate the direction towards the quickest path for each node of the environment. As shown in Fig. 4.25 (a), the change in the direction of the vectors pointing towards the quickest path is almost insignificant and a collision takes place instead of overtaking (see Fig. 4.25 (b)).

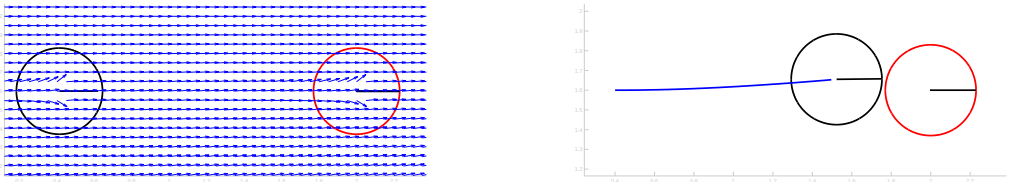

(a) (b)

Figure 4.25: The quickest path around an immobile pedestrian: If $V(\mathbf{x},t)$ is modified only for the red node (see Fig.4.24), (a) the change in the direction of the unit vectors pointing to the quickest path is insignificant and (b) a collision takes place instead of overtaking. The pedestrian to the left is mobile and the one to the right is immobile. The blue line represents the trajectory of the mobile pedestrian.

The second option is examined which consists of decreasing the value of $V(\mathbf{x},t)$ for the red and blue nodes (see Fig. 4.24). The same procedure described in the previous paragraph is repeated. This time, the change in the direction of the vectors pointing towards the quickest path is significant (see Fig. 4.26 (a).

However,as can be seen in Fig. 4.25 (b), this change is not enough for an overtaking to take place. However, if Fig. 4.25 (b) is closely examined, it can be noticed that the center of the disk representing the mobile pedestrian was able to overtake the immobile pedestrian. This means that the mobile pedestrian doesn't take his/her dimensions into consideration when trying to move around the pedestrian at rest. Therefore, we now examine a third option which is to decrease the value of $V(\mathbf{x},t)$ in an area equal to the double of the one occupied by a pedestrian (see Fig. 4.27 (a)). In this case, the change in the direction of the unit vectors toward the fastest path is enough for overtaking to take place as seen in Fig. 4.27 (b).

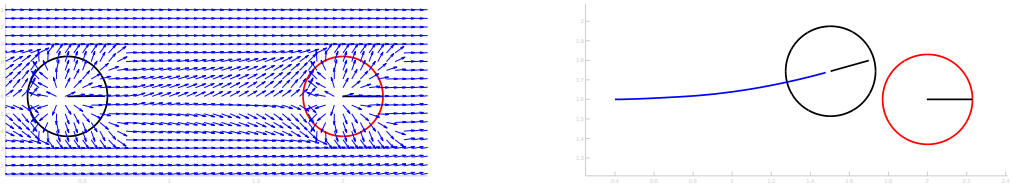

(a) (b)

Figure 4.26: The quickest path around an immobile pedestrian: If $V(\mathbf{x}, t)$ is modified for the area occupied by each pedestrian i represented by a disk of radius r_i, (a) the change in the direction of the unit vectors pointing to the quickest path is significant but (b) not enough for the mobile pedestrian to overtake the immobile one. The blue line represents the trajectory of the mobile pedestrian.

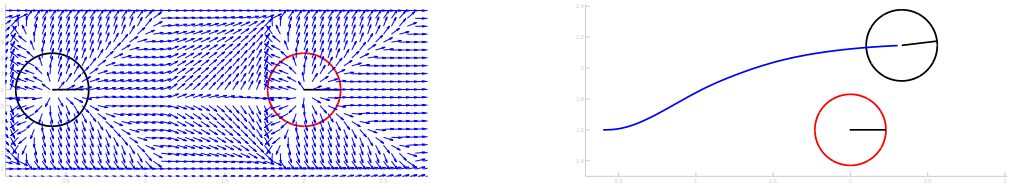

(a) (b)

Figure 4.27: The quickest path around an immobile pedestrian: If $V(\mathbf{x}, t)$ is modified for an area that is double the one occupied by a pedestrian, (a) the change in the direction of the unit vectors pointing to the quickest path is significant and (b) not enough for the mobile pedestrian to overtake the immobile one. The blue line represents the trajectory of the mobile pedestrian.

Case of overtaking a group of immobile pedestrians

The case of a pedestrian walking behind an immobile group of pedestrians is now considered. The solution that was found in the previous paragraph is first examined. The value of $V(\mathbf{x}, t)$ is decreased in an area equal to the double of the area occupied by a single pedestrian (the red and blue nodes). The unit vectors pointing toward the fastest path after modifying $V(\mathbf{x}, t)$ is illustrated in Fig. 4.28 (a). It can be seen in Fig. 4.28 (b) that the change in the direction of the unit vectors due to the presence of the group is not enough for the overtaking to happen. Instead, a collision takes place.

To be able to model the fastest path strategy in our continuous model for different cases, the area occupied by a pedestrian (where $V(\mathbf{x}, t)$ should be modified) has to be redefined. This is done in the next paragraph where the environment is partitioned using the Voronoi diagram.

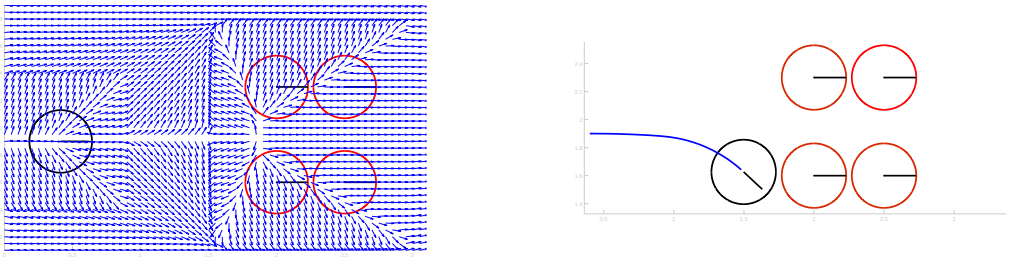

(a) (b)

Figure 4.28: The quickest path around a group of immobile pedestrians: If $V(\mathbf{x}, t)$ is modified for an area that is double the one occupied by a pedestrian, (a) the change in the direction of the unit vectors pointing to the quickest path is significant but (b) not enough for the mobile pedestrian to overtake the immobile group. The blue line represents the trajectory of the mobile pedestrian.

4.2.4 The dynamic floor field and the Voronoi diagram

As have been shown in the previous section, when trying to calculate the dynamic floor field for our model, the size of the area in which the value of $V(\mathbf{x}, t)$ is to be modified poses a problem. A solution to this problem that we propose is to partition the environment using a Voronoi diagram. A Voronoi diagram is a partitioning of a plane into regions based on distance to seeds specified beforehand. For each of these seeds, a Voronoi cell is attributed containing all points closer to that seed than to any other. The partitioning of the plane using a Voronoi diagram has never been used as a solution to apply floor fields for continuous models. It was used in [52] as a method to measure pedestrian densities with minimal scatter.

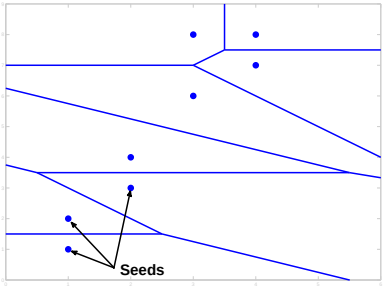

Figure 4.29: The discretization of an environment using a Voronoi diagram.

In our model, each pedestrian, whose center is considered as a seed, is attributed with a Voronoi cell (see Fig. 4.30). The difference between this representation and a cellular automate is that during the simulation, the size of the Voronoi cell varies with respect to the pedestrian's position and those in his/her surrounding.

We now reexamine the case of a pedestrian overtaking a group of immobile individuals. Since the Voronoi cell size is variable, it can be considered to represent a person's personal space. Therefore, we decrease the value of $V(\mathbf{x}, t)$ inside the Voronoi cell of each pedestrian. The change in the direction of the unit vectors, shown in Fig. 4.31 (a), allows the mobile individual to overtake the immobile group (see Fig. 4.31 (b))

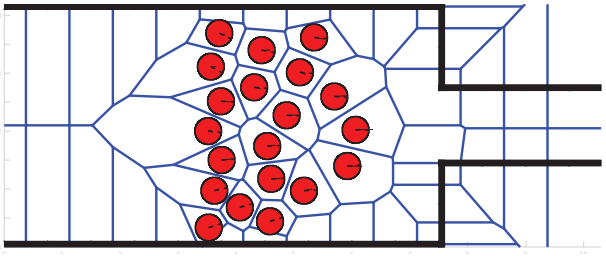

Figure 4.30: The discretization of an environment with 20 pedestrians using a Voronoi diagram.

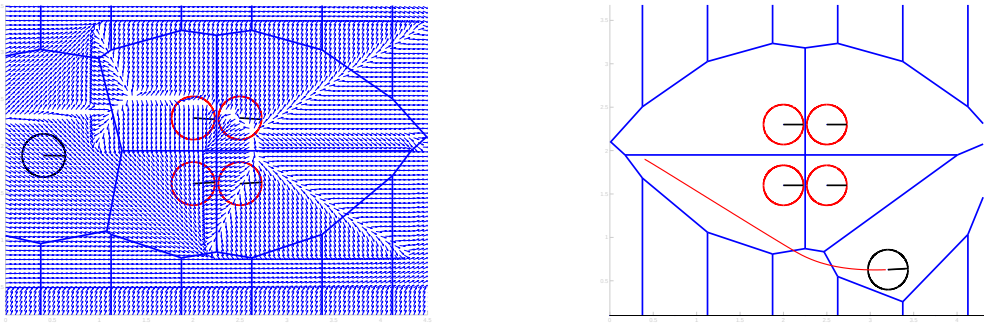

(a) (b)

Figure 4.31: The quickest path around a group of immobile pedestrians: If $V(\mathbf{x},t)$ is modified for an area that is double the one occupied by a pedestrian, (a) the change in the direction of the unit vectors pointing to the quickest path is significant and (b) enough for the mobile pedestrian to overtake the immobile group. The red line represents the trajectory of the mobile pedestrian.

Case of avoiding congestion

After having defined the area occupied by a pedestrian in which $V(\mathbf{x},t)$ is to be modified, we now address how congestions can be detected and avoided. The first step is to specify the criterion that identifies when a congestion is taking place. Since the Voronoi cell size is variable, it can be considered to represent an individual's personal space. In [53], it is noted that pedestrians prefer a body buffer zone space of $0.27 - 0.84\,m^2$, where also space needed to make a step is included. Therefore, whenever the size of the Voronoi cell is smaller than a chosen body buffer zone space and the velocity of the pedestrian is lower than a threshold, this implies that he/she doesnt have enough space to advance; thus a congestion is occurring.

Once a congestion is identified, the value of $V(\mathbf{x},t)$ should be modified in the area of the concerned Voronoi cell A_i^c. However, congestion occurs and then disappears progressively not instantaneously. Therefore, it is necessary to find a mechanism to modify $V(\mathbf{x},t)$ to be able to convey the evolution of traffic and its effect on the dynamics of the crowd. In our model, a mechanism similar to the one used by ants is adopted. When an ant finds a grain of rice, it deposits a chemical called pheromone that attracts other ants. The more ants use the food source path, the more the chemical accumulates and the more other ants are attracted (Fig. 4.32). Once the food source is depleted, less ants use the path and the pheromone chemical evaporates, making it less attractive. For pedestrians, a similar mechanism is used but with an opposite effect. For every time step, if the area of the Voronoi cell A_i^c of a pedestrian is smaller than a chosen body buffer zone space z_b, the value of $V(\mathbf{x},t)$ in his/her cell is decremented (see Eq. 4.21). With time, the value of $V(\mathbf{x},t)$ in the concerned Voronoi cell becomes small enough to start repulsing individuals from the zone occupied by the blocked pedestrian. When A_i^c becomes greater than z_b, the value of $V(\mathbf{x},t)$ is incremented until it reaches its original value (see Eq. 4.22). Then the

individuals are free to pass by the once congested zone.

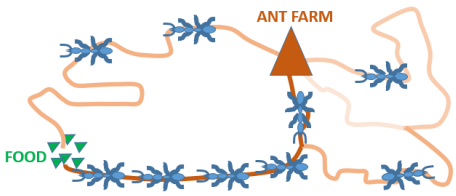

Figure 4.32: Spreading pheromone on the path that leads to the food source to attract more ants.

$$V(\mathbf{x}, t_{i+1}) = V(\mathbf{x}, t_i) - i_V \quad \text{if } A_i^c \leq z_b, \quad (4.21)$$

$$V(\mathbf{x}, t_{i+1}) = min\big(V(\mathbf{x}, t_0), V(\mathbf{x}, t_i) + j_V\big) \quad \text{if } A_i^c > z_b \quad (4.22)$$

where i_V and j_V are the incrementing and decrementing parameters respectively, to be chosen by the user. In the following sections, we demonstrate the capability of the dynamic field-Voronoi diagram method to reproduce macroscopic pedestrian behavior.

4.2.5 Applications

Two displacement strategies have been modeled using floor fields. In this section, the influence of each strategy on the overall dynamics of the crowd movement is demonstrated. We consider two cases: (i) exiting a room with two available exits and (ii) a U-turn.

Two exits

It is agreed on, that in the presence of several exits, pedestrians choose the one that allows them to reach their next destination while traversing the shortest distance. However, in the case of heavy pedestrian congestion, some individuals, who know the environment, prefer to take a longest but fastest path instead of waiting.

Using a static potential, the geodesic distance is constant throughout the simulation (Fig. 4.33(a-b)). Therefore, the traffic state is not updated and pedestrians continue to flow towards the heavily congested exit (Fig. 4.33(c-d)) which is far from reality.

However, when a dynamic potential is calculated, the geodesic distance varies with the evolution of traffic (Fig. 4.34(a-b)). As a result, it can be seen in Fig. 4.34(c-d) that pedestrians change their route and choose a longer path that will allow them to reach their destination in a shorter time.

A U-turn

Another case that shows how dynamic floor fields eliminate unrealistic congestion is a group of pedestrians making a U-turn around an obstacle. As can be seen in Fig. 4.35(a), using a static field, all agents insist on taking the shortest path resulting in an unrealistic congestion at the end of the wall. On the other hand, using a dynamic floor field, pedestrians use the available space to move around the congestion (Fig. 4.35(b)).

4.2.6 Short range navigation

Short range navigation can be summarized by a pedestrian's interaction with his/her surroundings (other pedestrians, obstacles,... at $1 \sim 10$ m, see Fig. 4.36). In our model, avoiding fixed obstacles is modeled through the floor fields. As for avoiding other pedestrians, a social repulsion for 'aggressive' behavior and a cognitive approach for 'civilized' behavior are implemented. The two approaches will be discussed in the chapter dedicated pedestrian behavior and interactions.

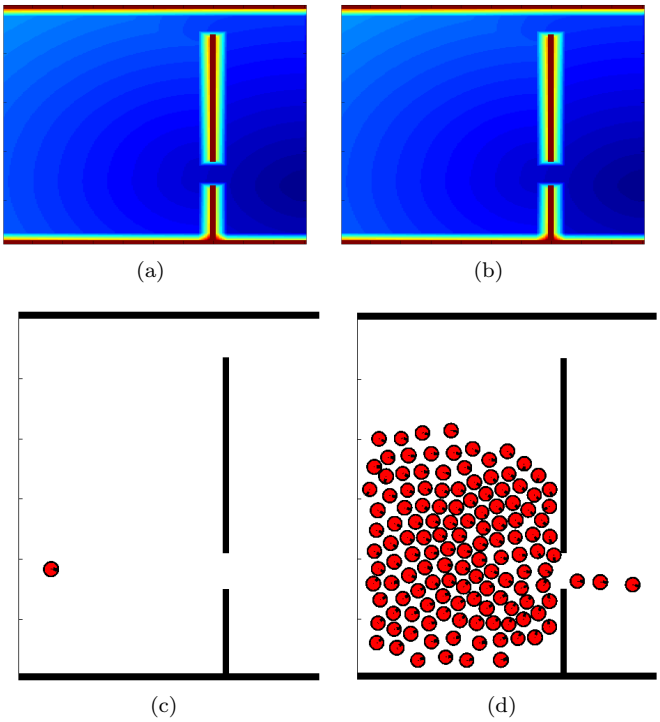

Figure 4.33: The static floor field for (a) t=0 and (b) t=60. The state of the system at (c) t=0 and (d) t=60.

4.2.7 Conclusion

Pedestrian route choice is one of the most important elements of any crowd model. In this chapter, we have enriched our model by adding new levels of navigation and new strategies. For medium distance navigation, two strategies are now available: (i) the shortest and (ii) the fastest path. The shortest path strategy is modeled using a static floor field. It has been found that the parameters of the latter (D_{shy} and $V(\mathbf{x})$) have an influence on pedestrians' trajectories and allow to obtain a funnel shape upstream of a bottleneck. However, static floor fields don't take into account the evolution of traffic. It has been shown that when applying dynamic floor fields in continuous models, the evolution of $V(\mathbf{x}, t)$ is problematic. That is why a dynamic floor field combined with a Voronoi diagram was introduced in order to add the fastest path strategy to our model. As a result, no more unrealistic congestions are obtained. Finally, short distance navigation, which is the content of the following chapter, was achieved by using two types of pedestrian-pedestrian interaction: (i) a social repulsion or a force-based approach and (ii) a cognitive approach.

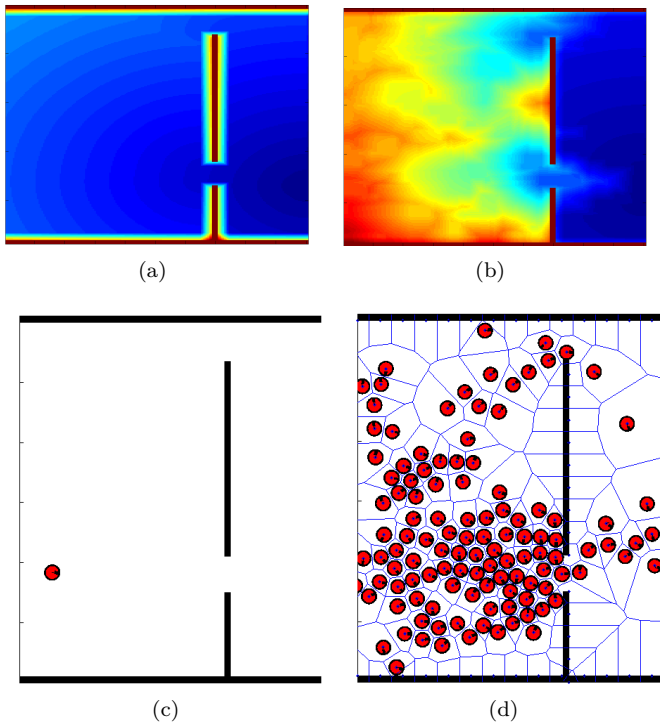

Figure 4.34: The dynamic floor field for (a) t=0 and (b) t=60. The state of the system at (c) t=0 and (d) t=60.

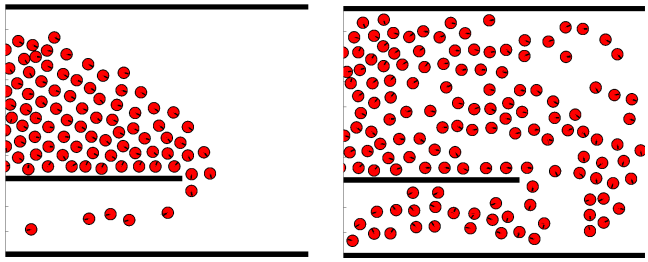

Figure 4.35: Moving around a 180° corner using (a) a static floor field and a (b) dynamic one.

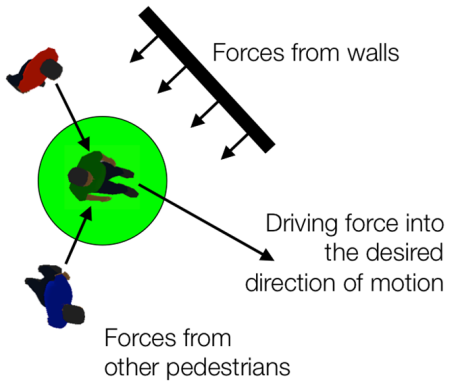

Figure 4.36: A pedestrian's interaction with its surrounding [54].

Bibliography

[1] D. Helbing, "A fluid-dynamic model for the movement of pedestrians," *Complex systems*, vol. 6, pp. 391–415, 1992.

[2] L. Henderson, "On the Fluid Mechanics of Human Crowd Motion," *Transportation Research*, vol. 8, no. 6, pp. 509–515, 1974.

[3] L. Huang, S. Wong, M. Zhang, C.-W. Shu, and W. H. Lam, "Revisiting Hughes' dynamic continuum model for pedestrian flow and the development of an efficient solution algorithm," *Transportation Research Part B: Methodological*, vol. 43, pp. 127–141, Jan. 2009.

[4] R. L. Hughes, "A continuum theory for the flow of pedestrians," *Transportation Research Part B: Methodological*, vol. 36, no. 6, pp. 507–535, 2002.

[5] P. Kachroo, ed., *Pedestrian dynamics: feedback control of crowd evacuation*. Understanding complex systems, Berlin: Springer, 2008.

[6] U. Weidmann, "Transporttechnik der Fußgänger," report Schriftenreihe Ivt- Berichte 90, ETH Zürich.

[7] P. Bovy and E. Stern, *Route Choice: Wayfinding in Transport Networks*, vol. 9. Springer Netherlands, 1990.

[8] D. Montello, "Navigation," in *The Cambridge handbook of visuospatial thinking* (P. Shah and M. A., eds.), pp. 257–294, Cambridge: Cambridge University Press, 2005.

[9] W. Daamen, *Modelling passenger flows in public transport facilities*. PhD thesis, Netherlands TRAIL Research School, Delft, the Netherlands, 2004.

[10] S. P. Hoogendoorn, "Normative pedestrian behaviour theory and applications," Tech. Rep. CTvk2001.002, Delft University of Technology, 2001.

[11] CROW, "ASVV - recommendations for traffic provisions in built-up areas," tech. rep., 1998.

[12] D. Hartmann and P. Hasel, "Efficient dynamic floor field methods for microscopic pedestrian crowd simulations," *Communications in Computational Physics*, vol. 16, no. 1, pp. 264–286, 2014.

[13] A. Kneidl, D. Hartmann, and A. Borrmann, "Using a multi-scale model for simulating pedestrian behavior," in *Pedestrian and Evacuation Dynamics 2012*, pp. 1029–1038, Springer, 2014.

[14] C. Burstedde, K. Klauck, A. Schadschneider, and J. Zittartz, "Simulation of pedestrian dynamics using a two-dimensional cellular automaton," *Physica A: Statistical Mechanics and its Applications*, vol. 295, no. 3, pp. 507–525, 2001.

[15] A. Schadschneider, W. Klingsch, H. Klpfel, T. Kretz, C. Rogsch, and A. Seyfried, "Evacuation Dynamics: Emprical Reuslts, Modeling and Applications," 2009.

[16] K. Yamamoto, S. Kokubo, and K. Nishinari, "Simulation for pedestrian dynamics by real-coded cellular automata (RCA)," *Physica A: Statistical Mechanics and its Applications*, vol. 379, pp. 654–660, June 2007.

[17] S. P. Hoogendoorn and P. Bovy, "Pedestrian route-choice and activity scheduling theory and models," *Transportation Research Part B*, vol. 38, pp. 169–190, 2004.

[18] W. Fleming and H. Soner, *Controlled Markov Processes and Viscosity Solutions*, vol. 25 of *Stochastic Modelling and Applied Probability*. New York: Springer-Verlag, 2006.

[19] S. P. Hoogendoorn, "Wayfinding under uncertainty in continuous time and space by dynamic programming," in *Proceedings of the 13th Mini-EURO Conference Handling Uncertainty in the Analysis of Traffic and Transportation Systems*, pp. 71–76, 2002.

[20] R. Kimmel and J. Sethian, "Fast Marching Methods for Computing Distance Maps and Shortest Paths," Tech. Rep. Technical Report 669, University of California, Berkley, 1996.

[21] J. A. Sethian and A. Vladimirsky, "Ordered upwind methods for static Hamilton-Jacobi equations: Theory and algorithms," *SIAM Journal on Numerical Analysis*, vol. 41, no. 1, pp. 325–363, 2003.

[22] W.-K. Jeong and R. T. Whitaker, "A Fast Iterative Method for Eikonal Equations," *SIAM Journal on Scientific Computing*, vol. 30, pp. 2512–2534, Jan. 2008.

[23] H. Zhao, "A fast sweeping method for eikonal equations," *Mathematics of computation*, vol. 74, no. 250, pp. 603–627, 2005.

[24] T. Kretz, A. Große, S. Hengst, L. Kautzcsh, A. Pohlmann, and P. Vortisch, "Quickest Path in Simulations of Pedestrians," *Advances in complex systems*, vol. 14, p. 733, 2011.

[25] D. Helbing and P. Molnar, "Social force model for pedestrian dynamics," *Physical review E*, vol. 51, no. 5, p. 4282, 1995.

[26] T. I. Lakoba, D. J. Kaup, and N. M. Finkelstein, "Modifications of the Helbing-Molnár-Farkas-Vicsek Social Force Model for Pedestrian Evolution," *SIMULATION*, vol. 81, pp. 339–352, Jan. 2005.

[27] R. Löhner, "On the modeling of pedestrian motion," *Applied Mathematical Modelling*, vol. 34, pp. 366–382, Feb. 2010.

[28] D. R. Parisi, M. Gilman, and H. Moldovan, "A modification of the Social Force Model can reproduce experimental data of pedestrian flows in normal conditions," *Physica A: Statistical Mechanics and its Applications*, vol. 388, pp. 3600–3608, Sept. 2009.

[29] M. Chraibi, A. Seyfried, and A. Schadschneider, "Generalized centrifugal-force model for pedestrian dynamics," *Physical Review E*, vol. 82, no. 4, p. 046111, 2010.

[30] V. Blue and J. Adler, "Cellular automata microsimulation of bidirectional pedestrian flows," *Transportation Research Record: Journal of the Transportation Research Board*, no. 1678, pp. 135–141, 1999.

[31] H. L. Klüpfel, *A cellular automaton model for crowd movement and egress simulation*. PhD thesis, Universität Duisburg-Essen, Fakultät für Physik, 2003.

[32] H. Yue, H. Hao, X. Chen, and C. Shao, "Simulation of pedestrian flow on square lattice based on cellular automata model," *Physica A: Statistical Mechanics and its Applications*, vol. 384, pp. 567–588, Oct. 2007.

[33] C. Gloor, P. Stucki, and K. Nagel, "Hybrid Techniques for Pedestrian Simulations," in *Cellular Automata* (P. M. A. Sloot, B. Chopard, and A. G. Hoekstra, eds.), no. 3305 in Lecture Notes in Computer Science, pp. 581–590, Springer Berlin Heidelberg, 2004.

[34] Mario Höcker, Volker Berkhahn, Angelika Kneidl, André Borrmann, and Wolfram Klein, "Graph-based approaches for simulating pedestrian dynamics in building models," in *eWork and eBusiness in Architecture, Engineering and Construction*, pp. 389–394, CRC Press, Sept. 2010.

[35] A. Kneidl, A. Borrmann, and D. Hartmann, "Generation and Use of Sparse Navigation Graphs for Microscopic Pedestrian Simulation Models," *Adv. Eng. Inform.*, vol. 26, pp. 669–680, Oct. 2012.

[36] A. Kneidl, D. Hartmann, and A. Borrmann, "A hybrid multi-scale approach for simulation of pedestrian dynamics," *Transportation Research Part C: Emerging Technologies*, 2013.

[37] G. Köster, D. Hartmann, and W. Klein, "Microscopic Pedestrian Simulations: From Passenger Exchange Times to Regional Evacuation," in *Operations Research Proceedings 2010* (B. Hu, K. Morasch, S. Pickl, and M. Siegle, eds.), Operations Research Proceedings, pp. 571–576, Springer Berlin Heidelberg, 2011.

[38] T. Kretz, "Pedestrian Traffic: on the Quickest Path," *Journal of Statistical Mechanics: Theory and Experiment*, vol. 2009, p. P03012, Mar. 2009. arXiv: 0901.0170.

[39] D. Hartmann, "Adaptive pedestrian dynamics based on geodesics," *New Journal of Physics*, vol. 12, p. 043032, Apr. 2010.

[40] A. U. Kemloh Wagoum, A. Seyfried, and S. Holl, "Modeling the dynamic route choice of pedestrians to assess the criticality of building evacuation," *Advances in Complex Systems*, vol. 15, p. 1250029, Sept. 2012.

[41] D. Quercia, R. Schifanella, and L. M. Aiello, "The shortest path to happiness: recommending beautiful, quiet, and happy routes in the city," pp. 116–125, ACM Press, 2014.

[42] P. Pécol, *Modélisation 2D discrète du mouvement des piétons - Application à l'évacuation des structures du génie civil et à l'interaction foule-passerelle.* PhD thesis, Université Paris Est, 2011.

[43] R. de Neufville and M. Grillot, "Design of Pedestrian Space in Airport Terminals," *Transportation Engineering Journal*, vol. 108, pp. 87–102, Jan. 1982.

[44] J. Pauls, "Calculating evacuation times for tall buildings," *Fire Safety Journal*, vol. 12, no. 3, pp. 213–236, 1987.

[45] J. Van Soeren, "User-Manual Station Version 2.01," report, Railinfrabeheer, 1996.

[46] H. Knoflacher, *Verkehrsplanung für den Menschen - Band 1 Grundstrukturen.* Verlag Orac, 1987.

[47] M. Campanella, S. Hoogendoorn, and W. Daamen, "Quantitative and Qualitative Validation Procedure for General Use of Pedestrian Models," in *Pedestrian and Evacuation Dynamics 2012* (U. Weidmann, U. Kirsch, and M. Schreckenberg, eds.), pp. 891–905, Springer International Publishing, 2014.

[48] T. Kretz, A. Grünebohm, and M. Schreckenberg, "Experimental study of pedestrian flow through a bottleneck," *Journal of Statistical Mechanics: Theory and Experiment*, vol. 2006, no. 10, p. P10014, 2006.

[49] A. Seyfried, O. Passon, B. Steffen, M. Boltes, T. Rupprecht, and W. Klingsch, "New Insights into Pedestrian Flow Through Bottlenecks," *Transportation Science*, vol. 43, pp. 395–406, May 2009.

[50] W. Song, W. Lv, and Z. Fang, "Experiment and Modeling of Microscopic Movement Characteristic of Pedestrians," *Procedia Engineering*, vol. 62, pp. 56–70, Jan. 2013.

[51] M. Davidich and G. Köster, "Predicting Pedestrian Flow: A Methodology and a Proof of Concept Based on Real-Life Data," *PLoS ONE*, vol. 8, p. e83355, Dec. 2013.

[52] B. Steffen and A. Seyfried, "Methods for measuring pedestrian density, flow, speed and direction with minimal scatter," *Physica A: Statistical mechanics and its applications*, vol. 389, no. 9, pp. 1902–1910, 2010.

[53] B. Pushkarev and J. M. Zupan, "Capacity of walkways," in *Transportation Research Record*, 1975.

[54] D. Helbing, "Social Forces - Revealing the Causes of Success or Disaster (Chapter 6 of Digital Society)," SSRN Scholarly Paper ID 2532002, Social Science Research Network, Rochester, NY, Nov. 2014.

Chapter 5

Pedestrian behavior in public places

Contents

5.1 Bibliographical study on pedestrian behavior

To most of us Crowds are disorderly. It is enough to witness the aftermaths of a shopping spree or a rock concert to believe so. However, several other aspects of daily life show that crowds also exhibit organization capacities without its members being aware. Take the example of pedestrian traffic in subways. People take advantage of the available space by developing lanes of opposite directions. This "pedestrian highway" happens spontaneously and is perfectly executed without any instructions or coordination between the individuals forming it.

At the same time, we cannot neglect the fact that observed individually, the unpredictable nature of pedestrian behavior in a crowd shows no sign or will for organization. It is characterized by sudden stops, avoidance or overtaking others, and sudden changes of direction. Moreover, individuals in crowds have different motivations and walking patterns. For example, while a passenger in a hurry walks in straight lines to catch his train, another who is shopping would be zigzagging at a low pace.

This paradox between individual behavior and self organization can be explained by the fact that crowds are complex systems whose collective dynamics rely on self organization processes. These systems function in a decentralized manner where pedestrians neither cooperate with each other nor follow general orders. They only interact with their surroundings. For example, an individual who prefers to walk at a relatively high velocity would be forced to slow down or even stop in a dense environment. This doesn't mean that pedestrians are not independent, but that they are all connected through a vast network of interactions. The global dynamics of the crowds result from these local interactions. As a result, collective behavior at group level may appear spontaneously without being planned by the pedestrians. One example is spatial and temporal separation of pedestrian counter flow.

In order to study the complex system that is pedestrian crowds, it is necessary to have a better understanding of the cognitive and behavioral mechanisms that govern its motion. First, we address the notion of self-organization. We start with a historical overview of this multidisciplinary concept. We then describe how a self-organized system operates. Secondly, different collective patterns of motion observed in the animal societies are examined. We also point out the similarities found between collective behavior observed in animal groups and pedestrian crowds. Finally, we focus on pedestrian and crowd motion and more precisely on the current empirical knowledge of the system. We describe the characteristics of the motion of an isolated pedestrian, individual interactions, and the different forms of collective organization.

5.1.1 Self organization phenomena

Collective motion based on self-organization processes isn't restricted to humans. In fact, more studies on collective animal behavior exist than on collective human behavior [1]. This is probably due to the simplicity of observing animals in their natural habitat and the obvious existence of collective behavior. Anyone who observes a school of fish escaping a predator (Fig. 5.1 a) or a perfectly synchronized flight of a flock of birds (Fig. 5.1 b) is astounded by the instantaneous motion coordination between the members of the group.

(a) (b)

Figure 5.1: A collective behavior by (a) a school of fish [2] and (b) a flock of birds (©Owen Humphreys).

There are two possible mechanisms that can explain this collective motion. The first one is **centralization**. Analogous to a command center, the leader (can be a unique member or a small group of individuals) collects the information provided by all the members of the group, analyzes it, takes a decision and transmits its instructions back to the members (Fig. 5.2(a)). While this mechanism is used in several organisms (armies, governments...), it is highly improbable in the systems we're studying. No animal species possess the required cognitive capacities to accomplish such a task (neither do human beings) [3]. As for humans, we all know that individuals in a crowd are independent and don't follow orders. The second mechanism is **decentralization**. It relies on self-organization processes where each member has its own unique information depending on its position within the group. Then by interacting with its surrounding, the information is locally exchanged (see Fig. 5.2(b)). For example, mimicry is a form of interaction that leads a group to adopt a unique behavior [4, 5]. This mechanism is the one that orchestrates the collective motion observed in flocks of birds, schools of fish and crowds of pedestrians.

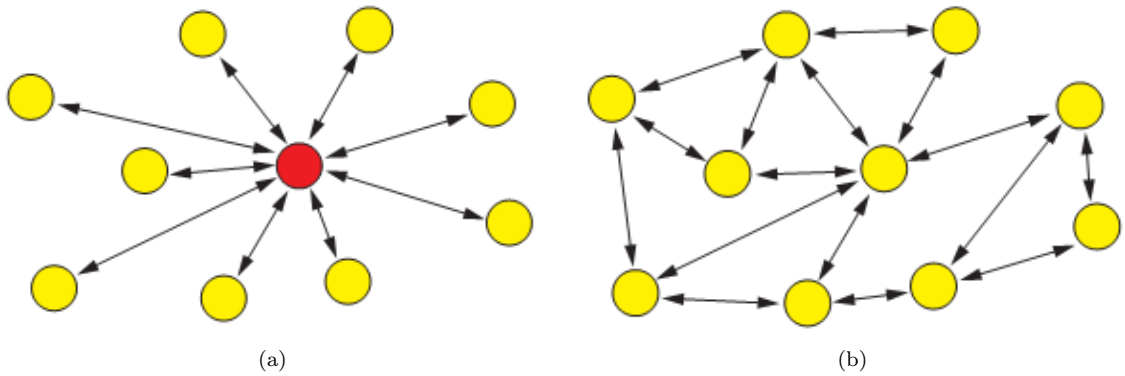

(a) (b)

Figure 5.2: Two systems using (a) a centralized and (b) a decentralized mechanism [1].

The theory of self-organization first appeared in the mid 1900's with the works of John Von Neumann on cellular automata [6]. The contributions of several scientists [7–9] then lead to the formalization of the basic concepts of the theory of self-organized systems. These concepts were first applied to animal groups by Jean-Louis Deneubourg who studied on the collective behavior of ants and termites [10]. In [11] and [12] the same concepts were applied but in a more general manner. It was shown that a set of local rules of interaction can lead to the emergence of a coordination between members of an animal group. Since then, the theory of self-organization is used to study numerous types biological systems. Concerning human beings, the same concepts were being developed in parallel during the 1960's [13, 14]. However, the first time collective behavior was examined in the context of the self-organization theory was in 1995 by Helbing [15].

Theoretical Concepts of Self-organization

Self-organization is defined as the spontaneous emergence of a global structure that is triggered by local interactions between members of a system. Self-organization phenomena are macroscopic effects reflecting the pedestrians' microscopic interactions. In the following, we describe the different mechanisms responsible for the functioning of a self-organized system, the resulting collective properties, and the methodology used to study self-organized collective behavior.

Mechanisms There are 4 main mechanisms responsible for the emergence of self-organized movement [16]:

- **Positive feedback or the snow ball effect** [1]: It is when an individual is encouraged to do a certain act since those who surround him are already doing it. Take for example the Mexican wave. It starts with a small group of fans then gets amplified to encompass the whole crowd of a football stadium.

- **Negative feedback**: without this mechanism, positive feedback leads the system to a state of dynamic amplification without control. This mechanism counteracts the amplification effect to bring the system back to a stable state.
- **Random perturbations**: If all members of a system had identical behavior, no positive and negative feedback can occur. Paradoxically, without random perturbations, no self-organization could take place [17].
- **Multiple interactions**: Interaction between two individuals occurs when one acquires new information from another leading the former to modify its behavior in light of what it had just learned. These interactions can be direct without leaving a trace (visual, audio, or sensory signs) or indirect leaving a trace (trails, chemical deposits, ...).

Properties A self-organized system can be characterized by the existence of emergent properties. **Emergence** is the phenomenon where a global behavior arises from the interactions between the particles of the system. It is the result of of a non linear combination of the contribution of each individual of the system (due to interaction among each other) generating positive feedback loops.

Emergent properties usually appear after a perturbation where certain parameters of the system change. This perturbation is then amplified by positive feedback loops, leading to a sudden transition from one state to another. That is why emergence is often associated to a **transition phase**. Take for example the case of a herd of buffalo attacked by a lion. At first, they are grazing with relatively large distances separating them. Once the danger represented by the lion is perceived, they regroup, closing the distance between each other, and chase the lion away.

The third property of self-organized systems is **dynamcitiy**. A collective organization emerges and is maintained as a result of permanent and repetitive interactions between the particles of the system. This means that the system can always react to new perturbations. Its equilibrium depends on the resistance of the positive feedback, amplifying the change, by the negative feedback suppressing it.

Methodology In order to study self-organized systems, Camazine et *al.* [16] proposed the methodology illustrated in Fig. 5.3. The first step is to observe and quantify the considered collective behavior and the conditions necessary for its emergence. The second step is an experimental phase and consists of characterizing isolated individual behavior and how it is affected by the presence of neighbors. These two serve as the base for developing a behavioral model. During the third step, the model is developed based on the data obtained from experimentation. Finally, the model is to be validated by verifying if it is capable of reproducing the initially observed collective phenomena under the same environmental conditions. For new predictions, the model has to be tested experimentally. Any failure in the validation step means that a critical individual behavior has not been properly included in the model.

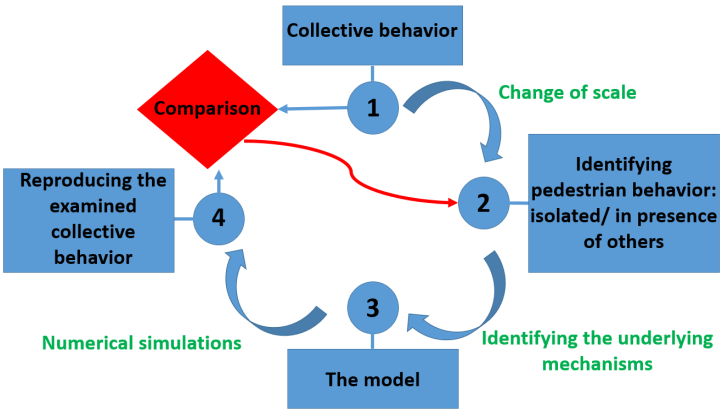

Figure 5.3: The four steps for studying self-organized collective behavior according to [16].

To sum up, using the approach introduced by [16], a model is first developed at the individual scale making use of direct observations, then parametrized according to the experimentally measured data

also at the individual level, and finally validated by testing its ability to reproduce what is observed and measure at the global or collective level. A model obtained using this methodology encompasses the mechanisms responsible for certain phenomena allowing not only to reproduce them but also to supply reliable and robust predictions to environmental variations.

Self-organized collective motion in animal groups

Self-organization processes are at the origin of the coordination of collective motion in several animal groups, like flocks of birds, schools of fish, and ant colonies [18–20]. Several similarities exist between collective motion in animal groups and crowds of pedestrians. That is why we start by describing the conditions that lead to the emergence of collective motion in certain species of animals in order to better understand the ones concerning human crowds.

Conditions for the emergence of collective motion in animal groups In systems like fish schools, bird flocks , and some other vertebrate groups, cohesive and polarized groups are formed exhibiting remarkable coordination and adaptability . Three conditions are necessary so that these systems demonstrate collective behavior [20]. The first condition is that the individuals should be moving in the same direction as their neighbors'. This is mainly observed in systems like schools of fish or flocks of birds where the tendency of each member of the group to move in the same direction as its neighbors creates a coordinated collective motion [18, 21, 22]. Concerning pedestrians, even though individuals don't usually try to follow their neighbors' direction, we do notice in streets for example, that there are mainly one or two main directions. The second condition is remaining close to one's neighbors. By keeping distances between members of the system small, the cohesion of the group is ensured and level of density is maintained allowing self-organization dynamics to take place. The third condition is avoiding collisions. This rule is particularly important when we are dealing with crowds of pedestrians.

From animal groups to crowds of pedestrians It is known that among existing complex systems, those existing in nature have been the most studied and observed. That is why the objective of the previous part was to gain knowledge on existing research on complex systems mainly animal groups to gain insight into the collective motion of pedestrian crowds. Two important points are to be retained. The first point concerns the self-organization phenomena observed in several systems. The qualitative resemblance of a phenomena in different species doesn't mean that the underlying mechanisms are also similar. Take for example the lane formation phenomena for bi-directional flows observed in ants and humans. It is clear that for humans a different mechanism than the building of pheromone trails is responsible for the emergence of this phenomenon. This leads us to the second point that concerns the validation of proposed crowd movement models. It is not sufficient to qualitatively reproduce a self-organization phenomenon to validate a certain model. It is imperative to ensure that the underlying mechanism is also identical to the one of the modeled system.

In general, before modeling any collective behavior, it is important to establish, in chronological order, the following elements [1]:

- Identification of the spontaneous behavior of an isolated individual,
- Identification of the change in behavior resulting from interacting with another individual,
- Formulation of a law of combination of the simultaneous interactions of the individual with its surroundings (other individuals, obstacles,...).

Whereas the first two elements can be observed, the last one is much more complex. It is a difficult task to evaluate the cognitive capacities of a certain species that allows them to process simultaneous interactions with others. Several studies exist that propose different laws of combination, in particular for animals [18, 22, 23]. However, how to combine simultaneous interactions remains an open subject both for animal groups and human crowds [24, 25].

5.1.2 Empirical knowledge of pedestrian collective motion

After having described the context of our research and the existing similarities with other complex systems, mainly animal groups, we will now explicitly address crowd collective behavior. In the coming sections, we will go over the characteristics of pedestrian behavior, pedestrian-pedestrian interactions and the collective dynamics resulting from the latter.

The characteristics of pedestrian motion

In a crowd, each pedestrian has two characteristics that affect the collective dynamics of the system. These are his/her velocity's speed and direction. Whether on a completely planned itinerary or getting from one point to another, each individual has a desired direction. Before arriving to a destination (temporary or final), this direction is always changing as a result of the pedestrian's interactions with obstacles and other pedestrians. After choosing a direction, an individual must choose its speed. In general, each individual possesses a desired speed that he/she tries to maintain whenever possible. Table. 5.1 illustrates several values of the desired speed found in literature.

Table 5.1: Different values of the desired speed.

Author	Desired velocity	Year
Weidmann [26]	$1.34\ m.s^{-1}$	1993
Bonhannon [27]	$1.27 - 1.46\ m.s^{-1}$	1997
Young [28]	$1.35\ m.s^{-1}$	1999
Helbing [29]	$1.3\ m.s^{-1}$	2000
Daamen [30]	$0.99 - 1.45\ m.s^{-1}$	2003

According to [26, 31], pedestrians traveling for business are the fastest ($1.61\,m/s$) while those traveling for lesiure are the lowest ($1.10\,m/s$). It was also found that in commuting, the average velocity is ($1.49\,m/s$) and during shopping is ($1.16\,m/s$). In general, the overall velocities in a crowd are Gaussian distributed with an average of ($1.34\,m/s$) and standard deviation of ($0.26\,m/s$) with men being approximately 10% faster than women ($1.41\,m/s$ versus $1.27\,m/s$) [31].

The influence of the characteristics of the walking infrastructure on pedestrian speed has also been investigated. In [32], it was found that the speed in unidirectional flows ($1.54\,m/s$) is larger than in bidirectional ones ($1.41\,m/s$) or crossing streams ($1.35\,m/s$). Moreover, certain studies have shown that cultural differences have an impact on typical walking speeds. For example, the study in [33] have shown that people in Singapore walk three times faster than people in Blantyre (Malawi) ($1.71\,m/s$ versus $0.57\,m/s$). For large cities, it is considered that average speed lies between $1.3\,m/s$ and $1.6\,m/s$ [34]. The desire speed also varies with respect to individual physical characteristics (age, sex, physical state,...).

The types of pedestrian interactions

An isolated pedestrian chooses to walk at his/her desired velocity (speed and direction) to reach a desired destination. People prefer to keep the same direction of motion since changing it is annoying, energy consuming and inefficient. However, in the presence of other pedestrians and obstacles, individuals are bound to adapt their velocity as a result of interacting with their surrounding. In what follows, we go over the types of pedestrian-pedestrian interaction.

The most frequent type of pedestrian-pedestrian interactions is **avoidance** or "repulsion". When a pedestrian detects a possible collision with an obstacle or another individual in his field of vision, he modifies his velocity in an attempt to avoid contact. This direct interaction is bilateral where interacting pedestrians coordinate their movement [35].

The second type of interactions involves a level of **attraction**. It is the case of social groups moving together, for example a family, a group of friends or a couple. Interactions between members of a group can be visual, tactile and acoustic [1]. Even though in a crowd, a great number of pedestrians belong to groups, group interaction has rarely been studied [36–38].

So far we have described types of interactions in normal situations. In panic situations or urgent evacuations it has been observed that pedestrians tend to change their desired direction for the one

adopted by the majority of their neighbors. This is called **imitation**. When densities reach critical levels, interactions become physical where individuals start pushing each other. This behavior is usually involuntary. Pedestrians push in a certain direction since themselves are being pushed by people behind them. At high densities, this behavior can lead to the emergence of the turbulence phenomenon where individuals get carried away several meters in random directions. This phenomenon often causes injuries and deaths.

In the presence of other pedestrians, interactions are direct. However, there are also **indirect interactions**. This is the case of surfaces that can be altered by the footsteps of pedestrians. Take the example illustrated in Fig. 5.4. With more and more people taking shortcuts through the greenfield, a new trail is formed. At one point, almost everybody uses the new trail instead of the ones designed for that purpose.

Figure 5.4: Indirect interactions between pedestrians create new paths [39].

Collective dynamics

Similar to groups of animals, collective motion in crowds of pedestrians emerge as a result of repetitive interactions between its members. In addition, the three conditions for the emergence of collective movement (see section 5.1.1) are also present in human crowds. The first condition is the existence of a repulsion between individuals and their surroundings (other pedestrians or obstacles). This element is crucial for the emergence of collective organization. The second one is a certain level of confinement so that individuals wont disperse in space and multiple interactions be ensured. Usually this is provided by the environment (walls, sidewalks, rooms...) where the pedestrians are found. The third and final condition is the existence of a form of alignment. This usually exists whether individuals are walking in a street in one direction or the other or trying to reach a certain destination.

Jamming Whenever the inflow in a certain location exceeds its capacity, jamming and clogging are expected to take place. These locations are called **bottlenecks**. Two different phenomena can occur in front of bottlenecks depending on the situation. In situations of panic and urgent evacuations, pedestrians usually "compete" to exit creating a form of an arch radiating from the exit, as illustrated in Fig. 5.5 a. In normal situations, where pedestrians try to keep a certain distance between each other and with obstacles, a funnel shape is obtained (Fig. 5.5 b).

Formation of lanes The formation of lanes is a form of collective organization that occurs when two crowds of pedestrians are moving in opposite directions in a street or a corridor (Fig. 5.6). By walking in lanes, strong interactions with oncoming pedestrians are reduced allowing higher walking speeds. However, in high density or nervous crowds, the formed lanes tend to break due to pedestrians trying to do overtaking manoeuvres. This is known as the **Freezing by heating** effect [40].

Though this form of self-organization is the most studied among collective phenomena[42], it has never been quantified under experimental conditions. While numerical simulations show a varying number of lanes as a function of the environment [15], simple observations show that regardless of the width of the street or corridor, two lanes form each occupying half of the available space [1] (see Fig. 5.7). Another characteristic of this phenomenon is its asymmetry. In Europe, lanes tend to form to the right with

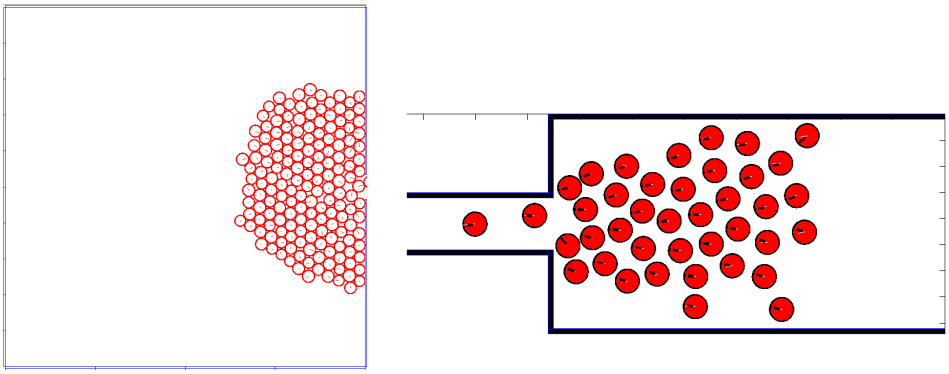

(a) (b)

Figure 5.5: Evacuation of a room: formation of (a) an arch and (b) a funnel shape.

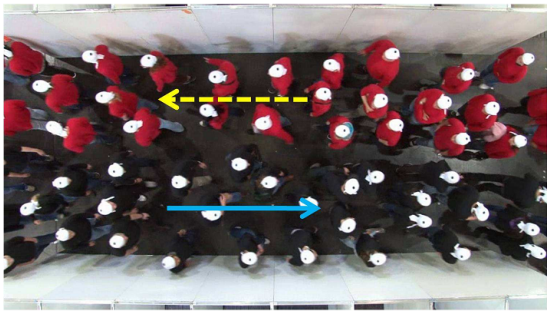

Figure 5.6: Lane formation observed during an experiment on bidirectional pedestrian flow [41].

respect to the walking direction while in Asia they form to the left [1]. So far, there have been no studies to quantify this characteristics. Only hypotheses exist to explain it one of which is the presence of social norms [43, 44].

Figure 5.7: Two groups walking in opposite direction: formation of two main lanes [45].

Oscillations at bottlenecks Most existing pedestrian models show exhibit oscillations at bottlenecks when two crowds moving in opposite directions meet at an exit Fig 5.8. Once a pedestrian manages to make his way through the opposing group, he is immediately followed by others of his side. While individuals are waiting on the other side, pressure starts building up until they manage to cut the opposing flow and force their passage. The same dynamics keeps repeating over and over. Again, this phenomenon has never been studied experimentally except once [46]. However, this experiment suffers from several

bias [1] leaving the oscillations at bottleneck phenomenon still unknown.

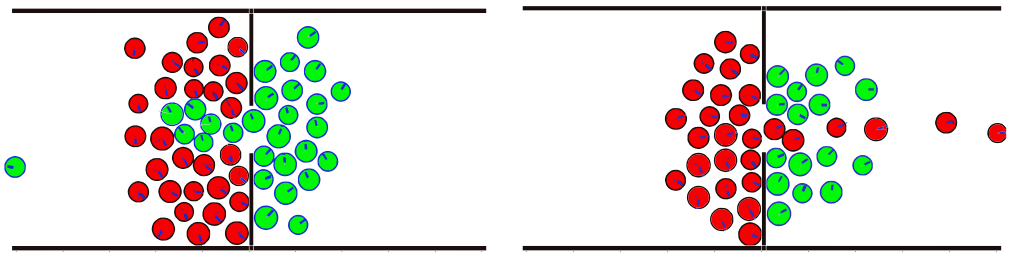

(a) (b)

Figure 5.8: Oscillation phenomenon.

Formation of Queues In several cultures, when a group of people want to do the same activity at the same time, they wait in queues. Queues of people form in various situations and locations such as in railway stations to book tickets, at large stores and supermarkets to pay, or at amusement parks to play. Depending on the situation and the location, queues can be structured or unstructured. In structured queues (Fig. 5.9 (a)), people form lines in a fixed, predictable position, such as at supermarket checkouts, banks, airport security, etc. In unstructured queues (Fig. 5.9 (b)), people form lines in unpredictable and varying locations and directions. This is can be observed in street markets, food stores, music concerts, etc.

(a) (b)

Figure 5.9: Structured [47] and unstructured queues [48].

Based on observations of pedestrian movement in airports, railway stations, department stores, and office buildings, three types of queuing behavior were identified [49]. In the first type (Fig. 5.10 a), pedestrians approach the queue formed in front of a counter, move forwards, get the service, and get out. In the second type (Fig. 5.10 b), pedestrians form lines in front of gates and turnstiles in order to pass through. The third queuing behavior is observed in front of doors of vehicles where boarding/alighting is expected. In this case, pedestrians either gather in front of the entrance without giving enough space for alighting pedestrians to get off (Fig. 5.10 c) or they do (Fig. 5.10 d).

The fundamental diagram The fundamental diagram represents the relation between the density of pedestrians and their average velocity. It is used as an input for engineering methods used in the design and dimensioning of pedestrian facilities [50, 51]. It also serves as a quantitative benchmark for pedestrian models [52, 53]. Due to its applicative interest, it has been often discussed in literature [54–58]. The fundamental diagrams obtained by different studies have in general a similar form. At low density ($0.7-1\,pedestrians/m^2$), the average speed of individuals varies slightly around the desired value of $1.3\,m/s$. Above that density, the average speed decreases drastically until it stabilizes at a value of

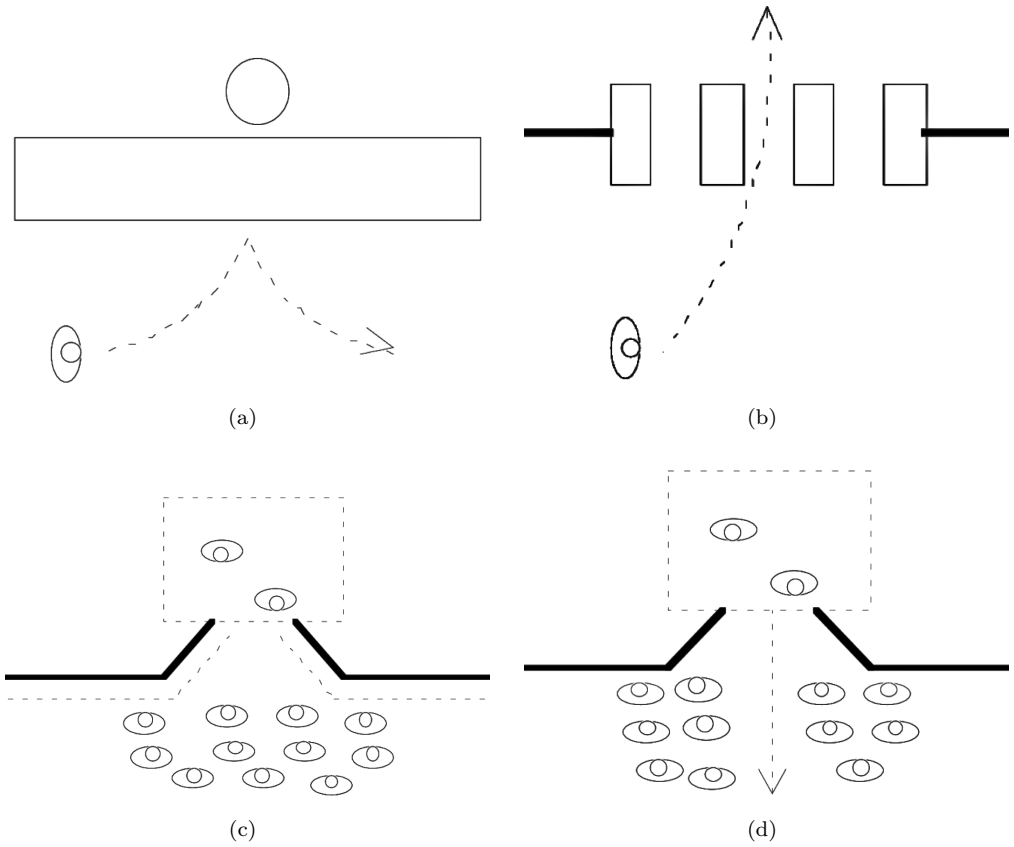

Figure 5.10: Types of queuing behavior [49].

$0 - 0.2\,m/s$ for a density of $3 - 4\,pedestrians/m^2$. Above this density, pedestrians are at risk and thus information is very rare. Most models assume gridlocks at these densities where the average speed is null. However, recent observations have shown that the velocity of the crowd can keep increasing at very high densities due to pushing [59] . Basically, the only similarity that exists between the fundamental diagrams obtained by different empirical studies is that the walking speed of pedestrians is a decreasing function of density. In [60], a simple mechanism was suggested that could explain the different empirical observations. In short, a pedestrian updates his velocity to keep a certain net-time headway with the pedestrian in front. In this way, if the latter stops, there wont be a collision between the two.

Though considered one of the most important elements of crowd management, the fundamental diagram is not always reliable. The velocity-density relation varies according to numerous factors [1]: (1) the size of the pedestrians' bodies, (2) their emotional state (calm, agitated, panicking...) [29], (3) their culture [61], (4) environmental and meteorological conditions, (5) ground slope, (6) the method used to measure the pedestrian density (7) unidirectional or bidirectional flows or even (8) presence of groups in the crowd.

Collective dynamics at very high densities

Beyond certain densities, it is impossible to conduct experiments to study crowd's movement since the participants' safety would be at risk. Only recently have we been able to gain an insight on human crowd dynamics thanks to a study based on the observation of the movement of Muslim pilgrims during The Hajj in Mecca [59]. Analyzing video footage of the unidirectional movement of pilgrims on a "pedestrian highway" that connects two sacred places, showed that in some zones local densities can reach a value of $9\,pedestrians/m^2$. In addition, the videos showed how the system responds to a progressive evolution of the pedestrian density where two new collective phenomena were observed: stop-and-go waves and crowd

turbulence. As the density increases, the system's state changes from fluid like to stop-and-go waves and finally reaches a state of turbulence.

Stop-and-go waves In unidirectional flows, an increase in the density of individuals lead to progressive decrease in the walking velocity. When this density reaches a certain critical level, the state of the system changes from a laminar to a stop-and-go flow. As a result, the velocity keeps decreasing (low individual velocity) interrupted by periods of successive forward movement waves (high individual velocity) and complete stops (zero individual velocity) Fig. 5.11. In the empirical study of pilgrim flows at Mecca it was found that stop-and-go waves start at a critical local density of $6\,pedestrians/m^2$.

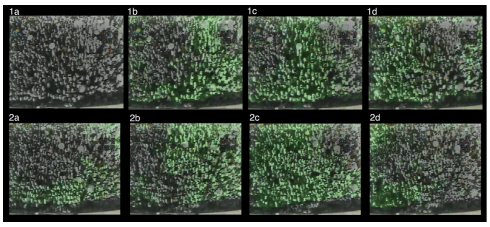

Figure 5.11: Image frames of a video of the pilgrimage in Mecca in 2006. The images illustrate the stop-and-go phenomenon throug the propagation of two successive waves (from 1a to 1d then from 2a to 2d). The pilgrims move from left to right. The green color indicates the pedestrians that are moving [59].

Stop-and-go waves have been well studied in vehicular traffic [62–64]. It has been established that two mechanisms are responsible for the emergence of this phenomenon. The first one is an external element perturbing the system and forcing the vehicles to slow down. Then, if the vehicular flow is high enough, the velocity reduction propagates rapidly in the opposite direction of the flow. Since a mechanical delay is inevitable for a vehicle to take off after a temporary halt, stop-and-go waves emerge.The same underlying mechanisms might also be at the origin of stop-and-go waves in pedestrian flows but with certain particularities. To start with, in a crowd, where the movement is less constraint than for vehicular traffic, the sources of perturbation are numerous. They can be temporary, for example if a pedestrian suddenly decides to stop or change direction. They can also be sustainable like the narrowing of a certain path. Concerning the take off delay that causes the stop-and-go waves, it is caused by the need of a certain space before a pedestrian takes a step forward.

Turbulence If after the transition from laminar to stop-and-go flow takes places the density keeps increasing, a new change in the collective dynamics occurs. When a second critical density is reached, a phenomenon called turbulence emerges. The effects of turbulent flows have been observed once during the pilgrimage at Mecca in 2006. It has never been reproduced under experimental conditions since the participants' security would be put in danger. At densities where turbulent flows appear, pedestrian interactions change dramatically. Each individual incurs very high pressure from his neighbors in all directions. In his turn, the pedestrian starts pushing to increase his personal space to be able to breathe. As a result, a local perturbation, like a new available space or a gap, is filled almost instantaneously resulting in shock waves that can propagate through the crowd and lift people off of their feet and propel them distances of 3 m or more [65]. This phenomenon has dramatic consequences on the lives of pedestrians.

> *"People may be literally lifted out of their shoes, and have clothing torn off. Intense crowd pressures, exacerbated by anxiety, make it difficult to breathe."* [65]

The empirical study of the pilgrimage in Mecca didn't precise an explicit value of the critical density beyond which the turbulence phenomenon emerges. It is though believed, that this value is close to 7 or $8\,pedestrians/m^2$. According to Fruin [65], at these levels of denisty, the crowd becomes almost a fluid mass. It seems that turbulence take place when individuals become in contact with each other. This means that the density have surpassed the capacity of the environment which is the maximum number of

people per square meter that an environment can encompass in the absence of physical contact between pedestrians. This is why the critical density value for turbulent flows can vary and depends on several parameters related to the individuals' physical characteristics.

Panic In situations of panic three types of pedestrian interactions exist [1]: (1) avoiding possible collisions with others while searching for an exit to escape; (2) pushing others using the same exit to be able to leave as quick as possible; and (3) imitating one's neighbors. The last behavior is often taken into consideration in pedestrian models based on a hypothesis that individuals tend to escape in the same direction of their neighbors. Some studies on the collective behavior of "panicking" individuals during evacuation of closed spaces exist as a form of postmortem analysis [66, 67]. In these incidents people were injured and lives were lost. For this reason, situations of panic have been mainly studied using numerical simulations [29, 68].

According to these studies, panic causes several changes in a pedestrian's "normal" behavior. To begin with, its desired velocity increases to exceed $5\,m/s$ coupled with a volatile and arbitrary movement. In simulation models, the latter is taken into consideration by adding random fluctuations to 'normal' movement. Concerning interactions, a "friction" term is added to slow down individuals in physical contact. The last modification concerns the desired direction of each pedestrian. Several pedestrian models have adopted the hypothesis that a pedestrian might change its direction for the one adopted by a group of its neighbors. A parameter representing the importance of each of the three effects of panic can be defined for each individual [29].

This change in individual behavior has two major consequences. The first one results from the increased speed and arbitrary movement of "panicking" individuals. This translates in a lack of coordination between the pedestrians when they are traversing a certain narrowing, like an exit. It was shown in [29], using numerical simulations, that evacuation times decreases as the level of panic increases. Pedestrians swarm exits obstructing it and resulting in lower discontinuous flows. The second consequence is caused by the 'imitation' behavior acquired during situations of panic. When individuals are not familiar with a certain environment or in cases of reduced visibility, imitation behavior leads to an unbalanced use of exists [69]. If someone finds a certain exit, those who can see him follow him. A positive feedback loop settles and the probability of pedestrians finding this specific exit increases. With time, the latter becomes congested while other available exits are overlooked or not efficiently used. This is called **herding behavior**.

In situations of panic, there's a great chance that people get injured or in worst cases lose their lives. This why it is very important to study and better understand the behavior of people under these circumstances. However, only fragile empirical results exits since it is impossible to study these situations under experimental conditions. This is why the hypotheses used by simulation models have never been properly validated.

5.1.3 Modeling pedestrian behavior

In human crowds, self-organized processes arising from local interactions among pedestrians lead to several collective phenomena that optimizes pedestrian traffic. For example, crowds moving in opposite directions tend to spontaneously form lanes of uniform walking direction to facilitate their movement. Modeling these collective phenomena is one of the objectives of crowd models. To reproduce self-organized processes, pedestrian-pedestrian and pedestrian-obstacle interactions, which are responsible for the appearance of the former, should be modeled. In the following paragraphs, a brief overview of the methods used to model pedestrian behavior is presented.

Avoidance behavior

Among the different forms of pedestrian interaction, the act of avoidance stands out as an essential component of the coordination of collective movement. Collision avoidance deals with applying forces that alter the agentâs trajectory to smoothly avoid static and dynamic obstacles. This action constitutes a central element of the majority of pedestrian movement models. Several approaches exist to model it each with different assumptions. Experimental studies exist to compare predictions from a model with certain observed global characteristics, such as flow intensity, velocity distribution or emerging collective

arrangements. However, the lack of control of the observed situations in these experiments creates a major obstacle for the process of identifying the interaction laws and validating the underlying assumptions of the available methods. At the same time, these approaches have been qualitatively validated by reproducing several observed self-organization phenomena. The three major ones are presented below.

Repulsive forces In force-based models (e.g. the social force model [70] or the centrifugal force model [71]), pedstrian motion is described as a combination of a driving force pointing towards the goal position, and repulsive forces originating from the obstacles (fixed or mobile). Individuals are treated as particles abiding the laws of Newtonian mechanics. As a result, pedestrians don't anticipate or predict collisions in order to avoid them. Instead, they exert repulsive forces on each other and only react once they are sufficiently close (Fig. 5.12). In addition, adjustments of the walking path are expected rather than adjustments of the walking speed. Consequently, the individuals' behavior and trajectories appear unnatural and contains undesirable oscillations. The problem becomes worse in dense crowds as pedestrians try to find an equilibrium position. The system's dynamics is closer to that of gas particles than to pedestrians. Several modifications and parameter calibrations were done in an effort to render pedestrian motion more natural [72, 73].

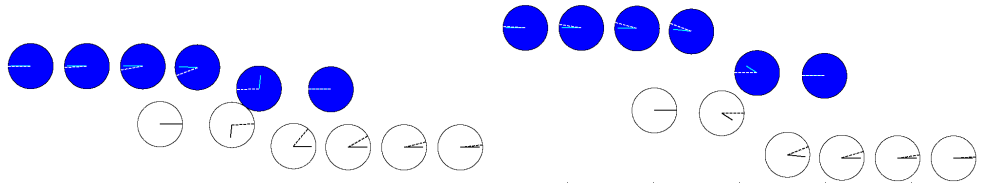

(a) (b)

Figure 5.12: Pedestrian-pedestrian interaction (a) without and (b) with introducing the repulsive force (for $A = 2000\,N$ and $B = 0.08\,m$)

Behavioral heuristics Several methods for modeling the avoidance behavior are based on collision prediction [74–77]. By linearly extrapolating the pedestrians' trajectories, the expected collisions in the near future are determined. These approaches are based on two behavioral heuristics:

- Taking into account the presence of obstacles, a pedestrian chooses the direction that allows the most direct path to a destination point.
- After choosing the walking direction, a pedestrian maintains a distance from the first obstacle or pedestrian on his path that ensures a minimum time to collision.

In this way, instead of being repelled by neighboring pedestrians and objects , individuals seek a collision free path through the crowd. This path is computed in three steps. In the first one, using their vision field, individuals explore the reachable space and identify the pedestrians and obstacles that are present in it. Then, among these "objects", they search for the ones with whom there will be possible collisions, i.e. the pedestrians and obstacles that are found in their sensory region. The visual field contains everything that can be spotted by an individual's vision while the sensory region contains only those that can influence the pedestrian's trajectory. Finally, the optimal path for the near future is determined so that all the possible collisions are avoided and with minimal effort.

Mobile robotics In mobile robotics, collision avoidance is of primary importance for mobile robots. Two main categories of collision avoidance algorithms exist. The first one directly calculates optimal collision free paths in an environment with stationary or moving obstacles whose motions are predictable. We will call them path planning algorithms. The second family of algorithms indirectly generate collision free paths by using the current kinematic and geometric information of the agent and all the obstacles.

We will call them trajectory planning algorithms. Since pedestrians' motion is unpredictable, only a literature on the trajectory planning algorithms will be reviewed.

Trajectory planning algorithms are based on the artificial potential field (APF) [78] or the virtual force field (VFF) [79]. These two approaches are similar and can be put in the same category since virtual forces can be obtained by using the gradient descent method on APFs. These algorithms assume that each obstacle is surrounded by a repulsive artificial potential field or a repulsive virtual force that push the agent or robot away from the obstacle. On the other hand, attractive APFs or VFFs exist to pull the robot towards a certain destination. These force functions or potential fields are related to the distance between the robot on one hand and the goal and the obstacles on the other. They can also be related to the velocities of the obstacles to help the agent avoid dynamic obstacles [78, 80, 81]. Then, through the dynamic interactions of the robot with the attractive and repulsive fields or forces, its desired acceleration is determined. The APF-based and VFF-based navigation algorithms can be applied to model pedestrian movement since they allow to avoid mobile obstacles whose moving directions are unpredictable, such as humans.

Queuing behavior

Queuing is a phenomenon in a number of fields, and has been extensively analyzed in the study of queuing theory. It has been used by several models to study pedestrian queues [82–84]. The number of waiting people and waiting time can be calculated by the Queuing theory. However, according to [49], queuing theory cannot be used in cases of extremely heavy congestions and complicated pedestrian movement. In this case, microscopic pedestrian models that incorporate pedestrian queuing behavior seem to be able to simulate these complicated movements in large spaces including queue spaces [49, 85]. Yet, no information was found in literature on the methods used to model queuing behavior in microscopic models.

In this section, we have done a bibliographical study on pedestrian behavior in public spaces. First, the self-organization phenomena in complex systems were presented. Its general theoretical concepts were introduced followed by a case study on animal groups and lessons to be learned for studying pedestrian crowds. Then, the current empirical knowledge of pedestrian collective motion were reviewed. We went over the characteristics of pedestrian motion and pedestrian interactions before presenting the resulting collective dynamics at normal and high densities. Finally, modeling pedestrian behavior, namely avoidance and queuing behavior, was addressed. The next section is dedicated for the work that has been done to model pedestrian behavior in our model.

5.2 Pedestrian behavior in the 2D model

One of the objectives of crowd modeling is to describe collective phenomena arising from local interactions among pedestrians. Among the different forms of interaction between pedestrians, the act of avoidance stands out as an essential component of the coordination of collective movement. This action constitutes a central element of the majority of pedestrian movement models. In an attempt to reproduce all self-organized processes and pedestrian behavior, these models are becoming increasingly complex. They either use complicated mathematical expressions or involve a considerable amount of parameters that is difficult to calibrate, notably for extreme crowd conditions. An approach based on behavioral heuristics and another based on repulsion forces have been integrated in our model. In the first part of this section, we compare the pedestrian behavior obtained by each method along with a collision approach (without avoidance).

As we have mentioned before, queuing is almost ubiquitous in public spaces. Whenever there are two or more people who want to perform the same activity at the same place, queues are formed. That is why it is important that a pedestrian model incorporates this pedestrian behavior. In the second part of this section, we demonstrate the method that was used to model pedestrians standing in line.

5.2.1 The social repulsive force

The social force model has been introduced in Chapter 1. It is based on physics: pedestrians are considered as particles moving according to a set of forces. An attractive force pulls the pedestrians towards their

destination and a repulsive one allows them to keep a distance with other pedestrians and obstacles in order to avoid collisions. In this section, only the repulsive force between pedestrians is revisited. This force was introduced by Helbing and was given by the following form in [29]:

$$\mathbf{f}_i^{soc} = \sum_{j \neq i} \mathbf{f}_{ij}^{soc} = \sum_{j \neq i} A e^{\left((R_{ij} - d_{ij})/B\right)} \left(\lambda + (1-\lambda)\frac{1+\cos\phi_{ij}}{2}\right) \mathbf{e}_{ji} \tag{5.1}$$

where $R_{ij} = r_i + r_j$ is the sum of the radii of pedestrians i and j, d_{ij} is the distance between their centers, A and B are constant parameters of the model representing the magnitude of the maximum sociopsychological force and its fall-off length respectively, λ with $0 < \lambda < 1$ reflects the anisotropic nature of the force, $\mathbf{e}_{ji}$ is the unit vector pointing from pedestrian j to pedestrian i, and ϕ_{ij} is the angle between i's desired direction $\mathbf{e}_{d,i}$ and $\mathbf{e}_{ji}$. As shown in Fig. 5.13, the social force $\mathbf{f}_i^{soc}$ acts on the particle i . If the parameters A, B, and $\lambda$are identical for both pedestrians, then the force acting on pedestrian j reads: $\mathbf{f}_j^{soc} = -\mathbf{f}_i^{soc}$.

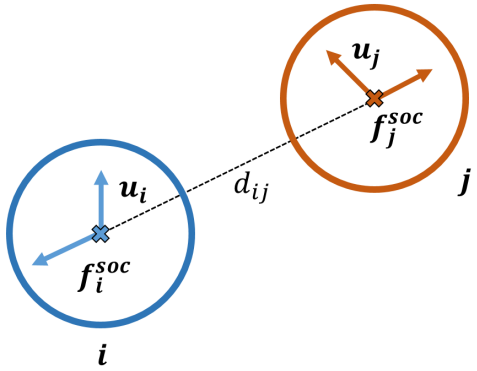

Figure 5.13: The direction of the social repulsive force for two pedestrians.

Force-based models have had great success in the academic world for many years. However, important limitations have then been identified. Indeed, it is hard to objectively evaluate the intensity of the different forces applied on pedestrians. In [29], Helbing chose $A = 2000\, kg.m.s^{-2}$ and $B = 0.08\, m$ (see Fig. 5.14). In [72], it is shown that for these values of A and B, a pedestrian's maximum deceleration exceed the acceleration of gravity by almost 40%. A value that does not seem realistic. Moreover, those models turned out to be unreliable for fitting experimental data. For instance, collisions are not well simulated: pedestrians tend to rebound against each other like rigid particles, which is of course far away from the observed phenomenon. For this reason, several modifications of the social repulsive force and calibrations of its parameters can be found in literature [72, 73, 86]. To compare the force-based interactions to other approaches, we use the traditional form of the social repulsive force given by Eq. (6.4).

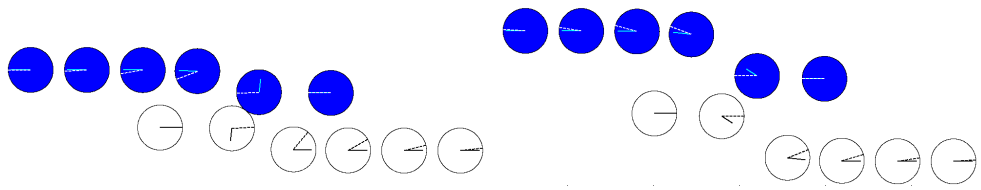

(a) (b)

Figure 5.14: Pedestrian-pedestrian interaction (a) without and (b) with introducing the repulsive force (for $A = 2000\, N$ and $B = 0.08\, m$)

5.2.2 Avoidance based on behavioral heuristics

In the field of decision making, it has been shown that individuals use simple and rapid heuristics in order to deal with daily situations in complex ever changing environments [87, 88]. A new modeling approach based on behavioral heuristics has been recently introduced to reproduce pedestrian avoidance behavior. The cognitive approach leads to much simpler behavioral principles than the physical one. Based on vision and relying on two simple heuristics, pedestrians adapt their movement to the surrounding conditions and choose (1) a walking direction α_{adap} and (2) a desired walking speed v_{adap}. In addition, individuals constantly adapt their current walking behavior to the desired one within a relaxation time. In the following, we demonstrate how these heuristics are introduced in our model.

The model

In our model, each agent is characterized by its current position $\mathbf{q}_i = (q_i^x, q_i^y)$, velocity $\mathbf{u}_i = (u_i^x, u_i^y)$, and its actual viewing direction represented by $\theta_i \in [-\pi, \pi]$ about the $\mathbf{e}_z$-axis ($\theta_i(t) = 0$ when the particle's walking direction is parallel to the x-axis in the positive direction and $\theta_i(t) > 0$ in the trigonometric sense). The pedestrian body is represented by a circular shape with radius r_i and density ρ_i. Each agent also possesses a comfortable walking speed $u_{d,i}$ and a relaxation time τ_i. The vision field of agent i ranges to the left and to the right by ϕ degrees with respect to the viewing direction (Fig. 5.15 (a)). Studies have shown that using neural mechanism at the retina and brain levels, human beings can estimate the time to collisions with surrounding obstacles [85, 89]. Therefore, for all $\alpha \in [\theta_i - \phi; \theta_i + \phi]$, we calculate $h(\alpha)$ which is the distance to the first anticipated collision if pedestrian i would move in the direction α at speed v_i^0 taking into consideration the speed and the body size of the other pedestrians present in his/her vision field. In the case that no collision is expected, $h(\alpha)$ is set to the horizon distance d_{max} (Fig. 5.15 (b)). As a reminder, a list of the different variables is given:

- $\mathbf{q}_i = (q_i^x, q_i^y)$: pedestrian i's current position
- $\mathbf{u}_i = (u_i^x, u_i^y)$: pedestrian i's current velocity
- θ_i is the direction in which pedestrian i is looking
- $[\theta_i - \phi; \theta_i + \phi]$: the vision field of pedestrian i and the set of all possible moving directions
- $h(\alpha)$: the distance before the first collision in the direction α
- $\alpha_{i,0}$: the direction of the destination point
- d_{max} the range of the pedestrians' vision field

We now discuss the two heuristics of this cognitive approach that will be used by the agents to choose their desired walking direction and walking speed. Concerning the choice of the walking direction, empirical evidence suggests that individuals prefer one with a low visual coverage through obstructing objects, and to follow the longest line of sight [90, 91]. Concurrently, pedestrians heading towards their destinations avoid deviations. These two observations lead to the first movement heuristic: "A pedestrian chooses the direction α_{adap} that comes closest to the destination point [77]. The chosen direction α_{adap} is computed through minimization of the distance to destination $d(\alpha)$ (see Fig. 5.16):

$$d^2(\alpha) = d_{max}^2 + h(\alpha)^2 - 2d_{max}h(\alpha)\cos(\alpha_{i,0} - \alpha) \tag{5.2}$$

where $\alpha_{i,0}$ represents the direction towards the destination. The pedestrian's desired walking speed v_{adap} is determined by the second movement heuristic. Since an individual needs a time τ to reach a sudden stop, he/she keeps a safe distance from others to avoid collisions [60, 92]. Therefore, the second heuristic is defined by the following statement: "A pedestrian keeps a time to collision of time period τ with respect to the first obstacle in the chosen walking direction" [77]. Accordingly, v_{adap} is given by :

$$v_{adap} = min(||\mathbf{u}_i||, \frac{d_{obs}}{\tau_i}) \tag{5.3}$$

where d_{obs} is the distance separating pedestrian i from the first obstacle found in his desired direction α_{adap}.

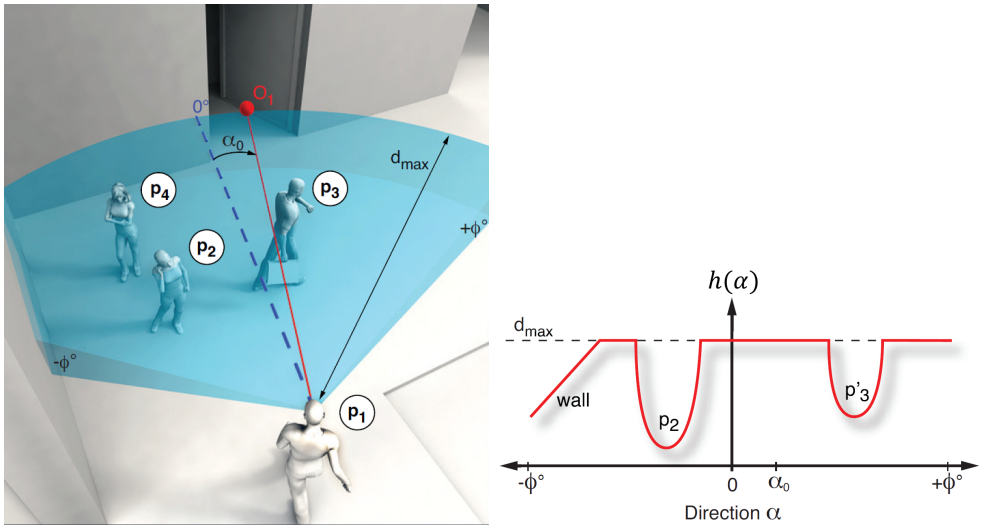

(a) (b)

Figure 5.15: (a) Illustration of a pedestrian p1 facing three other subjects and trying to reach the destination point marked in red. The blue dashed line corresponds to the line of sight and (b) a graphical representation of the function $h(\alpha)$ reflecting the distance to collision in direction α[77].

Calculating the time to collision

As we have mentioned earlier, for a given pedestrian i walking at a speed of $u_{d,i}$, $h(\alpha)$ represents the remaining distance towards the first expected collision in every direction $\alpha \in [\theta_i - \phi; \theta_i + \phi]$. It is given by $h(\alpha) = ||\mathbf{u}_i||t_\alpha$, where $t_\alpha = t_0 + \Delta t(\alpha)$ is the expected collision time. Therefore, the time to collision $\Delta t(\alpha)$ is found by solving the following equation:

$$d_{ij}(\Delta t(\alpha)) = r_i + r_j \tag{5.4}$$

where $d_{ij} = ||\mathbf{G}_i\mathbf{G}_j||$ represents the distance between pedestrians i and j's centers of mass. By denoting $(q_i^x(t), q_i^y(t))$ and $(u_i^x(t), u_i^y(t))$ the coordinates and velocity of agent i respectively, and for $t_0 = 0$ we get :

$$d_{ij}(\Delta t(\alpha)) = \sqrt{[q_i^x(\Delta t(\alpha)) - q_j^x(\Delta t(\alpha))]^2 + [q_i^y(\Delta t(\alpha)) - q_j^y(\Delta t(\alpha))]^2} \tag{5.5}$$

where the coordinates evolve according to the following equations :

$$\begin{cases} q_i^x(\Delta t(\alpha)) = q_i^x(t_0) + u_i^x \Delta t(\alpha) \\ q_i^y(\Delta t(\alpha)) = q_i^y(t_0) + u_i^y \Delta t(\alpha) \end{cases} \tag{5.6}$$

$$\begin{cases} q_j^x(\Delta t(\alpha)) = q_j^x(t_0) + u_j^x \Delta t(\alpha) \\ q_j^y(\Delta t(\alpha)) = q_j^y(t_0) + u_j^y \Delta t(\alpha) \end{cases} \tag{5.7}$$

and

$$\begin{cases} u_i^x = ||\mathbf{u}_i|| cos(\alpha) \\ u_i^y = ||\mathbf{u}_i|| sin(\alpha) \end{cases} \tag{5.8}$$

$$\begin{cases} u_j^x = ||\mathbf{u}_j|| cos(\theta_j) \\ u_j^y = ||\mathbf{u}_j|| sin(\theta_j) \end{cases} \tag{5.9}$$

We can then rewrite Eq. (5.5) in the following form:

$$\left(q_j^x(t_0) - q_i^x(t_0) + \Delta t(\alpha)(u_j^x - u_i^x)\right)^2 + \left(q_j^y(t_0) - q_i^y(t_0) + \Delta t(\alpha)(u_j^y - u_i^y)\right)^2 = (r_i + r_j)^2 \tag{5.10}$$

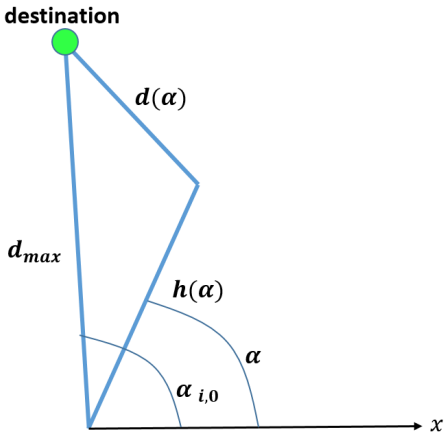

Figure 5.16: The distance to destination $d(\alpha)$.

By developing and rearranging Eq. (5.10), it can be written under the following form:

$$\boxed{U\Delta t(\alpha)^2 + Y\Delta t(\alpha) + Z = 0} \tag{5.11}$$

with

$$U = (u_j^x - u_i^x)^2 + (u_j^y - u_i^y)^2 \tag{5.12}$$
$$Y = 2(u_j^x - u_i^x)(q_j^x(t_0) - q_i^x(t_0)) + 2(u_j^y - u_i^y)(q_j^y(t_0) - q_i^y(t_0)) \tag{5.13}$$
$$Z = (q_j^x(t_0) - q_i^x(t_0))^2 + ((q_j^y(t_0) - q_i^y(t_0)))^2 - (r_i + r_j)^2 \tag{5.14}$$

By solving Eq. (5.11), we obtain two roots: Δt_1 and Δt_2. It is necessary to test these two roots to find out if a collision is expected within pedestrian i's visual field and if an eventual detour is going to be necessary.

Necessary and sufficient conditions for a collision within the visual field For a collision to take place within an individual's visual field, Eq. (5.11) must have at least one positive real root such that $\Delta t(\alpha) \leq d_{max}/||\mathbf{u}_i||$. Eq. (5.11) has at least one real root if its discriminant $D_{ij} \geq 0$. Assuming $D_{ij} \geq 0$, we have the relations (with Δt_1 and Δt_2 the polynomial roots) :

$$\frac{-Y}{U} = \Delta t_1 + \Delta t_2$$

$$\frac{Z}{U} = \Delta t_1 * \Delta t_2$$

Two cases are then possible :

- if U et Z have opposite signs $\Rightarrow$ Δt_1 and Δt_2 have opposite signs, then:

$$\Delta t(\alpha) = max(\Delta t_1, \Delta t_2) \tag{5.15}$$

- if U et Z have the same sign $\Rightarrow$ Δt_1 and Δt_2 have the same sign, then:
  - iff $\frac{-Y}{U} = \Delta t_1 + \Delta t_2 \geq 0$ then $\Delta t_1, \Delta t_2 \geq 0$ and:

$$\Delta t(\alpha) = min(\Delta t_1, \Delta t_2) \tag{5.16}$$

– If $\frac{-Y}{U} = \Delta t_1 + \Delta t_2 \leq 0$ then $\Delta t_1, \Delta t_2 \leq 0$ and:

$$\Delta t(\alpha) = d_{max}/||\mathbf{u}_i|| \tag{5.17}$$

If $D_{ij} < 0$, then Eq (5.11) has no real roots and $\Delta t(\alpha) = d_{max}/||\mathbf{u}_i||$. In case of physical contact between two pedestrians, $\Delta t(\alpha)$ is set to zero. Now that $\Delta t(\alpha)$ is found for all the possible collisions in an individual's visual field, $h(\alpha)$ can be obtained.

Calculating $h(\alpha)$

In [77], neither the expression of the function $h(\alpha)$ nor the method to evaluate it were defined. Only a graphical representation of the function was given for the case of 3 obstacles located within the vision field of the pedestrian (see Fig. 5.15 (b)).

In this section, we evaluate the function $h(\alpha)$ using two methods. In the first one, we approximate the curve from [77] with a polynomial function. In the second method, we determine $h(\alpha^i)$ by studying analytically the problem of a collision between two pedestrians and evaluating the remaining time before collision. We consider the case of a head-on encounter illustrated in Fig. 5.17.

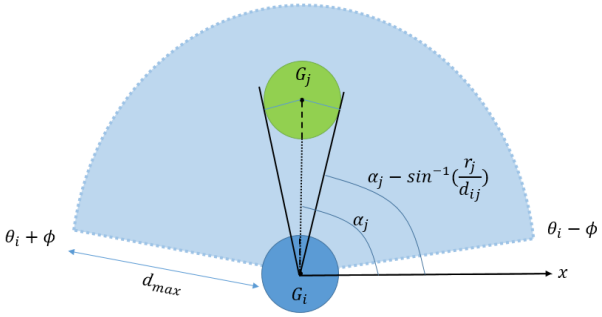

Figure 5.17: Head on encounter between pedestrians i and j.

Method 1: curve approximation

We first start by defining some additional notations that will be used later in this paragraph:

- α^j: the direction in which pedestrian j is found
- $h_j = h(\alpha = \alpha_j)$ the distance before the head-on collision when $\alpha = \alpha_j$

In this approach, the function $\alpha \to h(\alpha)$ is obtained by constructing a parabolic function centered at h_j. After evaluating the anticipated distance to collision h_j between the two pedestrians, we define the function $\alpha \to H_j(\alpha)$ by:

$$H_j(\alpha) = a_{ij}(\alpha - \alpha_j)^2 + h_j \tag{5.18}$$

$$\text{where } a_{ij} = \frac{(d_{max} - h_j)}{\left(arcsin\left(\frac{r_j}{d_{ij}}\right)\right)^2}$$

Agent j's center is found at α_j. However, due to its dimensions (disk of radius r_j), it is perceived by pedestrian i to be occupying the interval $[\alpha_j - arcsin(r_i/d_{ij}), \alpha_j + arcsin(r_i/d_{ij})]$. The function $\alpha \to h(\alpha)$ is now defined as:

$$h(\alpha) = \begin{cases} d_{max} & \text{if } \alpha \in \left[\theta_i - \phi, \alpha_j - arcsin(\frac{r_i}{d_{ij}})\right] \cup \left]\alpha_j + arcsin(\frac{r_i}{d_{ij}}), \theta_i + \phi\right] \\ H_j(\alpha) & \text{if } \alpha \in \left[\alpha_j - arcsin(\frac{r_i}{d_{ij}}), \alpha_j + arcsin(\frac{r_i}{d_{ij}})\right] \end{cases} \tag{5.19}$$

The shape of $h(\alpha)$ obtained using method 1 is illustrated in Fig. 5.18. By adopting the new direction which is supposed to be outside the interval occupied by pedestrian j, pedestrian i will be able to avoid the latter.

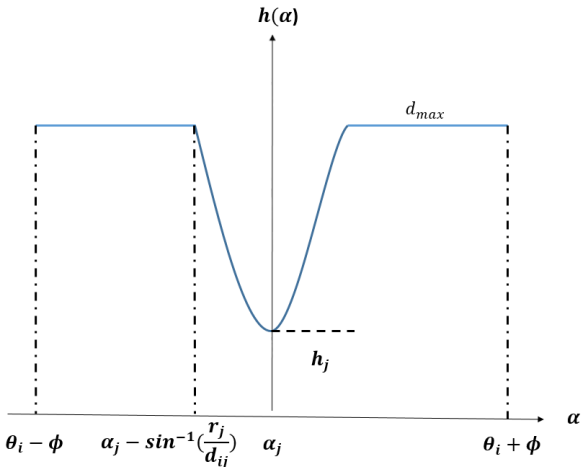

Figure 5.18: Representing $H_j(\alpha)$ by a parabolic function with a vertex at (α_j, h_j).

Method 2: analytical and numerical resolution of the collision problem - remaining time before collision The second method was developed with the help of Samy Mokhtari for his final semester project of his second year at the ENPC. In this paragraph, we consider a discretized vision field for the pedestrian i, with N_α possible moving directions (see Fig. 5.19). Then, we evaluate for each value of α within the discretized vision field, the coefficients U, Y and Z of Eq. (5.11), and its discriminant D_{ij}. For this method, some notations that were previously used must be redefined:

- $\boldsymbol{\alpha} = {}^t(\alpha_1, ..., \alpha_{N_\alpha})$ is now a vector (size $N_\alpha \times 1$) which contains all the possible directions of the speed vector $\mathbf{u}_i$ of pedestrian i (within his vision field)
- $\mathbf{h}(\boldsymbol{\alpha}) = {}^t(h(\alpha_1), ..., h(\alpha_{N_\alpha}))$ is the vector (size $N_\alpha \times 1$) of distances before collision for pedestrian i, for all possible directions α_n
- $\Delta t(\alpha_n^i)$ is the remaining time before collision in the direction α_n^i, for pedestrian i

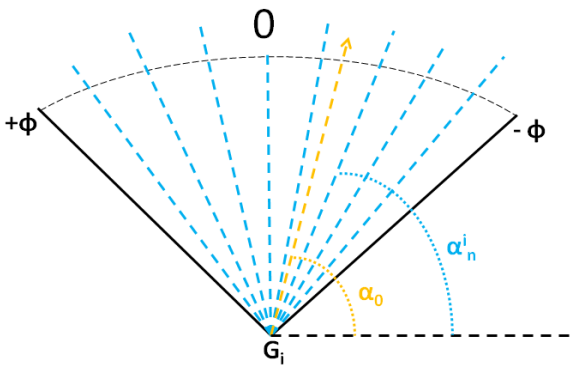

Figure 5.19: Discretized vision field of pedestrian i.

We evaluate, for each element α_n of $\boldsymbol{\alpha}$ ($n \in \{1, ..., N_\alpha\}$) in pedestrian i's discretized vision field, the remaining time before collision $\Delta t(\alpha_n)$. It can be evaluated from the following condition of collision: the distance between the pedestrians' centers of mass is equal to the sum of their radii. This condition can be written as a second degree polynomial (see Eq. 5.11) and $\Delta t(\alpha_n)$ must be a positive root of this polynomial for a collision to happen. Thus, we just have to multiply the remaining time before a collision by the speed of the pedestrian to obtain the row vector of remaining distances before collision :

$$\forall n \in \{1, ..., N_\alpha\},\ h(\alpha_n) = ||\mathbf{u}_i(\alpha_n)||_2 * \Delta t(\alpha_n)$$

For the case of a head-on encounter (see Fig. 5.17), Fig. 5.20 illustrates the row vector $\mathbf{h}(\boldsymbol{\alpha^i})$ as a function of the row vector $\boldsymbol{\alpha^i}$ and $\alpha^i \rightarrow h(\alpha^i)$, where α^i was a scalar $\in [-\phi, +\phi]$. In this example, pedestrians i and j are respectively located in $(1, 0.2)$ and $(1, 3.5)$.

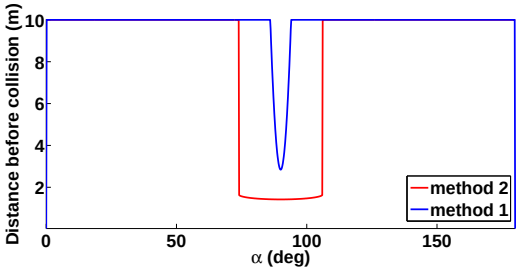

Figure 5.20: Head-on encounter between 2 pedestrians: the distance before collision obtained by method 1 (blue) and method 2 (red).

Before even testing those two methods on collision avoidance simulations, we can clearly see that for the case of a head-on encounter, methods 1 and 2 give very different curves for the distance before collision. Thus, we can guess that methods 1 and 2 will generate different pedestrian trajectories and number of collisions.

Numerical simulations

In this paragraph, we simulate several pedestrian-pedestrian interactions with the four different approaches we described:

- collision model
- social repulsive force model
- cognitive model : method 1
- cognitive model : method 2

To assess the differences between those four approaches, we compute four specific cases of pedestrian-pedestrian interactions : (a) head-on encounter, (b) overtaking a moving pedestrian, (c) overtaking two immobile pedestrians, and (d) the intersection of two pedestrian streams.

Head-on encounter At first, we consider a head-on encounter between two pedestrians moving in opposite directions. With both the collision and the social repulsive force models, pedestrians must not be placed on the exact same abscissa, otherwise they won't be able to go on towards their destination after the collision. That's why we placed, for this simulation, the two pedestrians respectively in $(1.23, 0.5)$ and $(1.1, 4)$.
With the collision model, the two pedestrians collide as expected, causing a little step back, but then are able to go back on the trajectory leading to their destination point (Fig. 5.21 a). With the social repulsive force model, the two pedestrians move towards each other as if they were going to collide. However, when the distance between them is short enough, the repulsive force enables them to avoid each other, and then to follow the trajectory towards their destination (Fig. 5.21 b).

With the cognitive model, whether it is computed with method 1 or 2, the two pedestrians change their trajectory from the start in order to avoid each other, then change it again in order to reach their destination. Moreover, we can notice that the safety distance that those pedestrians keep between each

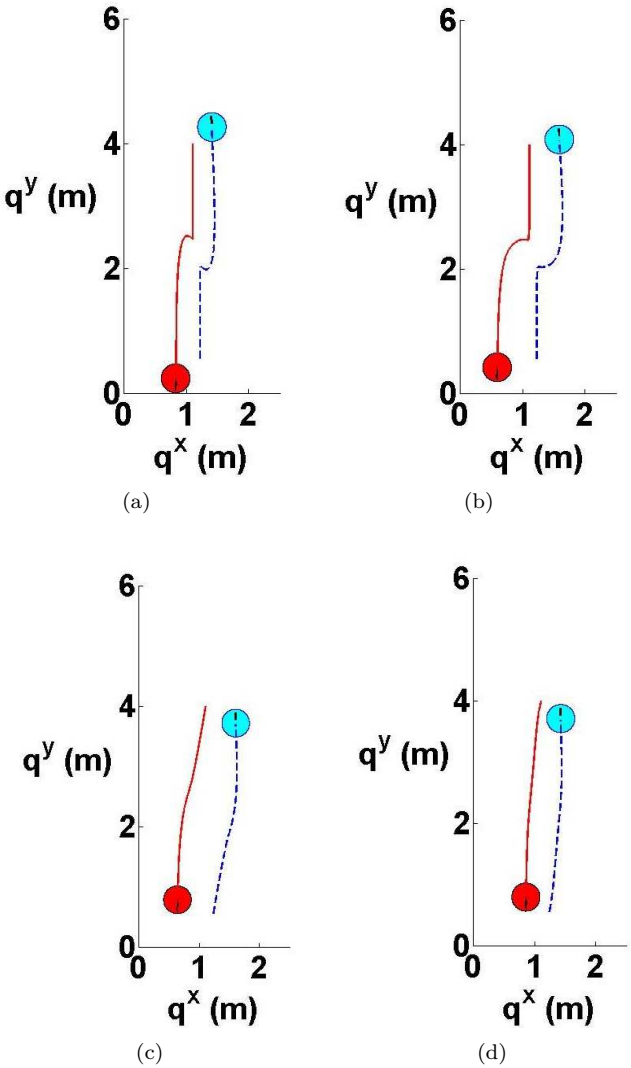

Figure 5.21: Head-on encounter between two pedestrians: (a) collision model, (b) social repulsive force model, and cognitive model (c) method 1 and (d) method 2.

other during the avoidance is shorter with the second method than with the first one (Fig. 5.21 c and d). Besides, contrary to the collision and social repulsive force models, we don't have to place the pedestrians on two different abscissas. Indeed, they are still able to avoid collision even if they are exactly in front of each other. However, the initial distance between them must be large enough to enable them to change their trajectory and avoid collision.

Overtaking a moving pedestrian This time, we consider the overtaking of a moving pedestrian by a second pedestrian moving in the same direction, at double speed. Both pedestrians have the same destination point. With the collision model, the overtaking maneuver is not successful. The two pedestrians collide at $y = 3.8\,m$ (see Fig. 5.22 a). This collision is the reason behind the slight deviation in their trajectories after $y = 3.8\,m$.

With the social repulsive model, no collision occurs. Similarly to the previous simulation, when the distance between the two pedestrians is short enough, the repulsive force pushes them away from each other. The pedestrian in the back has a greater trajectory deviation than the other one (Fig. 5.22 b).

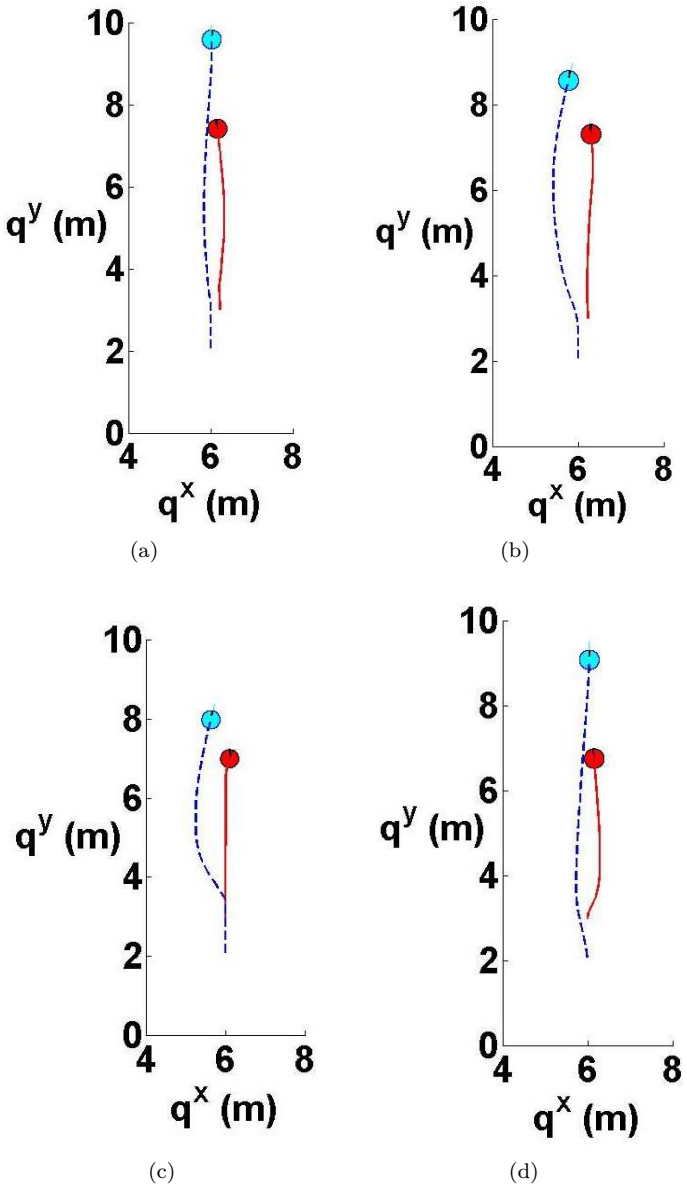

Figure 5.22: Overtaking of a moving pedestrian : (a) collision model, (b) social repulsive force model, and cognitive model (c) method 1 and (d) method 2.

This is due to anisotropic nature of the repulsive force represented by λ. As have been mentioned before, for a head-on encounter, for the collision and social repulsive force models the pedestrians cannot be on the exact same abscissa.

For the cognitive model, placing both pedestrians on the exact same abscissa poses no problems. With the first method, the second pedestrian moves straight towards the first one, slows down just before colliding, and then changes his trajectory in order to avoid collisions and reach eventually the destination point (Fig. 5.22 c). The first pedestrian almost does not change his trajectory. With the second method, both pedestrians change their trajectory from the beginning, and the safety distance between them during the overtaking is shorter than with the first method (Fig. 5.22 d).

Overtaking immobile pedestrians Let us now consider the overtaking of two pedestrians who are at rest. Naturally, when two individuals are together they keep a certain distance between each other. If

this distance is not large enough, a pedestrian who wants to overtake these two individuals will prefer to go around them rather than between them. With the collision and repulsive forces models, we are not able to reproduce this empirical behavior (see Fig. 5.23 a-b). However, the cognitive model gives better results (see Fig. 5.23 c-d).

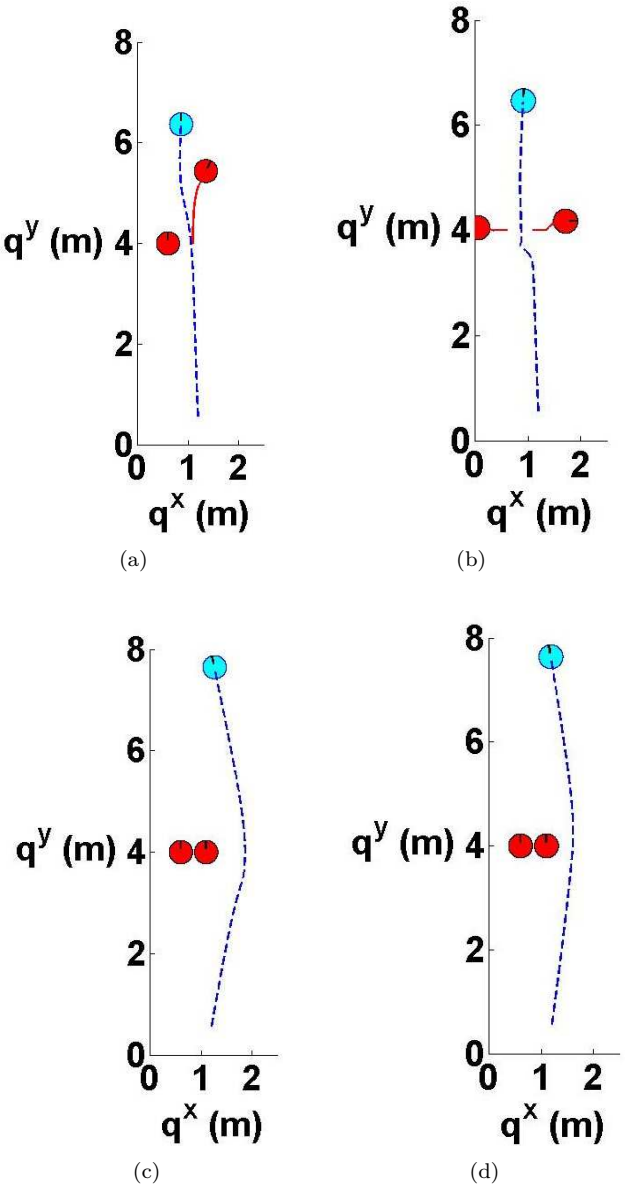

Figure 5.23: Overtaking of two immobile pedestrians : (a) collision model, (b) social repulsive force model, and cognitive model (c) method 1 and (d) method 2.

With the collision model, the moving pedestrian just strikes one of the immobile pedestrians and pushes him to the right. Then he moves forward towards his destination point (Fig. 5.23 a).
With the repulsive forces model, the two steady pedestrians begin to move away from each other, and then the moving pedestrian walks between them, in order to reach his destination (Fig. 5.23 b).
Finally, with the cognitive model, the two immobile pedestrians stand still and the moving pedestrian changes his trajectory from the beginning of the simulation, in order to avoid them. After being passed aside the obstacle, the moving pedestrian changes again his trajectory to reach his destination point

(Fig. 5.23 c and d). We can notice once again that the safety distance during the avoidance between the moving pedestrian and the steady pedestrians is shorter with the second method than with the first one.

Two intersecting pedestrian streams Finally, we study the case of two pedestrian streams intersecting each other shown in Fig. 5.24. For the following simulations, we defined a destination point located in $(9, 9.5)$ for the pedestrian stream starting from the bottom-left side of the screen. As for the other pedestrian stream, we defined a moving direction at 45 degrees under the horizontal line.

To assess the performance of the different models used to simulate the intersection of those two pedestrian streams, we selected the following criteria:

- number of collisions
- computation time
- pedestrians' speed to reach their destination point within the simulation time
- the pedestrians' ability to reach a speed close to the desired velocity

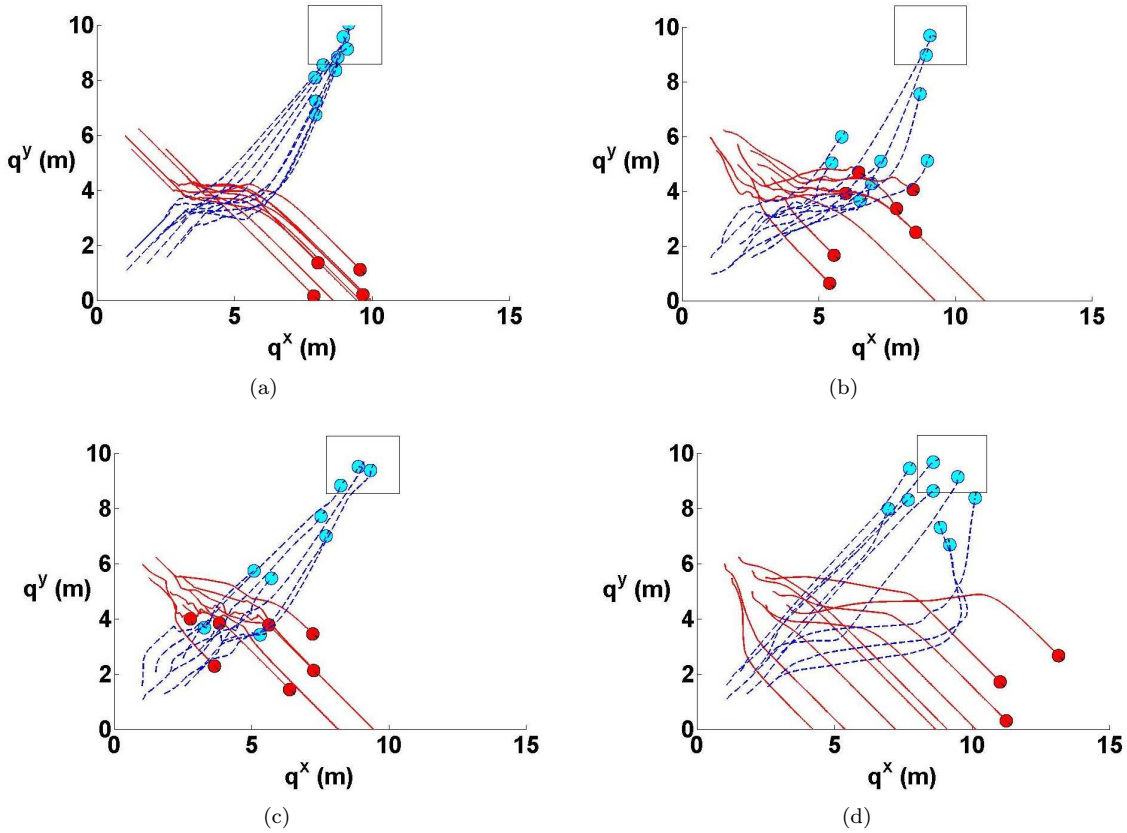

Figure 5.24: Intersection of 2 pedestrian streams: (a) collision model, (b) social repulsive force model, and cognitive model (c) method 1 and (d) method 2.

Number of collision The number of collisions obtained by each approach is given in Fig. 5.25. The least number of collisions were obtained by the social force model following by the cognitive model using the second method. It appears that the cognitive model using the first method is not efficient enough to enable pedestrians to avoid collisions properly. As for the collision model, it is not surprising to see that it gives the largest number of collisions.

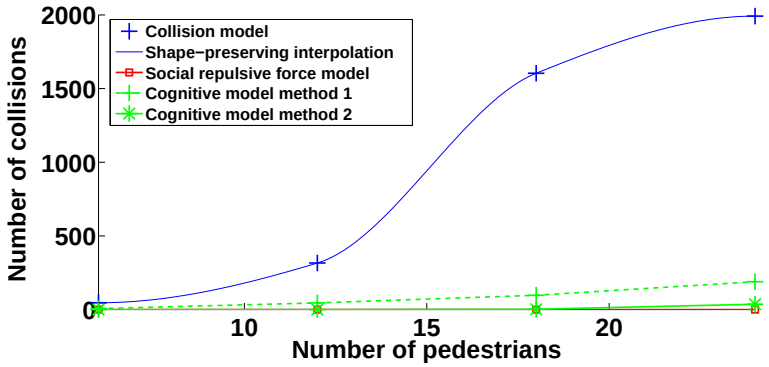

Figure 5.25: Intersection of 2 pedestrian streams : number of collisions, with the different models and an increasing number of pedestrians.

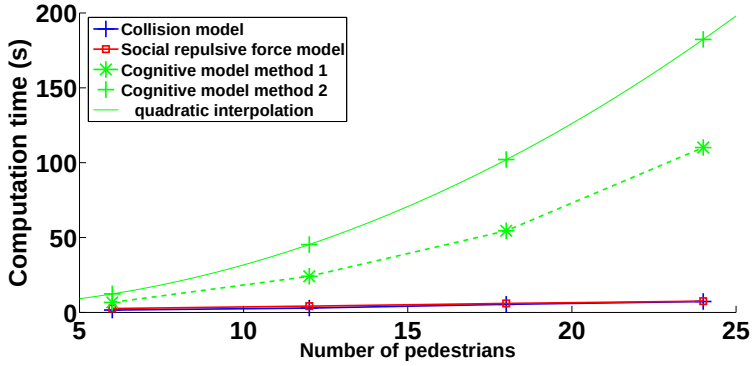

Figure 5.26: Intersection of 2 pedestrian streams : computation time, with the different models and an increasing number of pedestrians (Simulation time = 9 s).

Computation time In terms of computation time, Fig. 5.26 shows the most performant is the collision model followed by the social repulsive model. The cognitive model, whether it is computed with method 1 or 2, takes significantly more time. However, the second method clearly shows the slowest computation speed.

Pedestrians' speed to reach their destination point within the simulation time To assess the pedestrians' speed to reach their destination point, we drew a rectangle around it (see Fig. 5.24) in order to assess the number of pedestrians that are actually within this rectangle at the end of the simulation time (which is here 9.5 s) and also the approximate time when all the pedestrians are inside it.
The collision model shows the highest number of pedestrians within the rectangle as can be seen in Fig. 5.24 a. Those who did not have enough time to enter the rectangle are close. As for the cognitive model, both methods 1 and 2 enable several pedestrians to enter the rectangle. However, the remaining pedestrians are much closer to the destination point with the second method than with the first one. Finally, with the social repulsive force model, just two pedestrians entered the rectangle, and many of them are still far away.
Thus, it seems that, in terms of pedestrians' speed to reach their destination point, the collision model seems to be the best one, followed by the cognitive model computed with the second method, and finally the cognitive model computed with the first method and the social repulsive force model.

Pedestrians' ability to reach a speed close to the desired velocity In our previous simulations, the desired velocity of each pedestrian is defined by a normal distribution. For instance :

- mean (average speed) : 1 m/s
- standard deviation : 0.8

Thus, all the pedestrians do not have the exact same speed. It enables us to take into account for instance their age or their height, which affect their walking speed. In order to compare the results of the different approaches in terms of pedestrians' velocities, we chose in this part to give the exact same speed to all the pedestrians, for instance 1 m/s. In the following, the curves represent the amplitude of the pedestrians' mean walking speed, for both streams and with the different models we described earlier : collision, social repulsive force, and cognitive (method 1 and 2).

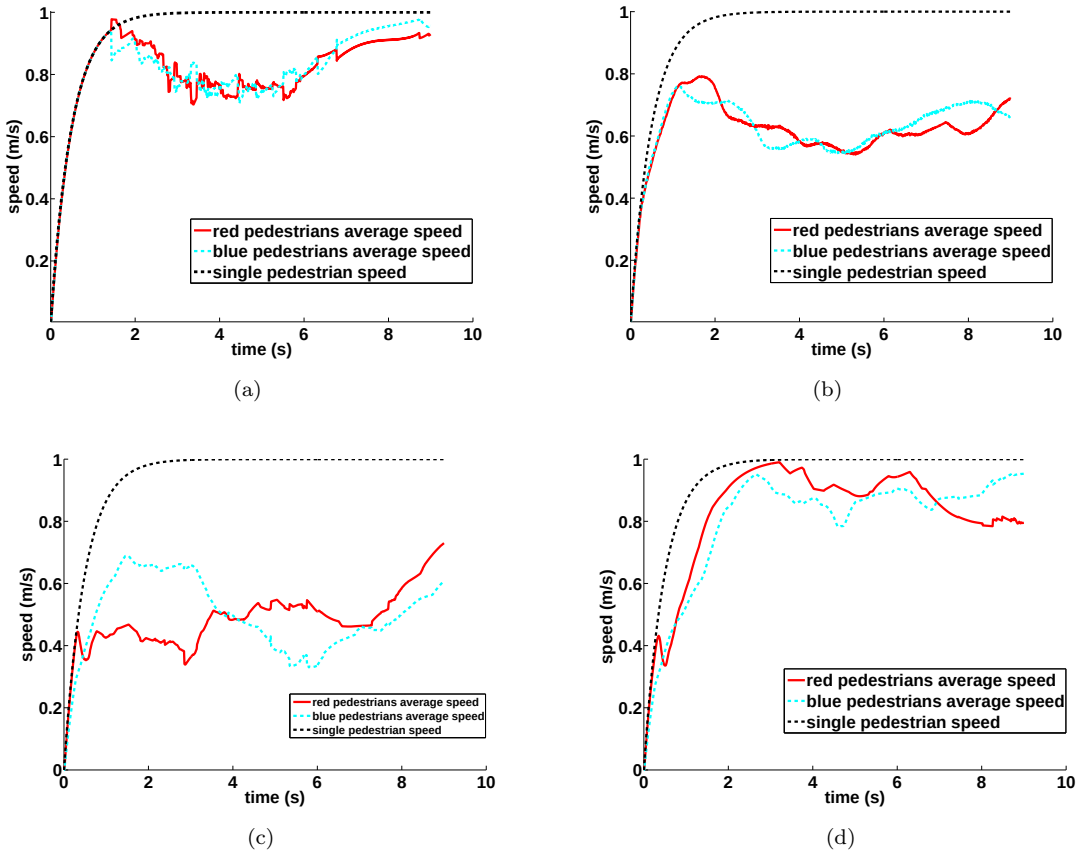

Figure 5.27: Intersection of 2 pedestrian streams: (a) collision model, (b) social repulsive force model, and cognitive model (c) method 1 and (d) method 2.

In terms of ability to reach and maintain a speed close to the desired velocity, which is here 1 m/s, Fig. 5.27 shows that the cognitive model based on method 2 seems to be the best option : pedestrians from both streams are able to quickly reach a speed close to 1 m/s and to maintain it. The collision model gives good results too, even if some pedestrians have to reduce their speed a little during the intersection.The cognitive model based on method 1 clearly seems to be the worst option : pedestrians from both streams have to reduce significantly their speed in order to walk through the intersection, and cannot reach their desired velocity before the end of the simulation.

Due to obvious reasons, only the social model and the cognitive model will be examined in the following section on queuing behavior. The capability of each approach to model this type of behavior will be tested.

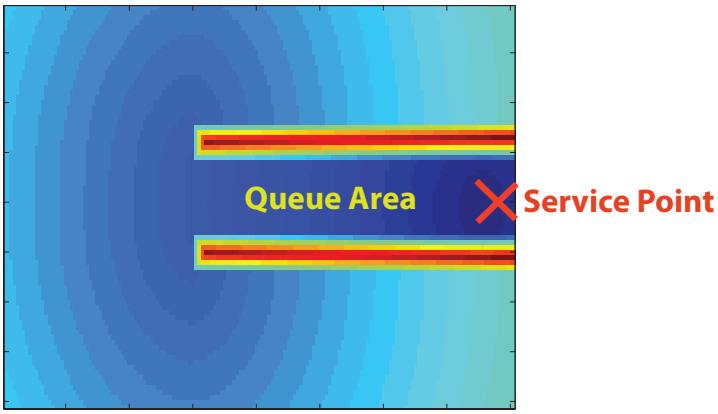

Figure 5.28: The static floor field used to create the queuing area that leads to the service point.

5.2.3 Queuing behavior

In public spaces, standing in queues seem to be inevitable. Whenever there are two or more individuals who want to do the same activity, queues are formed. Therefore, it is important that every pedestrian model incorporates this behavior. In the following paragraph, we demonstrate how queuing behavior can be modeled using floor fields and a stopping mechanism.

The queue

For pedestrians to stand in queue, the queue are must first be specified. These are usually found in front of a place offering a service (ATM machine, food truck, ...). The form queue can then either be predetermined with barriers such as in airports, banks, amusement parks, etc. or not such as in street markets, ATM machines, etc. In our model, we use the floor field method to specify the shape of the queue.

When the form of the queue is predetermined with barriers, the static floor field is used. In the floor field, the area where the service can be obtained is considered a destination, the queue area is modified to be attractive, and the rest of the environment is modified to be repulsive as illustrated in Fig. 5.28. In this way, pedestrians will walk through the queue area to get to the service area instead of taking the shortest or quickest path.

If the form of the queue is not predetermined then the dynamic floor field is used. In this case, the shape of the queue is recalculated every time a new pedestrians arrives and stands in it. As a result, pedestrians are not forced to walk in a predetermined queue area but they take the shortest path towards the position that is found just behind the last pedestrian in the formed queue.

The stopping mechanism

Queuing behavior is considered to be a 'civilized' behavior. People stand in line and wait for their turn. Therefore, the floor fields alone are not enough. A stopping mechanism is necessary so that pedestrians stop once they are at a certain distance from the person in front of them. This mechanism is defined as:

$$||\mathbf{u}_i|| = \begin{cases} 0 & \text{if } d_{ij} <= d \\ u_{d,i} & \text{if } d_{ij} > d \end{cases}$$

where $\mathbf{u}_i$ and $u_{d,i}$ are the actual and desired velocity of pedestrian i respectively, d_{ij} is the distance between pedestrians i and j, and d is a value chosen by the user. Then, out of the three three types of behavior that were introduced earlier in this chapter (collision, repulsion, avoidance) two were tested to see which one is the most appropriate for pedestrians standing in queues. Collision was eliminated for obvious reasons. As can be seen in Fig. 5.29 (a), using a repulsive force leads to undesired effects. The unbalanced repulsion forces causes oscillations among pedestrians which forces them to push forward. Using the second method based on behavioral heuristics, the desired queuing behavior is achieved. As

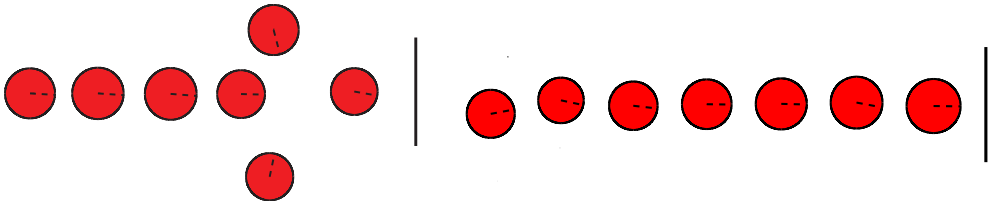

(a) (b)

Figure 5.29: Queuing behavior using (a) repulsive forces and (b) behavioral heuristics.

illustrated in Fig. 5.29, individuals stop at a safe distance from the person in front of them and wait without pushing for the line to move forward .

5.2.4 Conclusion

This chapter was dedicated to modeling pedestrian behavior, in particular avoiding and queuing behavior. In the first part, we described three approaches used to handle pedestrian-pedestrian interactions: (i) collision, (ii) avoidance using repulsive forces, and (iii) avoidance using behavioral heuristics. After comparing these approaches for different situations, it seems that none of them represents the totality of pedestrian behavior in public spaces. In normal situations with low to medium crowd densities, amongst the three methods, the one based on behavioral heuristics gives the best representation of real pedestrian trajectories, i.e. smooth trajectories without any sudden or acute deviations. In medium to high densities, collisions become inevitable. Therefore, it is necessary to be able to handle collisions to prevent interpenetration and to properly estimate the pressure felt by individuals. As for aggressive behavior, the method based on repulsive force gives the best representation of aggressive individuals who force their way through crowds. This behavior can be observed in transit stations, especially during boarding/alighting situations. In conclusion, it seems that a model should incorporate the three approaches to simulate different situations and scenarios.

In the second part of this chapter, queuing behavior was addressed. To model this behavior, two steps are necessary. First, one needs to define the queuing area and the queue type. Static and dynamic floor fields can be used to define structured and unstructured queues respectively. Then a stopping mechanism needs to be incorporated in the method based on behavioral heuristics to be able to model this behavior.

Bibliography

[1] M. Moussaïd, *Etude expérimentale et modélisation des déplacements collectifs de piétons*. PhD thesis, Université de Toulouse, Université Toulouse III-Paul Sabatier, 2010.

[2] "Follow my leader," *The Economist*, Feb. 2011.

[3] T. D. Seeley, "When is self-organization used in biological systems?," *The Biological Bulletin*, vol. 202, pp. 314–318, June 2002.

[4] I. D. Couzin, J. Krause, N. R. Franks, and S. A. Levin, "Effective leadership and decision-making in animal groups on the move," *Nature*, vol. 433, pp. 513–516, Feb. 2005.

[5] M. H. Pillot, J. Gautrais, J. Gouello, P. Michelena, A. Sibbald, and R. Bon, "Moving together: Incidental leaders and naïve followers," *Behavioural Processes*, vol. 83, pp. 235–241, Mar. 2010.

[6] J. V. Neumann, *Theory of Self-Reproducing Automata*. Champaign, IL, USA: University of Illinois Press, 1966.

[7] N. Wiener, *Cybernetics Or Control and Communication in the Animal and the Machine*. MIT Press, Jan. 1961.

[8] A. M. Turing, "The chemical basis of morphogenesis," *Philosophical Transactions of the Royal Society of London B: Biological Sciences*, vol. 237, no. 641, pp. 37–72, 1952.

[9] P. Glansdorff and I. Prigogine, *Structure, stabilité, et fluctuations*. Masson, 1971.

[10] J. L. Deneubourg, "Application de l'ordre par fluctuations à la description de certaines étapes de la construction du nid chez les Termites," *Insectes Sociaux*, vol. 24, pp. 117–130, June 1977.

[11] I. Aoki, "A Simulation Study on the Schooling Mechanism in Fish," *Nippon Suisan Gakkaishi*, vol. 48, no. 8, pp. 1081–1088, 1982.

[12] C. W. Reynolds, "Flocks, herds and schools: A distributed behavioral model," *ACM SIGGRAPH Computer Graphics*, vol. 21, no. 4, pp. 25–34, 1987.

[13] W. F. Buckley, *Sociology and modern systems theory*. Prentice-Hall, 1967.

[14] T. C. Schelling, "Models of Segregation," *The American Economic Review*, vol. 59, pp. 488–493, May 1969.

[15] D. Helbing, *Quantitative Sociodynamics*. Dordrecht: Springer Netherlands, 1995.

[16] S. Camazine, N. R. Franks, J. Sneyd, E. Bonabeau, J.-L. Deneubourg, and G. Theraula, *Self-Organization in Biological Systems*. Princeton, NJ, USA: Princeton University Press, 2001.

[17] F. Heylighen and others, "The science of self-organization and adaptivity," *The encyclopedia of life support systems*, vol. 5, no. 3, pp. 253–280, 2001.

[18] M. Ballerini, N. Cabibbo, R. Candelier, A. Cavagna, E. Cisbani, I. Giardina, V. Lecomte, A. Orlandi, G. Parisi, A. Procaccini, M. Viale, and V. Zdravkovic, "Interaction ruling animal collective behavior depends on topological rather than metric distance: Evidence from a field study," *Proceedings of the National Academy of Sciences*, vol. 105, pp. 1232–1237, Jan. 2008.

[19] C. K. Hemelrijk and H. Hildenbrandt, "Schools of fish and flocks of birds: their shape and internal structure by self-organization," *Interface Focus*, vol. 2, pp. 726–737, Dec. 2012.

[20] I. Giardina, "Collective behavior in animal groups: theoretical models and empirical studies," *HFSP Journal*, vol. 2, pp. 205–219, Aug. 2008.

[21] J. Buhl, D. J. T. Sumpter, I. D. Couzin, J. J. Hale, E. Despland, E. R. Miller, and S. J. Simpson, "From Disorder to Order in Marching Locusts," *Science*, vol. 312, pp. 1402–1406, Feb. 2006.

[22] A. Huth and C. Wissel, "The simulation of the movement of fish schools," *Journal of Theoretical Biology*, vol. 156, pp. 365–385, June 1992.

[23] I. D. Couzin and N. R. Franks, "Self-organized lane formation and optimized traffic flow in army ants," *Proceedings of the Royal Society of London B: Biological Sciences*, vol. 270, no. 1511, pp. 139–146, 2003.

[24] J. Ma, W.-g. Song, J. Zhang, S.-m. Lo, and G.-x. Liao, "-Nearest-Neighbor interaction induced self-organized pedestrian counter flow," *Physica A: Statistical Mechanics and its Applications*, vol. 389, pp. 2101–2117, May 2010.

[25] B. Steffen, "A Modification of the Social Force Model by Foresight," in *Pedestrian and Evacuation Dynamics 2008* (W. W. F. Klingsch, C. Rogsch, A. Schadschneider, and M. Schreckenberg, eds.), pp. 677–682, Berlin, Heidelberg: Springer Berlin Heidelberg, 2010.

[26] U. Weidmann, "Transporttechnik der Fuänger," report Schriftenreihe Ivt- Berichte 90, ETH Zürich, 1993.

[27] R. W. Bohannon, "Comfortable and maximum walking speed of adults aged 20-79 years: reference values and determinants," *Age and Ageing*, vol. 26, pp. 15–19, Jan. 1997.

[28] S. Young, "Evaluation of Pedestrian Walking Speeds in Airport Terminals," *Transportation Research Record: Journal of the Transportation Research Board*, vol. 1674, pp. 20–26, Jan. 1999.

[29] D. Helbing, I. Farkas, and T. Vicsek, "Simulating dynamical features of escape panic," *Nature*, vol. 407, pp. 487–490, 2000.

[30] W. Daamen and S. Hoogendoorn, "Controlled experiments to derive walking behaviour," *European journal of transport and infrastructure research EJTIR, 3 (1)*, 2003.

[31] S. Buchmueller, U. Weidmann, Eidgenössische Technische Hochschule Zürich, and Lehrstuhl für Verkehrssysteme, *Parameters of pedestrians, pedestrian traffic and walking facilities*. Zurich: Institute for Transport Planning and Systems (IVT), Chair of Transport Systems, ETH Zurich, 2006.

[32] W. Daamen and S. P. Hoogendoorn, "Free speed distributions based on empirical data in different traffic conditions," in *Pedestrian and Evacuation Dynamics 2005* (N. Waldau, P. Gattermann, H. Knoflacher, and M. Schreckenberg, eds.), pp. 13–25, Springer Berlin Heidelberg, 2007.

[33] R. Wiseman, "Pace of Life." http://www.richardwiseman.com/quirkology/pace_home.htm, 2007.

[34] A. Schadschneider, D. Chowdhury, and K. Nishinari, *Stochastic transport in complex systems: from molecules to vehicles*. Amsterdam: Elsevier, 2011.

[35] J. Pettré, J. Ondrej, A.-H. Olivier, A. Cretual, and S. Donikian, "Experiment-based Modeling, Simulation and Validation of Interactions Between Virtual Walkers," in *Proceedings of the 2009 ACM SIGGRAPH/Eurographics Symposium on Computer Animation*, SCA '09, (New York, NY, USA), pp. 189–198, ACM, 2009.

[36] D. Helbing, "A mathematical model for the behavior of pedestrians," *Behavioral Science*, vol. 36, no. 4, pp. 298–310, 1991.

[37] H. Singh, R. Arter, L. Dodd, P. Langston, E. Lester, and J. Drury, "Modelling subgroup behaviour in crowd dynamics DEM simulation," *Applied Mathematical Modelling*, vol. 33, pp. 4408–4423, Dec. 2009.

[38] P. Pécol, P. Argoul, S. Dal Pont, and S. Erlicher, "A new crowd movement modeling for pedestrians who hold hands," *Vibrations, Shocks and Noise*, 2012.

[39] "Desire paths lead to ergonomic crosswalks.." http://designapplause.com/2011/desire-paths-lead-to-ergonomic-crosswalks/19989/, 2011.

[40] D. Helbing, I. J. Farkas, and T. Vicsek, "Freezing by Heating in a Driven Mesoscopic System," *Physical Review Letters*, vol. 84, pp. 1240–1243, Feb. 2000.

[41] J. Zhang and A. Seyfried, "Comparison of bidirectional pedestrian flows by experiments," *Physica A: Statistical Mechanics and its Applications*, vol. 405, pp. 316–325, July 2014. arXiv: 1312.2475.

[42] S. Milgram, L. Bickman, and L. Berkowitz, "Note on the drawing power of crowds of different size.," *Journal of personality and social psychology*, vol. 13, no. 2, p. 79, 1969.

[43] D. Helbing, "A Mathematical Model for Behavioral Changes by Pair Interactions," in *Economic Evolution and Demographic Change* (G. Haag, U. Mueller, and K. G. Troitzsch, eds.), no. 395 in Lecture Notes in Economics and Mathematical Systems, pp. 330–348, Springer Berlin Heidelberg, 1992.

[44] D. Helbing, "Traffic and related self-driven many-particle systems," *Reviews of modern physics*, vol. 73, no. 4, p. 1067, 2001.

[45] A. Schadschneider, W. Klingsch, H. Klupfel, T. Kretz, C. Rogsch, and A. Seyfried, "Evacuation Dynamics: Emprical Reuslts, Modeling and Applications," 2009.

[46] D. Helbing, L. Buzna, A. Johansson, and T. Werner, "Self-Organized Pedestrian Crowd Dynamics: Experiments, Simulations, and Design Solutions," *Transportation Science*, vol. 39, pp. 1–24, Feb. 2005.

[47] P. Phelvin and D. Millward, "Airport queues longer than flights." http://www.telegraph.co.uk/news/uknews/1559410/Airport-queues-longer-than-flights.html, Aug. 2007.

[48] P. Gaspard, "Twenty Years of Democracy in South Africa." https://blogs.state.gov/stories/2014/04/26/twenty-years-democracy-south-africa, 2014.

[49] S. Okazaki and S. Matsushita, "A study of simulation model for pedestrian movement with evacuation and queuing," in *International Conference on Engineering for Crowd Safety*, pp. 271–280, 1993.

[50] J. J. Fruin, *Pedestrian planning and design*. Metropolitan Association of Urban Designers and Environmental Planners, 1971.

[51] V. M. Predtechenskii and A. I. Milinskii, *Planning for Foot Traffic Flow in Buildings*. Amerind, 1978.

[52] W. Daamen, P. H. L. Bovy, and S. P. Hoogendoorn, "Modelling pedestrians in transfer stations," *Pedestrian and evacuation dynamics*, pp. 59–73, 2002.

[53] A. Seyfried, B. Steffen, and T. Lippert, "Basics of Modelling the Pedestrian Flow," *Physica A: Statistical Mechanics and its Applications*, vol. 368, pp. 232–238, Aug. 2006. arXiv: physics/0506189.

[54] R. L. Carstens and S. L. Ring, "Pedestrian Capacities of Shelter Entrances," *Traffic Engineering, Inst Traffic Engr*, Dec. 1970.

[55] B. D. Hankin and R. A. Wright, "Passenger Flow in Subways," *OR*, vol. 9, pp. 81–88, June 1958.

[56] W. H. K. Lam, J. F. Morrall, and H. Ho, "Pedestrian Flow Characteristics in Hong Kong," *Transportation Research Record*, no. 1487, 1995.

[57] P. Navin and R. Wheeler, "Pedestrian flow characteristics," *Traffic Engineering*, vol. 39, no. 4, pp. 30–33, 1969.

[58] S. Older, "Movement of pedestrians on footways in shopping streets," *Traffic Engineering and Control*, vol. 10, pp. 160–163, 1968.

[59] D. Helbing, A. Johansson, and H. Z. Al-Abideen, "Dynamics of crowd disasters: An empirical study," *Physical Review E*, vol. 75, p. 046109, Apr. 2007.

[60] A. Johansson, "Constant-net-time headway as a key mechanism behind pedestrian flow dynamics," *Physical Review E*, vol. 80, Aug. 2009.

[61] U. Chattaraj, A. Seyfried, and P. Chakroborty, "Comparison of pedestrian fundamental diagram across cultures," *Advances in Complex Systems*, vol. 12, pp. 393–405, June 2009.

[62] D. Helbing, P. Molnàr, I. J. Farkas, and K. Bolay, "Self-organizing pedestrian movement," *Environment and Planning B: Planning and Design*, vol. 28, no. 3, pp. 361–383, 2001.

[63] D. Helbing and B. A. Huberman, "Coherent moving states in highway traffic," *Nature*, vol. 396, pp. 738–740, 1998.

[64] T. Nagatani, "The physics of traffic jams," *Reports on Progress in Physics*, vol. 65, p. 1331, Sept. 2002.

[65] J. J. Fruin, "The causes and prevention of crowd disasters," (England), 1993.

[66] R. L. Best and N. F. P. Association, *Reconstruction of a tragedy: the Beverly Hills Supper Club fire, Southgate, Kentucky, May 28, 1977*. National Fire Protection Association, Jan. 1978.

[67] N. R. Johnson, "Panic at "The Who Concert Stampede": An Empirical Assessment," *Social Problems*, vol. 34, pp. 362–373, Oct. 1987.

[68] M. Isobe, D. Helbing, and T. Nagatani, "Experiment, theory, and simulation of the evacuation of a room without visibility," *Physical Review E*, vol. 69, p. 066132, June 2004.

[69] Z. Fang, W. Song, J. Zhang, and H. Wu, "Experiment and modeling of exit-selecting behaviors during a building evacuation," *Physica A: Statistical Mechanics and its Applications*, vol. 389, pp. 815–824, Feb. 2010.

[70] D. Helbing and P. Molnàr, "Social force model for pedestrian dynamics," *Physical Review E*, vol. 51, pp. 4282–4286, May 1995.

[71] M. Chraibi, A. Seyfried, and A. Schadschneider, "Generalized centrifugal-force model for pedestrian dynamics," *Physical Review E*, vol. 82, no. 4, p. 046111, 2010.

[72] T. I. Lakoba, D. J. Kaup, and N. M. Finkelstein, "Modifications of the Helbing-Molnàr-Farkas-Vicsek Social Force Model for Pedestrian Evolution," *SIMULATION*, vol. 81, pp. 339–352, Jan. 2005.

[73] A. Johansson, D. Helbing, and P. K. Shukla, "Specification of the social force pedestrian model by evolutionary adjustment to video tracking data," *Advances in complex systems*, vol. 10, no. supp02, pp. 271–288, 2007.

[74] C. W. Reynolds, "Steering behaviors for autonomous characters," in *Game developers conference*, vol. 1999, pp. 763–782, 1999.

[75] S. Paris, J. Pettré, and S. Donikian, "Pedestrian Reactive Navigation for Crowd Simulation: a Predictive Approach," *Computer Graphics Forum*, vol. 26, pp. 665–674, Sept. 2007.

[76] I. Karamouzas, P. Heil, P. v. Beek, and M. H. Overmars, "A Predictive Collision Avoidance Model for Pedestrian Simulation," in *2015-07-05 14:41:33* (A. Egges, R. Geraerts, and M. Overmars, eds.), no. 5884 in Lecture Notes in Computer Science, pp. 41–52, Springer Berlin Heidelberg, 2009.

[77] M. Moussaïd, D. Helbing, and G. Theraulaz, "How simple rules determine pedestrian behavior and crowd disasters," *Proceedings of the National Academy of Sciences*, vol. 108, pp. 6884–6888, Apr. 2011.

[78] O. Khatib, K. Yokoi, O. Brock, K. Chang, and A. Casal, "Robots in Human Environments: Basic Autonomous Capabilities," *The International Journal of Robotics Research*, vol. 18, pp. 684–696, Jan. 1999.

[79] S. Masoud, A. Masoud, and others, "Constrained motion control using vector potential fields," *Systems, Man and Cybernetics, Part A: Systems and Humans, IEEE Transactions on*, vol. 30, no. 3, pp. 251–272, 2000.

[80] S. Loizou and K. Kyriakopoulos, "Navigation of Multiple Kinematically Constrained Robots," *IEEE Transactions on Robotics*, vol. 24, pp. 221–231, Feb. 2008.

[81] F. Fahimi, C. Nataraj, and H. Ashrafiuon, "Real-time Obstacle Avoidance for Multiple Mobile Robots," *Robotica*, vol. 27, pp. 189–198, Mar. 2009.

[82] D. Yanagisawa, A. Tomoeda, R. Jiang, and K. Nishinari, "Excluded volume effect in queueing theory," *JSIAM Letters*, vol. 2, no. 0, pp. 61–64, 2010.

[83] G. G. Lovas, "Modeling and simulation of pedestrian traffic flow," *Transportation Research Part B: Methodological*, vol. 28, pp. 429–443, Dec. 1994.

[84] D. Yanagisawa, A. Tomoeda, A. Kimura, K. Nishinari, K. Ohtsuka, and Y. Suma, *Theoretical and Experimental Study for Queueing System with Walking Distance*. INTECH Open Access Publisher, 2010.

[85] B. Hopkins, A. Churchill, S. Vogt, and L. Rönnqvist, "Braking Reaching Movements: A Test of the Constant Tau-Dot Strategy Under Different Viewing Conditions," *Journal of Motor Behavior*, vol. 36, pp. 3–12, May 2004.

[86] D. R. Parisi, M. Gilman, and H. Moldovan, "A modification of the Social Force Model can reproduce experimental data of pedestrian flows in normal conditions," *Physica A: Statistical Mechanics and its Applications*, vol. 388, pp. 3600–3608, Sept. 2009.

[87] P. M. Todd, "Simple inference heuristics versus complex decision machines," *Minds and Machines*, vol. 9, no. 4, pp. 461–477, 1999.

[88] G. Gigerenzer and P. M. Todd, *Simple Heuristics that Make Us Smart*. Oxford University Press, Jan. 1999.

[89] P. R. Schrater, D. C. Knill, and E. P. Simoncelli, "Mechanisms of visual motion detection," *Nature neuroscience*, vol. 3, no. 1, pp. 64–68, 2000.

[90] M. Batty, "Predicting where we walk," *Nature*, vol. 388, pp. 19–20, July 1997.

[91] A. Turner and A. Penn, "Encoding natural movement as an agent-based system: an investigation into human pedestrian behaviour in the built environment," *Environment and Planning B: Planning and Design*, vol. 29, no. 4, pp. 473 – 490, 2002.

[92] A. Seyfried, B. Steffen, W. Klingsch, and M. Boltes, "The fundamental diagram of pedestrian movement revisited," *Journal of Statistical Mechanics: Theory and Experiment*, vol. 2005, no. 10, p. P10002, 2005.

Chapter 6

Validation and Verification of crowd models

Contents

6.1 Bibliographical study on the Validation and Verification of crowd models

In occasions where crowd densities reach very high levels (increasing population and economy, rush hours, more sports events), the movement of pedestrians become difficult and possibly dangerous Fig. 6.1. In these situations, if an incident/accident takes place, people will not be able to escape quickly and the probability of casualties increases (love parade, Mekka,Cambodia water festival). Several questions arise: How to optimally design escape routes that can be used in emergency or critical situations? In case of an incident, how to guide people away from the source of danger as quickly as possible in order to decrease the number of casualties?

(a) (b)

Figure 6.1: Love Parade in Duisburg Germany [18] and a metro station in Paris during a strike of metro drivers [15]

To answer these questions and provide solutions, a deep understanding of crowd dynamics is inevitable. The reoccurring crowd disasters have attracted a lot of attention to research on pedestrian and traffic flow [2, 4, 62]. Several developed models were able to qualitatively reproduce some observed phenomena. However, to be used in practice, the development cycle of the simulation tool must contain all the elements illustrated in Fig. 6.2. This is when a process of verification and validation (V&V) becomes crucial. In [24], verification is defined as "the process of determining that a calculation method implementation accurately represents the developer's conceptual description of the calculation method and the solution to the calculation method". To put it simply, verification is about testing if the simulation results are as expected (have the models been correctly implemented). It can be accomplished by using a set of hypothetical test cases [24].

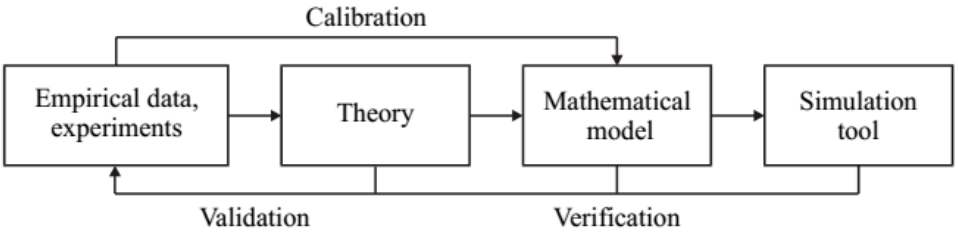

Figure 6.2: Development cycle of a simulation model.

Validation is defined as "process of determining the degree to which a calculation method is an accurate representation of the real world from the perspective of the intended uses of the calculation method" [24]. In other words, validation is about comparing the simulation results to observations in reality. One

has to distinguish between "qualitative" vs. "quantitative" and "macroscopic" vs. "microscopic" validation procedures. To be qualitatively validated, a pedestrian model is supposed to reproduce collective phenomena such as lane formation or the formation of jams. In quantitative validation, the relations between quantities such as velocity, density and flow must be correctly reproduced. Macroscopic means that the measured quantities were obtained by averaging over time or space. On the other hand, microscopic means that individual properties are verified such as individual velocities or single trajectories.

In the following, we present a brief literature review on the methods that are the most used to verify and validate pedestrian models.

6.1.1 Processes of Verification and Validation for building evacuation models

The process of V&V for pedestrian models for public spaces faces several difficulties. First of all, there is not a common standard procedure to perform V&V specifically designed for building evacuation models. A document provided by the International Standard Organization only provides general information on the assessment and V&V of calculation methods in the context of fire safety engineering. Another document was developed by the International Maritime Organization and contains guidelines for maritime evacuation tools, namely the MSC/circ.1238 [23]. Yet, the same guidelines are currently used to perform V&V for building evacuation models. Even though several efforts have been made to improve the MSC/Circ.1238 and extend its use to different application contexts (e.g., buildings, other means of transportation, etc.), several aspects of the V&V process for building evacuation models are still missing. As a result, model developers use inconsistent procedures in order to perform the V&V process. Second of all, the models must be calibrated with experimental data. It is surprising to know that the much of the data currently used in egress calculations and performance-based predictions were collected 40 years ago [9, 10]. Although some empirical data have been collected in the past few years, they are still insufficient to properly calibrate the existing models to guide the design of facilities. Not only are the available empirical data insufficient, they also show surprisingly large differences [54, 57]. One of the major differences is the fundamental diagram that represents the flow-density relationship and is associated with several qualitative self organization phenomena like lane formation and jams. The main divergences are in the maximum flow values and the corresponding densities in addition to the value of the density where the flow becomes null due to overcrowding [54]. It is not clear if the factors leading to these differences result from the specific properties of pedestrian flow or other external factors. Third of all, it has been recently found in [56], that the measurement methodologies applied on data sets have a significant effect on the fundamental diagram. Therefore, better data capture methods and data analysis methods are required [63].

According to the MSC/circ.1238, evacuation models should pass 4 main forms of tests : (1) component testing, (2) functional verification, (3) qualitative verification, and (4) quantitative verification. Component testing is done by verifying if each component of a model works as intended. In the process of functional verification, the analysis of the capabilities of the model, as in its ability to perform the required simulations, is performed. Qualitative and quantitative verification involves comparing the nature of predicted human behavior with informed expectations. In the guidelines, information on methods to assess the different forms of tests exist except for the 4th one (quantitative verification).

Currently, the MSC/Circ1.238 provides seven tests (IMO Tests 1-7) on component testing and four tests on qualitative verification (IMO Tests 8-11) along with recommendations on the methods that can be applied for functional verification. No tests are available for quantitative verification since, according to the MSC/Circ.1238 there is "insufficient reliable experimental data to allow a thorough quantitative verification of egress models". The set of experimental data that was recommended by the SAGEGUARD project [11, 12] to allow quantitative verification refers only to maritime applications and thus cannot be applied to the building context. These tests were developed for maritime evacuation tools. To be used in different application contexts (e.g., buildings, other means of transportation, etc.), they need to be expanded and modified. Even though several efforts have been made, several aspects of the V&V process for building evacuation models are still missing. First, the RIMEA project [34] failed to include validation tests in their proposed modifications. In addition, no new tests were added for the many of the features generally available in building evacuation models. Second, project SAFEGUARD [11, 12] suggested improvements to the MSC/Circ.1238 that focus on maritime applications and may not be

suitable for other models or scenarios. As a result, model developers use inconsistent procedures in order to perform the V&V process.

Suggested Verification and Validation Tests

In the NIST Technical Note 1822 [52] published in 2013, the list of tests presented in the MSC/Circ.1238 [23] were expanded and modified so that they can be used in the context of building evacuation. The IMO tests were used as a starting point to develop new guidelines applicable in the building context. In the following sections, some of the verification tests that are either based on the ones presented in [23] or developed by the authors in [52] in addition to the possible validation tests proposed in [52] are presented.

Verification Tests In [52], additional tests to the ones found in the MSC/Circ1.238 [23] were made in order to include the features that found in the review of building evacuation models by [32] which are: (1) Counterflow (2) exit block (3) fire conditions affecting behavior (4) toxicity (5) groups (6) disabled/slow occupants (7) delays preevacuation times (8) elevator use (9) route choice..

Each test is structured in five parts [52]: (i) Geometry: the test's configuration, (ii) Scenario(s): the simulated evacuation scenario, (iii) Expected result: the quantitative or qualitative result that the model should produce, (iv) Test method: the qualitative (e.g., visualization of the pedestrian behavior) or quantitative (e.g., comparing evacuation times, flows, etc.) method used to compare between the expected and the simulated results, and (vi) User's actions: the actions that the tester is required to accomplish while performing and presenting the tests. Different models might require different test methods depending on the input variables required for their calibration.

The suggested verification tests in [52] are organized to study the five core components of an evacuation model necessary for the most basic representation of a scenario [14]: (1) pre-evacuation time, (2) movement and navigation, (3) exit usage, (4) route availability, and (5) flow conditions/constraints. They are designed to analyze the current evacuation models' main features and divided into two categories. In the first category, called analytical verification (AN_VERIF), component testing is done. The expected results can be obtained using simple mathematical formulae or evidence. In the second category which is called the verification of emergent behaviors (EB_VERIF), the evacuation models' ability to qualitatively produce results reflecting the current knowledge on human behavior on fire is verified.

Validation tests A set of tests suggested in [52] for the validation of evacuation models are presented in this section. Before introducing these tests, it is necessary to go over certain facts that influence the validation procedure and the process of designing validation tests. These facts are [52]:

- The scarcity of experimental data sets on human behavior in fire limits the number of validation tests that can be performed.
- The definition of benchmark validation tests depends on the used techniques to collect evacuation experimental data (and the subsequent uncertainties), the presence and the availability to the public of documented experimental data sets.
- Current evacuation models are mostly deterministic or user dependent. The lack of human behavior data limits their behavioral predictions capabilities.
- Increasing the understanding of the limitations of evacuation models is the criterion used for choosing the validation tests.

Ideally, the list of validation tests should also include experimental data sets covering a full range of possible behaviors and scenarios representing the evacuation process. However, experimental data sets are very rare rendering the validation of all aspects of evacuation modeling tools very difficult.

While evacuation models may be developed using specific experimental data, they cannot be validated using the latter. As for models developed using hypothetical assumptions, the lack of understanding of actual occupant behavior makes it impossible to provide validation tests.

Due to the factors mentioned so far, a complete set of experimental data that can be used to validate the core behavioral components of evacuation models is not available. Nevertheless, we introduce in this section a set of examples of experimental/actual data sets that is suggested in [52] and that can be used to validate specific aspects of evacuation. This set must keep expanding and getting updated to encompass new data sets and new theories on human behavior. The NIST Technical Note 1822 suggests the data sets in Table 6.1 to be used for the analysis of the core behavioral components of evacuation models. Selecting data sets is based on three criteria: (1) availability to the public, (2) the documentation associated with them and (3) the methods used for data collection/analysis.

Core component	Sub-element	Suggested variable for the comparison	Experimental data
1	Pre-evacuaton time distribution	Evacuation times, exit choice	[3]
2	Stairwell evacuation	Evacuation times	[31]
3,4	Impact of way-finding installations	Exit choice	[42]
5	Small scale experiment	Evacuation times, movement speeds, flows	[8]
5	Small scale experiment	Evacuation times, movement speeds, flows	[20]
5	Small scale experiment	Evacuation times, movement speeds, flows	[55]
1,2,3,4,5	Full building evacuation	Evacuation times	[13]

Table 6.1: Examples of possible experimental data for the validation of the main core components of building evacuation models.

6.1.2 Quantitative validation using measured quantities

The complexity of estimating the parameters of microscopic pedestrian models arise from the relative large number of parameters and the lack of suitable data and calibration techniques. In general, pedestrian models are calibrated by comparing aggregate model outcomes (flows, speeds, densities, etc.), predicted macroscopic relations (e.g. speed density curves), or emerging spatio-temporal patters (dynamic lane formation) with macroscopic empirical data or expert opinion. Using those techniques, several models proved to be able to predict macroscopic flow conditions with reasonable accuracy.

Observables

The collective properties of pedestrian motion are often characterized using the density ρ and the flow J. These two quantities are related by the hydrodynamic relation:

$$J = \rho v b = J_s b \tag{6.1}$$

where v is the average velocity of the pedestrians, b the width of the environment where the crowd is, and J_s is the flow per unit width. The capacity of a certain facility is given by the maximum value of the flow. It allows to estimate the minimal time needed to empty a given facility or the minimal width of the facility to evacuate it in a given time. The flow or the specific flow are especially used to estimate how the capacity of a bottleneck increases with increasing width. While some studies found that the capacity increases as a function of width in a stepwise manner [20, 21], others found that the dependance is continuous and almost linear [57].

To obtain the three quantities (J, ρ and v), we either measure the three of them or only two and obtain the third one using Eq. (6.1). Several laboratory experiments were done to measure these quantities for different cases and different geometries [20, 29, 33, 37–39, 53]. Unfortunately, the use of different measurement methods by each study limits the comparability of the data. In [63], it was shown that using different measurement methods can lead to major differences between the results. Yet, the obtained experimental results are often used to validate pedestrian models by trying to reproduce them [5, 28, 45, 58, 60] (see Fig. 6.3).

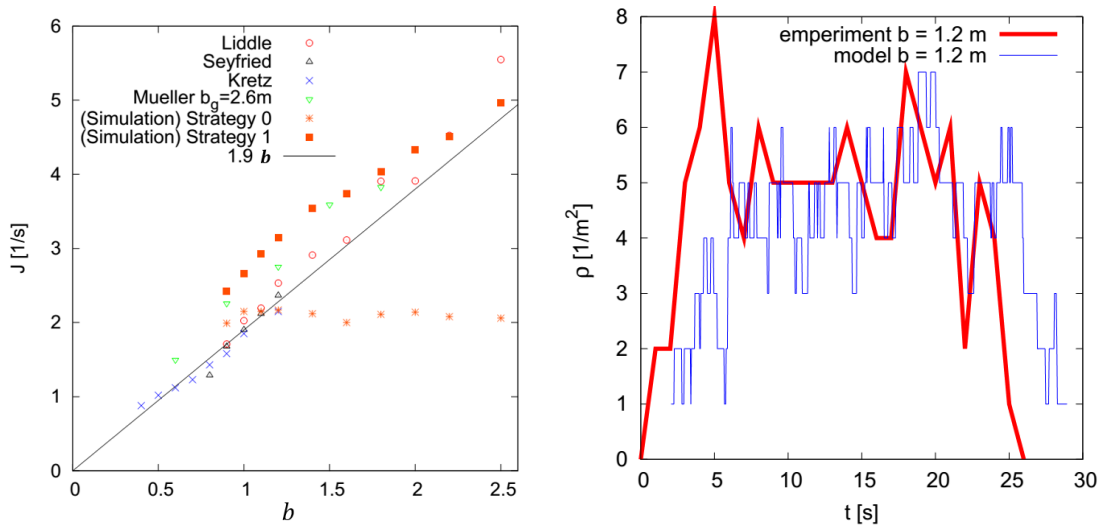

(a) (b)

Figure 6.3: Quantitative validation using flow [58] and density values [7]. Strategy 0 and Strategy 1 in (a) refer to direction choice strategies [58].

The fundamental diagram

The relation between the flow and the density, $J(\rho)$, is called the *fundamental diagram*. The hydrodynamic relation gives us two other equivalent forms: $v(\rho)$ and $v(J)$. Instead of calculating several fundamental diagrams for several values of the width of a facility b, the specific flow can be used to merge them into a single universal one.

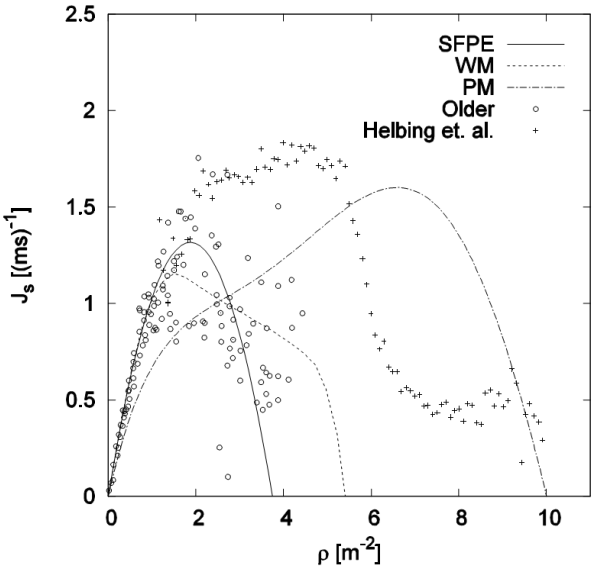

Figure 6.4: Fundamental diagrams for pedestrian movement in planar facilities. Lines refer to specifications in planning guidelines PM [50]; SFPE [41] and WM [61]. Data points are obtained from experimental measurements (Older, 1968) [44] and [17]

In most engineering methods developed for the design and dimensioning of pedestrian facilities, the fundamental diagram is used as a basic input [9, 41, 50]. For a given fundamental diagram in the representation $J(\rho)$, the capacity of a facility is defined as the maximum of this function. Fig. 6.4

shows the fundamental diagrams found in handbooks and planing guidelines for estimating the capacity of openings, doors, or bottlenecks along with two others that were obtained from empirical studies. The most elaborate one is given by Weidmann [61] who collected 25 data sets. He also gave an approximate analytical form:

$$v(\rho) = v_0\big[1 - exp\big(-\rho_0(1/\rho - 1/\rho_{max})\big)\big] \tag{6.2}$$

where $v_0 = 1.34\,m/s$ is the average walking speed, $\rho_{max} = 5.4\,P/m^2$ is the maximal observed density, and $\rho_0 = 1.913\,P/m^2$. The fundamental diagram is also used to evaluate pedestrian models [6, 19, 26, 45] and test their ability to describe pedestrian stream [27, 35]. It is associated with every qualitative self-organization phenomenon, like the formation of lanes or the occurrence of jams. It is very frequently used to calibrate pedestrian models. It is also used for quantitative validation. For a certain environment (usually corridors or bottlenecks), pedestrian models simulate a pedestrian stream and show that the resulting fundamental diagram is similar to an empirical one (see Fig. 6.5).

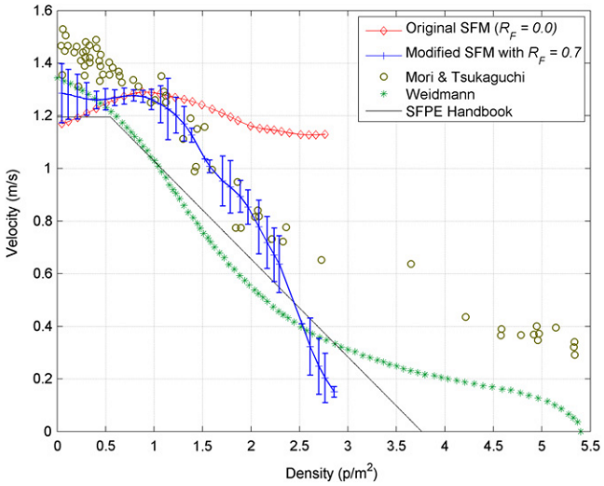

Figure 6.5: Fit of the simulations performed of the modified model [45] and comparison with the original one, experimental data given by Weidmann [61] and Mori et al.[36] and design data [41]. Error bars represent two standard deviations.

In spite of its importance, validation of models with fundamental diagrams is certainly not sufficient. The fundamental diagrams obtained by experimental studies, guidelines and handbooks shows important differences in maximal flow values (i.e. the capacity), the corresponding density, and the density where the flow vanishes due to overcrowding. In addition, in most cases, the error margins or even fluctuations are not shown. Several explanations for these discrepancies have been suggested:

- cultural and population differences [17],
- differences between uni- and multidirectional flow [40, 51],
- short-ranged fluctuations [51] also known as platooning,
- influence of psychological factors given by the incentive of the movement [50] or the type of traffic [43],
- measurement methods.

6.1.3 Discussion on validation and verification methods

Calibrating pedestrian models by comparing aggregate model outcomes (flows, speeds, densities, etc.), predicted macroscopic relations (e.g. speed density curves), or emerging spatio-temporal patters (dynamic lane formation) with empirical data or expert opinion is an important step in the calibration process.

However, they are not enough to achieve the desired results for a number of reasons. First of all, it is not possible to use macroscopic to data to obtain the inter-pedestrian differences expressed by the variability of model parameters. Moreover, it cannot be affirmed whether microscopic models properly describe individual walking behavior or just provide an acceptable 'average' macroscopic prediction. Therefore, the validity of the behavioral assumptions used by a microscopic model cannot be assessed. This means that the model is not reliable and may not be able to predict pedestrian behavior in other situations than the one used for calibration.

A generic calibration methodology for microscopic pedestrian models using pedestrian trajectory data was introduced in [22]. Using this method, a statistical analysis of the parameter estimates and their cross-correlations can be performed. In addition, it is possible to include prior information on the parameters of the model, their distribution, and their cross correlations. Moreover, a comparison between different versions of the same model (increasing its complexity) can be performed in order to find out which modifications are significant from a statistical point of view. The results obtained by this approach provide new insights into pedestrian behavior, inter-pedestrian differences, as well as the resulting pedestrian flow characteristics.

Without denying the importance of the previously mentioned methods in the calibration process, it is crucial to have an International Standards on the tests and methods to assess the V&V of building evacuation models. Such a guideline would obligate model developers to use consistent procedures to validate, verify and calibrate their models. Consequently, model users would be able to take better choices when selecting a model to be used for certain applications. This is why the NIST Technical Note 1822 [52] is very important. Though it offers a standard procedure for the verification and validation of building evacuation models, it doesn't provide a definitive guidance on the performance of V&V for building evacuation models. Instead, it aims at opening a debate on the issues associated with V&V for building evacuation models.

6.2 Validation and Verification of the 2D model

In the absence of codes or standards or any consensus in the community of crowd modeling on the methodologies to be adopted, every research group uses their own data sets and own methods to validate and verify their model. In most cases, a set of parameters are calibrated in order to reproduce results that are similar to the ones obtained by a particular experiment. Usually, only the results are published and one cannot reproduce the same simulations and repeat the validation process. For this reason, we have decided to tackle this problem using two approaches. In section 6.2.1, we adopt the mainstream approach and validate our model by finding the parameter values that allow us to reproduce experimental results. In section 6.2.2, we use an experimental design to find out the influence of the main parameters of our model and their interactions on the output.

6.2.1 Quantitative validation using experimental data: case of a bottleneck

In this section, we are interested in testing the performance of our model for the case of the flow of pedestrians through a bottleneck. Several experiments have been conducted in order to measure the influence of the bottleneck width on the pedestrian flow [29, 57, 59]. We will simulate the experimental set-up presented in [57]. Its configuration is shown in Fig. 6.6(a).

In [57], for every value of the bottleneck width $b \in [0.8\,m, 1.2\,m]$ with increments of $0.1m$, three runs are performed with $N = 20, 40$ and 60 pedestrians respectively. The pedestrians are placed in the holding area in a way that the density of each of the three sections is $\rho = 3.3\,individuals/m^2$ (Fig. 6.6(a)). It is important to note that the participants in this experiment were advised not to push and to walk with a normal velocity. To compare different tests, the authors introduced the specific flow J_s that was calculated for every run. The specific flow J_s is defined as the ratio of the flow J to the bottleneck width b:

$$J_s = \frac{J}{b} = \frac{N_b}{\Delta t \cdot b} \tag{6.3}$$

where J is defined here as a time-averaged flow equal to the ratio of the number of pedestrians N_b passing a certain facility to the duration Δt measured starting from the instant where the first individual

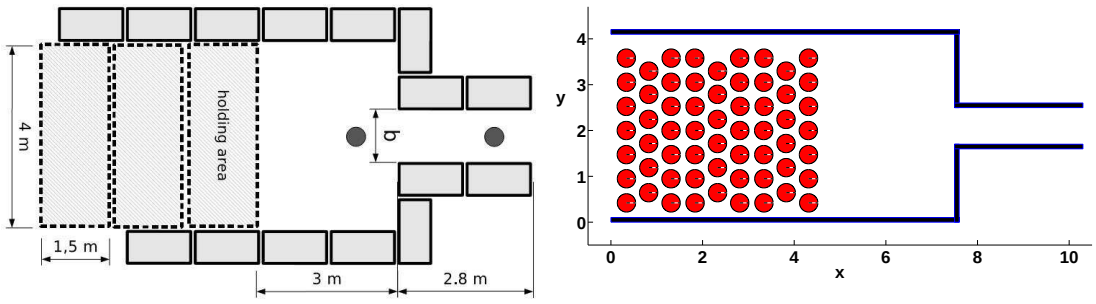

(a) (b)

Figure 6.6: Experimental setup (a) and the configuration of 60 pedestrians reproduced by our model (b)

exits and ending when the last one does.

Table 6.2: Experimental specific flow $J_{s,exp}$ $(individuals.m^{-1}.s^{-1})$ [57]. The time interval Δt is the time measured between the passage of the first person and the last one.

$b(m)$	$N_b = 20$	$N_b = 40$	$N_b = 60$
0.8	**1.86**	**1.77**	**1.61**
0.9	**2.06**	**1.91**	**1.86**
1.0	**2.19**	**2.08**	**1.9**
1.1	**1.78**	**1.93**	**1.93**
1.2	**2.31**	**1.81**	**1.97**

In [57], the specific flow J_s was calculated for three different group sizes N_b and five different values of the width b of the bottleneck as seen in Table 6.2. It allows to examine the influence of the dimensions of this type of exits on the evacuation procedure. In previous versions of our model, by fixing certain parameters ($K_n = 10^5\, kg$, $K_{tg} = 0\, kg$), several qualitative aspects of pedestrian dynamics was reproduced such as, lane formation, the arch phenomenon, oscillations at bottleneck exits, etc. In the following section, we will examine the quantitative results obtained using the same aforementioned parameter values.

A quantitative study

In this section, we study the quantitative results obtained by our model using the values of K_n and K_{tg} used in previous studies [46–49]. We first study the effect of introducing rotation to the pedestrian's movement. We then introduce the repulsive forces [16].

Adding rotation to the pedestrians' movement For $K_n = 10^5\, kg$ and $K_{tg} = 0\, kg$, we calculate J_s for two cases: with and without rotation. We aim to verify, when friction between pedestrians is not considered, if their rotations have any effect on the flow. For each case, fifty simulations were run, with different random initial pedestrian positions, and J_s is calculated for each one. The average value and the standard deviation of the specific flow are then calculated. The same procedure was repeated for the values of the parameters (b, N_b) found in Table 6.2. The results are illustrated in Fig. 6.7 along with the experimental ones [57]. They show that the agents' rotation introduced into our model does not affect the flow values. The reason behind this expected result is that we have not connected the agent's rotational motion to its translational one (pedestrians move even if they are not looking in the range of the direction of motion). As mentioned earlier, the interest of integrating the rotational motion was to

be able to reproduce subgroup behavior. Further investigation of the relation between the rotational and translational motion of a pedestrian will be done in order to study the effect of the rotational motion on the flow values.

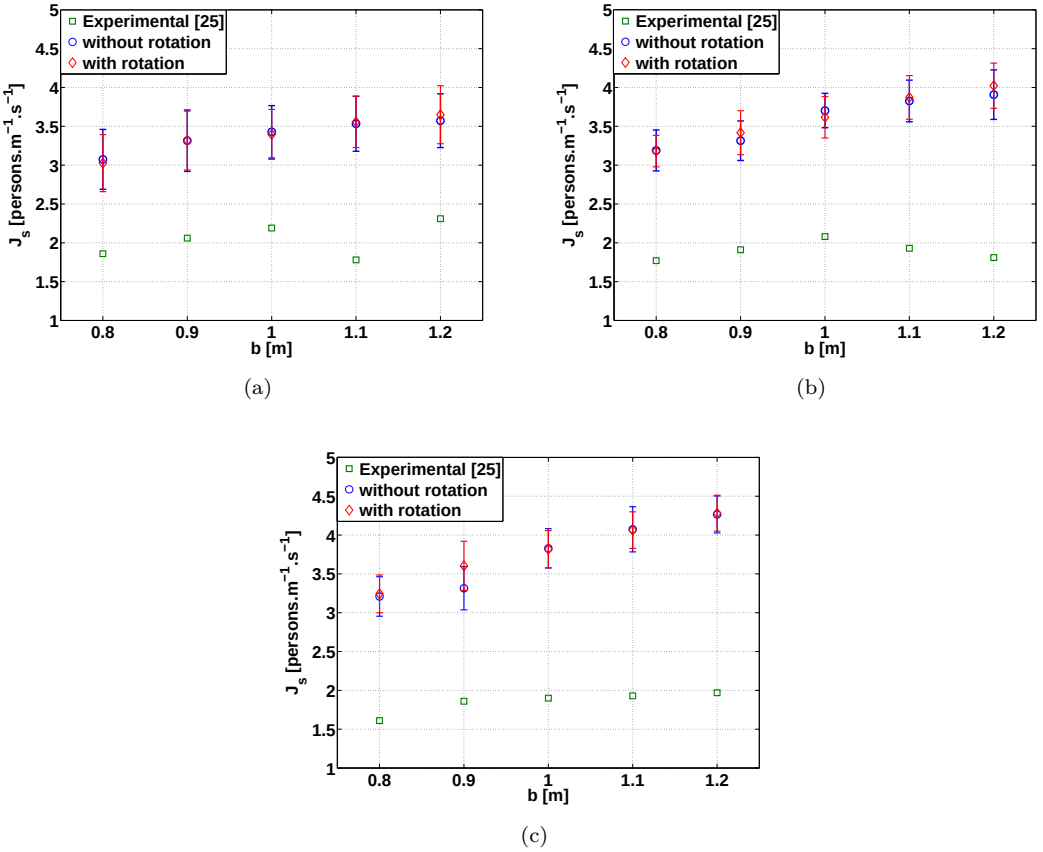

Figure 6.7: Values of J_s obtained with or without introducing the rotation for N= (a) 20, (b) 40 and (c) 60. The social force is not considered

Introducing the repulsive forces: a sensitivity analysis Since the experiment in [57] is held in normal conditions, introducing repulsive forces in our model is necessary to be able to approach the experimental data. However, the values of the parameters $A_i(kg.m.s^{-2})$ and $B_i(m)$ (Eq. (6.4)) for each pedestrian i have to be adapted to the scenario under study (flow through a bottleneck, multi-directional flows, stairs...). For this reason, we have decided to perform a sensitivity analysis to find the values of $A_i(kg.m.s^{-2})$ and $B_i(m)$ of the pedestrian-pedestrian repulsive force that will best reproduce the flow through a bottleneck under normal conditions (Eq. (6.4)). The parameters will be identical for all pedestrians: $A_i = A$ and $B_i = B$. The form of the social repulsive force is recalled here:

$$\mathbf{f}_{ij} = Ae^{\left((R_{ij}-d_{ij})/B\right)}\left(\lambda + (1-\lambda)\frac{1+\cos\phi_{ij}}{2}\right)\mathbf{e}_{ji} \tag{6.4}$$

where $R_{ij} = r_i + r_j$ is the sum of the radii of pedestrians i and j, d_{ij} is the distance between their centers, A and B are constant parameters of the model representing the magnitude of the maximum sociopsychological force and its fall-off length respectively, λ with $0 < \lambda < 1$ represents the anisotropic nature of the force, $\mathbf{e}_{ji}$ is the unit vector pointing from pedestrian j to pedestrian i, and ϕ_{ij} is the angle between i's desired direction $\mathbf{e}_{d,i}$ and $\mathbf{e}_{ji}$.

Therefore, for twenty linearly spaced values of A and B in the intervals $[10; 1000]$ N and $[0.01; 0.2]$ m respectively, all the experiments conducted in [57]. This means that for each value of b and N, 400

Table 6.3: Parameters used in the simulations for pedestrian flow through a bottleneck

Parameters	Symbol	Value	Unit
Walking speed	$\parallel \mathbf{u}_{d,i} \parallel$	$\mathcal{N}$ (1.34,0.26)	$\mathrm{m.s}^{-1}$
Radius	r_i	0.23	m
Mass	m_i	83	kg
Relaxation time	τ_i	0.5	s
Normal coefficient of dissipation	K_n	10^5	kg
Tangential coefficient of dissipation	K_{tg}	0	kg
Time step	h	10^{-2}	s

simulations were run. An example of the configuration of the participants (N=60) along with the different parameters used in the simulations are shown in Fig. 6.6(b) and Table 6.3 respectively. The parameters that vary from one simulation to another are A, B, N and b.

For each N_b^j ($N_0.8^1$ corresponds to $N = 20$ and $b = 0.8$), an error criterion in the least mean square sense has been studied:

$$\varepsilon_j(A,B) = \frac{1}{n_b}\sum_{i=1}^{n_b}\Big(\frac{J_s(A,B,b_i,N_b^j)}{J_{s,exp}(b_i,N_b^j)} - 1\Big)^2 \tag{6.5}$$

where $n_b = 5$ is the number of bottleneck widths considered (see Table. 6.2), $J_{s,exp}$ the experimental value of the specific flow found in Table 6.2, and J_s the value of the specific flow obtained by our model.

The n_b corresponding errors are then added together in a way to conserve the value of the mean, and the global error is given by:

$$\varepsilon_T(A,B) = \frac{1}{n_g\, n_b}\sum_{j=1}^{n_g}\sum_{i}^{n_b}\Big(\frac{J_s(A,B,b_i,N_b^j)}{J_{s,exp}(b_i,N_b^j)} - 1\Big)^2 \tag{6.6}$$

where $n_g = 3$ is the number of studied groups. The optimized values $\tilde{A}$ and $\tilde{B}$ are obtained by minimizing ε_T in the least-mean square:

$$(\tilde{A},\tilde{B}) = \arg\min \varepsilon_T(A,B) \tag{6.7}$$

By plotting ε_T as a function of A and B, the surface illustrated in Fig. 6.8 is obtained. After interpolating and smoothing the surface, using the curve fitting toolbox of Matlab, several functions that fit the local minima represented by red circles in Fig. 6.8 can be found. The best fit was achieved by the exponential function shown in Fig. 6.8. We ran simulations for three points of the curve and got the specific flow values illustrated in Fig. 6.9. The first point was chosen so as to use the same value of B found in [16]. The other two were chosen to be around the latter. Fig. 6.9 shows that the specific flow values obtained for the three points are in good agreement with the experimental results.

Another validation of our model comes from the density measurements inside and in front of the bottleneck. The results are also in good agreement with the experimental data as shown in Fig. 6.10.

Linear dependence of the flow on the bottleneck-width In [57], the relationship between the flow and the width of a bottleneck is examined. Using the experimental findings of [57] along with several others, it is argued that the relationship is linear rather than stepwise, as suggested by [20]. To verify which $J - b$ relationship ($J = J_s \cdot b$) would be obtained by our model using one of the values of (A, B) found in the previous section, i.e. $A = 790\,N$ and $B = 0.08\,m$, we calculated the flow for each b. The results of the simulations and the experimental data [57] along with their linear regressions are plotted in Fig. 6.11. The norm of residuals of the linear regressions are presented in Table 6.4.

It is clear that the flow values given by our model increase rather linearly with the bottleneck width. We can also notice that the difference between the simulation and experimental results decrease as N increases. This can be explained by the fact that, for small N, the time allotted to the experiment was not enough to reach a stationary state [57].

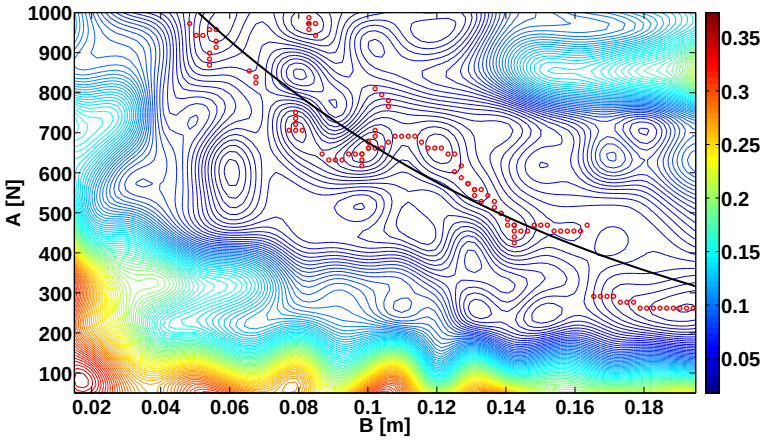

Figure 6.8: The surface representing ε_T as a function of A and B. The curve is given by the exponential function $A = 1501 * e^{-7.98B}$

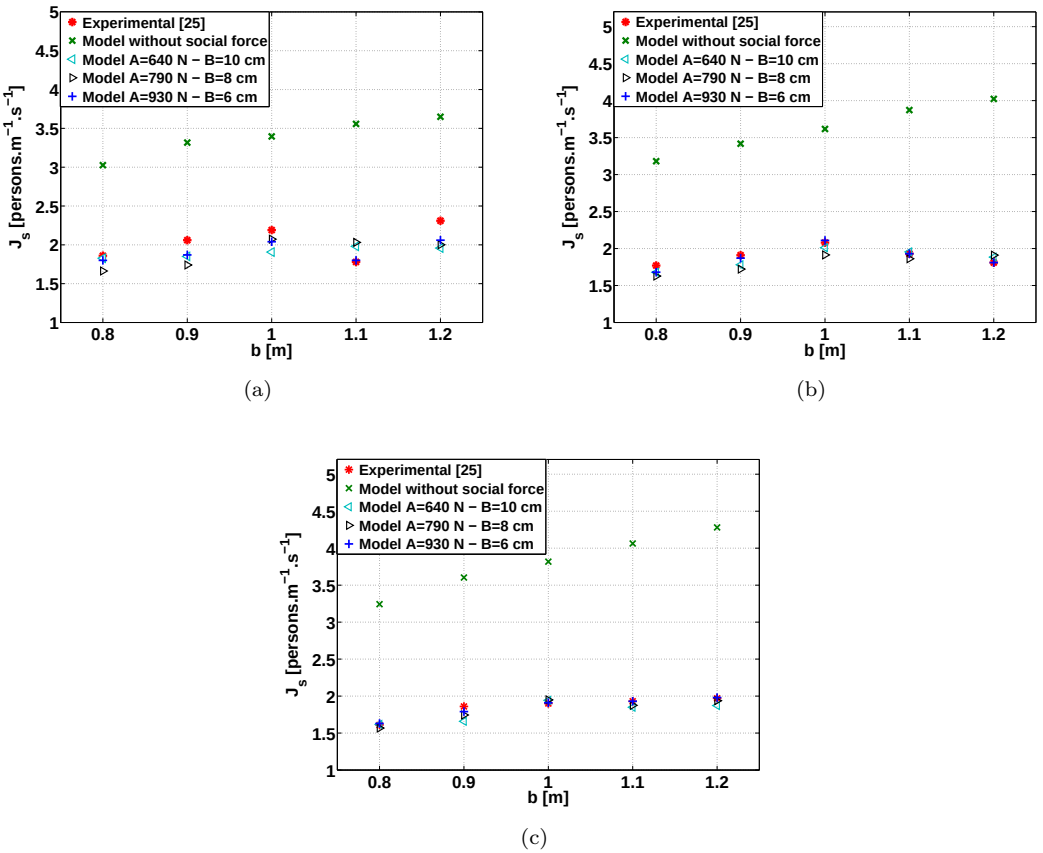

Figure 6.9: Specific flow measurements obtained by our model (considering the social repulsive force) in comparison with empirical data [57] for N= (a) 20, (b) 40, and (c) 60

Lane formation inside the bottleneck

In [29, 57, 59], pedestrians formed lanes inside the bottleneck. The number of lanes depends on the bottleneck width. In order to verify if our model can reproduce the same phenomenon, we ran fifty

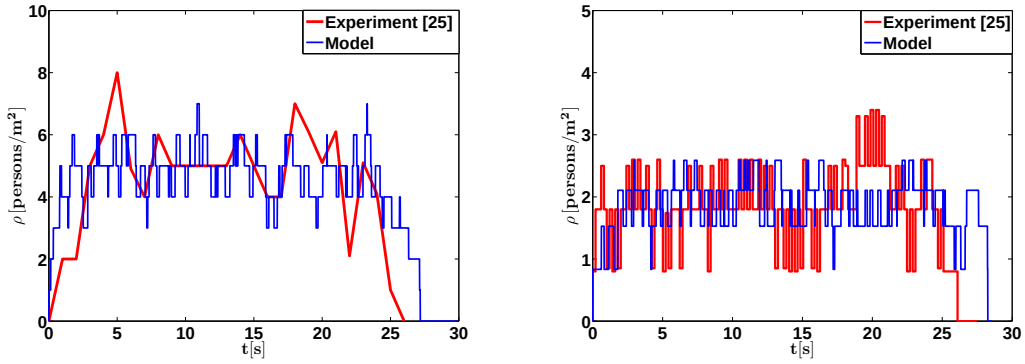

(a) (b)

Figure 6.10: Density measurements for 60 pedestrians obtained by the experiment [57] and by our model ($A = 790\,kg.m.s^{-2}$, $B = 0.08\,m$): (a) density in front of the entrance of the bottleneck and (b) density inside the bottleneck

simulations for each bottleneck width b and for $N = 60$. For each run, we saved the probability of finding a pedestrian at position x inside the bottleneck (see Fig. 6.6). The probability is given by $X_i/(\sum_{j=1}^{m} X_j)$ where X_i represents the number of times pedestrians were detected in an interval centered at position x of magnitude $0.01\,m$ and $\sum_{j=1}^{m} X_j$ represents the total number of detections made inside the bottleneck. The probabilities were plotted in Fig. 6.12. Lane formation is illustrated by the double peak structure in the probability distribution of the positions for $b \geq 0.9\,m$. Starting with one lane for $b = 0.8\,m$ and ending with two lanes for $b = 1.2\,m$, it is clear that the lanes continue to separate with the width of the bottleneck.

Discussion

In this section, we discuss and analyze results obtained by the 2D model for the simulation of the movement of pedestrians through a bottleneck. The discussed results concern the specific flow and the lane formation. We show that they agree with the findings of several bottleneck experiments.

Concerning the specific flow J_s, two criteria are to be examined: the value of J_s for each bottleneck width and its variation. Without introducing the social force, the specific flow values obtained by our model were very far from the experimental ones found in [57]. The main reason behind this expected result is the different pedestrian behavior in the two studies. While in [57] the participants are asked not to push and to move normally, pedestrians were clearly more aggressive in our model when the social respulsive force wasn't added (Fig. 6.13 (a)). This behavior might increase the flow for some bottleneck widths and decrease it for others (clogging phenomenon). For this reason, we repeated the study after introducing the social force. The obtained results approach the experimental ones better than the case without the repulsive forces. However, the sudden drop of the specific flow value for $b = 1.1\,m$ and $N = 20$ (Fig. 6.11), that was not explained in [57], was not reproduced for all the simulations we ran. This could be explained by the fact that, for small N, the time allotted to the experiment was not enough to reach a stationary state. This means that the value of J_s found in [57] might not be representative of the specific

Table 6.4: Norms of residuals of the linear regressions plotted in Fig. 6.11

	Experimental	Model
$N_b = 20$	**0.436**	**0.192**
$N_b = 40$	**0.237**	**0.104**
$N_b = 60$	**0.098**	**0.136**

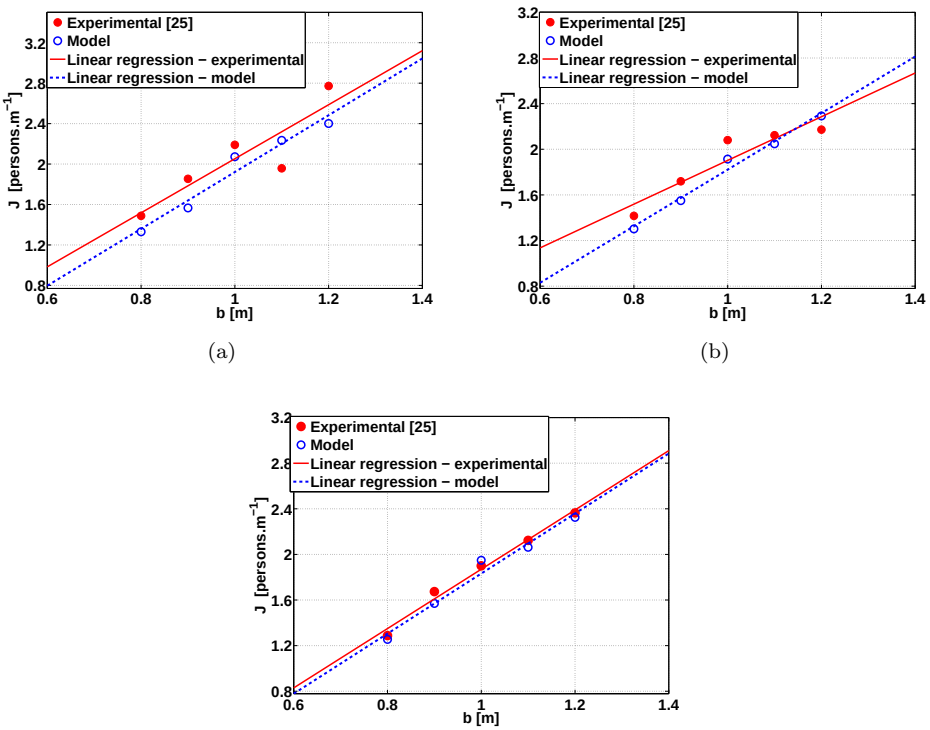

Figure 6.11: Flow values obtained by the 2D discrete model ($A = 790\,N$, $B = 0.08\,m$) compared to the experimental data [57] for N = (a) 20, (b) 40, and (c) 60

flow value for $b = 1.1\,m$ and $N = 20$. The difference between the characteristics of the pedestrians in each study might have also contributed to the small gap between the results obtained by our model and the empirical ones. As for the variation of the flow ($J = b \cdot J_s$), we have found that it increases rather linearly with the bottleneck width.

The second result obtained by the 2D model was the lane formation inside the bottleneck. This phenomenon was found in all the experiments done on the bottleneck with a difference in the number of lanes formed. The simulation results conform with what was obtained experimentally in [57].

Eventhough we obtained satisfying results by the previous study, we realized that the procedure was not efficient and optimal. For only two parameters, over 6000 simulations were performed. Since our model has about 13 input parameters, a more efficient procedure is essential. For this reason, we turn towards the design of experiments to extract a maximum amount of information for a least number of simulations.

6.2.2 Experimental design

When conducting experiments, we usually seek to observe how one or more response variables change when we deliberately change one or more process variables, also called factors. The design of experiments (DOE) is an efficient procedure that can be used to plan experiments so that the analysis of the obtained data leads to valid and objective conclusions. Constructing a detailed experimental plan before doing the experiment allows to obtain a maximum amount of information for a given amount of experimental effort. Before discovering the different aspects of an experimental plan, we define some of the fundamental terms that will be used throughout this section.

A *factor* is one of the controlled (known without an error) or uncontrolled variables (a random perturbation) whose influence on the response is being studied in the experiment [1, 25]. A factor is

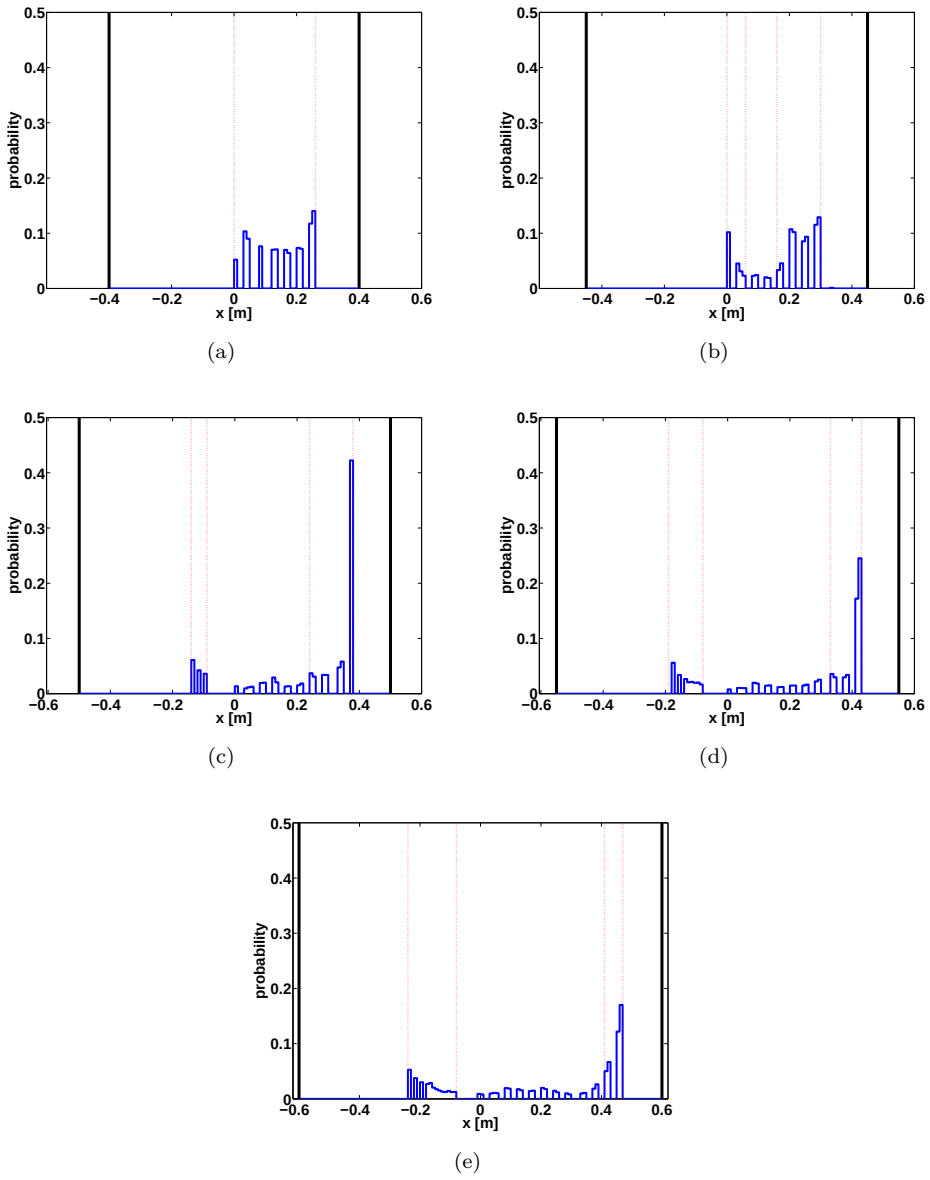

Figure 6.12: The probability of finding a pedestrian at position x for 50 runs with $N = 60$, $A = 790\,N$, $B = 0.08\,m$, and b= (a) 0.8, (b) 0.9, (c) 1, (d) 1.1 and (e) 1.2

quantitative if the values it takes can be classed in a logical order, e.g., temperature in degrees, times in seconds. If not, it is qualitative, e.g., different operators, switch on or off.

A *level* is one of the particular values that an examined factor can take in the experiment. The necessary number of levels for each factor is chosen in a way to correctly describe the factor's effect on the process and possible interactions between factors [1].

A *treatment* is one chosen level for a single factor during an experimental run, e.g., temperature at 800 degrees. A *treatment combination* is the set of chosen levels for the considered factors in a given experimental run, e.g., an experimental run using an 800-degree temperature, machine number 3, operator A and switch off is using the following treatment combination: $\{800, 3, A, off\}$. Therefore, a treatment defines an elementary experiment that could be repeated to enhance the precision of the targeted model.

An *experimental design* is the formal plan that will be used to conduct the experiment. This plan includes the choice of the responses, factors and their levels, and the treatments. It is usually represented

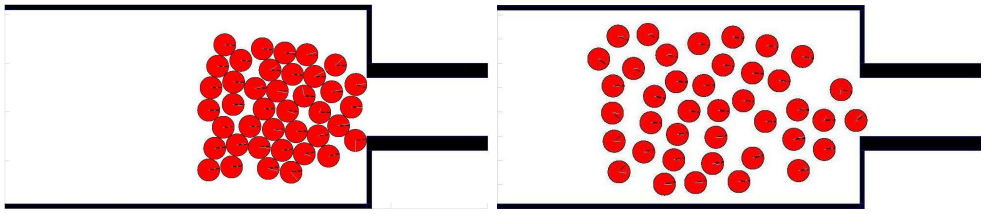

(a) (b)

Figure 6.13: Pedestrian behavior when $N = 40$ at $t = 2.5\,s$ (a) without and (a) with the social repulsive force

by a matrix having as much columns as the number of factors and as much rows as the number of tests to be realized [1].

A *response* is a quantifiable observed yield of the process for a certain treatment combination. There can be several responses for the same treatment combination if the experiment is replicated.

Now that some basic definitions are introduced, the different aspects of an experimental design will be addressed in more detail. We start with the two main objectives of using an experimental plan:

- Out of all of the considered factors, find the statistically significant ones. This also allows to answer the following questions:
  - How to estimate and compare the different factors of a process?
    - What are the most influencing factors?
    - Are there interactions between the factors (correlations)?
- Build a regression model or a good quality analysis of variance in order to understand and/or predict and/or search for an optimum. The process of building this meta model is illustrated in Fig 6.14. This also allows to answer the following questions:
  - How to choose an efficient plan?
  - How to adjust the factors of a process to reach an optimum?
    - How to minimize the necessary measurement points of a process while obtaining the maximum amount of information?
    - Are there biased measurements?

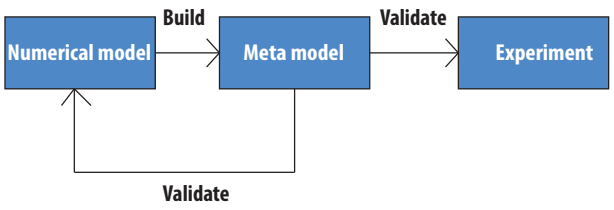

Figure 6.14: The steps of validating a meta model.

Answering all these questions, an experimental plan helps reduce the number of tests to what is essential for taking a decision. In the scope of our work, we are interested in finding the statistically significant factors or input parameters of our model building a regression model. But first, let us define the experiment.

Table 6.5: The factors and their levels.

Factor	**Symbol**	**Interval**
Velocity of wavefront in buffer zone	$V_b(\mathbf{x})$	[0.1,0.3]
Repulsion distance from wall	D_{shy}	[0.1,0.35]
Viscosity of collision (kg)	K_{tg}	$[0, 1e^4]$
Nature of collision (kg)	K_n	$[500, 1e^5]$
Social force: anisotropy	λ	[0,1]
Repulsive zone around pedestrian	z_{rep}	[0.8,5]
Social force: fall-off length	B	[0,0.25]
Social force: magnitude	A	[0,800]
Radius of pedestrians	R	[0.18,0.24]
Number of pedestrians	N	[20,40]
Agressivity	τ	[0.4,1]
Desired speed	v_0	[0.5,2.2]
Time step	h	[0.001,0.01]

The experiment

Working with crowds, the environment of the experiment was the first to be chosen. A bottleneck configuration as the one shown in Fig. 6.15 is adopted. Pedestrians start in the wide corridor and head towards the exit at the end of the small corridor. The response to be measured is the flow $J = \frac{\nabla N}{\nabla t}$ through the small corridor. Other responses can be measures such as density or velocity. Since in our model the parameters don't have particular levels, a minimum and maximum value for each of the factors that will be examined was chosen. The factors to be varied and their corresponding levels are shown in Table 6.5.

Figure 6.15: The bottleneck configuration to be used for the experiments.

Choice of experimental design

Several experimental designs exist depending on the type of application [25]. We have decided to use a factorial design since it is appropriate when several factors are to be investigated at two or more levels and interaction of factors may be important. By using a factorial design, the following can be achieved:

- estimate and compare effects of several factors.
- estimate possible interaction effects.
- estimate variance.

As illustrated in Table 6.5, each varied factor has two levels, a minimum and a maximum value. Therefore, a two level full factorial design is selected with 2^k experiments to be done, where k is the number of factors to be examined. This allows to obtain all k main effects (first-order effects), all $k(k-1)/2$ two-factor interactions, all $k(k-1)(k-2)/3!$ three-factor interactions, etc.. In our case, we have done $2^{13} = 8192$ experiments. We did not seek a fractional-factorial design because we had enough

Table 6.6: The obtained 2^{13} full factorial design.

	Factors												
Run no.	$V_b(\mathbf{x})$	D_{shy}	K_{tg}	K_n	λ	z_{rep}	B	A	R	N	τ	v_0	h
1	-	-	-	-	-	-	-	-	-	-	-	-	-
2	+	-	-	-	-	-	-	-	-	-	-	-	-
3	-	+	-	-	-	-	-	-	-	-	-	-	-
4	+	+	-	-	-	-	-	-	-	-	-	-	-
5	-	-	+	-	-	-	-	-	-	-	-	-	-
6	+	-	+	-	-	-	-	-	-	-	-	-	-
							⋮						
							⋮						
8192	+	+	+	+	+	+	+	+	+	+	+	+	+

time to implement all the experiments. The obtained experimental design is illustrated in Table 6.6. The + and the − signs represent respectively, the maximum and the minimum values of a factor.

Estimation of main effects and interactions

The effect of each factor can be estimated by using a statistic of the form $\bar{y}_+ - \bar{y}_-$ which is the difference between two averages each containing 2^{k-1} observations. So to study the effect of factor k, all the observations corresponding to a + in column k go into $\bar{y}_+$ and the rest goes into $\bar{y}_-$. As for the interactions between factors, additional column vectors of + and − signs must be constructed by algebraically multiplying the columns of the main factors. For example, to obtain the vector AB, column A is multiplied by column B. However, this method is very tedious for 8192 vectors.

A more rapid method to calculate the estimates of main effects and interactions for two-level factorials is *Yates algorithm*. After listing the observed data in Yates order (see Table 6.6), the calculation of the effects' estimates proceeds as follows [25]:

1. Create a table with $k+2$ columns and place all the experimental design (Table 6.6) in column 1.
2. Enter all the obtained responses corresponding to each treatment combination in column 2.
3. Place the sum of consecutive pairs from column 2 in the first half of column 3, e.g., add the first and the second element of column 2 and place it in the first row of column 3.
4. Place the difference of consecutive pairs from column 2 in the second half of column 3, e.g., subtract the first and the second element of column 2 and place it in the first row of the second half of column 3.
5. Obtain the columns $4, 5, \ldots, k+2$ by repeating steps 3 and 4 by using each time the previous column, e.g., to obtain column 4 use column 3, etc.
6. In colmun $k+2$, the entries are labeled $g(T), g(V_b(\mathbf{x})), g(D_{shy}), g(V_b(\mathbf{x})\, D_{shy}), etc.$. For each row, each factor having a + sign is found inside the parantheses of $g(\ldots)$. For example, if in row i, factors v_0 and A both have a plus sign, then we obtain $g(v_0 A)$. The grand average is obtained by dividing $g(T)$ by $N = 2^k$. The estimates of the main effects and interactions are obtained by dividing each $g(\ldots)$ by $N/2$. The estimated effects $E(\ldots)$ are found in the last column.
7. Verify that the sum of all individual responses (column 2) is equal to $g(T)$.
8. Verify that the sum of the squares of the quantities in column 2 is equal to the sum of squares of the quantities in column $k+2$ divided by 2^k.

The results obtained from Yates algorithm are illustrated in Table 6.7

Table 6.7: Yates method of analysis using the data from Table 6.6.

$V_b(\mathbf{x})$ D_{shy} $\cdots$h	2 (response)	3	4	$\cdots$	15			Estimated effects		
- - - $\cdots$ −	2.4655	4.9310	9.8619		**1.5788e^4**	=	$g(T)$	Average	=	1.9272
+ - - $\cdots$ −	2.4655	4.9310	5.4636		7.566	=	$g(V_b(\mathbf{x}))$	$E(V_b(\mathbf{x}))$	=	0.0018
- + - $\cdots$ −	2.4655	2.7318	9.0567		10.8394	=	$g(D_{shy})$	$E(D_{shy})$	=	0.0026
+ + - $\cdots$ −	2.4655	2.7318	8.7169	$\cdots$	-2.3343	=	$g(V_b(\mathbf{x})\, D_{shy})$	$E(V_b(\mathbf{x})\, D_{shy})$	=	$-5.7e^{-4}$
- - + $\cdots$ −	1.3659	4.5284	9.8619		$-7.9e^3$	=	$g(K_{tg})$	$E(K_{tg})$	=	-1.9276
+ - + $\cdots$ −	1.3659	4.5284	5.4636		14.7048	=	$g(V_b(\mathbf{x})\, K_{tg})$	$E(V_b(\mathbf{x})\, K_{tg})$	=	0.0036
			⋮							
+ + + $\cdots$ +	0.6135	0.0106	0.0106		-73.9056	=	$g(V_b(\mathbf{x})\cdots, h)$	$E(V_b(\mathbf{x})\cdots h)$	=	-0.018
Total	**1.5788e^4**									
Sum of squares	5.8508e^4				4.7929$e^8/2^{13}$	=	5.8508e^4			

Table 6.8: Analysis of variance table for the 2^{13} factorial design.

Source of Variation			SSq	DF
Total	=	$\sum (y_i - \bar{y})^2$	$2.8082e^4$	8192
$V_b(\mathbf{x})$ effect	=	$2^{13}(0.0018)^2/4$	0.007	1
D_{shy} effect	=	$2^{13}(0.0026)^2/4$	0.0143	1
$V_b(\mathbf{x})\, D_{shy}$ effect	=	$2^{13}(-5.7e^4)^2/4$	$6.65e^{-4}$	1
K_{tg} effect	=	$2^{13}(-1.9276)^2/4$	$7.6093e^3$	1
$V_b(\mathbf{x})\, K_{tg}$ effect	=	$2^{13}(0.0036)^2/4$	0.0264	1
		⋮		
$V_b(\mathbf{x})\cdots h$ effect	=	$2^{13}(-0.018)^2/4$	0.6668	1
Residual sum of squares			0	0

Testing main effects and interactions- the analysis of variance

Now that the effects of the factors and their interactions have been calculated, it is necessary to find out which ones are statistically significant. This can be done by calculating the following interval:

$$Effect \pm t_{\nu,\alpha/2} * (SE(effect)) \tag{6.8}$$

where $t_{\nu,\alpha/2}$ is the student's t-distribution for ν degrees of freedom, $100(1-\alpha)\%$ is the confidence interval, and $SE(effect)$ is the standard error of each estimated effect. SE is defined as:

$$SE(effect) = SE(\bar{y}_+ - \bar{y}_-) = 2s/\sqrt{N} \tag{6.9}$$

where s^2 is the estimate of the experimental error variance σ^2. For replicated trails, an estimate of σ^2 can be obtained by pooling the variance estimates calculated for each set of repetitions. Since in our case only one trail was performed for each treatment combination, an alternative procedure is necessary to estimate σ^2. To do so, the analysis of variance for 2^k factorial designs will be used.

It is possible to measure the total variability of the observations by calculating $\sum (y_i - \bar{y})^2 = \sum y_i^2 - (\sum y_i)^2/N$, for $i = 1, 2, \ldots, N$. If it is considered that all variability comes from random errors, then an estimate of σ^2 is given by $s^2 = \sum (y_i - \bar{y})^2/(N-1)$. However, the influences of the controlled factors making up the experimental design usually contribute to the variability of the observations. To find out the contribution of each factorial effect, we calculate its sum of squares given by $SSQ = N * (effect)^2/4$ with one degree of freedom as shown in Table 6.8.

After all assignable causes have been subtracted, the remaining variability is represented by the residual sum of squares. In Table 6.8, all 8192 degrees of freedom with their assigned SSq are present which explains why the residual sum of squares and degrees of freedom are both equal to 0.

In order to estimate σ^2 for this unreplicated factorial design, it is necessary to consider some of the estimated effects as manifestations of noise, i.e., they have no real effect [25]. As an example, consider the case where 7 factor interactions and higher are considered to be noise. By summing their squares and their degrees of freedom from Table 6.8 we obtain the estimate of the variance $s^2 = 602.81/4096 = 0.1472$ with $\nu = 4096$ degrees if freedom. The estimated standard deviation is then $s = 0.3837$. The standard

error of an effect can now be calculated $SE(effect) = 2s/\sqrt{N} = 0.0085$ and the $100(1-\alpha)\%$ confidence limits for an effect are:

$$\pm\, t_{\nu,\alpha/2} * SE(effect) = \pm t_{4096,0.025} * 0.0085 = \pm 0.0167 \tag{6.10}$$

All the remaining terms (4096) now have a 95% confidence interval given by effect ± 0.0167. If 0 is not included in the confidence interval of a term then it is considered to be statistically significant. Of the 4096 remaining terms, 461 are declared statistically significant with 10 main effects, 41 two-factor , 74 three-factor , 112 four-factor , 121 five-factor, and 103 six-factor interactions. A Pareto diagram is plotted in Fig. 6.16 showing all the retained terms in decreasing order of significance. The first appearance of an i^{th} order interaction is marked by a red stem (see Fig. 6.16). For clarity, only the first 30 terms are displayed (there are 461). The main factors and their second order interactions are also shown in Figures 6.17 and 6.18.

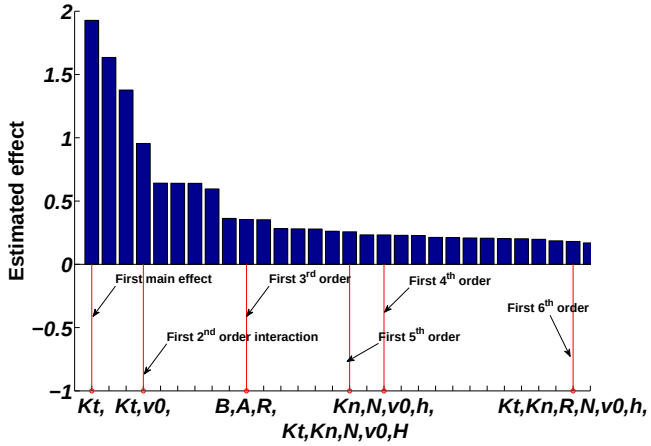

Figure 6.16: The terms of the 6^{th} order model in decreasing order of significance.

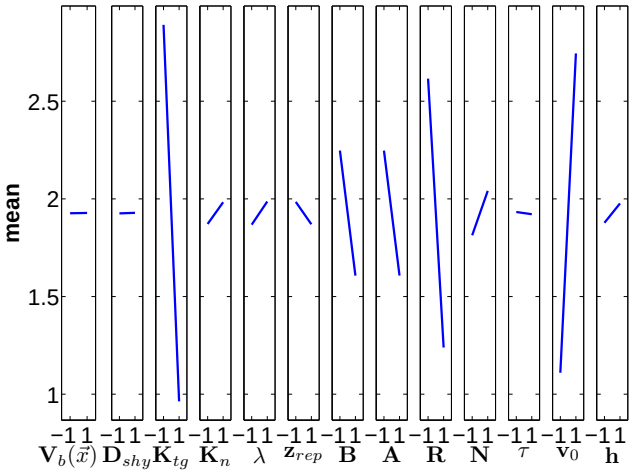

Figure 6.17: Illustration of the main effects of the 2^{13} complete factorial design.

The regression model

Since all the factors are quantitative, it is interesting to construct a regression model that would allow us to predict the response of our pedestrian model at the intermittent levels of the factors. The regression

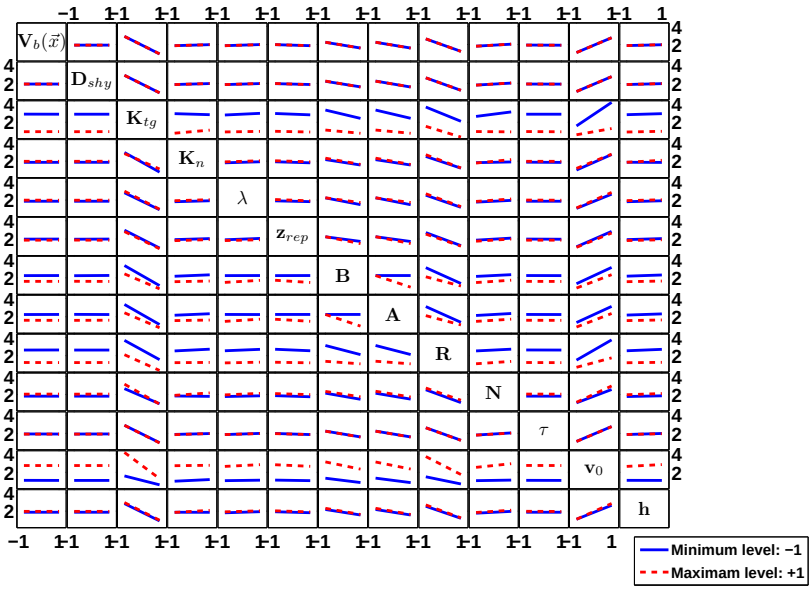

Figure 6.18: Illustration of the 2-factor interactions of the main effects of the 2^{13} complete factorial design.

model is constructed of the p significant effects that were identified for each case and is given by:

$$Y = \beta_0 + \beta_1 X_1 + \beta_2 X_2 + \cdots + \beta_{12} X_1 X_2 + \cdots + \epsilon \tag{6.11}$$

where X_i is a statistic (a main effect or an i^{th} order interaction), β_i is a regression coefficient and β_0 is the total average. The regression coefficient for each statistic is equal to half of its estimated effect found in the last column of Table 6.7 ($\beta_i = E(X_i)/2$) [30]. We have built 13 models each time considering an interaction order. For example, for the first model we consider only the significant factors, for the second model we consider the significant factors and the significant second order interactions and so on. We then perform an analysis of variance, also called ANOVA, that will provide us with information about levels of variability within each regression model. First we rewrite the basic regression line concept, $Data = Fit + Residual$, as follows:

$$(y_i - \bar{y}) = (\hat{y}_i - \bar{y}) + (y_i - \hat{y}_i) \tag{6.12}$$

In other words, the total variation of the observed data y_i is equal to the sum of the variations of the fitted model $\hat{y}_i$ and the residual values. By squaring each of these terms and adding over all of the $N = 2^k$ observations, one obtains:

$$\sum_{i=1}^{N} (y_i - \bar{y}) = \sum_{i=1}^{N} (\hat{y}_i - \bar{y}) + \sum_{i=1}^{N} (y_i - \hat{y}_i) \tag{6.13}$$

It is possible to rewrite Eq. (6.13) as $SST = SSM + SSE$, where SS is a notation for sum of squares and T, M, and E are notations for total, model, and error, respectively. The source of each error and its degrees of freedom are given in Table 6.9.

To determine how well data fit each of the obtained regression models, the coefficient of determination, R^2, is computed using the following expression:

$$R^2 = \frac{SSM}{SST} \tag{6.14}$$

Table 6.9: The ANOVA table.

Source	SS	Degrees of freedom
Model	$SSM = \sum_{i=1}^{N} (\hat{y}_i - \bar{y})^2$	p-1
Error	$SSE = \sum_{i=1}^{N} (y_i - \hat{y}_i)^2$	N-p
Total	$SST = \sum_{i=1}^{N} (y_i - \bar{y})^2$	N-1

The value of R^2 is interpreted as the fraction of variability in the data explained by the regression model. The value of R^2 for each obtained regression model is given in Fig. 6.19. We remind the reader that for each regression model only the significant terms up to certain order of interaction are considered.

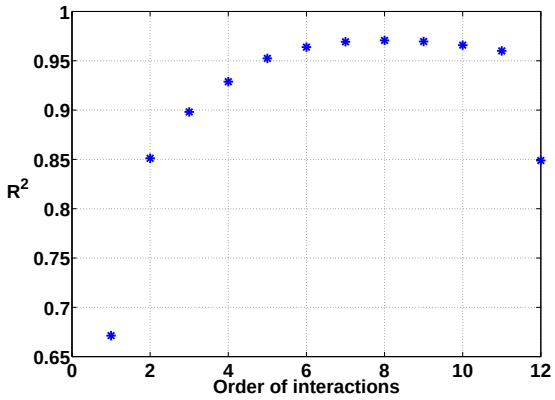

Figure 6.19: The value of R^2 for each regression model where each time the terms up to a certain order of interactions is considered.

Out of all the built regression models, the one with interactions up to order 8 (with 664 coefficients) gives the best R^2 value of 97%. However, it is interesting to note that by taking only 3^{rd} order interactions (regression model with 104 coefficients), we obtain $R^2 = 90\%$. The choice of the best representative model is then a trade-off between the precision required and the complexity of the meta model.

6.2.3 Conclusion

In this chapter, the validation and verification of the discrete model was addressed. First, we examined the capacity of the discrete model to reproduce experimental results. A parametric study was done in order to find a series of values of the social repulsive force parameters (A and B) that allowed us to obtain simulation results (specific flow, flow rate, density inside and outside the bottleneck) close to the empirical ones found in [57]. It was also shown that our model is capable of reproducing the lane formation phenomenon inside bottleneck that was observed in several experiments [29, 57, 59]. Although we obtained important information from this study, they were not enough nor efficient compared to the number of simulations that had to be done. For this reason, an experimental plan was used in order to identify the most statistically significant parameters of our model and the interactions between them. The influence of varying one of the input parameters on the response of the discrete model can now be predicted. This study also allowed us to construct regression models with different complexity levels that can predict the results of the numerical model with different precision levels. The importance of these meta models is the possibility to obtain responses without having to perform simulations that are time consuming.

Bibliography

[1] Pierre Argoul. Introduction aux plans d'expériences. In Denis Duhamel, editor, *Faire une mesure en mécanique*, pages 33–74. Presses des Ponts, 2014.

[2] Stefania Bandini, Sara Manzoni, Hiroshi Umeo, and Giuseppe Vizzari. *Cellular Automata: 9th International Conference on Cellular Automata for Research and Industry, ACRI 2010, Ascoli Piceno, Italy, September 21-24, 2010, Proceedings*. Springer Science & Business Media, 2010.

[3] Klas Bayer and Tobias Rejnö. Utrymningslarm. Technical Report 5053, Department of Fire Safety Engineering, Lund University, Lund, Sweden, 1999.

[4] Ana L. C. Bazzan and Franziska Klugl. *Multi-Agent Systems for Traffic and Transportation Engineering*. Information Science Reference - Imprint of: IGI Publishing, Hershey, PA, 2009.

[5] Mohcine Chraibi. *Validated force-based modeling of pedestrian dynamics*. PhD thesis, Forschungszentrum J'ulich GmbH, March 2012.

[6] Mohcine Chraibi, Armin Seyfried, and Andreas Schadschneider. Generalized centrifugal-force model for pedestrian dynamics. *Physical Review E*, 82(4):046111, 2010.

[7] Mohcine Chraibi, Armin Seyfried, Andreas Schadschneider, and Wolfgang Mackens. Quantitative Verification of a Force-based Model for Pedestrian Dynamics. *arXiv preprint arXiv:0912.4044*, 2009.

[8] Haakan Frantzich, Daniel Nilsson, and Oskar Eriksson. *Utvärdering och validering av utrymningsprogram*. 2007.

[9] J.J. Fruin. *Pedestrian planning and design*. Metropolitan Association of Urban Designers and Environmental Planners, 1971.

[10] J.J. Fruin and Jake Pauls. Human Factors of Means of Egress: History, Current Problems, and Implications for the Future. Boston, 2007.

[11] E.R. Galea, S. Deere, R. Brown, and L. Filippidis. An Evacuation Validation Data Set for Large Passenger Ships. ETH, Zurich, 2012.

[12] E.R. Galea, S. Deere, R. Brown, I. Nicholls, Y. Hifi, and N. Bresnard. The SAFEGUARD validation data - set and recommendations to IMO to update MSC Circ 1238. In *SAFEGAURD Passenger Evacuation Seminar*, pages 41–60, London, UK, 2012.

[13] William Grosshandler, Nelson Bryner, Daniel Madrzykowski, and Kenneth Kuntz. Report of the technical investigation of The Station Nightclub fire: appendices. Technical report, National Institute of Standards and Technology, 2005.

[14] S. Gwynne, E. Kuligowski, and D. Nilsson. Representing evacuation behavior in engineering terms. *Journal of Fire Protection Engineering*, 22(2):133–150, May 2012.

[15] Laurie Hanna. Commuter chaos in Paris after train drivers go on strike following attack on colleague Daily Mail Online. *Mail Online*, 2015.

[16] Dirk Helbing, IllÃ©és Farkas, and Tamàs Vicsek. Simulating dynamical features of escape panic. *Nature*, 407:487–490, 2000.

[17] Dirk Helbing, Anders Johansson, and Habib Zein Al-Abideen. Dynamics of crowd disasters: An empirical study. *Physical Review E*, 75(4):046109, 2007.

[18] Eva Herman. 20 Minuten - "Ferngesteuert, betrunken, vollgekifft" - International. *20 Minuten*, 2010.

[19] S.P. Hoogendoorn and Piet Bovy. Gas-kinetic modeling and simulation of pedestrian flows. *Transportation Research Record: Journal of the Transportation Research Board*, (1710):28–36, 2000.

[20] S.P. Hoogendoorn and W. Daamen. Pedestrian Behavior at Bottlenecks. *Transportation Science*, 39(2):147–159, 2005.

[21] S.P. Hoogendoorn, W. Daamen, and P.H.L. Bovy. Microscopic pedestrian traffic data collection and analysis by walking experiments. In E.R. Galea, editor, *Pedestrian and evacuation dynamics 2003*, pages 89–100. CMS Press, London, 2003.

[22] S.P. Hoogendoorn and Winnie Daamen. Microscopic Calibration and Validation of Pedestrian Models: Cross-Comparison of Models Using Experimental Data. In Andreas Schadschneider, Thorsten Pöschel, Reinhart Kühne, Michael Schreckenberg, and Dietrich E. Wolf, editors, *Traffic and Granular Flow'05*, pages 329–340. Springer Berlin Heidelberg, 2007.

[23] International Maritime Organization. Guidelines for evacuation analyses for new and existing passenger ships. Technical Report MSC/Circ.1238, 2007.

[24] International standards organization. Fire safety engineering - Assessment, verification and validation of calculation methods. Technical Report ISO 16730, 2008.

[25] J.M. Juran and A.D.F. Joseph. *Juran's Quality Handbook: The Complete Guide to Performance Excellence, Sixth Edition*. McGraw Hill, 1999.

[26] Andreas Ke, Hubert Klüpfel, Joachim Wahle, and Micael Schreckenberg. Microscopic simulation of pedestrian crowd motion. *Pedestrian and evacuation dynamics*, pages 193–202, 2002.

[27] Ansgar Kirchner, Hubert Klüpfel, Katsuhiro Nishinari, Andreas Schadschneider, and Michael Schreckenberg. Discretization effects and the influence of walking speed in cellular automata models for pedestrian dynamics. *Journal of Statistical Mechanics: Theory and Experiment*, 2004(10):P10011, 2004.

[28] T. Kretz, S. Hengst, and P. Vortisch. Pedestrian flow at bottlenecks: validation and calibration of VISSIM's social force model of pedestrian traffic and its empirical foundations. *International symposium on transport simulation, 8th, 2008, Surfers paradise, Queensland, Australia*, 2008.

[29] Tobias Kretz, Anna Grünebohm, and Michael Schreckenberg. Experimental study of pedestrian flow through a bottleneck. *Journal of Statistical Mechanics: Theory and Experiment*, 2006(10):P10014, 2006.

[30] K. Krishnaiah and P. Shahabudeen. *Applied design of experiments and Taguchi methods*. PHI Learning Pvt. Ltd., 2012.

[31] Erica D. Kuligowski and Richard D. Peacock. Building Occupant Egress Data. Report of Test FR 4024, National Institute of Standard s and Technology, Gaithersburg, MD (US), 2010.

[32] Erica D. Kuligowski, Richard D. Peacock, and Bryan L. Hoskins. *A review of building evacuation models, 2nd edition*. US Department of Commerce, National Institute of Standards and Technology Gaithersburg, MD, 2nd edition, 2010.

[33] Weichen Liao, Armin Seyfried, Jun Zhang, Maik Boltes, Xiaoping Zheng, and Ying Zhao. Experimental Study on Pedestrian Flow through Wide Bottleneck. *Transportation Research Procedia*, 2:26–33, 2014.

[34] T. Meyer-Köig, N. Waldau, and H. Klüpfel. The RiMEA Project-Development of a new Regulation. In *Pedestrian and Evacuation Dynamics 2005*, pages 309–313. Springer, 2007.

[35] Tim Meyer-König, Hubert Klüpfel, and Michael Schreckenberg. Assessment and analysis of evacuation processes on passenger ships by microscopic simulation. *Schreckenberg and Sharma*, pages 297–302, 2002.

[36] Masamitsu Mori and Hiroshi Tsukaguchi. A new method for evaluation of level of service in pedestrian facilities. *Transportation Research Part A: General*, 21(3):223–234, 1987.

[37] Helen C. Muir, David M. Bottomley, and Claire Marrison. Effects of Motivation and Cabin Configuration on Emergency Aircraft Evacuation Behavior and Rates of Egress. *The International Journal of Aviation Psychology*, 6(1):57–77, 1996.

[38] Klaus Müller. *Zur Gestaltung und Bemessung von Fluchtwegen für die Evakuierung von Personen aus Bauwerken auf der Grundlage von Modellversuchen.* PhD thesis, Technische Hochschule Magdeburg, 1981.

[39] Ryoichi Nagai, Masahiro Fukamachi, and Takashi Nagatani. Evacuation of crawlers and walkers from corridor through an exit. *Physica A: Statistical Mechanics and its Applications*, 367:449–460, 2006.

[40] PD Navin and RJ Wheeler. Pedestrian flow characteristics. *Traffic Engineering*, 39(4):30–33, 1969.

[41] H.E. Nelson and F.W. Mowrer. Emergency Movement. In P.J. DiNenno and W. Douglas Walton, editors, *SFPE handbook of fire protection engineering*, pages 3–367. National Fire Protection Association, Quincy, MA, 3 edition, 2002.

[42] Daniel Nilsson. *Exit choice in fire emergencies - Influencing choice of exit with flashing lights.* PhD thesis, Lund University, Lund, 2009.

[43] Detlef Oeding. *Verkehrsbelastung und Dimensionierung von Gehwegen und anderen Anlagen des Fussgängerverkehrs.* Bundesminister für Verkehr, Abt. Strassenbau, Bonn, 1963.

[44] SJ Older. Movement of pedestrians on footways in shopping streets. *Traffic Engineering and Control*, 10:160–163, 1968.

[45] Daniel R. Parisi, Marcelo Gilman, and Herman Moldovan. A modification of the Social Force Model can reproduce experimental data of pedestrian flows in normal conditions. *Physica A: Statistical Mechanics and its Applications*, 388(17):3600–3608, 2009.

[46] Philippe Pécol. *Modélisation 2D discrète du mouvement des piétons: application à l'évacuation des structures du génie civil et à l'interaction foule-passerelle.* PhD thesis, Université Paris-Est, 2011.

[47] Philippe Pécol, Pierre Argoul, Stefano Dal Pont, and Silvano Erlicher. A new crowd movement modeling for pedestrians who hold hands. *Vibrations, Shocks and Noise*, 2012.

[48] Philippe Pécol, Pierre Argoul, Stefano Dal Pont, and Silvano Erlicher. The non-smooth view for contact dynamics by Michel Frémond extended to the modeling of crowd movements. *Discrete and Continuous Dynamical Systems - Series S*, 6(2):547–565, November 2012.

[49] Philippe Pécol, StÃ©fano Dal Pont, Silvano Erlicher, and Pierre Argoul. Smooth/non-smooth contact modeling of human crowds movement: numerical aspects and application to emergency evacuations. *Annals of Solid and Structural Mechanics*, 2(2-4):69–85, 2011.

[50] V. M. Predtechenskii and A. I. Milinskii. *Planning for Foot Traffic Flow in Buildings.* Amerind, 1978.

[51] B. Pushkarev, J. M. Zupan, Boris Pushkarev, and Jeffrey M. Zupan. Capacity of walkways. In *Transportation Research Record*, 1975.

[52] Enrico Ronchi, Erica D. Kuligowski, Paul A. Reneke, Richard D. Peacock, and Daniel Nilsson. The Process of Verification and Validation of Building Fire Evacuation Models. *NIST Technical Note*, 2013.

[53] T. Rupprecht, W. Klingsch, and A. Seyfried. Influence of Geometry Parameters on Pedestrian Flow through Bottleneck. In Richard D. Peacock, Erica D. Kuligowski, and Jason D. Averill, editors, *Pedestrian and Evacuation Dynamics*, pages 71–80. Springer US, January 2011.

[54] A. Schadschneider, W. Klingsch, H. Klüpfel, T. Kretz, C. Rogsch, and A. Seyfried. Evacuation Dynamics: Empirical Results, Modeling and Applications, 2009.

[55] A. Seyfried, T. Rupprecht, A. Winkens, O. Passon, B. Steffen, W. Klingsch, and M. Boltes. Capacity Estimation for Emergency Exits and Bottlenecks. In *Interflam 2007*, 2007. Record converted from VDB: 12.11.2012.

[56] Armin Seyfried, Maik Boltes, Jens Kähler, Wolfram Klingsch, Andrea Portz, Tobias Rupprecht, Andreas Schadschneider, Bernhard Steffen, and Andreas Winkens. Enhanced empirical data for the fundamental diagram and the flow through bottlenecks. In *Pedestrian and Evacuation Dynamics 2008*, pages 145–156. Springer, 2010.

[57] Armin Seyfried, Oliver Passon, Bernhard Steffen, Maik Boltes, Tobias Rupprecht, and Wolfram Klingsch. New Insights into Pedestrian Flow Through Bottlenecks. *Transportation Science*, 43(3):395–406, May 2009.

[58] Armin Seyfried, Andreas Schadschneider, Ulrich Kemloh, and Mohcine Chraibi. Force-based models of pedestrian dynamics. *Networks and Heterogeneous Media*, 6(3):425–442, August 2011.

[59] Weiguo Song, Wei Lv, and Zhiming Fang. Experiment and Modeling of Microscopic Movement Characteristic of Pedestrians. *Procedia Engineering*, 62:56–70, January 2013.

[60] Armel Ulrich Kemloh Wagoum, Mohcine Chraibi, Jonas Mehlich, Armin Seyfried, and Andreas Schadschneider. Efficient and validated simulation of crowds for an evacuation assistant: Simulation of crowds for an evacuation assistant. *Computer Animation and Virtual Worlds*, 23(1):3–15, February 2012.

[61] U. Weidmann. Transporttechnik der Fuänger. Report Schriftenreihe Ivt- Berichte 90, ETH Zürich, 1993.

[62] Ulrich Weidmann, Uwe Kirsch, and Michael Schreckenberg, editors. *Pedestrian and Evacuation Dynamics 2012*. Springer International Publishing, Cham, 2014.

[63] Jun Zhang. *Pedestrian fundamental diagrams comparative analysis of experiments in different geometries*. PhD thesis, Forschungszentrum, Zentralbibliothek, Jülich, 2012.

[latin1]inputenc [french]babel

Chapter 7

Modeling pedestrian flow at the Noisy-Champs train station

Contents

7.1 Crowd dynamics and pedestrian trajectories in public transit

With a rising demand for public transport in the region of ile-de-France, it has become crucial to assess the design of pedestrian areas in railway and transfer stations as well as the impact of changes in the timetables of public transit systems. To this end, the 2D model was recently used in a study aimed at estimating the train dwell time (the time a train spends at a scheduled stop) at "Noisy-Champs" station (RER-A) in the region of ile-de-France for a given demand of boarding and alighting passengers [1]. This study has been a part of evaluating public transport in Paris and its suburbs.

"Noisy-Champs" station is on the RER A that links the east of ile-de-France to the west (see Fig. 7.1). One of the reasons for which it has been chosen is that according to the Grand Paris Express project, it will be the connection point between metro lines 11, 15, 16, and RER A (see Fig. 7.2). To be able to estimate the train dwell time (the time a train stays in a train station from arrival till departure) at this station using our 2D discrete model, data concerning the station's geometry, the traffic organization, and passenger flows are needed (see Fig. 7.3). In this chapter, the data collection and modeling techniques that were used to simulate traffic flow in "Noisy-Champs" station are demonstrated. In the first section, we show how the geometry of the station was partitioned into 3 zones in order to model pedestrian navigation. In section 2, pedestrian behavior according to the performed activity is addressed. In the third section, the obtained results are presented. The last section is dedicated to the conclusion and perspectives.

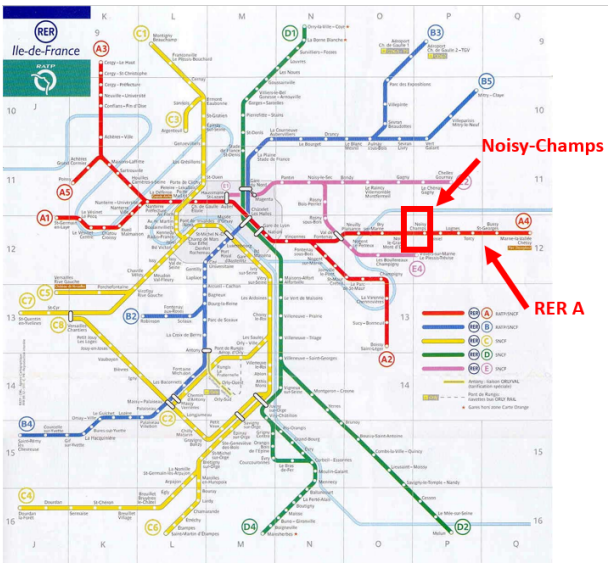

Figure 7.1: The actual RER lines of ile-de-France.

7.2 Geometry of "Noisy-Champs" station - pedestrian navigation

"Noisy-Champs" station has two entrances/exits to the east and one entrance/exit to the west (see Fig. 7.4). With the train platform it extends over 300 meters. Due to its size, we had to divide the station into several zones in order to model pedestrian navigation. The division has been done by taking into consideration three stages in transfer stations : Entrance-exit, platform access, boarding alighting.

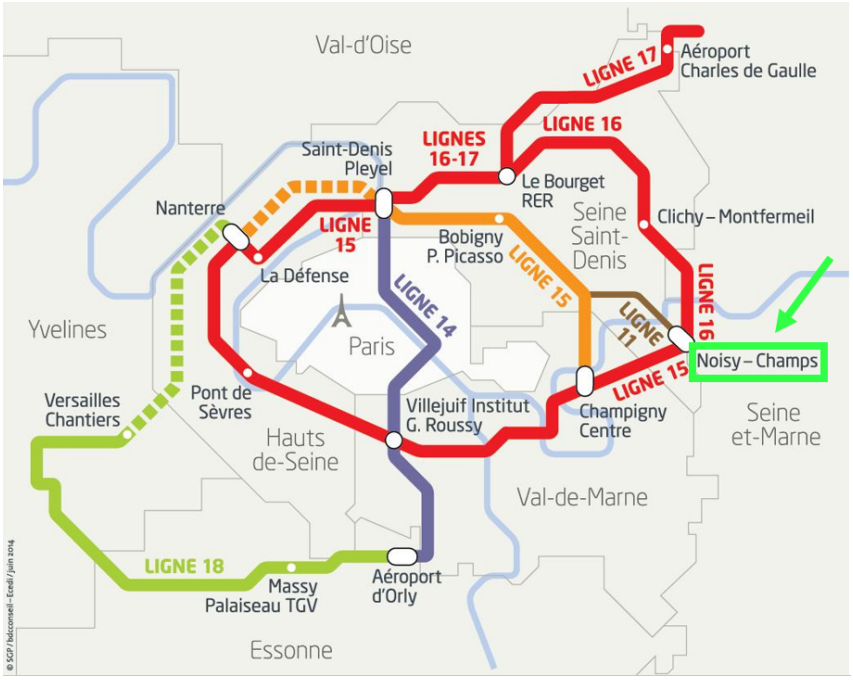

Figure 7.2: The new lines of the Grand Paris Express project.

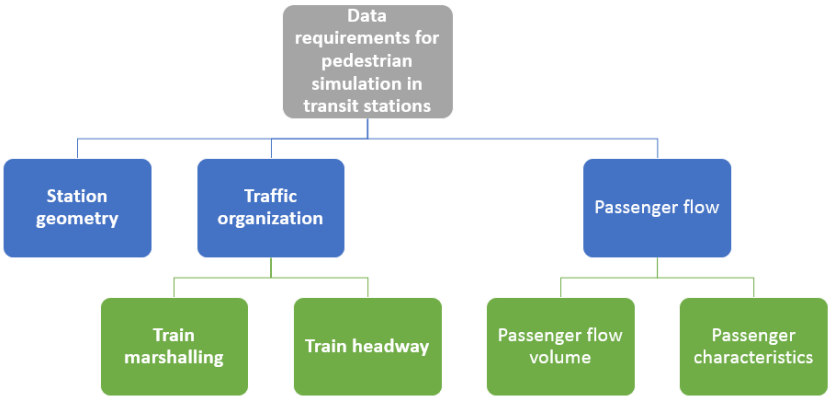

Figure 7.3: Data requirements for pedestrian simulation in transit stations.

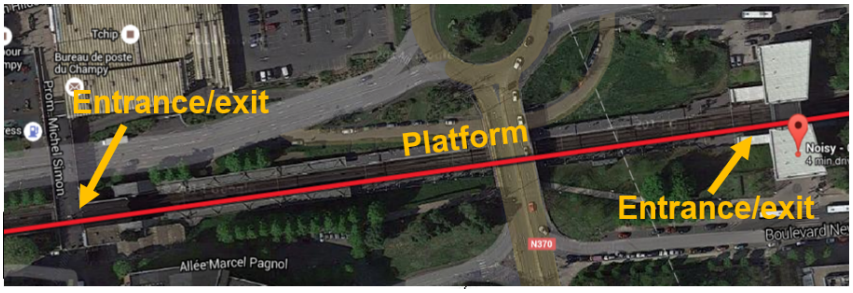

Figure 7.4: Aerial view of "Noisy-Champs" station.

7.2.1 Entrance/exit: Zone 1

The area that gives access to the train platforms is considered Zone 1. The eastern entrance is Zone 1-E and the western entrance is Zone 1-W (see Fig. 7.5). From Zone 1 pedestrians can enter the train to station or leave it. When they enter, they have the choice of heading to the northern or southern platform. For this study, only pedestrians heading to Paris are considered (southern platform). Zone 1 is only connected to the train platform (Zone 2).

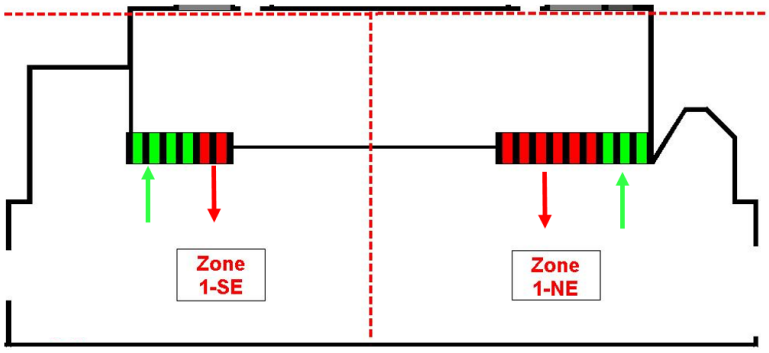

(a)

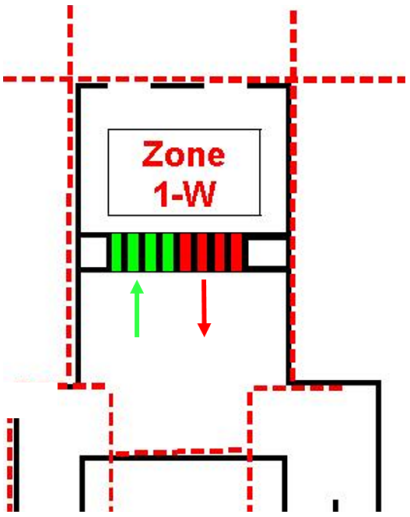

(b)

Figure 7.5: Entrance/exit areas of Noisy-Champs : (a) eastern and (b) western sides.

7.2.2 Access to platforms: Zone 2

Once pedestrians arrive at one of the stairs that lead to the train platform, they are considered to be in Zone 2 (see Fig. 7.6). In this zone, pedestrians wait for the train on the platform or board/alight the train. Zone 2 is connected to Zone 1 (entrance/exit) and Zone 3 (train).

7.2.3 Boarding/alighting- Zone 3

Boarding/alighting takes place between the train platform (Zone 2) and the train (Zone 3 illustrated in Fig. 7.7). Pedestrians who want to alight get off the train and head to one of the exits. Those who are on the platform assemble next to the doors of the train and either wait for others to descend or force their

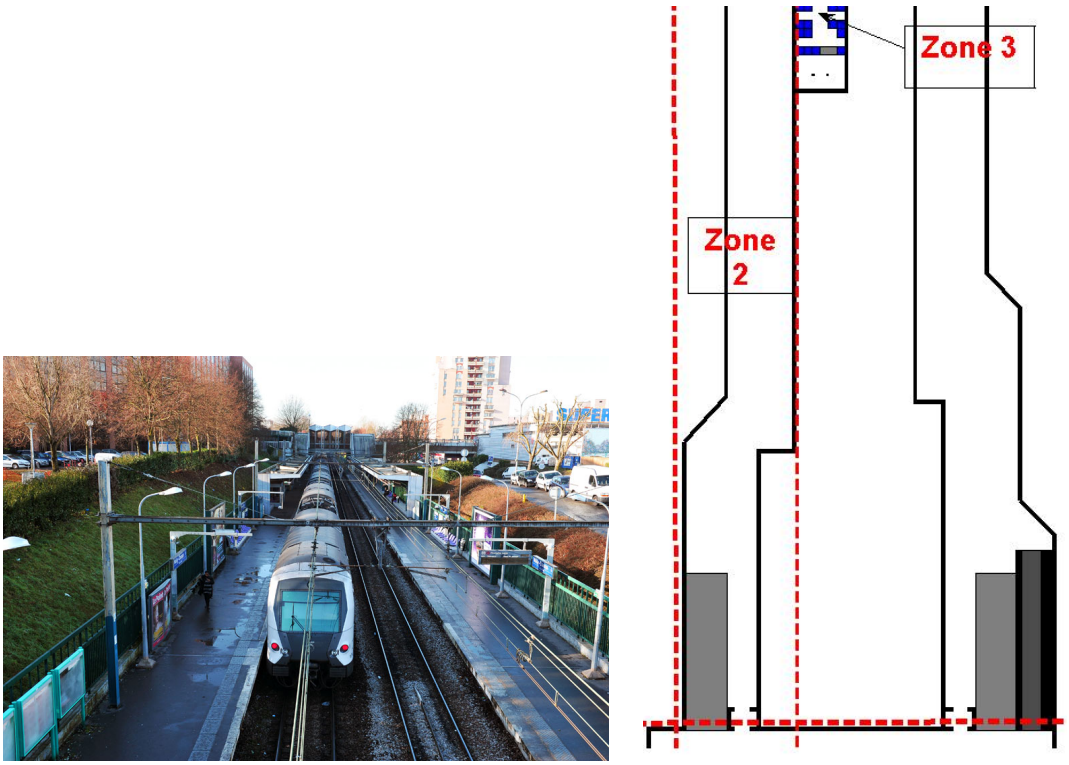

(a) (b)

Figure 7.6: Platform (direction Paris) of "Noisy-Champs": (a) real and (b) modeled.

way into the train. Next, they either search for a seating place or stay standing. Zone 3 is connected to Zone 2.

(a) (b)

Figure 7.7: Zone 3 which is the train (a) real and (b) modeled.

7.3 Activities

7.3.1 Zone 1

Pedestrians can enter the train station by one of the three available entrances (Zone 1-W, Zone 1-SE, and Zone 1-NE). In this zone, three main activities accompanied with three types of pedestrian behavior can be identified:

- Buy a ticket: type 1 queuing behavior (Fig. 7.8 a).
- Pass the turnstile: type 2 queuing behavior (Fig. 7.8 b).
- Head towards the train platform: navigation and avoidance behavior.

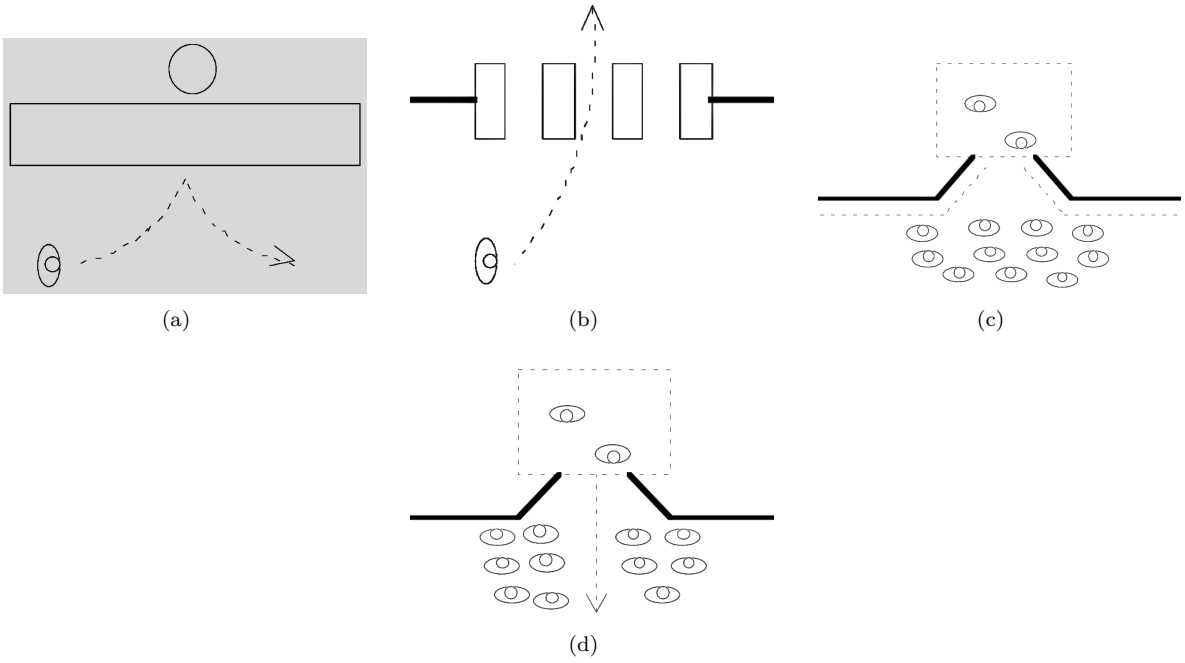

Figure 7.8: Queuing behavior: (a) type 1, (b) type 2, (c) type 3, and (d) type4).

Each of these types of pedestrian behavior can be modeled using one or a combination of the following methods: (i) floor fields, (ii) respect mechanism, and (iii) avoidance behavior based on heuristics. Fig 7.9 illustrates pedestrians entering the train station, standing in line to buy tickets, passing the turnstiles and heading to the train platform. We consider aggressive behavior (pushing or forcing one's way) to be rare at this stage and don't model it in this zone.

7.3.2 Zones 2 and 3

At this stage, pedestrians will either be waiting for the train on the platform (Zone 2) in order to board the train (Zone 3) or waiting in the train to alight. In these zones, 3 main activities can be identified:

- Finding a position on the platform to wait for the train: navigation and avoidance behavior
- Assembling next to the train's doors: type 3 a-b queuing behavior (Fig. 7.8 c,d)
- Boarding/alighting the train: navigation, avoidance or aggressive behavior

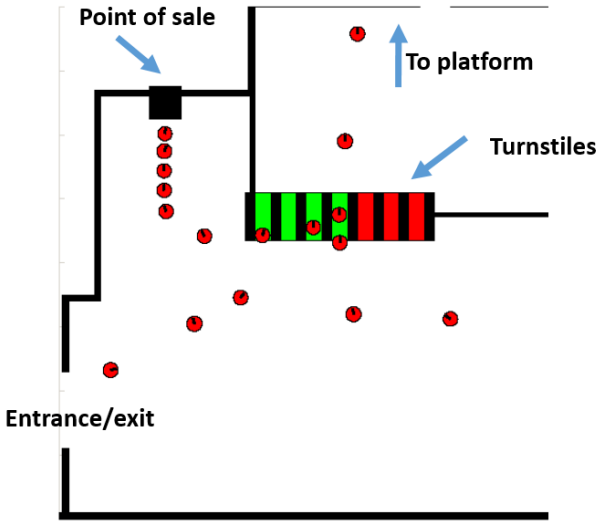

Figure 7.9: Pedestrians entering the train station, buying tickets, and passing the turnstiles to head to the platform.

The pedestrian behavior necessary to perform these activities is modeled using one or a combination of the following: (i) avoidance based on heuristics, (ii) avoidance based on repulsive forces or collision, and (iii) floor fields. Fig. 7.10 shows pedestrians waiting on the platform, waiting at the train's doors, and boarding/alighting. It should be note that repulsive forces or collision were used to model aggressive avoidance and pushing respectively [2]. This is especially observed during boarding/alighting.

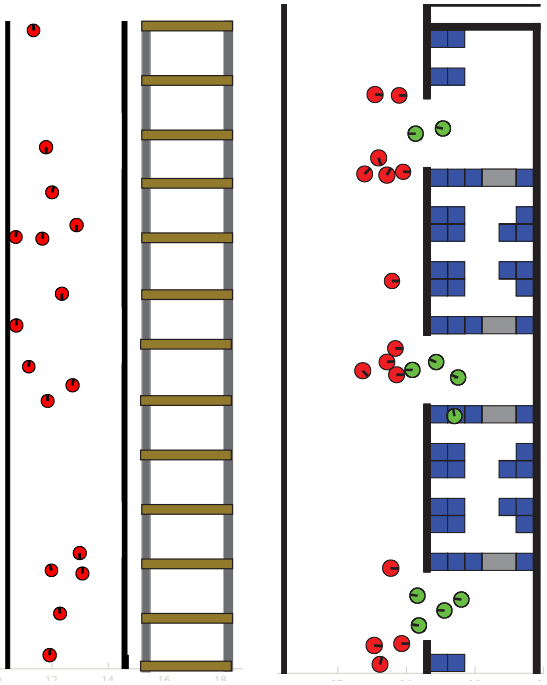

Figure 7.10: Pedestrians (a)waiting for the train on the platform and (b) boarding/alighting.

7.4 Traffic organization

The time interval between trains in a transit system is a very important factor influencing the inflow/outflow of pedestrians into the station and the timetables. This time interval is known as headway and is defined as:

$$H = \frac{60}{f} \tag{7.1}$$

where H is the headway in minutes and f the observed train frequency in one hour. Theoretically, 12 trains per hour should pass by "Noisy-Champs" station. However, Fig. 7.11 shows that actually this value is never attained.

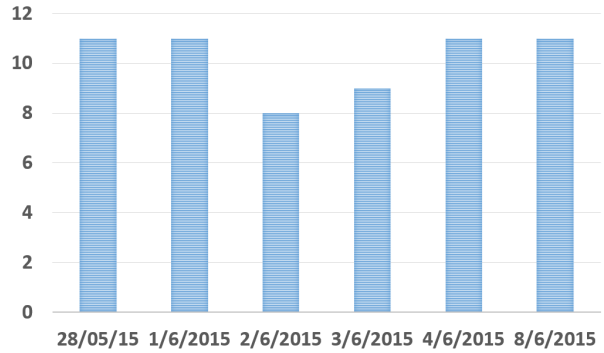

Figure 7.11: Train frequency for "Noisy-Champs" station.

The values of the train frequency from Fig. 7.11 give a mean value of 10 trains/hour. Using Eq. (7.1), the headway is then obtained, $H = 6\,min$. This value allows us to construct the simulation scenario (Fig. 7.12). The train arrives at the 4^{th} minute and the doors opens after 30 seconds. In these simulations, boarding time is attained when no passengers are present at a distance of $3\,m$ from the train's extremities. The next step is to add the pedestrian flow data.

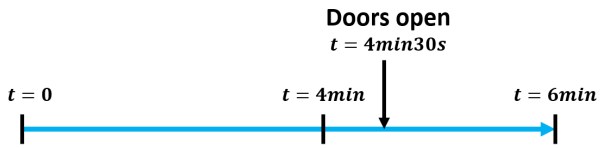

Figure 7.12: Simulation scenario.

7.5 Passenger flow

For a proper estimation of the train dwell times, it is important to have enough data concerning passenger flow volume and passenger characteristics. In the following section, we demonstrate how the pedestrians' enter and exit volume, repartition on the platform, and velocities were obtained.

7.5.1 Passenger demand

Passenger demand consists of knowing how many pedestrians will get off and on the train at the examined train station. To estimate the passenger flow during the morning rush hour for the east-west direction of the RER A the CapTA model has been used. CapTA is a model developed at the Laboratoire Ville Mobilité Transport (LVMT, or City, Mobility, Transport Laboratory) that aims to capture the capacity phenomena related with the vehicle seat capacity, the total capacity and the interplay of passenger flows

at access and egress with the dwell time and the service frequency [3]. It allows to estimate the passenger demand for each possible itinerary in a public transportation network. The CapTA model . Table 7.1 shows the origins and the number of passengers that will alight the train at "Noisy-Champs" (see Fig. 7.13). Table 7.2 shows the destinations and the number of passengers that will board the train at "Noisy-Champs" station (see Fig. 7.14).

Figure 7.13: Origins of passengers alighting the train at "Noisy-Champs".

Table 7.1: Flow of pedestrians alighting at "Noisy-Champs"

Station	**Train freq.**	**Flow** (per hour)	**Flow** (per train)
Marne-la-Vallée	7	115	16
Val d'Europe	7	49	7
Bussy-Saint-Georges	7	99	14
Torcy	14	161	12
Lognes	10	84	8
Noisiel	10	15	2
Total		**522**	**59**

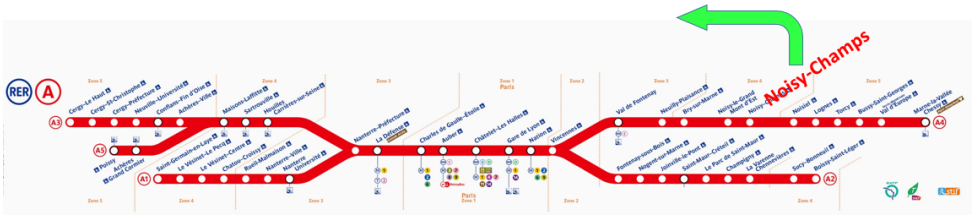

Figure 7.14: Destinations of passengers boarding the train at "Noisy-Champs".

7.5.2 Pedestrian distribution along the train platform

In order to determine the pedestrian distribution along the train platform, the train is divided into three zones (A,B, and C) as illustrated in Fig. 7.15. Then, for each zone and for each origin/destination, the percentage of passengers who alight/board was observed. Using these percentages along with the flow values per train from Tables 7.1 and 7.2, the pedestrian distribution along the train platform was obtained. Table 7.3 shows how many passengers get off the train at "Noisy-Champs". The same procedure was done for the passengers that get on the train at "Noisy-Champs", giving the following results: 39 for zone A, 184 for zone B, and 81 for zone C.

Table 7.2: Flow of pedestrians boarding at "Noisy-Champs"

Station	**Train freq.**	**Flow** (per hour)	**Flow** (per train)
Noisy-le-Grand	14	134	9
Bry-sur-Marne	5	0	0
Neuilly plaisance	9	34	4
Val de Fontenay	14	176	13
Vincennes	14	70	5
Nation	14	811	58
Gare de Lyon	14	446	32
Chatelet	14	629	45
Auber	14	699	50
Charles de Gaulle-Etoile	14	620	44
La Défense	14	438	31
Nanterre Pr.	7	19	3
Sartrouville	6	8	1
Achères Ville	4	15	1
Conflans- fin d'Oise	4	2	1
Neuville Univ.	4	2	1
Cergy Pref.	4	23	5
Cergy St. Chris.	4	5	1
Cergy le Haut	4	1	0
Total		**4117**	**304**

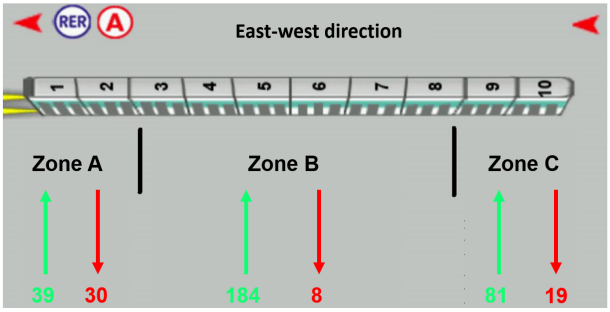

Figure 7.15: Pedestrian distribution along the train platform for "Noisy-Champs" train station for the east-west direction.

Table 7.3: Distribution of pedestrians alighting at "Noisy-Champs" for each of the three zones.

Station	**Flow** (per train)	**A**		**B**		**C**	
		Dist. (%)	**Flow** (per train)	**Dist.** (%)	**Flow** (per train)	**Dist.** (%)	**Flow** (per train)
Marne-la-Vallée	16	65	10.68	5	0.82	30	4.93
Val d'Europe	7	30	2.14	10	0.71	60	4.29
Bussy-St.-Georges	14	65	9.12	25	3.51	10	1.4
Torcy	12	55	6.33	13	1.5	22	2.53
Lognes	8	17	1.43	18	1.52	65	5.49
Noisiel	2	17	0.17	16	0.16	67	0.69
Total			**30**		**8**		**19**

7.5.3 Pedestrian enter volume

To estimate the pedestrian enter volume for the "Noisy-Champs" train station, the number of arriving passengers per minute was observed. This observation was performed during the morning rush hour

(7h30-8h30) for each train and for 4 consecutive days. An example of the observations for the eastern entrance is illustrated in Table 7.4.

Table 7.4: An example of the pedestrian enter volume from the eastern entrance of "Noisy-Champs" train station.

	Time	**Number of Arrivals**	**Counter**
	7h26	11	11
	7h27	6	17
	7h28	21	38
	7h29	7	45
	7h30	9	54
	7h31	7	61
	7h32	17	78
	7h33	45	123
Train doors close	7h34	15	**138**

By observing the rate of arriving passengers, it has been noticed that there were three main waves. For each wave, duration and velocity of pedestrians were measured. The obtained values are the following:

- **Wave 1**:
  - duration: 4 min
  - number of arriving passengers: 202
  - average velocity of pedestrians: 1.15 m/s for the eastern entrance and 0.95 m/s for the western entrance
- **Wave 2**:
  - duration: 1 min
  - number of arriving passengers: 51
  - average velocity of pedestrians: 1.91 m/s for the eastern entrance and 1.5 m/s for the western entrance
- **Wave 3**:
  - duration: 1 min
  - number of arriving passengers: 52
  - average velocity of pedestrians: 3.28 m/s for the eastern entrance and 2 m/s for the western entrance

By adding this data into the scenario (see Fig. 7.16), it is now possible to start simulations to estimate the train dwell time with out model.

7.6 Results

As we have already mentioned, the main objective of this study is to estimate the influence of pedestrian behavior at the platform-train interface on train traffic at the "Noisy-Champs" train station. In total, 10 simulations were performed. On average, 238 pedestrians managed to get on the train and 59 got off in 32 seconds. The obtained results were compared to observations (Table 7.5).

Other interesting results can be supplied by our model. In Fig. 7.17, the number of embarked and disembarked passengers along with the exchange time is plotted for each of the 30 doors of the train. This

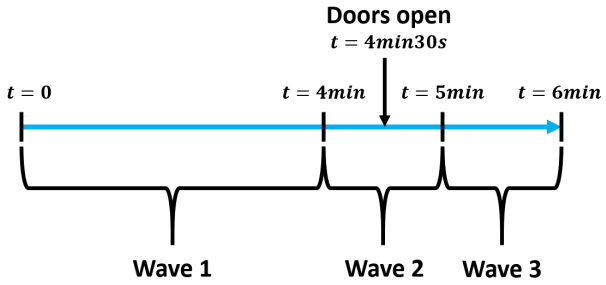

Figure 7.16: Simulation scenario with passenger flow data.

Table 7.5: Train dwell times in the "Noisy-Champs" station.

	Observations			Simulation
Embarked passengers	257	242	240	238
Disembarked passengers	57	28	64	59
Total	314	270	304	297
Dwell time (s)	**27**	**35**	**38**	**32**

could be a good indicator of the train dwell time. In Fig. 7.18, the pedestrian demand on the turnstiles of the south eastern part of the train station is calculated. This result can be analyzed to verify if the turnstile capacity have been reached or not. Unfortunately, there were no available observations in order to compare these results to.

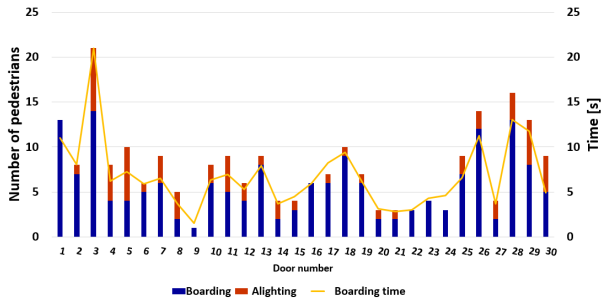

Figure 7.17: Number of embarked and disembarked passengers and the corresponding exchange time for each door of the train.

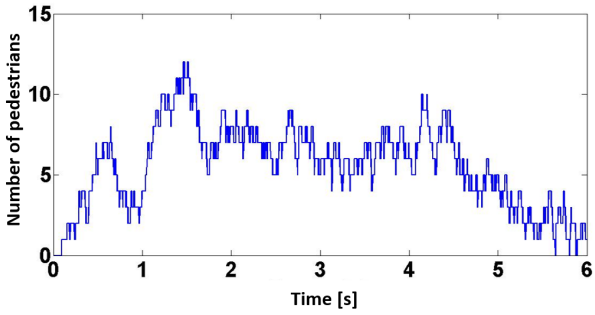

Figure 7.18: Demand on the turnstiles of the south eastern side of the train station.

7.7 Conclusion

We have presented in this chapter, a preliminary study on modeling pedestrian movement in the "Noisy-Champs" train station. The geometrical data obtained by measuring all the necessary dimensions of the station allowed us to create the simulation environment. Then by using the CapTA model, developed by the LVMT, and by observing the train traffic and the pedestrian flow, we were able to create the simulation scenarii. Several simulations were performed and the train dwell time was calculated. The simulation results were compared to observations and were shown to be satisfactory. Other results were obtained by our model but were not validated because of the lack of empirical data. These promising test results will allow us to further develop the study by considering additional pedestrian characteristics such as their age, size, aggressiveness, etc. We can also further expand the studied area by integrating the bus arrivals to the "Noisy-Champs" train station. This will allow us to study the efficiency of intermodality (combining several means of transport during the same journey) at "Noisy-Champs". It is also interesting to consider other train stations that are more complex (number of lines, several modes of transportation, geometry, etc.) than "Noisy-Champs".

Bibliography

[1] S. Mokhtari, Z. Christoforou, F. Leurent, B. Kabalan, P. Argoul, and G. Cumunel, "Crowd dynamics and pedestrian trajectories in public transit," in *Railway Stations and Urban Integration' 5th NEXTSTATION CONGRESS*, (Marrakech, Morocco), 2015.

[2] B. Kabalan, P. Argoul, A. Jebrane, G. Cumunel, and S. Erlicher, "A crowd movement model for pedestrian flow through bottlenecks," *Annals of Solid and Structural Mechanics*, Accepted.

[3] E. Chandakas, F. Leurent, and A. Poulh
'es, "Les contraintes de capacité dans les trafics de voyageurs et de véhicules en transport collectif: un modèle de simulation et son application au Grand Paris," pp. 1–10, Congrès ATEC ITS France 2014 : Les Rencontres de la Mobilité Intelligente, 2014.

Chapter 8

Modeling the lateral pedestrian force on a rigid floor by a self-sustained oscillator

Contents

8.1 Introduction

The modeling of walking and running phenomena is an important subject of investigation in several research fields, from bio-mechanics to robotics and cybernetics; from medical applications to the analysis of the crowd-structure dynamical interaction in civil engineering. Depending on the saught refinement level, several approaches can be used. For instance, in the most complex models, the movement is studied in the three-dimensional space. In some other cases [1, 2], only the vertical 1D motion of the main parts of the body is studied. In other articles, e.g. [3, 4] , only the lateral direction is analyzed (in the frontal plane, orthogonal to the direction of progression).

A hybrid version of the Van der Pol self-sustained oscillator has been developed in [5] in order to model the lateral walking force of a pedestrian. First of all, the Fast Fourier Transform is used to illustrate the quasi-periodicity of the lateral force. This allows us to write the latter under the form of a Fourier series of odd harmonic cosines only. Next, based on the shape of the force-velocity relationship and the phase plot, a modified Van der Pol oscillator (mVdP) is proposed. Then, the parameters of the mVdP oscillator are identified by using the method of least squares. Last, the use of the method is validated by comparing the results obtained using the mVdP oscillator with the periodical approximation of the measured lateral walking force.

In [5], the previously described method was applied for 12 pedestrians walking at 4 different velocities between $3.75\,km/h$ and $6\,km/h$. In this work, we will reapply the method for 31 participants (20 males and 11 females) and for 4 different walking velocities (between $1.87\,km/h$ and $3.35\,km/h$). This will allow us to further validate the proposed model and to identify if there is a difference between the way the two genders walk. These 31 participants participated in an experiment conducted by the University of Sheffield to measure the pedestrian force on a rigid floor.

8.2 Modeling the lateral walking force of a pedestrian on a rigid floor

The lateral walking force of a pedestrian on a rigid floor have been measured for several pedestrians as a part of an experiment conducted at the University of Sheffield. The experimental data were analyzed in order to determine certain aspects of the walking movement and model the resulting force. In what follows, the experiment is described. Then the data processing is illustrated. Finally, the obtained results are presented.

8.2.1 Description of the laboratory experiment

In the experiment, the participants were asked to walk for a certain time duration on a treadmill adjusted to a certain velocity (see Fig. 8.1). The vertical, lateral and longitudinal components of the force applied by the pedestrian on the treadmill were then measured by four Kistler 9077B three-axial piezoelectric force sensors using a sampling frequency of $200\,Hz$ [6]. Each participant repeated the same activity for several velocities (between $1.87\,km/h$ and $9\,km/h$). It is interesting to note that the majority of people usually walk comfortably at an average velocity of $v_M = 5km/h$ [7]. The characteristics of the male and female participants are illustrated in Table 8.1 and Table 8.2. BMI (kg/m^2), which is the body mass index, will be used in plotting the different parameters related to the lateral walking force. To avoid confusion, we refer to a male or a female participant by adding the letters "msc" and "fmn" respectively.

8.2.2 Fourier analysis of the lateral walking force

To examine their periodicity, the Fast Fourier Transform (FFT) was used to analyze the experimental signals. The expression of the FFT is defined by :

$$\hat{F}_y(r) = \frac{2}{\tilde{N}} FFT(F_{y,\tilde{N}}, \tilde{N}) \;\; r = 1, ..., \tilde{N} \tag{8.1}$$

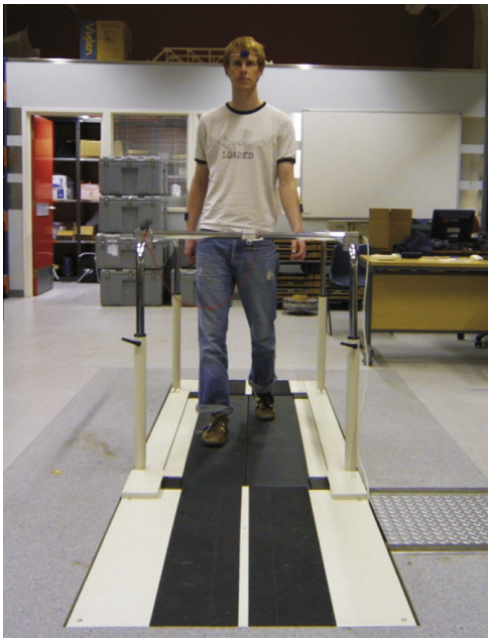

Figure 8.1: Experimental setup [6].

Table 8.1: Mass and height of the 20 male participants.

Participant	**1**	**2**	**3**	**4**	**5**	**6**	**7**	**8**	**9**	**10**
Mass (kg)	67.5	81.6	81.2	86.6	89.9	86.3	79.6	63.3	89.8	81.7
Height (cm)	180	175	180	173	174	188	173	188	180	175
BMI (kg/m^2)	20.83	26.64	25.06	28.94	29.69	24.4	26.6	17.91	27.72	26.68
Participant	**11**	**12**	**13**	**14**	**15**	**16**	**17**	**18**	**19**	**20**
Mass (kg)	77.1	94.8	80.3	69.2	95.9	68.1	75.4	82.7	73.2	79.8
Height (cm)	173	173	173	176	183	175	167	178	175	181
BMI (kg/m^2)	25.76	31.67	26.83	22.34	28.64	22.24	27.04	26.1	23.9	24.36

where $F_{y,\tilde{N}}$ represents the measured signal in the interval $[t_{n_1}, t_{n_2}]$ subtracted by its mean and $\tilde{N} = n_2 - n_1 + 1$. The interval can be modified in order to obtain an integer value of periods. The expression $FFT(F_{y,\tilde{N}}, \tilde{N})$ refers to the FFT function in MATLAB.

Eq.(8.1) was applied to the measured signals. By plotting modulus of $\hat{F}_y$ against the frequencies given by $\tilde{f}_r = (r-1)/(\tilde{N}\Delta t)$, it can be noticed that the equally spaced peaks, corresponding to frequencies less than $15\,Hz$, are odd multiples of the fundamental one f_1 (ratios 3,5,7,9,...). For example, the modulus of $\hat{F}_y$ for the lateral walking force of pedestrians 1-msc and 1-fmn are illustrated in Fig. 8.2 and 8.3 respectively. It can be seen that the main peaks correspond to the harmonics of order 1,3,5,7, and 9. Therefore, the signal can be considered nearly periodic with small even harmonics (see also [8–10]) and a fundamental frequency f_1. The lateral walking force can then be written under the following form :

$$F_y(t) \simeq F_y^{(\infty)}(t) = \sum_{i=1}^{+\infty} C_i cos(2\pi i f_1 t - \varphi_i) \tag{8.2}$$

By defining $\tilde{t} = t - t_0$, we can compare more easily the Fourier series of the signal representing $F_y(t)$. Eq. (8.2) is now given by:

Table 8.2: Mass and height of the 11 female participants.

Participant	**1**	**2**	**3**	**4**	**5**	**6**	**7**	**8**	**9**	**10**	**11**
Mass (kg)	55.8	59.6	57.3	50.7	61.9	49.7	49.1	54.5	69.9	55.9	71.6
Height (cm)	160	160	170	160	171	163	158	166	165	165	160
BMI (kg/m^2)	21.8	23.28	19.83	21.17	18.7	19.67	19.78	25.67	20.53	27.97	

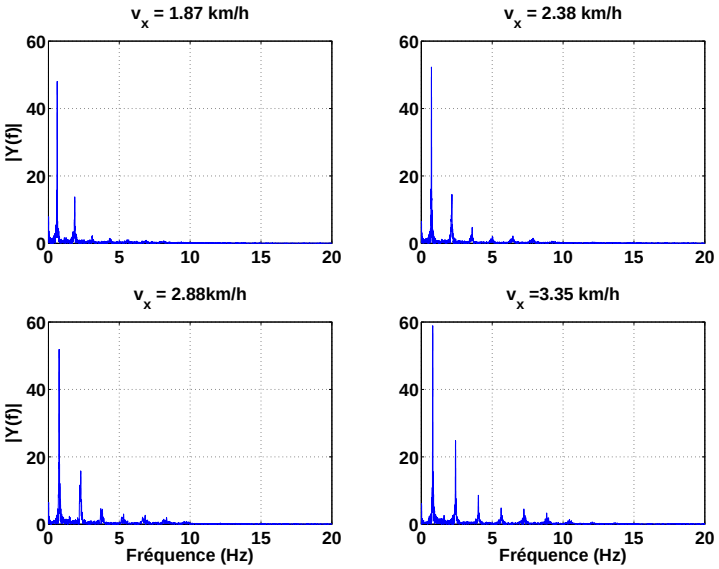

Figure 8.2: Modulus of $\hat{F}_y$ (Eq.(8.1)) for the lateral force of pedestrian 1-msc for different walking velocities.

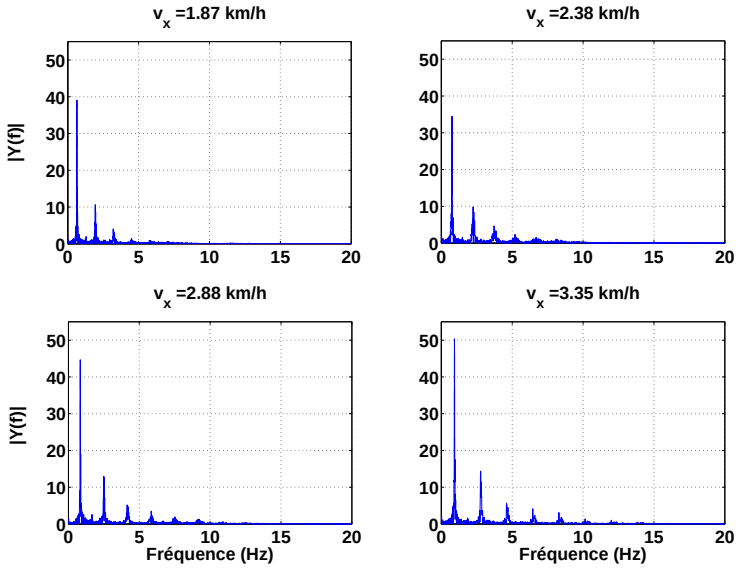

Figure 8.3: Modulus of $\hat{F}_y$ (Eq.(8.1)) for the lateral force of pedestrian 1-fmn for different walking velocities.

$$\tilde{F}_y^{(\infty)}(\tilde{t}) = F_y^{(\infty)}(\tilde{t}+t_0) = \sum_{i=1}^{+\infty} C_i cos(2\pi i f_1 \tilde{t} - \Delta\varphi'_{1,i}) \tag{8.3}$$

where $\Delta\varphi'_{1,i} = \varphi_i - 2\pi i f_1 t_0$ for $i \geq 1$. By choosing $t_0 = \varphi_1/2\pi f_1$ ($\Delta\varphi'_{1,1} = 0$), Eq. (8.3) becomes:

$$\tilde{F}_y^{(\infty)}(\tilde{t}) = C_1 cos(2\pi f_1 \tilde{t}) + \sum_{i=2}^{+\infty} C_i cos(2\pi i f_1 \tilde{t} - \Delta\varphi_{1,i}) \tag{8.4}$$

where $\Delta\varphi_{1,i} = \Delta\varphi'_{1,i} + k'2\pi$ and k' ,that depends on i, ensures that $\Delta\varphi_{1,i} \in [0, 2\pi)$. Fig. 8.2 and 8.3 show that the principal harmonics are the odd ones up to the 9^{th} order. We can then estimate the lateral force by a Fourier series given by :

$$F_y(t) \simeq F_y^{(5)}(t) = C_1 cos(2\pi f_1 t) + \sum_{i=2}^{5} C_{2i-1} cos(2\pi(2i-1) f_1 t - \Delta\varphi_{1,2i-1}) \tag{8.5}$$

The measured force $F_y(t)$ and its periodic approximation $F_y^{(5)}(t)$ are plotted and compared in Fig. 8.4 and 8.5 for pedestrians 1-msc and 1-fmn respectively. The quality of the fitting is rather good. Similar plots have been obtained for the other pedestrians.

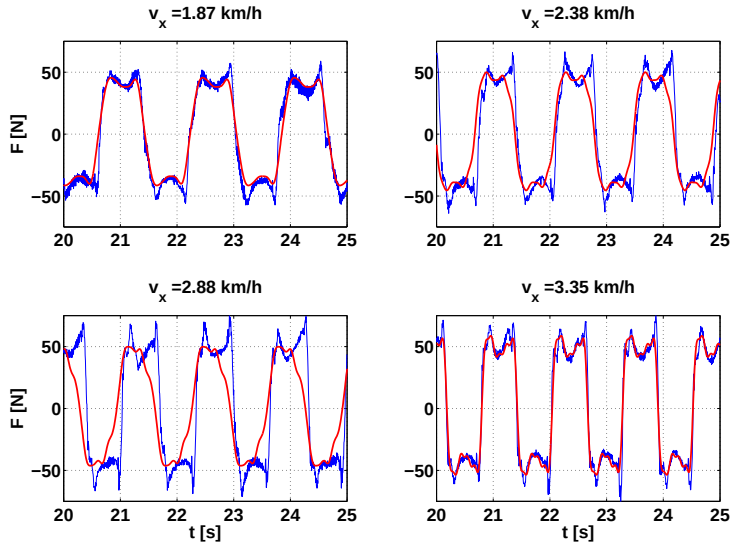

Figure 8.4: Time-histories of the lateral force of pedestrian 1-msc for different walking speeds. Experimental results (thin line) vs. truncated Fourier Series (Eq. 8.5, thick line).

In MATLAB, $\hat{F}_y(m)$ (Eq. (8.1)) is obtained under the form of a column of complex numbers representing the harmonics. The magnitudes of these numbers gives the amplitudes of the harmonics. The fundamental frequency f_1 is the one corresponding to the harmonic having the maximum amplitude. The amplitudes of the odd harmonics are the ones corresponding to the odd multiples of f_1 ($3f_1$, $5f_1$,...). As for the phase, it is calculated using the function $atan2$ in MATLAB:

$$\phi_i = atan2(-Im_i, Re_i) \tag{8.6}$$

where Im_i and Re_i are the imaginary and real parts of the complex number representing the harmonics. The fundamental frequency, the amplitudes, and the phase differences (see Eqs. (8.2-8.4)) of participants 1-msc and 1-fmn obtained by Fourier analysis are illustrated in Tables 8.3 and 8.4 respectively. Then, the average values for the 20 male and 11 female participants are given in Tables 8.5 and 8.6 respectively. They show that the female participants have a higher lateral walking frequency and lower

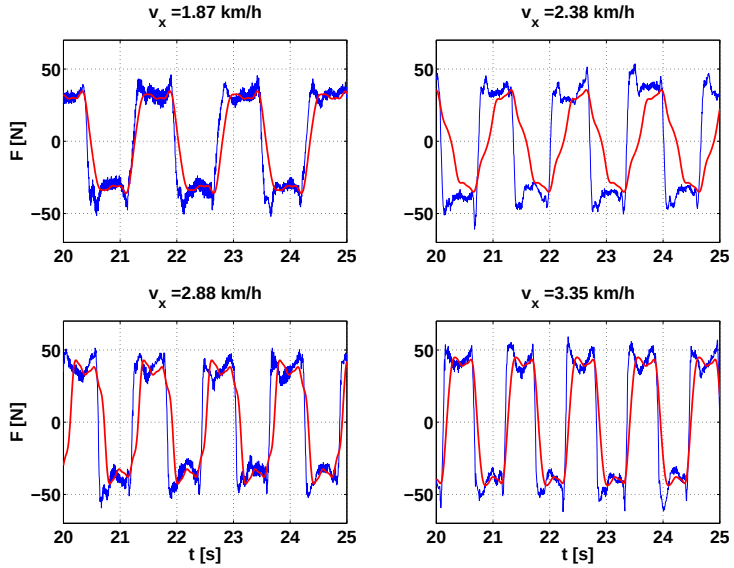

Figure 8.5: Time-histories of the lateral force of pedestrian 1-fmn for different walking speeds. Experimental results (thin line) vs. truncated Fourier Series (Eq. 8.5, thick line).

harmonic amplitudes for the four velocities. Since the female participants have a lower average height ($163.5\,cm$) than the male participants ($177\,cm$), it is possible that the walking frequency decreases with the height of the person. As for the harmonic amplitudes, their values decrease when the harmonic rank increases and increase when the walking velocity increases. Regarding the phase difference $\Delta\phi_{1,3}$, it is smaller for the male pedestrians. It can be noticed that the fundamental frequency and the harmonic amplitudes are correlated to the walking velocity whereas the phase difference is not. Moreover, the dynamic load factors were calculated for the odd harmonics up to the 9^{th} order for four walking velocities. These factors are given by:

$$DLF_k = (1/N_p)\sum_{j=1}^{N_p} C_{2k-1}^{(j)}/(m^{(j)}g) \tag{8.7}$$

where N_p is the total number of participants, m is the mass of pedestrian j, g is gravity and k is the harmonic rank. The obtained DLF values for the male and female participants are illustrated in Tables 8.7 and 8.8 respectively. We can notice that female participants have a higher DLF_1 than their male counterparts.

Table 8.8: Fourier analysis of the lateral walking force for the female pedestrians : the average values of the dynamic load factors (DLF) of the odd harmonics up to the 9^{th} order for 4 different walking velocities.

	1.87 km/h	**2.38 km/h**	**2.88 km/h**	**3.35 km/h**
$C_1/(mg)$ (%)	6.42	7.03	7.85	8.27
$C_3/(mg)$ (%)	1.31	1.34	2.37	2.44
$C_5/(mg)$ (%)	0.27	0.42	0.6	0.59
$C_7/(mg)$ (%)	0.12	0.2	0.31	0.22
$C_9/(mg)$ (%)	0.08	0.10	0.18	0.10

Fig. 8.6 (a) and (b) illustrate the lateral walking frequencies for all the participants. It is obvious that the fundamental frequency increases as the walking velocity increases. Fig. 8.7 and 8.8 give the values of C_1, C_2 and $\Delta\phi_{1,3}$ for all the pedestrians and all the walking velocities. It can be noticed that the average value of $\Delta\phi_{1,3}$ for all pedestrians and all of the 4 walking velocities is very close to π.

Table 8.3: Fourier series for pedestrian 1-msc : fundamental frequency, amplitudes and phase difference for the odd harmonics up to the 9^{th} order for four walking velocities.

	1.87 km/h	**2.38 km/h**	**2.88 km/h**	**3.35 km/h**
f_1 (Hz)	0.618	0.714	0.754	0.806
C_1 (N)	48.0	52.3	51.9	58.8
C_3 (N)	13.5	11.8	6.9	24.7
C_5 (N)	2.1	1.7	3.6	8.6
C_7 (N)	1.0	1.6	1.1	4.7
C_9 (N)	0.6	1.4	0.8	3.8
$\Delta\phi_{1,3}$ (rad)	3.30	3.31	3.81	3.22
$\Delta\phi_{1,5}$ (rad)	5.81	1.17	1.93	0.25
$\Delta\phi_{1,7}$ (rad)	1.07	3.96	3.96	3.03
$\Delta\phi_{1,9}$ (rad)	3.33	0.69	4.74	6.19

Table 8.4: Fourier series for pedestrian 1-fmn : fundamental frequency, amplitudes and phase difference for the odd harmonics up to the 9^{th} order for four walking velocities.

	1.87 km/h	**2.38 km/h**	**2.88 km/h**	**3.35 km/h**
f_1 (Hz)	0.647	0.754	0.834	0.929
C_1 (N)	39.06	34.47	44.62	50.36
C_3(N)	10.67	0.78	12.95	13.65
C_5 (N)	2.43	3.55	3.99	2.37
C_9 (N)	0.78	0.74	1.64	0.45
$\Delta\phi_{1,3}$ (rad)	3.17	2.99	3.36	3.23
$\Delta\phi_{1,5}$ (rad)	5.78	2.13	1.29	6.08
$\Delta\phi_{1,7}$ (rad)	1.17	4.56	4.78	1.81
$\Delta\phi_{1,9}$ (rad)	2.88	4.78	1.73	3.45

Table 8.5: Fourier analysis of the lateral walking force for the male participants: average values and standard deviations of the fundamental frequency, amplitudes and phase differences of the odd harmonics up to the 9^{th} order for 4 walking velocities.

	1.87 km/h		**2.38 km/h**		**2.88 km/h**		**3.35 km/h**	
	av.	s.d	av.	s.d	av.	s.d	av.	s.d
f_1 (Hz)	0.625	0.054	0.695	0.065	0.760	0.066	0.823	0.052
C_1 (N)	49.45	6.8	56.07	10.41	59.63	9.18	63.02	10.04
C_3(N)	8.97	5.12	14.41	5.87	15.48	6.92	22.41	9
C_5 (N)	1.77	0.98	3.43	2.14	4.85	2.75	7.83	4.27
C_7 (N)	0.93	0.38	1.47	0.64	2.19	1.23	4.05	2.11
C_9 (N)	0.67	0.29	1.14	0.61	1.29	0.81	2.25	1.27
$\Delta\phi_{1,3}$ (rad)	2.99	0.78	2.91	0.72	3.04	0.61	3.06	0.72
$\Delta\phi_{1,5}$ (rad)	3.63	2.37	3.29	2.54	2.44	2.1	1.72	2.1
$\Delta\phi_{1,7}$ (rad)	2.81	1.69	3.07	1.58	2.82	1.58	3	1.39
$\Delta\phi_{1,9}$ (rad)	3.36	1.75	2.99	2.04	3.2	1.94	2.78	2.34

By comparing the results obtained in this study with the ones obtained in [5], we have found qualitative similarities and quantitative differences. For example, both studies showed that the walking frequency

Table 8.6: Fourier analysis of the lateral walking force for the female participants: average values of the fundamental frequency, amplitudes and phase differences of the odd harmonics up to the 9^{th} order for 4 walking velocities.

	1.87 km/h		**2.38 km/h**		**2.88 km/h**		**3.35 km/h**	
	av.	s.d	av.	s.d	av.	s.d	av.	s.d
$f_1(Hz)$	0.681	0.14	0.758	0.12	0.837	0.098	0.892	0.079
C_1 (N)	37.09	9.31	40.63	9.68	45.39	10.62	47.80	9.63
C_3 (N)	7.59	3.47	7.77	6.5	13.72	6.65	14.11	6.66
C_5 (N)	1.58	0.79	2.41	1.99	3.47	2.59	3.4	1.35
C_7 (N)	0.72	0.3	1.17	1	1.77	1.05	1.27	0.87
C_9 (N)	0.45	0.3	0.59	0.3	1.05	0.63	0.58	0.43
$\Delta\phi_{1,3}$ (rad)	3.65	0.94	3.16	0.63	3.34	0.26	3.30	0.15
$\Delta\phi_{1,5}$ (rad)	2.95	2.12	3.14	2.01	2.98	2.63	2.29	2.5
$\Delta\phi_{1,7}$ (rad)	3.35	1.98	3.02	1.85	3.33	1.77	2.89	1.42
$\Delta\phi_{1,9}$ (rad)	3.43	1.74	3.98	1.66	3.56	1.98	2.51	2.22

Table 8.7: Fourier analysis of the lateral walking force for the male pedestrians: the average values of the dynamic load factors (DLF) of the odd harmonics up to the 9^{th} order for 4 different walking velocities.

	1.87 km/h	**2.38 km/h**	**2.88 km/h**	**3.35 km/h**
$C_1/(mg)$ (%)	6.17	6.99	7.43	7.86
$C_3/(mg)$ (%)	1.12	1.8	1.93	2.79
$C_5/(mg)$ (%)	0.22	0.43	0.61	0.98
$C_7/(mg)$ (%)	0.12	0.18	0.27	0.51
$C_9/(mg)$ (%)	0.08	0.14	0.16	0.28

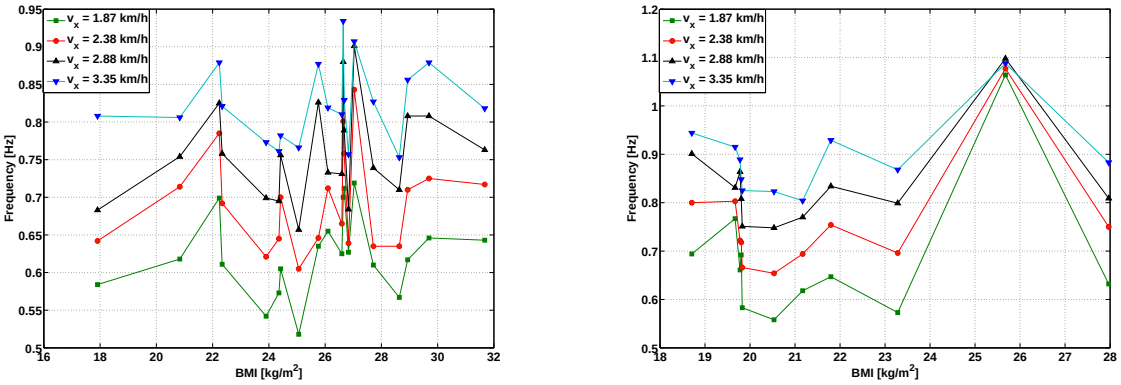

(a) (b)

Figure 8.6: Walking frequency for all (a) the male and (b) female participants.

and the amplitudes of the odd harmonics increase with increasing walking velocity. Moreover, it was found in both studies that the amplitudes of the harmonics decrease rapidly as we increase the harmonic rank. On the other hand, the values of the amplitudes that were found in this work are different than the ones in [5]. We have found the average value of C_1 for $v_x = 3.35\,km/h$ to be $63\,N$ for the male participants and $47.8\,N$ for the female ones. For a velocity higher than $v_x = 3.35\,km/h$ we expect a value of C_1 higher than $63\,N$ for male participants and $47.8\,N$ for female ones. However, in [5], $C_1 = 39.3\,N$

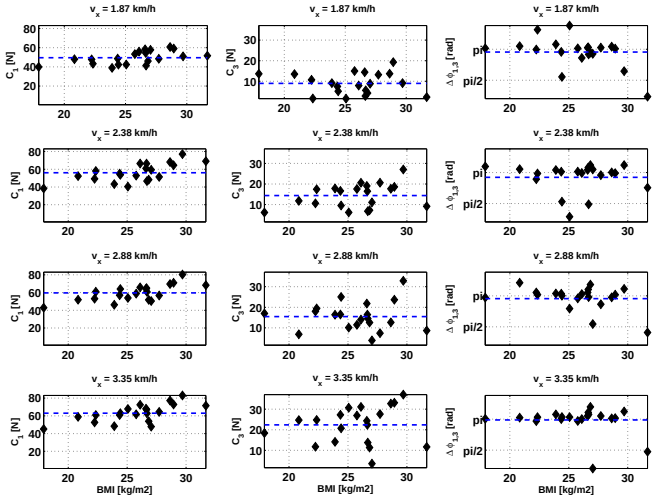

Figure 8.7: Fourier series approximation of the lateral walking force of the male participants: the amplitudes C_1, C_3, and the phase difference $\Delta\varphi_{1,3}$. The average values are represented by the dotted lines.

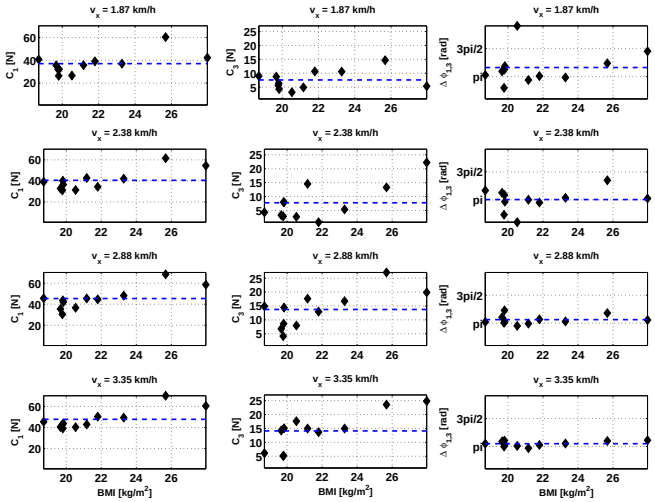

Figure 8.8: Fourier series approximation of the lateral walking force of the female participants: the amplitudes C_1, C_3, and the phase difference $\Delta\varphi_{1,3}$. The average values are represented by the dotted lines.

for $v_x = 6.0\,km/h$.

8.2.3 Study of the pedestrian lateral force as a function of displacement and velocity

By using Eq.(8.5), we can obtain an estimation of the lateral acceleration of a pedestrian of mass m:

$$\ddot{u}_y(t) \simeq \ddot{u}_y^{(5)}(t) = -\frac{F_y^{(5)}(t)}{m} = -\frac{\alpha_1}{m}cos(2\pi f_1 t) - \frac{1}{m}\sum_{i=2}^{5}\alpha_{2i-1}cos(2\pi(2i-1)f_1 t - \Delta\varphi_{1,2i-1}) \quad (8.8)$$

By integrating Eq. (8.8) successively, we obtain the expressions of the lateral velocity and displacement of a pedestrian:

$$\dot{u}_y(t) \simeq \dot{u}_y^{(5)}(t) = -\frac{\alpha_1}{2\pi m f_1}sin(2\pi f_1 t) - \frac{1}{m}\sum_{i=2}^{5}\frac{\alpha_{2i-1}}{2\pi(2i-1)f_1}sin(2\pi(2i-1)f_1 t - \Delta\varphi_{1,2i-1}) \quad (8.9)$$

$$u_y(t) \simeq u_y^{(5)}(t) = -\frac{\alpha_1}{m(2\pi f_1)^2}cos(2\pi f_1 t) + \frac{1}{m}\sum_{i=2}^{5}\frac{\alpha_{2i-1}}{(2\pi(2i-1)f_1)^2}cos(2\pi(2i-1)f_1 t - \Delta\varphi_{1,2i-1}) \quad (8.10)$$

Fig. 8.9 and 8.10 show the evolution of $\ddot{u}_y(t)$, $\dot{u}_y(t)$ and $u_y(t)$ for the pedestrians 1-msc and 1-fmn respectively. The evolution of $u_y(t)$ seems to be close to that of a pure cosine. The amplitude of the maximum displacement is plotted as a function of the walking velocities for the 20 male and 11 female participants (Fig. 8.11 (a) and (b) respectively). We note that the amplitudes decrease with increasing walking velocity. We can also notice that the values of the maximum displacement of the male participants fluctuates much more than those of the female pedestrians.

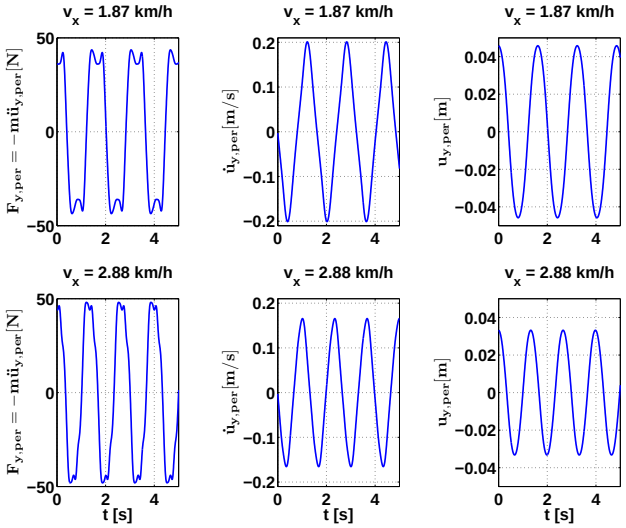

Figure 8.9: Fourier series for 2 different walking velocities for pedestrian 1-msc : the lateral force $F_y(t)$ (left), the lateral velocity $v_y(t) = \dot{u}_y(t)$ (center), and the lateral displacement $u_y(t)$ (right)

In [5], it was found that the maximum and minimum of the velocity $\dot{u}_y(t)$ in the phase plot will be in the second and fourth quadrants if $\Delta\phi_{1,3} \lesssim \pi$ ($\lesssim$ is used instead of $\leq$ since all the experimental values of $\Delta\phi_{1,3}$ have been found close to π as illustrated in Fig. 8.7 and 8.8). This implies that the pedestrian's foot touches the floor before the pedestrian arrives to his reference vertical configuration ($u_y = 0$). If $\Delta\phi_{1,3} \gtrsim \pi$, the maximum and minimum of the velocity $\dot{u}_y(t)$ in the phase plot will be in the first and third quadrants, implying that the pedestrian's foot touches the floor after the pedestrian arrives to his vertical configuration ($u_y = 0$). Fig. 8.12 and 8.13 represent the phase plots and the 3D parametric plots "displacement-velocity-force" for pedestrians 1-msc and 1-fmn. In both figures, the maximum and minimum of $\dot{u}_y(t)$ are in the first and third quadrants because $\Delta\phi_{1,3}$ is always greater than π (see Tables 8.3 and 8.4).

The phase plots of all the pedestrians are also given for 4 walking velocities (Fig. 8.14 (a) and (b)). It can be noticed that the displacement decreases with increasing walking velocity. We can also remark that

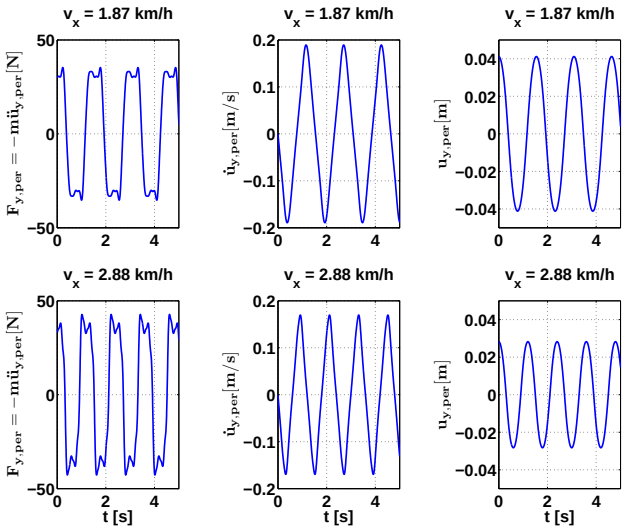

Figure 8.10: Fourier series for 2 different walking velocities for pedestrian 1-fmn : the lateral force $F_y(t)$ (left), the lateral velocity $v_y(t) = \dot{u}_y(t)$ (center), and the lateral displacement $u_y(t)$ (right)

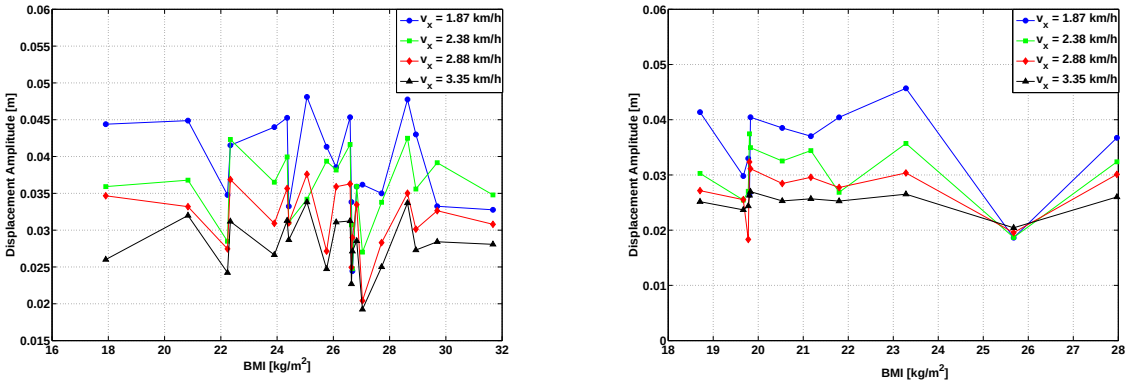

(a) (b)

Figure 8.11: Amplitude of the maximum displacement for 4 different walking velocities for (a) the male and (b) female participants.

the limit cycle in the phase plot tends to converge for the considered velocities for the female participants. We cannot say the same for the male pedestrians.

8.2.4 A self sustained oscillator for the modeling of the lateral pedestrian force

In this paragraph, we test the validity of the hybrid Van der Pol/Rayleigh oscillator developed in [5] to model the lateral walking force of a pedestrian. In [5], two aspects of the lateral walking force inspired the authors to use a self-sustained oscillator to model it. The first one is to consider the lateral force $F_y(t)$, the displacement $u_y(t)$, and the velocity $\dot{u}_{y(t)}$ as nearly periodic time signals. The second one is that pedestrians self-sustain their motion during walking, i.e. they produce their own energy needed for walking [5]. Therefore, it was decided to use a self-sustained oscillator satisfying the following criteria:

- has an equation of motion given by Eq. 8.11 and a restoring force given by Eq. 8.12 with

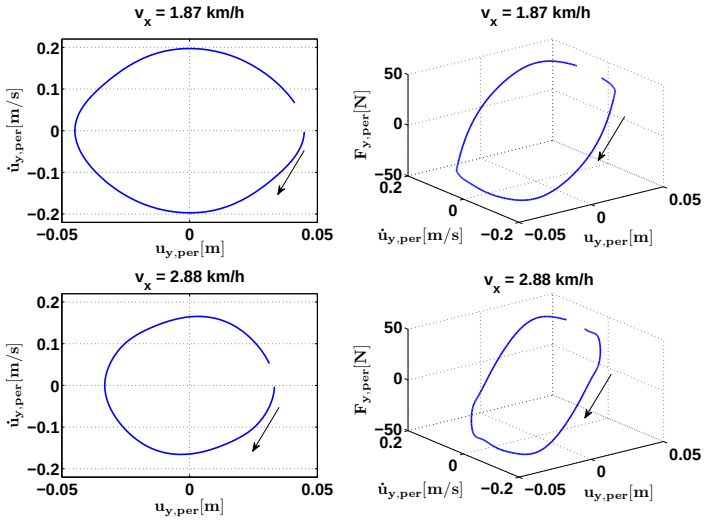

Figure 8.12: Fourier series approximation of the lateral force, velocity and displacement for pedestrian 1-msc for two walking velocities.The phase plot (left) and the lateral force as a function of displacement and velocity (right).

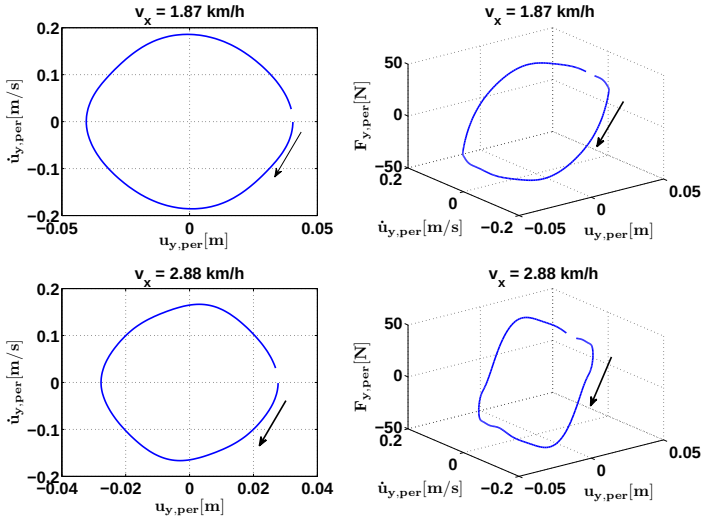

Figure 8.13: Fourier series approximation of the lateral force, velocity and displacement for pedestrian 1-fmn for two walking velocities.The phase plot (left) and the lateral force as a function of displacement and velocity (right).

$h(u_y(t), \dot{u}_y(t))$ under polynomial form.

$$m\ddot{u}_y(t) + F_y(u_y(t), \dot{u}_y(t)) = 0 \tag{8.11}$$

$$F_y(u_y(t), \dot{u}_y(t)) = 2\mu m\omega_0 \dot{u}_y(-1 + h(u_y(t), \dot{u}_y(t))) + m\omega_0^2 u_y \tag{8.12}$$

where μ is strictly positive, $\omega_0 > 0$ is the circular frequency of the underlying linear system and m the mass of a pedestrian.

- has a stable limit cycle

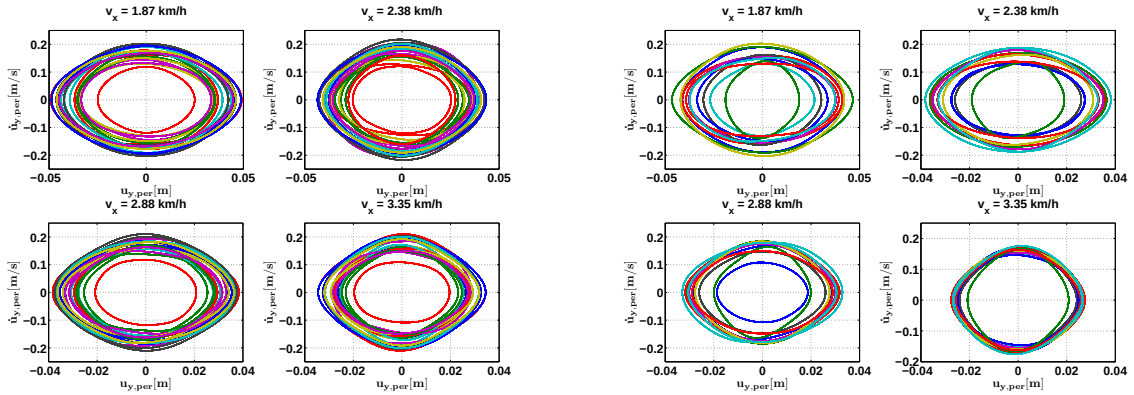

(a) (b)

Figure 8.14: Experimental phase plots for 4 different walking velocities of (a) the male and (b) female participants.

- has a limit cycle whose shape and size is close to the periodic orbits in the phase-plane obtained from the analysis of the experimentally measured lateral forces (Fig. 8.12 and 8.13). In addition, along the limit cycle, F_y should be close to the experimental forces (Fig. 8.12 and 8.13).

After having examined the phase and force plots of the Van der Pol/Rayleigh oscillator and the experimental measurements, a hybrid Van der Pol/Rayleigh oscillator with an additional term $F_\gamma = m2\gamma u_y \dot{u}_y^2$ was proposed where γ is any real. The additional term is responsible for the softening effect observed in the shape of the lateral force for the largest displacement amplitudes (Fig. 8.15 and 8.16). As a result, the restoring force of this hybrid oscillator is given by :

$$F_y(u_y, \dot{u}_y, \mu, \omega_0, \beta, \gamma, \delta) = 2\mu\omega_0 m\dot{u}_y(-1 + \beta u_y^2 + \frac{\gamma}{\omega_0} u_y\dot{u}_y + \frac{\delta}{\omega_0^2}\dot{u}_y^2) + m{\omega_0}^2 u_y \tag{8.13}$$

where $\beta \geq 0$, $\delta \geq 0$ with $\beta + \delta \neq 0$, γ is a real number, $\omega_0 > 0$ and $\mu > 0$. By inserting Eq. 8.13 in Eq. 8.11, we obtain :

$$\ddot{u}_y(t) - 2\mu\omega_0 m\dot{u}_y(1 - \beta u_y^2 - \frac{\gamma}{\omega_0} u_y\dot{u}_y - \frac{\delta}{\omega_0^2}\dot{u}_y^2) + m{\omega_0}^2 u_y = 0 \tag{8.14}$$

In order to calculate the parameters of the mVdP model, a least squares identification procedure is used [5]. To do so, Eq. 8.13 is rewritten under the following form:

$$F = F(u_y, \dot{u}_y, b) = b_1 u_y + b_2\dot{u}_y + b_3 {u_y}^2\dot{u}_y + b_4 u_y\dot{u}_y^2 + b_5\dot{u}_y^3 \text{ avec } b = [b_1, b_2, b_3, b_4, b_5]^T \tag{8.15}$$

The components of vector b correspond to the parameters of the mVdP model:

$$b = [m{\omega_0}^2,\ -2\mu m\omega_0,\ 2\mu m\omega_0\beta,\ 2\mu m\gamma,\ \frac{2\mu m}{\omega_0}\delta]^T \tag{8.16}$$

The optimal parameters are then obtained by a constrained minimization procedure:

$$b^* = min[\frac{1}{2}\sum_{i=1}^{N_{id}}((F_{y,per}^{(i)} - F(u_{y,per}^{(i)}, \dot{u}_{y,per}^{(i)}, b)))^2] \tag{8.17}$$

where $F_{y,per}^{(i)}$ is the Fourier series approximation of the lateral force, $\dot{u}_{y,per}^{(i)}$ and $u_{y,per}^{(i)}$ are obtained by successive integration of $\ddot{u}_{y,per}^{(i)} = F_{y,per}^{(i)}/m_i$, and N_{id} is the number of points used for the identification procedure corresponding to one period. The optimization constraints are given by:

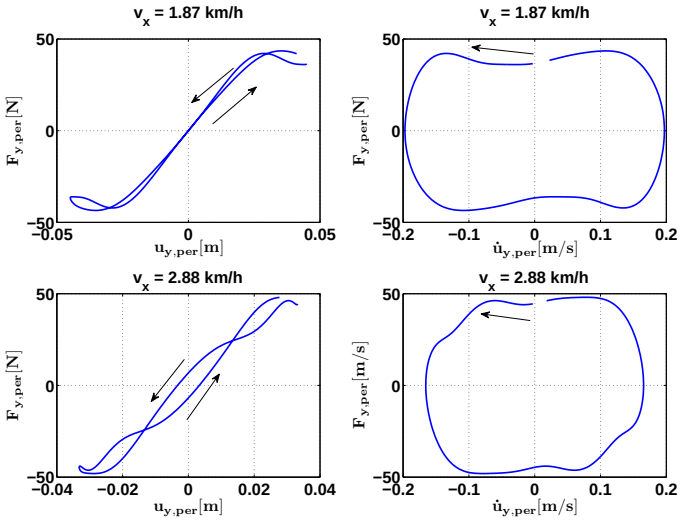

Figure 8.15: Fourier series of the force, velocity and displacement for one cycle for pedestrian 1-msc : $F_y(t) - u_y(t)$ (left) and $F_y(t) - u_y(t)$ (right).

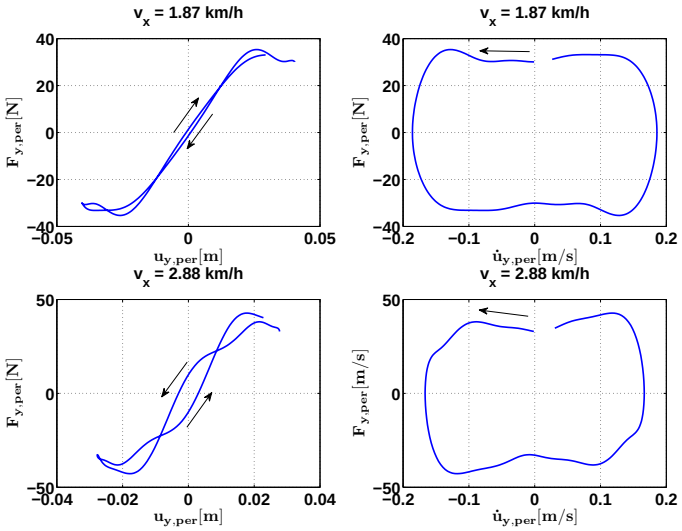

Figure 8.16: Fourier series of the force, velocity and displacement for one cycle for pedestrian 1-fmn : $F_y(t) - u_y(t)$ (left) and $F_y(t) - u_y(t)$ (right).

$$b_1 \geq 0, b_2 \leq 0, b_3 \geq 0 \text{ and } b_5 \geq 0 \tag{8.18}$$

Eqs. 8.17 and 8.18 define a constrained linear optimization problem. The function $fmincon$ in MATLAB was used to solve this problem. Once b^* is obtained, the model parameters can be calculated knowing that:

$$\omega_0 = \sqrt{\frac{{b_1}^*}{m}},\ \mu = -\frac{{b_2}^*}{2{b_1}^*}\sqrt{\frac{{b_1}^*}{m}},\ \beta = -\frac{{b_3}^*}{{b_2}^*},\ \gamma = -\frac{{b_4}^*}{{b_2}^*}\sqrt{\frac{{b_1}^*}{m}},\ \delta = -\frac{1}{m}\frac{{b_1}^*}{{b_2}^*}{b_5}^*,\ R = \frac{1}{n}\int \frac{F_{y,per}}{F_y}dt.$$

The parameters of pedestrians 1-msc and 1-fmn were calculated by the method described previously (see Tables 8.9 and 8.10). Finally, by using the identified parameters, the response of the oscillator (Eq. 8.14) is computed by ODE solver by choosing suitable initial conditions. The comparison between the

periodic-experimental and identified signals for pedestrians 1-msc and 1-fmn shows a very good agreement, as illustrated in Fig. 8.17-8.19. The identified parameters for all the participants are found in Fig. 8.23 and 8.24.

Table 8.9: Hybrid Van der Pol/Rayleigh oscillator with the γ-term: the identified parameters associated with pedestrian 1-msc.

	1.87 km/h	**2.38 km/h**	**2.88 km/h**	**3.35 km/h**
$\omega_0(rad/s)$	3.468	4.092	4.531	4.223
μ	0.844	0.024	0.044	0.026
$\beta(m^{-2})$	592.3	2601.7	3396.6	3105.4
$\gamma(m^{-2})$	248.6	11037.6	3632.6	26708.5
$\delta(m^{-2})$	308.5	0	0	0
R	0.99	0.99	0.99	0.99

Table 8.10: Hybrid Van der Pol/Rayleigh oscillator with the γ-term: the identified parameters associated with pedestrian 1-fmn.

	1.87 km/h	**2.38 km/h**	**2.88 km/h**	**3.35 km/h**
$\omega_0(rad/s)$	3.612	4.696	4.663	5.212
μ	0.692	0.001	0.049	0.418
$\beta(m^{-2})$	697.5	160.9	4511.2	1882.0
$\gamma(m^{-2})$	403.8	38325.2	12103.7	1634.8
$\delta(m^{-2})$	387.5	1758.7	0	975.5
R	0.99	0.99	0.99	0.99

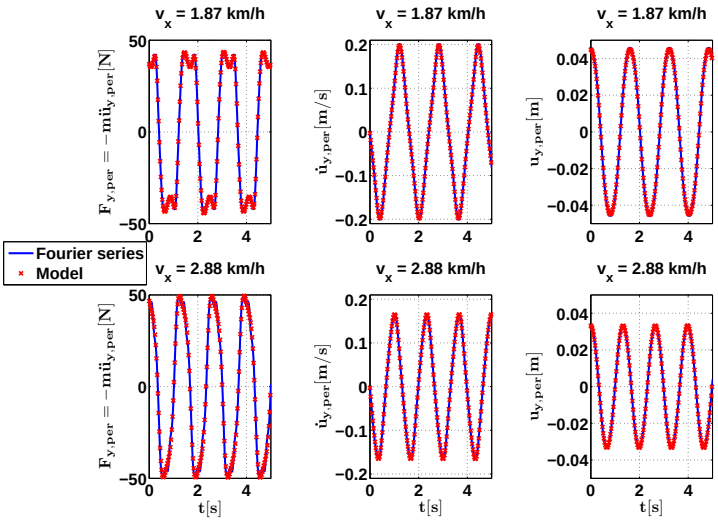

Figure 8.17: Lateral oscillation of the pedestrian 1-msc. Model (cross symbol) vs. truncated Fourier series results (solid line): the lateral force (left), velocity (middle), and displacement (right).

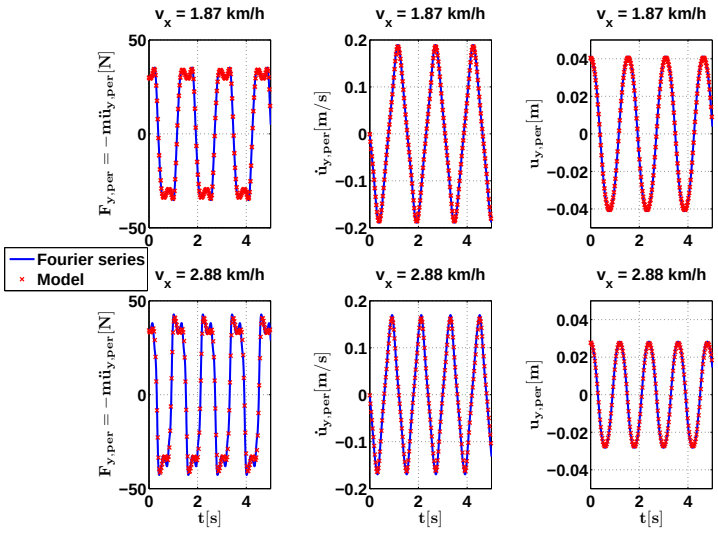

Figure 8.18: Lateral oscillation of the pedestrian 1-fmn. Model (cross symbol) vs. truncated Fourier series results (solid line): the lateral force (left), velocity (middle), and displacement (right).

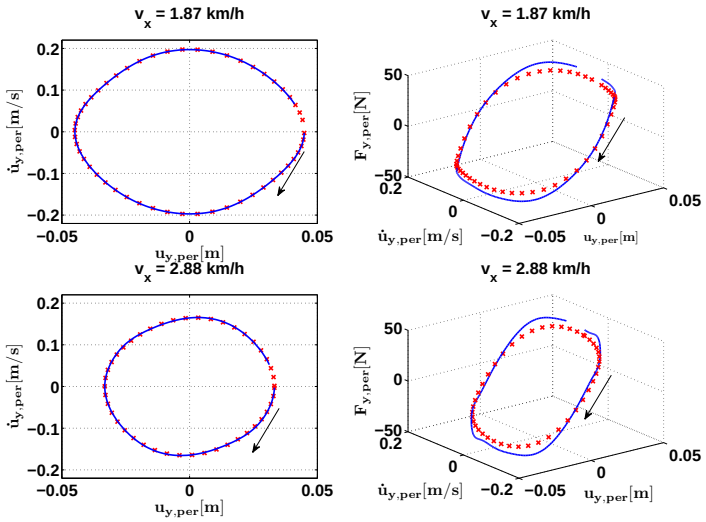

Figure 8.19: Lateral oscillations of the pedestrian 1-msc. Model (cross symbol) vs. truncated Fourier series results (solid line) over one cycle. The limit cycle in the phase-plane (left) and the lateral force as a function of displacement and velocity (right).

8.3 Conclusion

The objective of this study is to validate the representation of the dynamic behavior of a pedestrian by a self-sustained oscillator [5]. A modified version of a hybrid Van der Pol/Rayleigh oscillator was used for the reasons mentioned previously. The use of such an oscillator dictates that the lateral walking force of a pedestrian has to be periodic. For this reason, the measured lateral force signals of 31 participants (20 male and 11 female pedestrians) were treated. First, the Fast Fourier Transform (FFT) was used to represent the measured signals in the frequency domain. This representation helped to conclude on the quasi-periodicity of the lateral force. The latter was then approximated by a Fourier series of odd harmonics up to the 9^{th} order. Second, the lateral force was studied as a function of the lateral velocity and displacement. The limit cycle, the force-displacement, and force-velocity plots had the same shapes

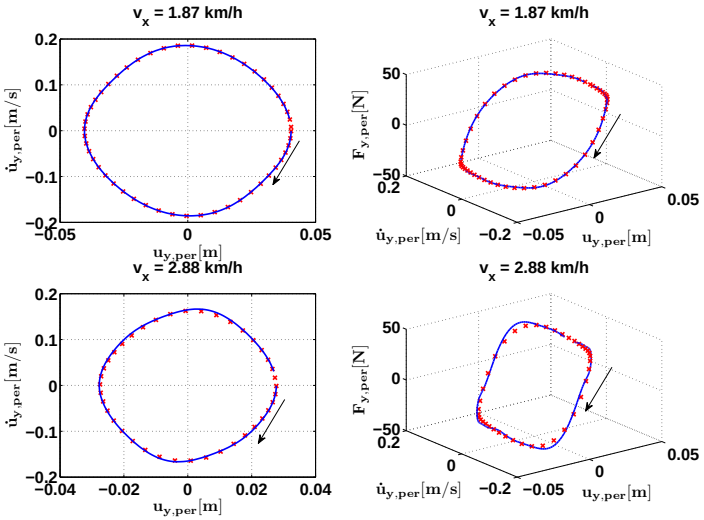

Figure 8.20: Lateral oscillations of the pedestrian 1-fmn. Model (cross symbol) vs. truncated Fourier series results (solid line) over one cycle. The limit cycle in the phase-plane (left) and the lateral force as a function of displacements and velocity (right).

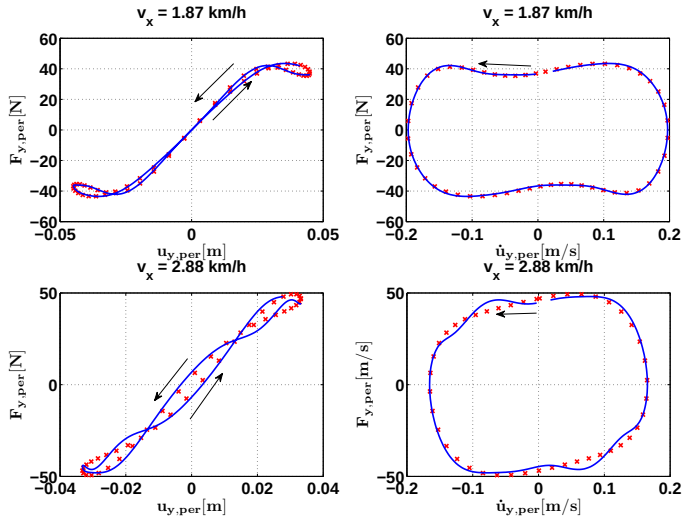

Figure 8.21: Force-displacement and force-velocity diagrams for pedestrian 1-msc over one cycle. Truncated Fourier series (solid line) vs. model results (cross symbol). Parametric plot $F_y(t) - u_y(t)$ (left) and $F_y(t) - u_y(t)$ (right).

as the ones obtained in [5]. Finally, the parameters of the mVdP model were identified. The comparison between periodic-experimental and identified signals showed a very good agreement thus validating the use of the hybrid Van der Pol/Rayleigh oscillator to model the lateral pedestrian force.

On the other hand, some results obtained in this study were not in line with what was found in [5]. Both found that the amplitude of the harmonics increase with increasing walking velocity. Yet, we obtained amplitude values higher than the ones found in [5] for lower values of the walking velocity. The same results were found for the maximum displacements. For the male participants, this quantitative difference could be justified by a higher average mass than the participants' in [5]. However, a similar quantitative difference was obtained for the female pedestrians who had a lower average mass than the participants' in [5].

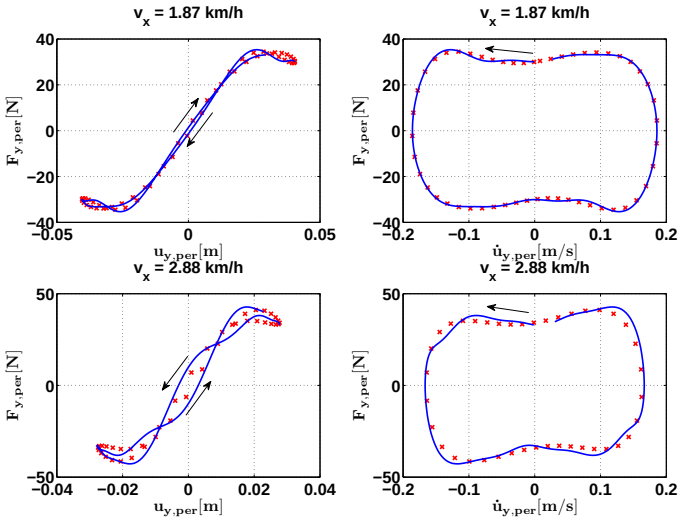

Figure 8.22: Force-displacement and force-velocity diagrams for pedestrian 1-fmn over one cycle. Truncated Fourier series (solid line) vs. model results (cross symbol). Parametric plot $F_y(t) - u_y(t)$ (left) and $F_y(t) - u_y(t)$ (right).

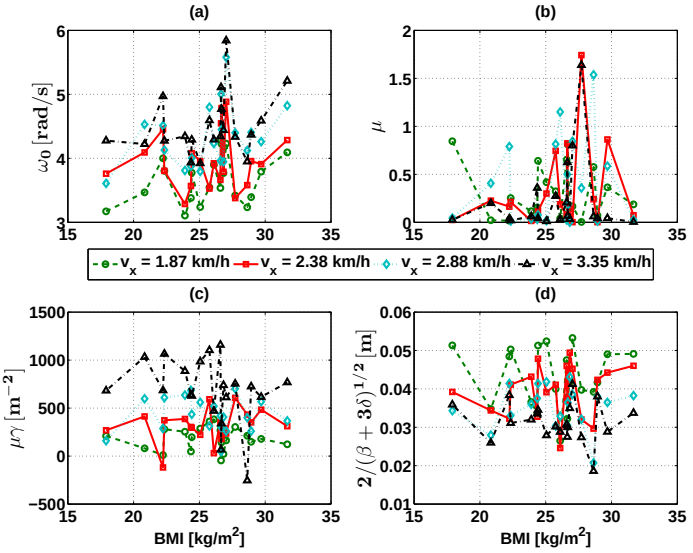

Figure 8.23: Identified model parameters for all of the male participants.

By applying the previously described method on 20 male and 11 female subjects, we tried to determine the differences in the dynamic behavior between the two genders if any exist. To start with, we have found that the female participants had a higher walking frequency than the men's. Second, the phase difference between the first and the third harmonic ($\Delta\phi_{1,3}$) was slightly higher than π for the women and slightly lower than π for the men. Finally, whereas the limit cycle tend to converge as walking velocity increases for the female participants, it doesn't seem to be the case for the male pedestrians. To conclude, it is difficult to precise the origin of these findings. The small diversity in the female population versus a higher one in the male population might be the main reason behind the obtained results. Another study where the population is more diverse could be more conclusive.

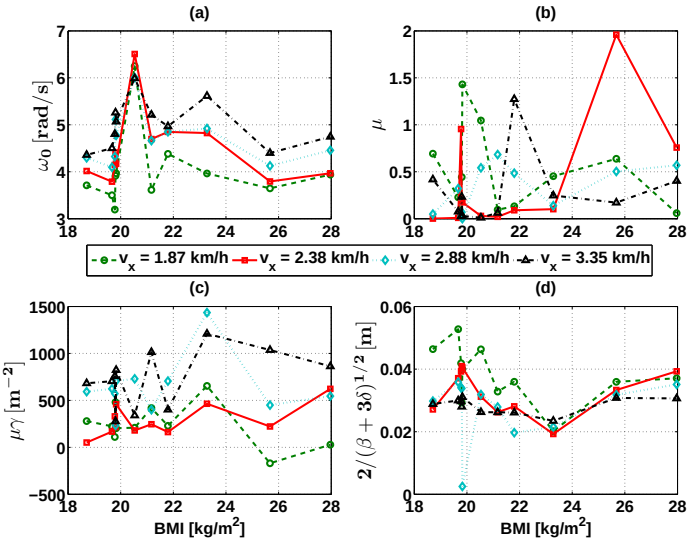

Figure 8.24: Identified model parameters for all of the female participants.

8.4 Appendix

In an effort to identify inter-pedestrian differences that might have an influence on a number of parameters related to the lateral walking force, we have plotted these parameters as a function of the pedestrians' height, mass, and Body Mass Index (BMI).

8.4.1 Lateral walking frequency

By examining Fig. 8.25 (a) and (b), it seems that the lateral walking frequency is inversely proportional to the pedestrians' height. Therefore it is proportional to the pedestrians' BMI (see Fig. 8.26 (a) and (b)). We could not observe a pattern regarding the participants' mass (see Fig. 8.27 (a) and (b)).

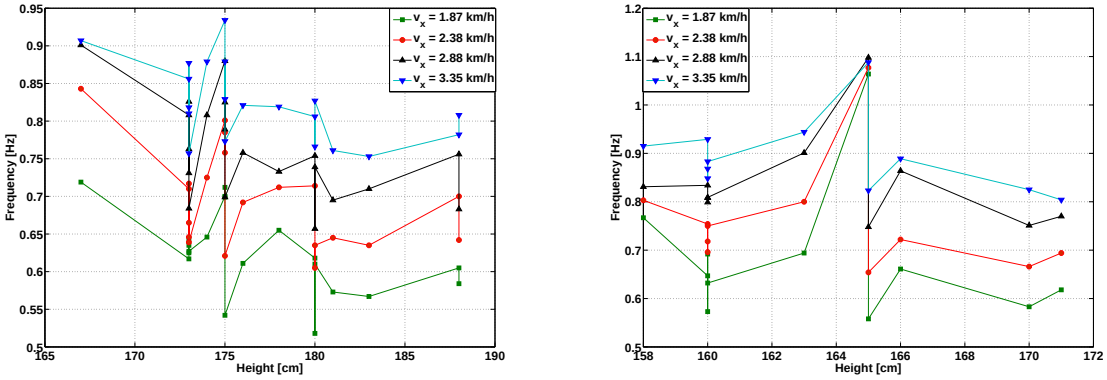

(a) (b)

Figure 8.25: Lateral walking frequency as a function of height for (a) the male and (b) female participants.

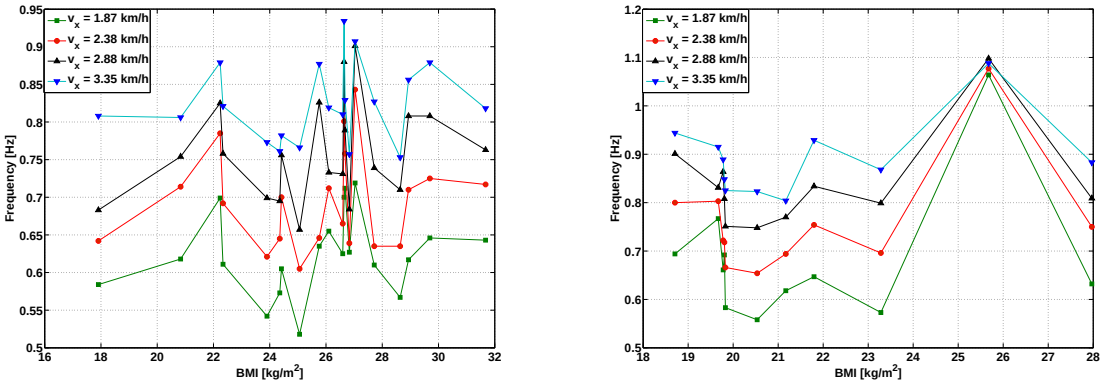

(a) (b)

Figure 8.26: Lateral walking frequency as a function of BMI for (a) the male and (b) female participants.

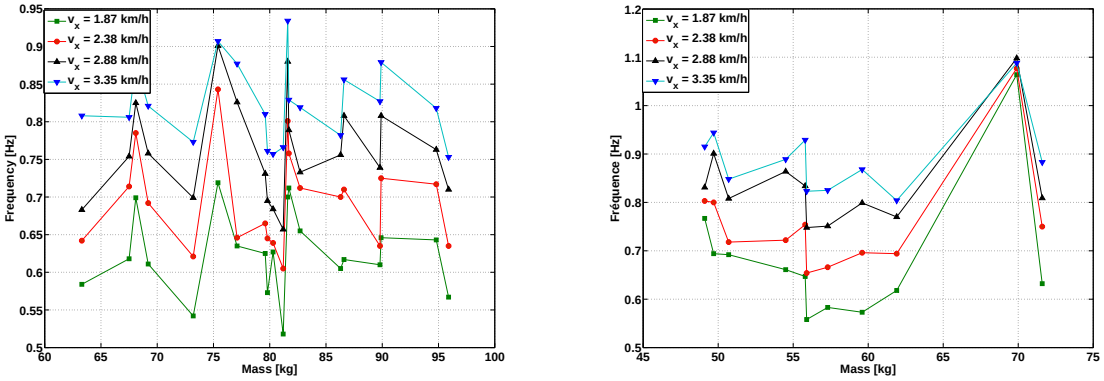

(a) (b)

Figure 8.27: Lateral walking frequency as a function of mass for (a) the male and (b) female participants.

8.4.2 C_1, C_3, and $\Delta_{1,3}$

It is difficult to observe any pattern regarding the participants' height, mass or BMI for the male (see Fig. 8.28, 8.29, and 8.30) and female participants (see Fig. 8.31, 8.32, and 8.33).

8.4.3 Amplitude of displacement

By examining Fig. 8.34 (a) and (b), it seems that the displacement amplitude is proportional to the pedestrians' height. Therefore it is inversely proportional to the pedestrians' BMI (see Fig. 8.35 (a) and (b)). We could not observe a pattern regarding the participants' mass (see Fig. 8.36 (a) and (b)).

8.4.4 Identified parameters of the proposed oscillator

By examining Fig. 8.37 (a) and (b), it seems that ω_0 is inversely proportional to the pedestrians' height. Therefore it is proportional to the pedestrians' BMI (see Fig. 8.38 (a) and (b)). We could not observe any other pattern for the other identified parameters or regarding the participants' mass (see Fig. 8.39 (a) and (b))..

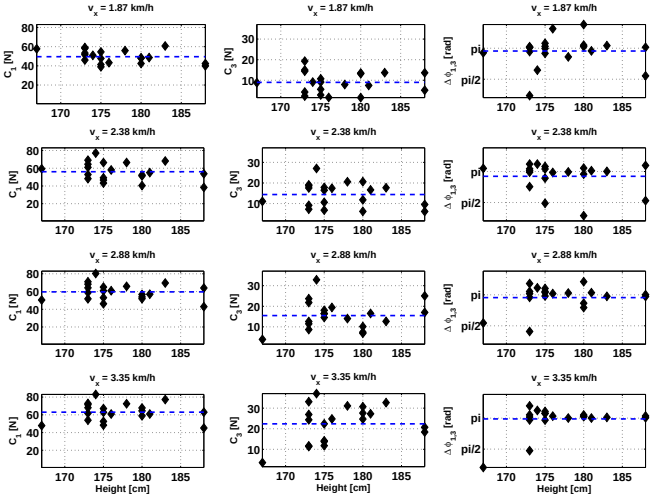

Figure 8.28: Fourier series approximation of the lateral walking force of the male participants: the amplitudes C_1, C_3, and the phase difference $\Delta\varphi_{1,3}$ as a function of their height. The average values are represented by the dotted lines.

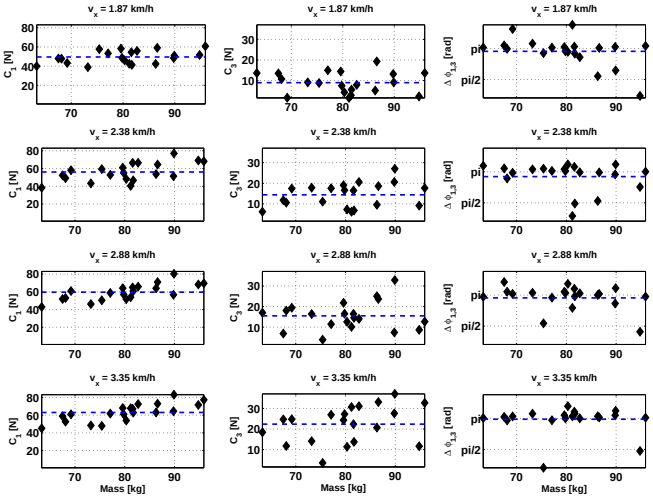

Figure 8.29: Fourier series approximation of the lateral walking force of the male participants: the amplitudes C_1, C_3, and the phase difference $\Delta\varphi_{1,3}$ as a function of their mass. The average values are represented by the dotted lines.

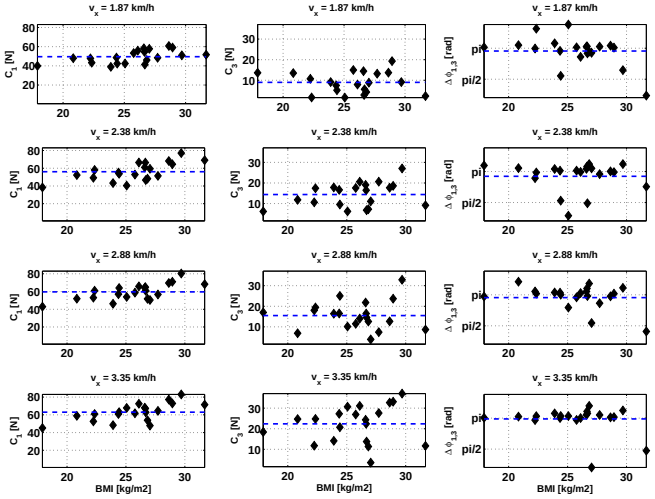

Figure 8.30: Fourier series approximation of the lateral walking force of the male participants: the amplitudes C_1, C_3, and the phase difference $\Delta\varphi_{1,3}$ as a function of their BMI. The average values are represented by the dotted lines.

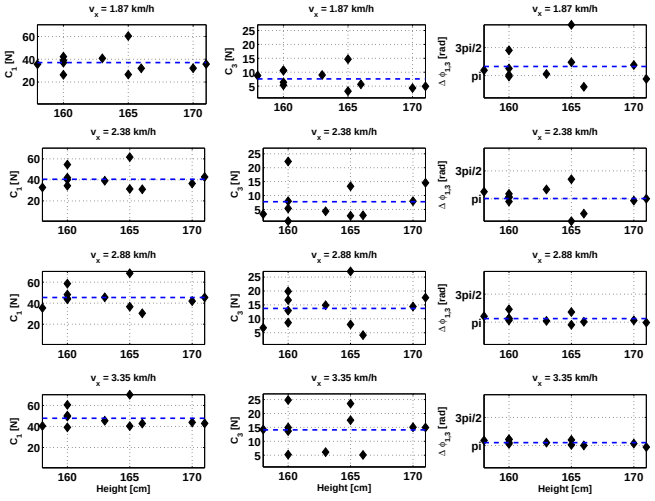

Figure 8.31: Fourier series approximation of the lateral walking force of the female participants: the amplitudes C_1, C_3, and the phase difference $\Delta\varphi_{1,3}$ as a function of their height. The average values are represented by the dotted lines.

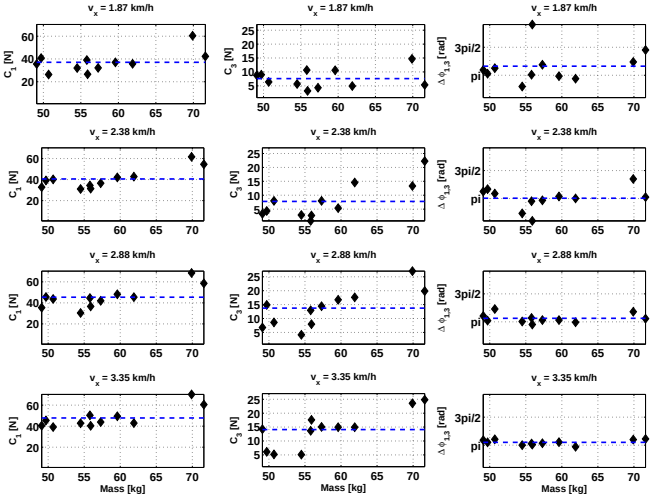

Figure 8.32: Fourier series approximation of the lateral walking force of the female participants: the amplitudes C_1, C_3, and the phase difference $\Delta\varphi_{1,3}$ as a function of their mass. The average values are represented by the dotted lines.

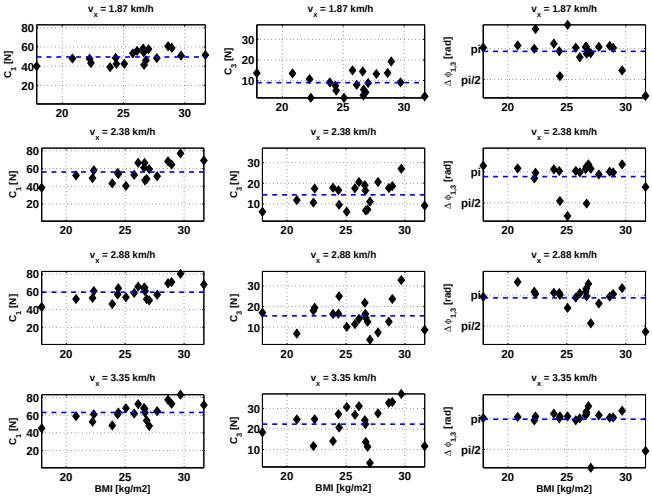

Figure 8.33: Fourier series approximation of the lateral walking force of the female participants: the amplitudes C_1, C_3, and the phase difference $\Delta\varphi_{1,3}$ as a function of their BMI. The average values are represented by the dotted lines.

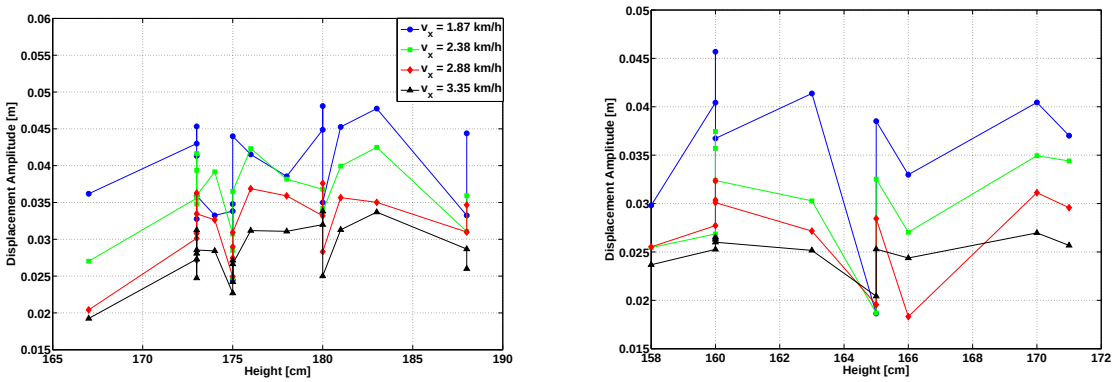

(a) (b)

Figure 8.34: Amplitude of the maximum displacement as a function of height for (a) the male and (b) female participants.

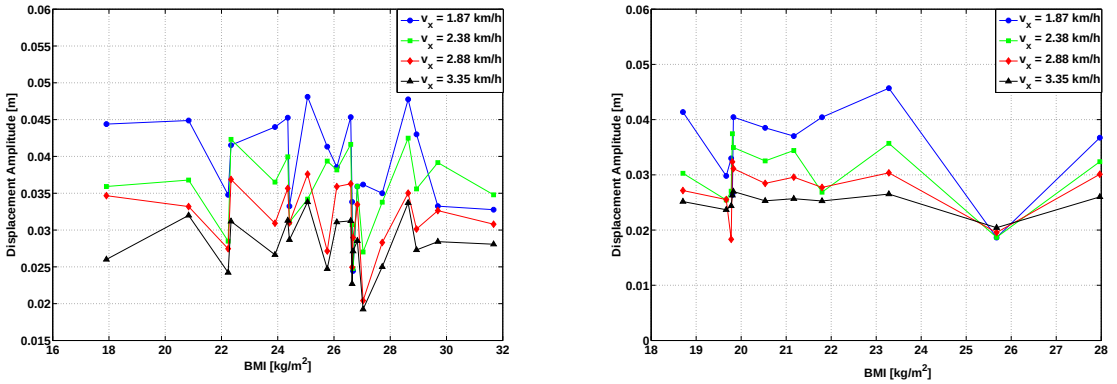

(a) (b)

Figure 8.35: Amplitude of the maximum displacement as a function of their BMI for (a) the male and (b) female participants.

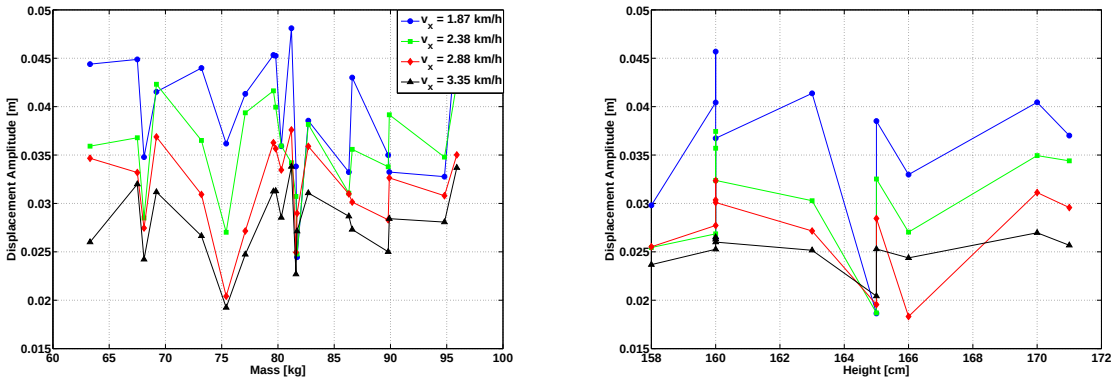

(a) (b)

Figure 8.36: Amplitude of the maximum displacement as a function of mass for (a) the male and (b) female participants.

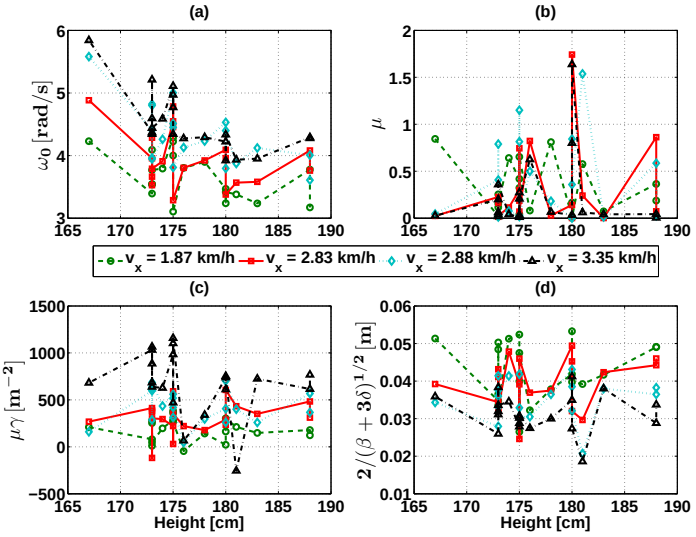

(a)

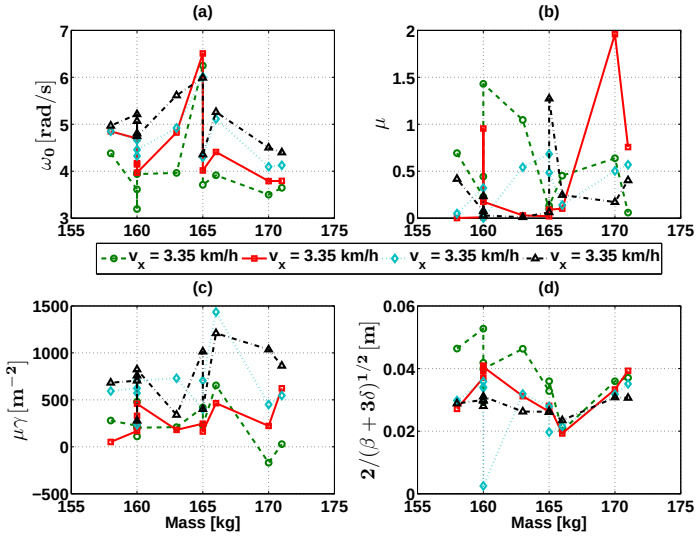

(b)

Figure 8.37: Identified parameters of the mVdP model as a function of height for (a) the male and (b) female participants.

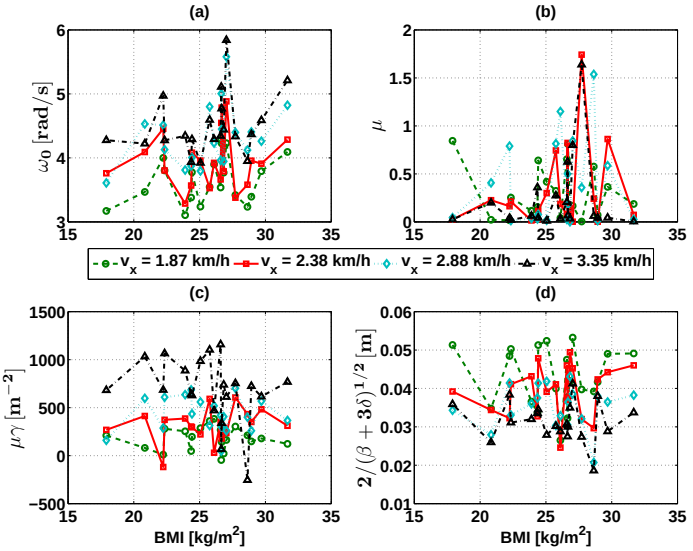

(a)

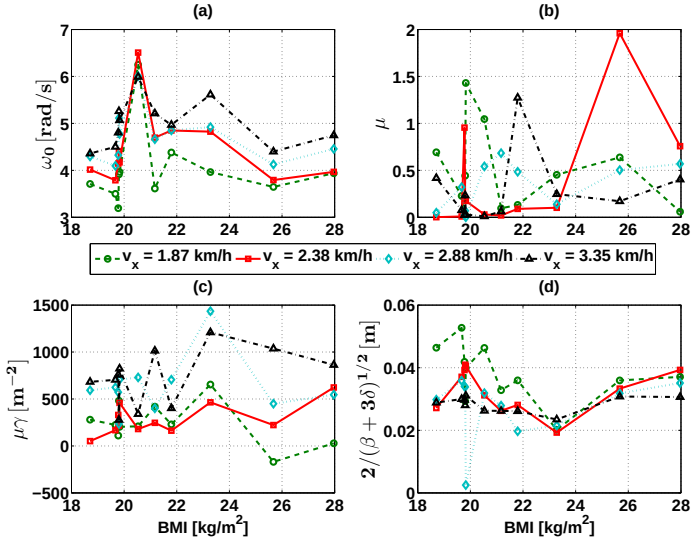

(b)

Figure 8.38: Identified parameters of the mVdP model as a function of BMI for (a) the male and (b) female participants.

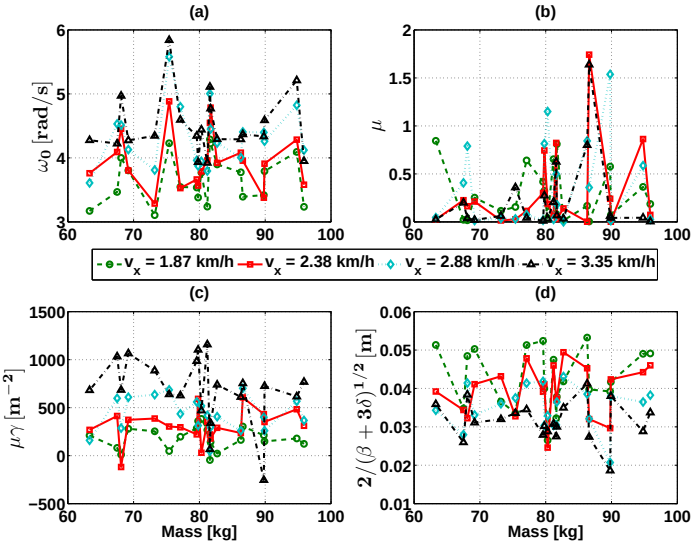

(a)

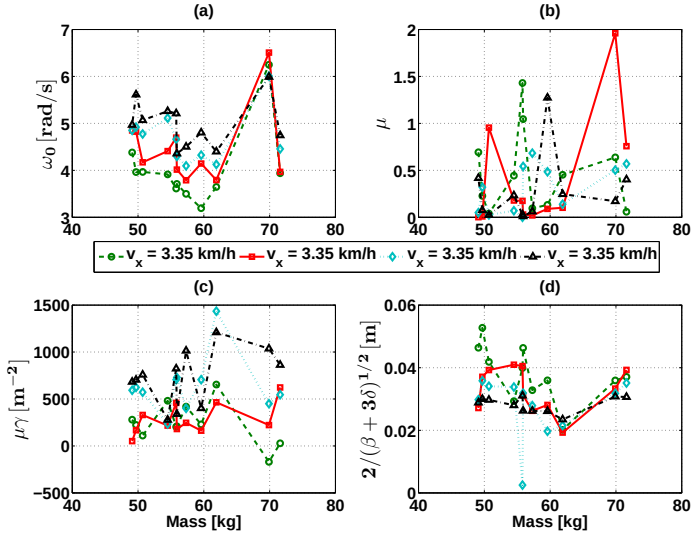

(b)

Figure 8.39: Identified parameters of the mVdP model as a function of mass for (a) the male and (b) female participants.

Bibliography

[1] Q. H. Ly, A. Alaoui, S. Erlicher, and L. Baly, "Towards a footwear design tool: influence of shoe midsole properties and ground stiffness on the impact force during running," *Journal of Biomechanics*, vol. 43, pp. 310–317, Jan. 2010.

[2] W. Liu and B. M. Nigg, "A mechanical model to determine the influence of masses and mass distribution on the impact force during running," *Journal of Biomechanics*, vol. 33, pp. 219–224, Feb. 2000.

[3] A. L. Hof, R. M. van Bockel, T. Schoppen, and K. Postema, "Control of lateral balance in walking: Experimental findings in normal subjects and above-knee amputees," *Gait & Posture*, vol. 25, pp. 250–258, Feb. 2007.

[4] J. H. G. Macdonald, "Lateral excitation of bridges by balancing pedestrians," *Proceedings of the Royal Society of London A: Mathematical, Physical and Engineering Sciences*, vol. 465, pp. 1055–1073, Apr. 2009.

[5] S. Erlicher, A. Trovato, and P. Argoul, "Modeling the lateral pedestrian force on a rigid floor by a self-sustained oscillator," *Mechanical Systems and Signal Processing*, vol. 24, pp. 1579–1604, July 2010.

[6] V. Racic and J. Brownjohn, "Mathematical modelling of random narrow band lateral excitation of footbridges due to pedestrians walking," *Computers & Structures*, vol. 90-91, pp. 116–130, Jan. 2012.

[7] L. Henderson, "The Statistics of Crowd Fluids," vol. Nature, 229, pp. 381–383, 1971.

[8] J. H. Rainer, G. Pernica, and D. E. Allen, "Dynamic loading and response of footbridges," *Canadian Journal of Civil Engineering*, vol. 15, pp. 66–71, Feb. 1988.

[9] F. Ricciardelli and A. D. Pizzimenti, "Lateral Walking-Induced Forces on Footbridges," *Journal of Bridge Engineering*, vol. 12, pp. 677–688, Nov. 2007.

[10] H. Bachmann and W. Ammann, *Vibrations in Structures: Induced by Man and Machines*. IABSE, 1987.

Conclusions and perspectives

A discrete pedestrian model has been developed at the Navier laboratory to simulate urgent evacuations and the pedestrian-structure interaction. In this thesis, the model was evolved by adding several levels of complexity. The objective is to be able to simulate normal situations so that the model can be used to reproduce experiments and applied in some applications such as public transportation. Three main aspects were addressed: (i) pedestrian navigation and displacement strategies, (ii) pedestrian-pedestrian interactions, and (iii) the validation and verification of the model.

In the first chapter of this thesis, the main core of the discrete model, based on the theory of rigid body collisions, is introduced. Certain modifications and investigations that were done concerning the main collision parameters and their effect on pedestrian rotation are illustrated.

The second part is dedicated to pedestrian navigation. The first section is a bibliographical study on this theme. The different approaches to classify the different levels of pedestrian navigation are elaborated. We then review some of the existing methods on modeling displacement strategies that take into account the evolution of traffic. In the second section, the method that we have adopted to model the shortest and fastest path strategies is demonstrated. It is shown how solving the eikonal equation can result in a floor field that gives a desired direction to each pedestrian according to his/her position and the adopted strategy. A static floor field attributes a direction towards the shortest path while a dynamic one takes into consideration the presence of other individuals and directs the pedestrian towards the fastest path. The influences of the two strategies on the overall dynamics of the crowd movement are compared. Connecting the notion of personal space with dynamic floor fields is an original approach that has never been used for continuous models. Its simplicity and intuitiveness allow us to believe that it can have other applications in pedestrian modeling.

The third part concerns pedestrian behavior or pedestrian-pedestrian interaction. In the first section, a bibliographical study is conducted on this aspect of pedestrian modeling. Several approaches that are found in literature on modeling pedestrian-pedestrian interactions are reviewed. In the second section of this part, we demonstrate the methods that are adopted in our model. The social repulsive force is used to model aggressive avoidance when a pedestrian needs to force his/her way. As for normal avoidance, where a pedestrian avoids others without disturbing them, is modeled by using a cognitive approach based on two heuristics. The performances of the two methods along with the one use for collision modeling are illustrated and compared for several criteria. The work done in this chapter leads us to the conviction that none of the existing methods can be used by itself to model pedestrian behavior. Instead, a combination of the three methods can be able to represent pedestrian behavior in different situations and density levels.

The fourth chapter is dedicated to the validation and verification of crowd models. A survey of the existing validation techniques and methods for crowd models is done in the first part. The work that have been done on our model concerning this issue is demonstrated in the second part of this chapter. First of all, an experimental plan was used in order to identify the most statistically significant input parameters of our model. The effects of the main parameters and their interactions on the model's output are also investigated. We then examine the capability of our model to reproduce empirical results. The case of a bottleneck was considered and a comparison between the simulation and experimental results gave satisfying results. In the absence of a unified code or standard to validate an verify pedestrian models, we have decided to use mathematical and statistical methods to better understand our model and how the input parameters interact and affect the output. However, we are also keeping up with the pedestrian modeling community by using mainstream techniques to validate and verify our model.

The fifth part is devoted to the application of the model in the field of public transportation. The objective of the study was to estimate train dwell time in the Noisy-Champs train station. In the first place, the field work that has been done to obtain the geometrical, traffic, and pedestrian data is shown. Then, we demonstrated how these data were introduced into the model in order to create the simulation scenario. Finally, the simulation results were compared to field observations giving promising results.

In the last part, modeling the lateral walking force of a pedestrian on a rigid floor was addressed. An already developed hybrid version of the Van der Pol self-sustained oscillator that is used to model the lateral walking force of a pedestrian on a rigid floor was further validated. This was done by processing the experimental data of 31 participants. The obtained results for male (20) and female (11) participants were separated in order to spot the differences between the two genders.

After going over the accomplished work in this thesis, several tracks for future research can be identified. There are still much more areas and aspects that are very interesting to investigate.

Concerning pedestrian route choice, the modeled displacement strategies can be improved in several ways. First of all, the concept of field of vision should be introduced so that pedestrians don't avoid congestions before actually "seeing" them. For example, if an exit is hidden behind a corner, a pedestrian should not avoid it before trying to take it and spotting the congestion at it. Second of all, it is important to differentiate between pedestrians who are familiar or unfamiliar with the environment. Familiar pedestrians will take the global fastest or shortest paths while the unfamiliar ones will use the local fastest or shortest paths. Third of all, the methods that were used in this PhD thesis to model displacement strategies are more adapted to small or medium areas. It will be interesting to investigate other methods that might be more suitable to model route choice in large areas such as airports or football stadiums. Finally, new displacement strategies can be introduced into our model. For example, the most comfortable path seems to be very important when elderly or disabled pedestrians are present in a crowd.

As for pedestrian-pedestrian interactions, there are several tracks to be investigated. Starting with cognitive approach to model pedestrian avoidance, it is important to verify its ability to reproduce the phenomena of auto-organization such as lane formation. Then, we can try to connect the notion of personal space (Voronoi diagram) to the behavior of pedestrians. According to the available personal space, an individual can change his/her behavior between pushing (collision model), aggressive avoidance (social repulsive force model), and normal avoidance (cognitive approach). Allowing a pedestrian to change his/her behavior according to the evolution of density in the environment seems to be an important subject that is not addressed in literature.

All of the above research should always be validated and verified in order to be useful in pedestrian modeling. The work that has been done in this PhD thesis using experimental plans should be carried on. As a first step, the constructed regression model has to be validated with the numerical model. Then, it should be validated with the experimental results on bottlenecks. Since the validation part in this PhD thesis was focused on bottlenecks, other scenarios should be considered in future work, e.g., unidirectional and bidirectional flows in corridors, T-junctions, intersections, etc.. At this stage, it is important to acquire empirical data to be able to calibrate our model using pedestrian trajectory data.

During this PhD thesis, the model evolved to a level that allowed us to use it to study pedestrian flow at a real train station. The promising results that were obtained by this preliminary study encourage us to continue and extend the work on similar projects. However, precise data is needed concerning pedestrian characteristics, trajectories, origins-destinations, etc.. This will allow us to calibrate our model and identify the different types of pedestrian behavior on platforms, train doors, queues, etc.. The results obtained by our model are as good as the input data that we introduce.